

# **Predictability of Hydroclimatic Variability over Eastern South Africa under Climate Change**

Report to the  
**WATER RESEARCH COMMISSION**

by

**Francois Engelbrecht, Zane Dedekind, Mavhungu Muthige, Johan Malherbe,  
Asmerom Beraki, Christien Engelbrecht, Isaac Ngwana, Trevor Lumsden, Willem  
Landman, Robert Maisha, Lerato Mpheshea, Jacobus van der Merwe  
and Karen Eatwell**

CSIR

**WRC Report No 2457/1/19**

**ISBN 978-0-6392-0162-7**

**March 2020**

**Obtainable from**

Water Research Commission  
Private Bag X03  
GEZINA, 0031

[orders@wrc.org.za](mailto:orders@wrc.org.za) or download from [www.wrc.org.za](http://www.wrc.org.za)

**DISCLAIMER**

This report has been reviewed by the Water Research Commission (WRC) and approved for publication. Approval does not signify that the contents necessarily reflect the views and policies of the WRC nor does mention of trade names or commercial products constitute endorsement or recommendation for use.

## Executive Summary

This Water Research Commission research project (project K5/2457) explored the climate change futures of eastern South Africa, given the importance of this region for South Africa's water security and thus its future industrial and socio-economic development. Key areas of interest in this project included South Africa's eastern escarpment, Lesotho and the mega-dam area. The research was focussed on projecting changes in a wide range of variables that are important to the hydroclimate of eastern South Africa, such as changes in rainfall totals, average temperatures, extreme rainfall events, droughts, soil moisture, run-off, streamflow and dam levels. It was also explored whether climate change may result in changes in climate variability over eastern southern Africa under climate change, for example, whether the frequency of occurrence of seasons of below and/or above normal rainfall will increase or decrease during the 21<sup>st</sup> century. A baseline for the project research was Assessment Reports Four and Five (AR4 and AR5) of the Intergovernmental Panel on Climate Change (IPCC), which both concluded that the larger southern African region is likely to become generally drier under low mitigation climate change futures. However, uncertainty exists in the AR4 and AR5 projections in terms of the rainfall futures over eastern South Africa, with some models projections indicative of rainfall increases and roughly the same number of models indicative of rainfall decreases. Against this background, the project proceeded to generate high-resolution projected climate change futures over southern Africa. This involved generating a large ensemble of 50-km resolution global projections of future climate change as a contribution to the Coordinated Regional Downscaling Experiment (CORDEX) of the World Climate Research Programme (WCRP). The CSIR thereby became the first African institute contributing projections of future climate change to CORDEX, which is an important long-term legacy of the project. Moreover, the CORDEX simulations were downscaled to a resolution of 8 km in the horizontal over eastern South Africa, thereby generating the most detailed projections of climate change obtained to date over this region. Although the statistical analysis of future climate change and hydrological modelling as presented in the project are based on the detailed projections generated by the project, all findings are interpreted within the larger body of evidence reported on in AR4 and AR5 of the IPCC.

The research performed demonstrated that pronounced changes in rainfall and temperature may occur over the mega-dam region under climate change. In terms of potential impacts on hydrology, there are three main messages of change that may be considered to be most important:

- Multi-year droughts may occur frequently over the mega-dam region as early as the mid-future period of 2046-2065, presumably in response to the more frequent occurrence of El Niño events, and with detrimental implications for dam levels;
- Despite the region projected to become generally drier, extreme convective rainfall events may occur more frequently over the mega-dam region;
- Both statistical and dynamic hydrological modelling are indicative of the plausibility of increased streamflow over eastern South Africa;
- Drastic increases in temperature are likely to result in increased evaporation in the mega dams and also in drastic reductions in soil moisture.

Moreover, climate of the mega-dam region is projected to become more variable in terms of the annual anomalies of both temperature and rainfall. This does not translate into a decrease in predictability, however, since a stronger ENSO signal over the region is likely to increase predictability at the seasonal time-scale. Also at shorter-range time-scales, whether systems associated with high predictability are projected to occur more frequently under climate change. This implies that short-range and seasonal forecasts may become increasingly important adaptation tools to climate change, towards providing early warning of extreme events occurring over eastern South Africa.

## **Acknowledgements**

The project team is indebted to the project Reference Group, who has actively participated in the project meetings and whom have made a number of useful suggestions towards improving and extending research. Special thanks are due to in particular to Prof. Chris Reason (UCT), Dr Chris Jack (UCT), Dr Christien Engelbrecht and Mr Abel Moatshe for their specialist advice. Dr Brilliant Petja of the WRC is thanked for his expert leadership in initializing and managing the project. The WRC is thanked for supporting the research, and the CHPC is acknowledged for providing the computational resources required to perform the CCAM simulations. Mr Zane Dedekind's MSc research on high-resolution climate modelling was supported through the project, and SAWS is acknowledged to provide weather station data to aid the model verifications performed. Mr Isaac Ngwana's PhD research on short-range predictability was similarly supported by the project, and ACCESS (Alliance for Collaboration in Climate and Earth Sciences) is thanked for the co-funding provided.

# Table of Contents

<b>Executive Summary .....</b>	<b>iii</b>
<b>Acknowledgements .....</b>	<b>iv</b>
<b>Chapter 1 Introduction.....</b>	<b>1</b>
<b>Chapter 2 Projections of regional climate change over southern Africa and implications for the mega-dam region.....</b>	<b>5</b>
2.1 Introduction .....	5
2.2 The conformal-cubic atmospheric model and experimental design .....	6
2.3 Projected climate change futures over southern Africa.....	7
2.3.1 Projected changes in temperature.....	7
2.3.2 Projected changes in rainfall .....	8
2.3.3 Projected changes in wetness and dryness over southern Africa .....	18
2.4 Summary .....	19
<b>Chapter 3 Detailed projections of future climate change over the eastern escarpment and mega-dam regions of South Africa .....</b>	<b>20</b>
3.1 Introduction .....	20
3.2 Data and design of the model simulations of present-day climate .....	21
3.3 Results: simulations of present-day climate .....	22
3.3.1 Verification of the CCAM simulations against station data .....	22
3.3.2 Annual rainfall totals .....	24
3.3.3 Seasonal rainfall totals .....	27
3.3.4 Monthly rainfall totals .....	27
3.3.5 Diurnal rainfall cycle .....	32
3.3.6 Intra-annual rainfall .....	32
3.3.7 Inter-annual rainfall .....	32
3.4 Summary – detailed simulations of present-day climate.....	34
3.5 Experimental design of the detailed downscalings of future climate change .....	35
3.6 Results: detailed projections of future climate change.....	35
3.6.1 Average temperature .....	36
3.6.2 Maximum temperature .....	40
3.6.3 Minimum temperature .....	43
3.6.4 Rainfall.....	43
3.6.5 Extreme rainfall events.....	47
3.7 Summary of the detailed projections of future climate change .....	53
<b>Chapter 4 Climate variability and predictability over eastern South Africa under climate change .....</b>	<b>54</b>
4.1 Introduction .....	54
4.2 Methodology .....	55
4.2.1 AMIP-style simulations as an upper boundary for seasonal forecast skill .....	55
4.2.2 High-resolution CCAM seasonal forecasts .....	55
4.2.3 Short-range predictability under climate change.....	56
4.3 Results.....	56
4.3.1 Projected changes in climate variability over eastern South Africa .....	56
4.3.2 Seasonal forecast skill in rainfall and streamflow over eastern South Africa .....	72
4.3.3 High resolution seasonal forecasting over eastern South Africa .....	76
4.3.4 Changes in short-range predictability over southern Africa .....	77
4.4 Summary .....	81

<b>Chapter 5 Projected changes in hydrology over the eastern escarpment and mega-dam region of South Africa .....</b>	<b>83</b>
5.1 Introduction .....	83
5.2 Methodology .....	83
5.2.1 Time-series analysis of dam levels .....	83
5.2.2 Dynamic hydrological modelling .....	84
5.2.3 Observed streamflow data and statistical projections of stream-flow .....	84
5.3 Results – variability, trends and projected changes in dam levels .....	85
5.3.1 Present-day variability .....	85
5.3.2 Projections of future climate change – rainfall and dam levels.....	93
5.3.3 Dynamic projections of changes in the hydro-climate of eastern South Africa ...	103
5.3.4 Projections of streamflow over eastern South Africa under climate change .....	107
5.4 Summary .....	113
<b>Chapter 6 Conclusions .....</b>	<b>114</b>
<b>References .....</b>	<b>117</b>
<b>Appendix A List of publications and post-graduate students related to/contributing to WRC project K5/2457.....</b>	<b>134</b>

## List of Figures

<b>Figure 1.1:</b> Observed October to December SST anomalies over the Niño 3.4 region (y-axis) and corresponding observed December-February rainfall anomalies (mm) over Lesotho for the summers of 1901/02 through to 2013/14. The SST anomalies were obtained from the Atmospheric Model Intercomparison Project (AMIP) data set whilst the rainfall anomalies were calculated from the Climatic Research Unit (CRU) data set CRU 3.24. ....	2
<b>Figure 2.1:</b> C192 quasi-uniform conformal-cubic grid (every 4th grid point is shown), which provides a horizontal resolution of about 200 km globally.....	7
<b>Figure 2.2:</b> CCAM-CABLE projected changes in annual mean temperature (°C) under RCP 8.5 for the period 2046-2065 relative to 1961-1990.....	9
<b>Figure 2.3:</b> CCAM-CABLE projected changes in annual mean temperature (°C) under RCP 4.5 for the period 2046-2065 relative to 1961-1990.....	10
<b>Figure 2.4:</b> CCAM-CABLE projected changes in annual mean temperature (°C) under RCP 8.5 for the period 2070-2099 relative to 1961-1990.....	11
<b>Figure 2.5:</b> CCAM-CABLE projected changes in annual mean temperature (°C) under RCP 4.5 for the period 2070-2099 relative to 1961-1990.....	12
<b>Figure 2.6:</b> CCAM-CABLE projected changes in annual rainfall (mm) under RCP 8.5 for the period 2046-2065 relative to 1961-1990.....	13
<b>Figure 2.7:</b> CCAM-CABLE projected changes in annual rainfall (mm) under RCP 4.5 for the period 2046-2065 relative to 1961-1990.....	14
<b>Figure 2.8:</b> CCAM-CABLE projected changes in annual rainfall (mm) under RCP 8.5 for the period 2070-2099 relative to 1961-1990.....	15
<b>Figure 2.9:</b> CCAM-CABLE projected changes in annual rainfall (mm) under RCP 8.5 for the period 2070-2099 relative to 1961-1990.....	16
<b>Figure 2.10:</b> CCAM simulated annual temperature anomalies (°C, y-axis) and corresponding rainfall anomalies (mm, x-axis) over Lesotho for the period 1971-2099.....	17
<b>Figure 2.11:</b> SPI evolution over the period 1971-2099, for (a) southern Africa, (b) West Africa and (c) East Africa. The light-pink shade represents the CCAM ensemble spread; red and black lines are the CCAM ensemble mean and observations, respectively. ....	18
<b>Figure 3.1:</b> Location of South African Weather Service (SAWS) stations around Lesotho measuring at daily (coloured) and hourly (black) time intervals. ....	25
<b>Figure 3.2:</b> a) Vertical cross-section at 29.25°S for annual rainfall in mm/day (solid line – CCAM; long stripes – CRU; short stripes – TRMM). Annual rainfall totals (mm) for b) CCAM (1979-2004), c) CRU (1979-2007) and d) TRMM (1998-2010). Bias (mm) for e) CCAM-CRU and f) CCAM-TRMM. ....	26
<b>Figure 3.3:</b> a) Vertical cross-section at 29.25°S for DJF rainfall in mm/day (solid line – CCAM; long stripes – CRU; short stripes – TRMM). DJF rainfall totals (mm) for b) CCAM (1979-2004), c) CRU (1979-2007) and d) TRMM (1998-2010). Bias (mm) for e) CCAM-CRU and and f) CCAM-TRMM. ....	28
<b>Figure 3.4:</b> a) Vertical cross-section at 29.25°S for November rainfall in mm/day (solid line – CCAM; long stripes – CRU; short stripes – TRMM). November rainfall totals (mm) for b) CCAM (1979-2004), c) CRU (1979-2007) and d) TRMM (1998-2010). Bias (mm) for e) CCAM-CRU and f) CCAM-TRMM. ....	29
<b>Figure 3.5:</b> a) Vertical cross-section at 29.25°S for December rainfall in mm/day (solid line – CCAM; long stripes – CRU; short stripes – TRMM). December rainfall totals (mm) for b) CCAM (1979-2004), c) CRU (1979-2007) and d) TRMM (1998-2010). Bias (mm) for e) CCAM-CRU and f) CCAM-TRMM. ....	30
<b>Figure 3.6:</b> a) Vertical cross-section at 29.25°S for January rainfall in mm/day (solid line – CCAM; long stripes – CRU; short stripes – TRMM). January rainfall totals (mm) for b) CCAM (1979-2004), c) CRU (1979-2007) and d) TRMM (1998-2010). Bias (mm) for e) CCAM-CRU and f) CCAM-TRIMM. ....	31

<b>Figure 3.7:</b> 6-Hourly diurnal cycle for CCAM a) annually, b) DJF, c) November, d) December and e) January. Intervals are 00h to 06h (dark blue), 06h-12h (light blue), 12h-18h (green) and 18h-24h (yellow).....	33
<b>Figure 3.8:</b> Intra-annual rainfall totals (mm) for CCAM AMIP (1979-2004), NCEP reanalysis (1979-2009), CRU (1979-2004) and TRMM (1998-2010) over the regions of a) LES, b) NESa and c) ESA. ....	34
<b>Figure 3.9:</b> Inter-annual DJF rainfall totals (mm) for CCAM (1979-2004) and CRU (1979-2004) over the regions of LES. In brackets is the Spearman Rank Correlation level of significance. ....	34
<b>Figure 3.10a:</b> CCAM simulated annual average temperature (°C) over eastern South Africa at 8 km resolution, for the baseline period 1961-1990. The median of simulations is shown for the ensemble of downscalings of six GCM simulations. ....	48
<b>Figure 3.10b:</b> CCAM projected change in the annual average temperature (°C) over eastern South Africa at 8 km resolution, for the time-slab 2021-2050 relative to 1961-1990. The 10 <sup>th</sup> , 50 <sup>th</sup> and 90 <sup>th</sup> percentiles are shown for the ensemble of downscalings of six GCM projections under RCP4.5 (left) and RCP8.5 (right). ....	49
<b>Figure 3.10c:</b> CCAM projected change in the annual average temperature (°C) over eastern South Africa at 8 km resolution, for the time-slab 2070-2099 relative to 1961-1990. The 10 <sup>th</sup> , 50 <sup>th</sup> and 90 <sup>th</sup> percentiles are shown for the ensemble of downscalings of six GCM projections under RCP4.5 (left) and RCP8.5 (right).....	50
<b>Figure 3.11a:</b> CCAM simulated annual average maximum temperature (°C) over eastern South Africa at 8 km resolution, for the baseline period 1961-1990. The median of simulations is shown for the ensemble of downscalings of six GCM simulations.....	51
<b>Figure 3.11b:</b> CCAM projected change in the annual average maximum temperature (°C) over eastern South Africa at 8 km resolution, for the time-slab 2021-2050 relative to 1961-1990. The 10 <sup>th</sup> , 50 <sup>th</sup> and 90 <sup>th</sup> percentiles are shown for the ensemble of downscalings of six GCM projections under RCP4.5 (left) and RCP8.5 (right). ....	52
<b>Figure 3.11c:</b> CCAM projected change in the annual average maximum temperature (°C) over eastern South Africa at 8 km resolution, for the time-slab 2021-2050 relative to 1961-1990. The 10 <sup>th</sup> , 50 <sup>th</sup> and 90 <sup>th</sup> percentiles are shown for the ensemble of downscalings of six GCM projections under RCP4.5 (left) and RCP8.5 (right).....	53
<b>Figure 3.12a:</b> CCAM simulated annual average minimum temperature (°C) over eastern South Africa at 8 km resolution, for the baseline period 1961-1990. The median of simulations is shown for the ensemble of downscalings of six GCM simulations.....	445
<b>Figure 3.12b:</b> CCAM projected change in the annual average minimum temperature (°C) over eastern South Africa at 8 km resolution, for the time-slab 2021-2050 relative to 1961-1990. The 10 <sup>th</sup> , 50 <sup>th</sup> and 90 <sup>th</sup> percentiles are shown for the ensemble of downscalings of six GCM projections under RCP4.5 (left) and RCP8.5 (right).....	56
<b>Figure 3.12c:</b> CCAM projected change in the annual average minimum temperature (°C) over eastern South Africa at 8 km resolution, for the time-slab 2070-2099 relative to 1961-1990. The 10 <sup>th</sup> , 50 <sup>th</sup> and 90 <sup>th</sup> percentiles are shown for the ensemble of downscalings of six GCM projections under RCP4.5 (left) and RCP8.5 (right).....	57
<b>Figure 3.13a:</b> CCAM simulated annual average rainfall totals (mm) over eastern South Africa, for the baseline period 1961-1990 at 8 km resolution. The median of simulations is shown for the ensemble of downscalings of six GCM simulations. ....	478
<b>Figure 3.13b:</b> CCAM projected change in the annual average rainfall totals (mm) over eastern South Africa at 8 km resolution, for the time-slab 2021-2050 relative to 1961-1990. The 10 <sup>th</sup> , 50 <sup>th</sup> and 90 <sup>th</sup> percentiles are shown for the ensemble of downscalings of six GCM projections under RCP4.5 (left) and RCP8.5 (right).....	59

<b>Figure 3.13c:</b> CCAM projected change in the annual average rainfall totals (mm) over eastern South Africa, for the time-slab 2071-2100 relative to 1961-1990. The 10 <sup>th</sup> , 50 <sup>th</sup> and 90 <sup>th</sup> percentiles are shown for the ensemble of downscalings of six GCM projections under RCP4.5 (left) and RCP8.5 (right).....	60
<b>Figure 3.14a:</b> CCAM simulated annual average number of extreme rainfall days (units are number of days per grid point per year) over eastern South Africa, for the baseline period 1961-1990. The median of simulations is shown for the ensemble of downscalings of six GCM simulations.....	61
<b>Figure 3.14b:</b> CCAM projected change in the annual average number of extreme rainfall days (units are numbers of grid points per year) over eastern South Africa at 8 km resolution, for the time-slab 2021-2050 relative to 1961-1990. The 10 <sup>th</sup> , 50 <sup>th</sup> and 90 <sup>th</sup> percentiles are shown for the ensemble of downscalings of six GCM projections under RCP4.5 and RCP8.5.....	62
<b>Figure 3.14c:</b> CCAM projected change in the annual average number of extreme rainfall days (units are numbers of grid points per year) over eastern South Africa, for the time-slab 2071-2100 relative to 1961-1990. The 10 <sup>th</sup> , 50 <sup>th</sup> and 90 <sup>th</sup> percentiles are shown for the ensemble of downscalings of six GCM projections under RCP4.5 (left) and RCP8.5 (right).....	63
<b>Figure 4.1a:</b> 11-year moving average of projected summer temperature (°C) over the mega-dam area, obtained through downscaling of the ACCESS1-0 GCM using CCAM (top). Standard deviation of the detrended 11-year moving time series, depicting summer temperature variability (°C) over the mega-dam area.....	58
<b>Figure 4.1b:</b> 11-year moving average of projected summer temperature (°C) over the mega-dam area, obtained through downscaling of the GFDL-CM3 GCM using CCAM (top). Standard deviation of the detrended 11-year moving time series, depicting summer temperature variability (°C) over the mega-dam area.....	69
<b>Figure 4.1c:</b> 11-year moving average of projected summer temperature (°C) over the mega-dam area, obtained through downscaling of the MPI-ESM-LR GCM using CCAM (top). Standard deviation of the detrended 11-year moving time series, depicting summer temperature variability (°C) over the mega-dam area.....	70
<b>Figure 4.1d:</b> 11-year moving average of projected summer temperature (°C) over the mega-dam area, obtained through downscaling of the NorESM1M GCM using CCAM (top). Standard deviation of the detrended 11-year moving time series, depicting summer temperature variability (°C) over the mega-dam area.....	71
<b>Figure 4.1e:</b> 11-year moving average of projected summer temperature (°C) over the mega-dam area, obtained through downscaling of the CCSM4 GCM using CCAM (top). Standard deviation of the detrended 11-year moving time series, depicting summer temperature variability (°C) over the mega-dam area.....	72
<b>Figure 4.1f:</b> 11-year moving average of projected summer temperature (°C) over the mega-dam area, obtained through downscaling of the CNRM GCM using CCAM (top). Standard deviation of the detrended 11-year moving time series, depicting summer temperature variability (°C) over the mega-dam area.....	73
<b>Figure 4.2a:</b> 11-year moving average of projected summer rainfall (mm) over the mega-dam area, obtained through downscaling of the ACCESS1-0 GCM using CCAM (top). Standard deviation of the detrended 11-year moving time series, depicting summer rainfall variability (mm) over the mega-dam area.....	64
<b>Figure 4.2b:</b> 11-year moving average of projected summer rainfall (mm) over the mega-dam area, obtained through downscaling of the GFDL-CM3 GCM using CCAM (top). Standard deviation of the detrended 11-year moving time series, depicting summer rainfall variability (mm) over the mega-dam area.....	75

<b>Figure 4.2c:</b> 11-year moving average of projected summer rainfall (mm) over the mega-dam area, obtained through downscaling of the MPI-ESM-LR GCM using CCAM (top). Standard deviation of the detrended 11-year moving time series, depicting summer rainfall variability (mm) over the mega-dam area.....	76
<b>Figure 4.2d:</b> 11-year moving average of projected summer rainfall (mm) over the mega-dam area, obtained through downscaling of the NorESM1M GCM using CCAM (top). Standard deviation of the detrended 11-year moving time series, depicting summer rainfall variability (mm) over the mega-dam area.....	77
<b>Figure 4.2e:</b> 11-year moving average of projected summer rainfall (mm) over the mega-dam area, obtained through downscaling of the CCSM4 GCM using CCAM (top). Standard deviation of the detrended 11-year moving time series, depicting summer rainfall variability (mm) over the mega-dam area.....	78
<b>Figure 4.2f:</b> 11-year moving average of projected summer rainfall (mm) over the mega-dam area, obtained through downscaling of the GFDL-CM3 GCM using CCAM (top). Standard deviation of the detrended 11-year moving time series, depicting summer rainfall variability (mm) over the mega-dam area.....	79
<b>Figure 4.3:</b> Projected changes in the standard deviation of austral summer near-surface atmospheric temperature (°C) over southern Africa for the period 2071-2100 relative to 1971-2000. The projections were obtained by downscaling the simulations of six different GCMs integrated under RCP8.5 to a high resolution global grid, using the variable-resolution atmospheric model CCAM. ....	70
<b>Figure 4.4:</b> Projected changes in the standard deviation of austral summer rainfall (mm) over southern Africa for the period 2071-2100 relative to 1971-2000. The projections were obtained by downscaling the simulations of six different GCMs integrated under RCP8.5 to a high resolution global grid, using the variable-resolution atmospheric model CCAM. ....	71
<b>Figure 4.5:</b> Rank probability skill score of the CCAM AMIP-style simulations in representing 850 hPa inter-annual circulation variability over southern Africa, for the austral summers of 1978-2004 (top). The effects of enhanced greenhouse gas forcing on changing this predictability are depicted in the bottom figure. ....	73
<b>Figure 4.6:</b> Rank probability skill-score for the CCAM-AMIP simulations in predicting summer (top) and winter (bottom) inter-annual circulation variability over southern Africa, for the period 1979-2005.....	74
<b>Figure 4.7:</b> Kendal Tau correlation between the CCAM-AMIP predictions of summer season streamflow over the mega-dam area and observed natural streamflow, over the period 1979-2005.....	75
<b>Figure 4.8:</b> Daily Precipitation (mm/day) averaged over the period from DJF 2000/01 to DJF 2012/13. (a) CHIRP satellite estimates, (b) ensemble mean CCAM-CABLE C192, and (c) ensemble mean CCAM-CABLE C96.....	76
<b>Figure 4.9:</b> Southern Africa kill distribution as measured with ROC area daily accumulated rainfall (mm/day) the CCAM 8 km horizontal resolution mid-austral summer (DJF) one month lead for (a) below- and (b) above-normal categories. Only statistically significant values at the 95% level shades are shown.....	77
<b>Figure 4.10:</b> First ever probabilistic seasonal rainfall forecast release of the CCAM-CABLE operation ensemble prediction system (C192 stretched grid with 8 km zoom in over the southern Africa region). The forecast is based on the November initialization consist of 12 ensembles built as a function of 12 slightly different NCEP Environmental Modelling Center's (EMC) Global Forecasting System (GFS) atmospheric states and forced with multi-model SSTs (Landman et al., 2014). Worth noting is that the probabilities shown here were computed from the AMIP2 style climatology and the skill presented here is not the true reflection of this forecast. ....	77
<b>Figure 4.11:</b> SOM characterisation of 35 dominant synoptic types over southern Africa based on NCEP reanalysis data for the period 1979-2014.....	78

<b>Figure 4.12:</b> Rainfall patterns associated with each of the synoptic types, as deduced from GPCP data for the period 1997-2014. ....	79
<b>Figure 4.13:</b> Rainfall patterns associated with each of the synoptic types, as deduced from the CCAM predictions for the period 1997-2014. ....	79
<b>Figure 4.14:</b> Pattern correlations between the CCAM (predicted) and GPCP (observed) rainfall fields for each of the 35 synoptic types .....	80
<b>Figure 4.15:</b> Projected changes in the frequency of occurrence of synoptic types over southern Arica (% change) for the far-future period (2070-2099) relative to the present-day (1961-1990). ....	80
<b>Figure 5.1:</b> Gariep dam (a) Rainfall and (b) Dam fill (%). ....	86
<b>Figure 5.2:</b> Vaal dam (a) Rainfall and (b) Dam fill (%). ....	87
<b>Figure 5.3:</b> Sterkfontein dam (a) Rainfall and (b) Dam fill (%). ....	88
<b>Figure 5.4:</b> Katse dam (a) Rainfall and (b) Dam fill (%). ....	90
<b>Figure 5.5:</b> Van der Kloof dam (a) Rainfall and (b) Dam fill (%). ....	91
<b>Figure 5.6a:</b> Projections of future rainfall patterns (mm) over the Gariep dam catchment region, as obtained from the CCAM dynamic downscalings of six different GCMs. ....	93
<b>Figure 5.6b:</b> Projections of dam levels (standardised % anomalies) over the Gariep dam catchment region, as obtained from the CCAM dynamic downscalings of six different GCMs. ....	104
<b>Figure 5.7a:</b> Projections of future rainfall patterns (mm) over the Vaal dam catchment region, as obtained from the CCAM dynamic downscalings of six different GCMs. ....	95
<b>Figure 5.7b:</b> Projections of dam levels (standardised % anomalies) over the Vaal dam catchment region, as obtained from the CCAM dynamic downscalings of six different GCMs. ....	106
<b>Figure 5.8a:</b> Projections of annual rainfall totals (mm) over the Sterkfontein dam catchment region, as obtained from the CCAM dynamic downscalings of six different GCMs. ....	97
<b>Figure 5.8b:</b> Projections of dam levels (standardised % anomalies) over the Sterkfontein dam catchment region, as obtained from the CCAM dynamic downscalings of six different GCMs. ....	108
<b>Figure 5.9a:</b> Projections of changes in annual rainfall totals (mm) over the Katse dam catchment region, as obtained from the CCAM dynamic downscalings of six different GCMs. ....	99
<b>Figure 5.9b:</b> Projections of dam levels (standardised % anomalies) over the Katse dam catchment region, as obtained from the CCAM dynamic downscalings of six different GCMs. ....	110
<b>Figure 5.10a:</b> Projections of changing rainfall totals over Vanderkloof dam catchment region, as obtained from the CCAM dynamic downscalings of six different GCMs. ....	101
<b>Figure 5.10b:</b> Projections of dam levels (standardised % anomalies) over the Vanderkloof dam catchment region, as obtained from the CCAM dynamic downscalings of six different GCMs. ....	112
<b>Figure 5.11:</b> Annual average climatologies over the mega-dam area, for the variables of potential pan evaporation ( $W/m^2$ ; top left), evaporation (mm; top right), runoff (mm/day; bottom left and near-surface soil moisture ( $m^3/m^3$ ; bottom right). ....	104
<b>Figure 5.12:</b> Projected changes in annual average climatologies over the mega-dam area, for the variables of potential pan evaporation ( $W/m^2$ ; left) and evaporation (mm; right). Changes are shown for the future period 2070-2099 relative to the present-day baseline period of 1961-1990, and across three different downscaled GCMs. ....	105
<b>Figure 5.13:</b> Projected changes in annual average climatologies over the mega-dam area, for the variables of runoff (mm/day; right and near-surface soil moisture ( $m^3/m^3$ ; left). Changes are shown for the future period 2070-2099 relative to the present-day baseline period of 1961-1990, and across three different downscaled GCMs. ....	106

<b>Figure 5.14:</b> SOM characterisation of 12 dominant summer (DJF) rainfall anomalies over southern Africa as calculated from CRU TS_3.2 data.....	108
<b>Figure 5.15:</b> Accumulated summer (DJF) streamflow anomalies mapped onto the SOM characterisation of 12 dominant summer (DJF) rainfall anomalies over southern Africa. ....	109
<b>Figure 5.16:</b> CCAM projected change in the annual average rainfall totals (units mm/day) over southern Africa for the time-slab 2070-2099 relative to 1961-1990. The downscalings were obtained from six different CMIP5 GCM projections under low mitigation (RCP8.5). .	110
<b>Figure 5.17:</b> CCAM projected change in the summer average rainfall totals (units mm/day) over southern Africa for the time-slab 2070-2090 relative to 1961-1990. The downscalings were obtained from six different CMIP5 GCM projections under low mitigation (RCP8.5). .	111
<b>Figure 5.18:</b> CCAM projected change in the summer half-year (ONDJFM) streamflow over South Africa for the time-slab 2070-2090 relative to 1961-1990. The downscalings were obtained from six different CMIP5 GCM projections under low mitigation (RCP8.5).....	112

## List of Tables

<b>Table 3.1:</b> Daily SAWS station rainfall compared to rainfall from CCAM at the points of the SAWS stations. Highlighted blocks show large over estimations (larger than 2x the observed rainfall).....	23
<b>Table 3.2:</b> The diurnal cycle from SAWS station data compared to CCAM data at the location of the particular station. The location from the stations is marked in Figure 3.1.....	24
<b>Table 3.3:</b> Relevant climate variables.....	36
<b>Table 5.1:</b> Location of Dams.....	84
<b>Table 5.2:</b> Statistics for Gariep Dam: Catchment Rainfall and dam fill.....	85
<b>Table 5.3:</b> Statistics for Vaal Dam: Catchment Rainfall and Dam fill (%).....	87
<b>Table 5.4:</b> Statistics for Sterkfontein Dam: Catchment Rainfall and Dam fill (%).....	89
<b>Table 5.5:</b> Statistics for Katse dam: Catchment Rainfall and Dam fill (%).....	89
<b>Table 5.6:</b> Statistics for Van der Kloof Dam (a) Rainfall and (b) Dam fill (%) for the climate record in Table 5.1.....	91

## Chapter 1 Introduction

Southern Africa's climate exhibits a great deal of natural variability and is prone to the frequent occurrence of droughts and floods (e.g. Dyer and Tyson, 1977; Reason and Rouault, 2002; Rouault and Richard, 2003; Fauchereau et al., 2003). Moreover, the region is thought to be highly vulnerable to anthropogenically-induced climate change. Temperatures are projected to rise rapidly over southern Africa under the enhanced greenhouse effect, at about twice the global rate of temperature increase (e.g. Jones et al., 2012; Engelbrecht et al., 2015), and the region is likely to become general drier (Christensen et al., 2007; Niang et al., 2014; Engelbrecht et al., 2015). Moreover, the frequencies of extreme weather events such as droughts, dry spells, heat waves and high fire danger days are projected to increase in association with the rapidly rising surface temperatures (e.g. Christensen et al., 2007; Niang et al., 2014; Engelbrecht et al., 2015; Garland et al., 2015). It is also plausible for heavy rainfall events to increase in frequency, despite the general decreases in rainfall projected for southern Africa (e.g. Engelbrecht et al., 2013). Such events may lead to the occurrence of flash floods and high flow volumes in the region's major river systems. The skilful prediction of weather and in particular extreme weather events over the region, at both short-range (days ahead) and seasonal time-scales (months ahead), is therefore of the utmost importance as an adaptation tool within a changing climate (e.g. Winsemius et al., 2014). For present-day climate, probabilistic seasonal predictions of rainfall and temperatures are known to be skilful over southern Africa, at least over the summer rainfall region during summers associated with strong El Niño Southern Oscillation (ENSO) forcing (e.g. Landman and Beraki, 2012, Lazenby et al., 2014). Deterministic event-forecasting of high impact weather events has been shown to be skilful about four days ahead over southern Africa (e.g. Potgieter et al., 2006). However, climate change may not only affect weather patterns over southern Africa, but also their predictability. For example, with seasonal predictive skill over southern Africa depending largely on the ENSO signal (Landman and Beraki, 2012), any decreases (increases) in the strength or stability of the ENSO teleconnection to the region may impact negatively (positively) on the seasonal forecast skill. At shorter time-scales, more intense thunderstorms may occur more frequently in a changing climate, with detrimental effects on the skill of short-range deterministic forecasts if weather forecast models do not sufficiently represent the intricate attributes of convection. With short-range and seasonal forecasts being potentially important adaptation tools within a changing climate (by providing early warnings) there is a clear need to investigate the impacts of climate change on predictability over southern Africa.

Of particular interest in this project are the potential impacts of climate change on the hydroclimate of eastern South Africa, given the impact that such changes may have on water security in the country. This stems from the fact that the Lesotho Highland water schemes and all of South Africa's mega-dams are located in eastern South Africa. Moreover, the Gauteng province of South Africa – the economic heartland of the country – has a critical dependence on the Lesotho Highland water schemes for both the quantity and quality of its water supply. It may be noted that the 2015/16 El Niño and associated drought brought water restrictions to Gauteng, given that it was the third season in a row associated with below-normal rainfall over eastern South Africa. A water crisis was looming, but good rains in the late summer of 2016/17, which occurred in association with a La Niña event, broke the drought. Nevertheless, South Africa's vulnerability to multi-year drought in the mega-dam region was demonstrated through this event. Currently, in March 2018, multi-year drought has brought an extensive crisis to Cape Town in South Africa, with dam levels being 20% below average in the relevant catchments. Another season of drought would in fact create the distinct possibility of the city running out of water. These recent and current droughts in the summer and winter rainfall regions of South Africa clearly demonstrate the need to investigate the plausibility of climate change bringing more frequent drought to the mega-dam region of eastern South Africa.

Eastern South Africa receives almost all of its rainfall in summer, with the inter-annual variability in rainfall being strongly controlled by ENSO events. Figure 1.1 serves to demonstrate the relationship between sea-surface temperatures (SSTs) in the Niño 3.4 region and rainfall anomalies over Lesotho. The driest years in recorded history have been associated with El Niño events, whilst the wettest years have occurred in association with La Niña events. However, this relationship is not linear. An example is the super El Niño event of 1997/1998, which was associated with near-normal rainfall over Lesotho and in fact over most of South Africa. About 80% of the rainfall occurs in the form of thunderstorms (which are mostly embedded in tropical-temperate cloud bands).

## NINO3.4 and LES rainfall 1901–2013

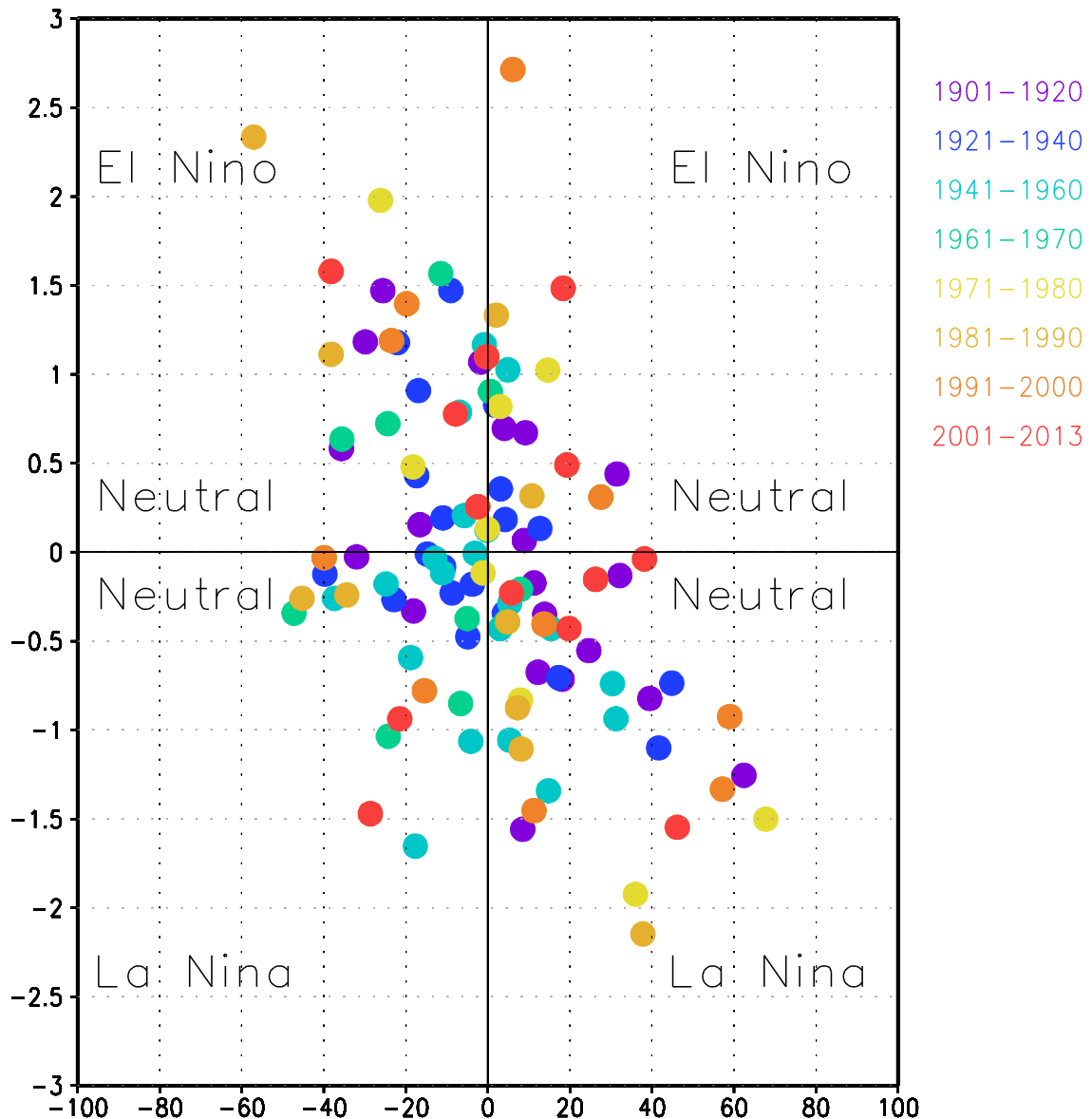


**Figure 1.1** Observed October to December SST anomalies over the Niño 3.4 region (y-axis) and corresponding observed December-February rainfall anomalies (mm) over Lesotho for the summers of 1901/02 through to 2013/14. The SST anomalies were obtained from the Atmospheric Model Intercomparison Project (AMIP) data set whilst the rainfall anomalies were calculated from the Climatic Research Unit (CRU) data set CRU 3.24.

It is thus important to understand how climate change may alter the occurrence of convective rainfall over the region, as well as teleconnection to ENSO and other modes of global variability, such as the Southern Annular Mode (SAM). Of particular importance from a water security perspective are the potential changes in rainfall rates, evaporation, run-off, streamflow and dam levels.

Recent drought in the mega-dam region, as well as seasons of good falls of rain, have once again demonstrated the need for skilful of weather and seasonal forecasts in predicting this hydroclimatic variability. Should climate change alter this variability, for example by resulting in the more frequent occurrence of drought and large-scale flood events, it may be argued that the availability of skilful forecasts will become even more important (Winsemius et al., 2014). That is, skilful weather and seasonal forecasts may well become an increasingly important adaptation tool for water management in this region within a changing climate. Both the short-term management of flood events and planning at seasonal time-scales during times of drought can greatly benefit from skilful forecasts. Also, at multidecadal time scales, plausible projections of the hydroclimate of the mega-dam region can inform water managers and economists on the water security of the country within a changing climate. The sustained economic growth of South Africa and an enhanced industrial development programme critically depend on water availability. This project was thus undertaken with the aim of providing detailed and plausible projections of the changing hydroclimate of eastern South Africa, including direct estimates of rainfall patterns, streamflow and dam levels in a changing climate. These projections should be of valuable to water managers concerned with South Africa and Gauteng's water security in a changing climate. Moreover, the project benchmarks the skill of short-range and seasonal forecast systems as an adaptation tool for water management within the context of a changing climate. It may be noted that numerous rural communities in Lesotho rely on dam-levels and associated stream flow of the megadams in the Lesotho Highlands water scheme. These communities may potentially benefit from more robust multi-decadal planning concerned with the changing hydroclimate of Lesotho, and also from skilful short-range and seasonal forecasts of climate and hydroclimate variability over the region.

This project reports commences by considering regional projections of future climate change over southern Africa, towards providing a regional context for climate change over eastern South Africa. Of particular importance are changes in rainfall patterns, including the occurrence of drought and large-scale flood producing systems. This chapter considers projections in the regional climate of southern Africa performed at the CSIR, but also the larger body of evidence from global projections of future climate change as described in Assessment Reports Four and Five (AR4 and AR5) of the Intergovernmental Panel on Climate Change (IPCC). From this foundation the project team proceed to generated detailed projections in future climate change over eastern South Africa, at a resolution of 8 km in the horizontal. These are the most detailed simulations obtained to date for the region, and are presented in Chapter 3. The 8 km resolution simulations of present-day climate are first verified in detail against observations, to gain some insight into the description of the meso-scale details of rainfall in the simulations, before the projected changes in future climate are presented. Chapter 4 is focussed on a description of present-day climate variability over eastern South Africa, how this variability may change under climate change, and the use of short-range and seasonal forecasts to predict this variability. The projected changes in hydrology of the mega-dam region under climate change are presented in Chapter 5, with a focus on changes in streamflow and dam levels. Here a new method of projecting streamflow, which relies on combining the technologies of dynamic regional climate modelling with statistical downscaling, is outlined and applied. Simulations performed with a highly sophisticated and new dynamic river routing scheme coupled to a dynamic regional climate model are also presented. The report concludes in Chapter 6 with providing a summary of the main findings and a set of recommendations of the risks and opportunities that South Africa is to face in terms of its water security under climate change, through

changes in the hydroclimate of eastern South Africa. It may finally be noted that understanding the climate change futures of the mega-dam region also presents a rich set of research questions to post-graduate students in climatology and hydrology. As such, this project was associated with a strong capacity building programme, with three post-graduate students contributing to the research. Their contributions and involvement, as well as a list of external publications generated in relation to the project research, are presented in Appendix A of this report.

## **Chapter 2 Projections of regional climate change over southern Africa and implications for the mega-dam region**

### **2.1 Introduction**

Climate change is projected to impact drastically on southern Africa during the 21<sup>st</sup> century under low mitigation futures (Niang et al., 2014). Temperatures are projected to rise rapidly, at 1.5 to 2 times the global rate of temperature increase (Engelbrecht and Bopape, 2011; James & Washington, 2013; Engelbrecht et al., 2015). Moreover, the region is likely to become generally drier under enhanced anthropogenic forcing, the exception being Mozambique, where wetter conditions are likely to occur over the central and northern parts (Christensen et al., 2007; Niang et al., 2015; Engelbrecht et al., 2015). In fact, East Africa is projected to become generally wetter under low mitigation climate change futures. This implies that the projected climate change signal over Africa exhibits a distinct El Niño signal, with East Africa projected to become generally wetter and southern Africa projected to become generally drier. A minority of climate models are projecting the wetter conditions over northern and central Mozambique to also extend southwards, to southern Mozambique and eastern South Africa, whilst some models are indicative of rainfall increases over central South Africa. Further to the south, over South Africa's winter rainfall region and along the Cape south coast, a robust pattern of decreases in rainfall is projected. Thus, there is some uncertainty in rainfall projections for the southern African region, although overarching decreases in rainfall seem likely to occur. This pattern of change has been linked to a general strengthening of the subtropical high-pressure belt over southern Africa (Engelbrecht et al., 2009), a pattern associated with the poleward displacement of the westerlies and a strengthening of the easterlies north of the high-pressure belt over the Indian Ocean. This simple conceptual model is sufficient to explain the main pattern of rainfall change projected for southern Africa and renders the rainfall projections physical defensible. Moreover, it has been shown that changes in mid-level highs (the mid-level component of the sub-tropical high-pressure belt), in combination with heat-induced increases in the continental trough over southern Africa, can plausibly explain the rainfall increases projected by some climate models over the eastern and central parts of South Africa (Engelbrecht et al., 2009).

The projected changes in southern African climate are simulated to occur in association with changes in the attributes of extreme weather events over the region. The generally drier conditions over southern Africa are projected to occur in association with the more frequent occurrence of dry spells and drought (Christensen et al., 2007; Engelbrecht et al., 2009). Cut-off low related flood events are projected to occur less frequently over South Africa (e.g. Engelbrecht et al., 2013) in response to a poleward displacement of the westerly wind regime. Tropical cyclones are projected to plausibly make landfall over central to northern Mozambique more frequently, with some models extending this signal of change to southern Mozambique (Malherbe et al., 2013). Intense thunderstorms are plausible to occur more frequently over tropical and subtropical Africa in a generally warmer climate (e.g. Engelbrecht et al., 2013). Drastic increases in extreme temperature events, including heat-wave days and high fire-danger days are projected to occur across the region (Niang et al., 2014; Engelbrecht et al., 2015).

The changing southern African climate is likely to have a range of impacts across the continent, including impacts on energy demand (in terms of achieving human comfort within buildings and factories), agriculture (e.g. reductions of yield in the maize crop under higher temperatures and reduced soil moisture), livestock production (e.g. higher cattle mortality as a result of oppressive temperatures), water security (through reduced rainfall and enhanced evapotranspiration) (Thornton et al., 2011; Engelbrecht et al., 2015; Garland et al., 2015)

and infrastructure (mostly through the occurrence of more large-scale floods in particular regions).

It is against this background that the project “Predictability of hydroclimatic variability over eastern South Africa under climate change” was initiated. This chapter explores in particular the regional climate change futures of southern Africa, towards providing regional context to the climate change futures over eastern South Africa. It should be noted that conclusions are drawn by considering the larger body of evidence of projected climate change futures over southern Africa, as described using the global and regional model projections reported on in AR4 and AR5 of the IPCC. Evidence from peer-reviewed papers published since AR5, including some recent work generated through the Coordinated Regional Downscaling Experiment (CORDEX) are also interpreted to this effect. The key concepts are illustrated through the analysis of an ensemble of climate change projections generated at high resolution over Africa at the CSIR as a contribution to CORDEX. Having such an ensemble of locally generated projections available offered two main advantages to the project: firstly further downscaling to very high resolution was possible over the eastern escarpment of South Africa, potentially resulting in new insights into the effects of orography on convective rainfall under climate change; and secondly the high-temporal resolution of the regional projections and the large number of atmospheric variables generated made feasible application modelling, such as dynamic river routing, required by the project to further explore the hydroclimatic futures of eastern South Africa.

## **2.2 The conformal-cubic atmospheric model and experimental design**

The regional climate model used in the project and in this chapter is the conformal-cubic atmospheric model (CCAM) developed by the Commonwealth Scientific and Industrial Research Organisation (CSIRO) (McGregor, 1996, 2005a, 2005b; McGregor and Dix, 2001, 2008). CCAM is a variable-resolution global atmospheric model, which can be applied in at quasi-uniform resolution to function as an atmospheric global circulation model, or alternatively in stretched-grid mode to provide high resolution over an area of interest. It employs a semi-implicit semi-Lagrangian method to solve the hydrostatic primitive equations. The model includes a fairly comprehensive set of physical parameterizations. The GFDL parameterizations for long-wave and short-wave radiation are employed, with interactive cloud distributions determined by the liquid and ice-water scheme of Rotstayn (1997). A stability-dependent boundary layer scheme based on Monin Obukhov similarity theory is employed (McGregor et al., 1993), together with the non-local treatment of Holtslag and Boville (1993). The cumulus convection scheme uses a mass-flux closure, as described by McGregor (2003), and includes downdrafts, entrainment and detrainment. CCAM is coupled to the dynamic land-surface model CABLE (CSIRO Atmosphere-Biosphere Land Exchange). CABLE includes six layers for soil temperatures, six layers for soil moisture (solving Richard's equation) and three layers for snow (Kowalczyk et al., 2006). Fig. 2.1 shows a quasi-uniform conformal-cubic grid, of C192 (about 50 km) resolution in the horizontal.

This chapter analyses the high-resolution regional projections of future climate change over Africa generated at the Council for Scientific and Industrial Research as a contribution to CORDEX. Six GCM simulations of the Coupled Model Intercomparison Project Phase Five (CMIP5) and Assessment Report Five (AR5) of the Intergovernmental Panel on Climate Change (IPCC), obtained for the emission scenarios described by Representative Concentration Pathways 4.5 and 8.5 (RCP4.5 and 8.5) were downscaled to 50 km resolution globally. The simulations span the period 1960-2100. RCP4.5 is a high mitigation scenario, whilst RCP8.5 is a low mitigation scenario. The GCMs downscaled are the Australian Community Climate and Earth System Simulator (ACCESS1-0); the Geophysical Fluid Dynamics Laboratory Coupled Model (GFDL-CM3); the National Centre for Meteorological

Research Coupled Global Climate Model, version 5 (CNRM-CM5); the Max Planck Institute Coupled Earth System Model (MPI-ESM-LR); the Norwegian Earth System Model (NorESM1-M) and the Community Climate System Model (CCSM4). The simulations were performed on supercomputers of the Centre for High Performance Computing (CHPC) of the Meraka Institute of the CSIR in South Africa. In these simulations CCAM was forced with the bias-corrected daily sea-surface temperatures (SSTs) and sea-ice concentrations of each host model, and with CO<sub>2</sub>, sulphate and ozone forcing consistent with the RCP4.5 and RCP8.5 scenarios. The model's ability to realistically simulate present-day southern African climate has been extensively demonstrated (e.g. Engelbrecht et al., 2009; Engelbrecht et al., 2011; Engelbrecht et al., 2013; Malherbe et al., 2013; Winsemius et al., 2014; Engelbrecht et al., 2015). Most current coupled GCMs do not employ flux corrections between atmosphere and ocean, which contributes to the existence of biases in their simulations of present-day SSTs – of more than 2°C along the West African coast. An important feature of the downscalings performed here is that the model was forced with the bias-corrected sea-surface temperatures (SSTs) and sea-ice fields of the GCMs. The bias is computed by subtracting for each month the Reynolds (1988) SST climatology (for 1961-2000) from the corresponding CGCM climatology. The bias-correction is applied consistently throughout the simulation. Through this procedure the climatology of the SSTs applied as lower boundary forcing is the same as that of the Reynolds SSTs. However, the intra-annual variability and climate-change signal of the CGCM SSTs are preserved (Katzfey et al., 2009).

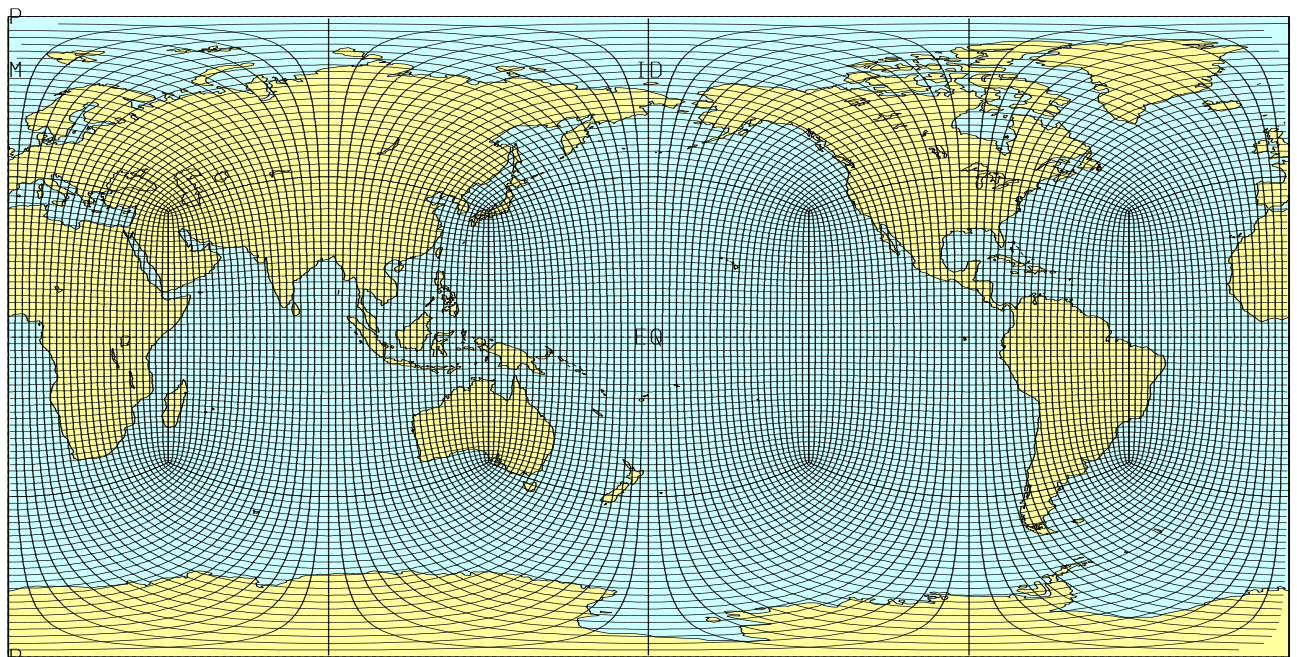


**Figure 2.1:** C192 quasi-uniform conformal-cubic grid (every 4th grid point is shown), which provides a horizontal resolution of about 200 km globally.

## 2.3 Projected climate change futures over southern Africa

### 2.3.1 Projected changes in temperature

The CCAM projected changes in average annual temperature for the mid-future period 2046-2065 relative to 1961-1990 under low mitigation (RCP8.5) are shown in Figure 2.2. General temperature increases of 2-3.5°C are projected over the interior regions of southern Africa, with increases of 1-2.5°C projected for the coastal areas. One of the projections is indicative of temperature increases larger than 3.5°C over parts of the western interior, including the Free State and North West provinces. Under modest-high mitigation (RCP4.5)

the ensemble of projections is indicative of temperature increases of 2-3°C over the interior, and 1-2°C over the coastal areas (Figure 2.3).

For the far-future time-slab of 2070-2099, drastic warming of more than 4°C is projected for most of the southern African region, with only the southern and eastern coastal areas and adjacent interiors projected to experience relatively smaller increases (Figure 2.4). Increases of more than 5°C are likely to occur over much of Namibia and Botswana, and southwards into the western interior of South Africa. The amplitude of far-future temperature increases may be significantly reduced by achieving a modest-high mitigation future (Figure 2.5). Temperature increases over the interior may well be reduced to 2-3.5°C, although increases higher than 4°C remains plausible over the western interior of South Africa. Temperature increases over the coastal areas of South Africa are projected to be limited to 1-2.5°C.

### *2.3.2 Projected changes in rainfall*

The CCAM projected changes in average annual rainfall totals for the mid-future period 2046-2065 relative to 1961-1990 under low mitigation (RCP8.5) are shown in Figure 2.6. The general pattern that emerges from the CCAM projections is one of a generally drier southern Africa, but with rainfall increases projected for the northern half of Mozambique. The wetter conditions over Mozambique are projected to extend westwards to Zambia, and in some projections in a broader band that also includes Zimbabwe, southern Mozambique and northeastern South Africa. The substantial rainfall increases projected over northern Mozambique may be attributed to more frequent tropical cyclone landfall (Muthige et al., 2018), consistent with the earlier findings of Malherbe et al. (2013). Most of the projections are indicative of rainfall reductions over the eastern escarpment areas of South Africa, and in two of the downscalings these losses are substantial. Many of the projections are also indicative of modest rainfall increases over the central interior regions of South Africa, including the western Free State and Lesotho. This physically defensible pattern of change under low mitigation futures was first identified by Engelbrecht et al. (2009) and may be attributed to a deepening of the heat low over the western interior of South Africa, which would induce the more frequent outbreak of convection east of the trough axis. This deepening of the heat low is also projected to occur in conjunction with the more frequent southward advection of moisture into southern Africa occurring to the east of stronger mid-level high-pressure systems (Engelbrecht et al., 2009). A similar regional pattern of change is projected under RCP4.5 (Figure 2.7), with the exception that two of the ensemble members are indicative of wide-spread rainfall increases over the central to eastern regions of South Africa. The majority of ensemble members are nevertheless still indicative of rainfall reductions over Lesotho and the mega-dam region, but with a decrease in the amplitude of the projected changes.

In the far-future under low mitigation (Figure 2.8) the pattern of change projected for southern Africa is similar to that of the mid-future period (Figure 2.6), but with a general strengthening in the amplitude of change. Most ensemble members are indicative of substantial reductions in rainfall over the eastern escarpment of South Africa, Lesotho and the mega-dam region. Slight rainfall increases are still projected for the western interior by some ensemble members. Most ensemble members remain indicative of rainfall increases over central and northern Mozambique, with these increases extending westwards to Zambia, and southward into Zimbabwe and southern Mozambique. This pattern of rainfall increases may plausibly also reach the northeastern parts of the Limpopo province in South Africa. The pattern of change projected under RCP4.5 is remarkably different. The maxima of rainfall increases over Mozambique is shifted to the central and southern parts, with associated rainfall increases over much of central and eastern South Africa. The dynamics of this pattern of change remains to be explored, but it seems as if the intensification of mid-

level highs and associated subsidence is not occurring, or is less of a factor, under modest-high mitigation.

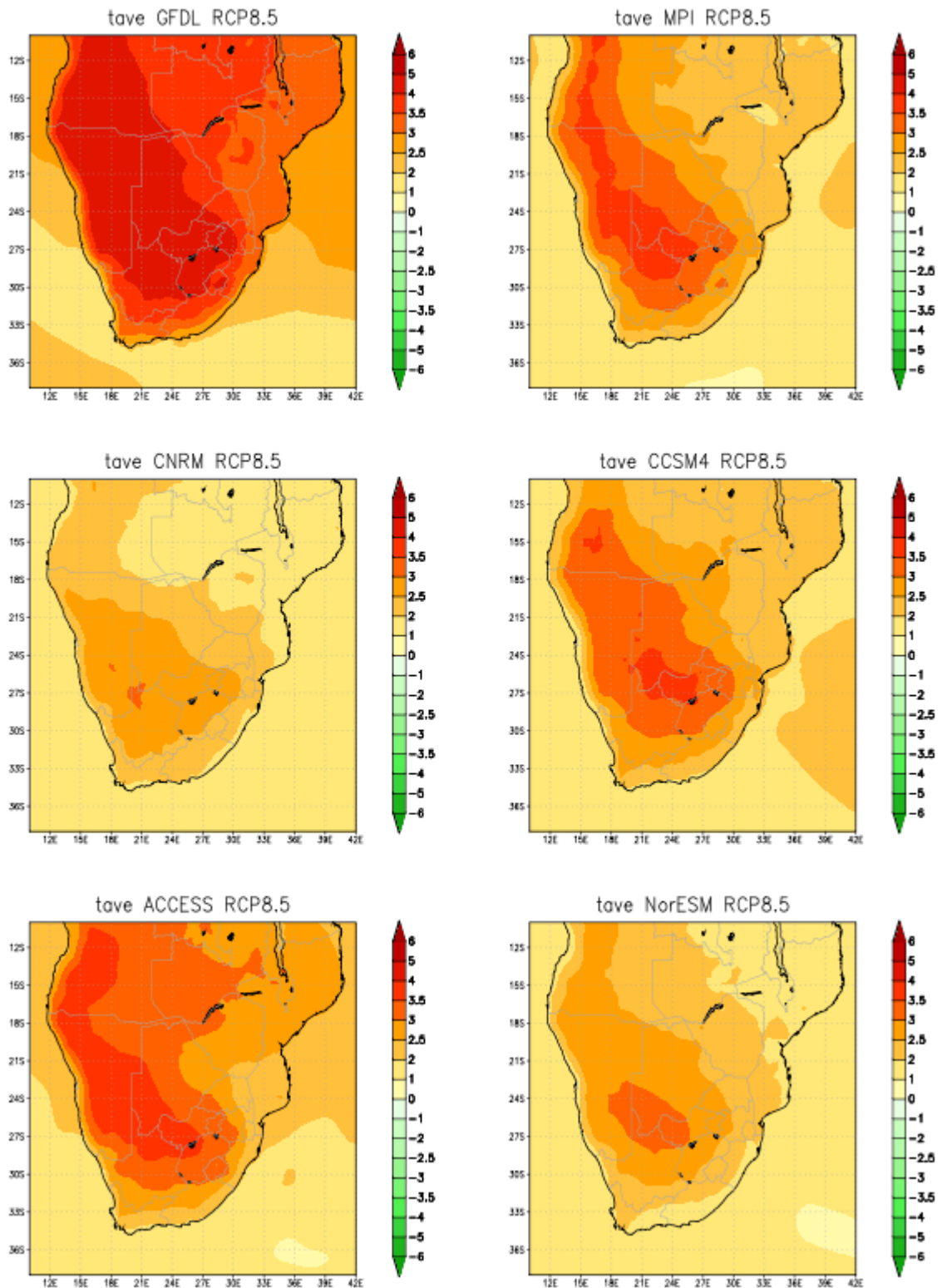


**Figure 2.2:** CCAM-CABLE projected changes in annual mean temperature (°C) under RCP 8.5 for the period 2046-2065 relative to 1961-1990.

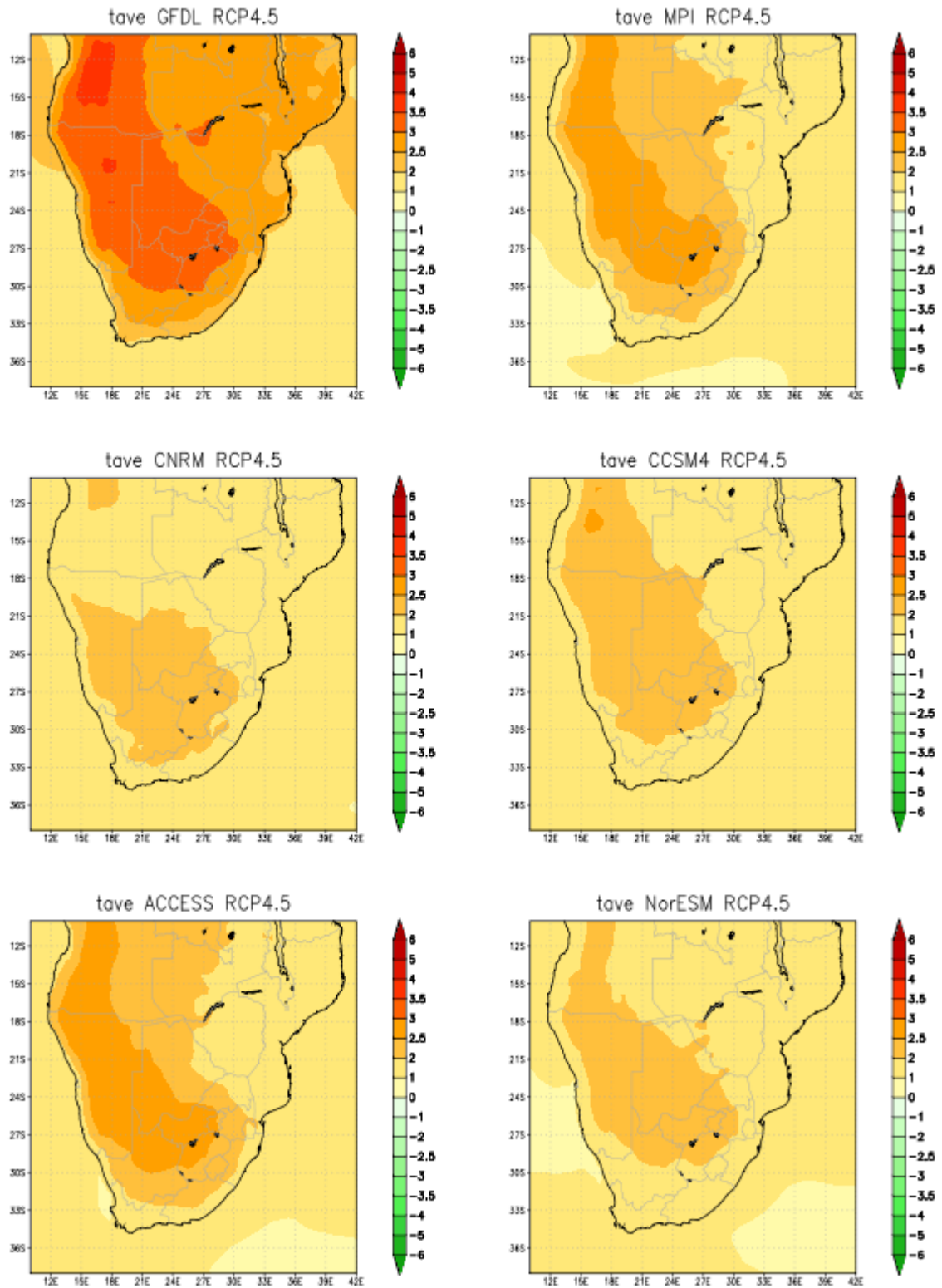


**Figure 2.3:** CCAM-CABLE projected changes in annual mean temperature (°C) under RCP 4.5 for the period 2046-2065 relative to 1961-1990.

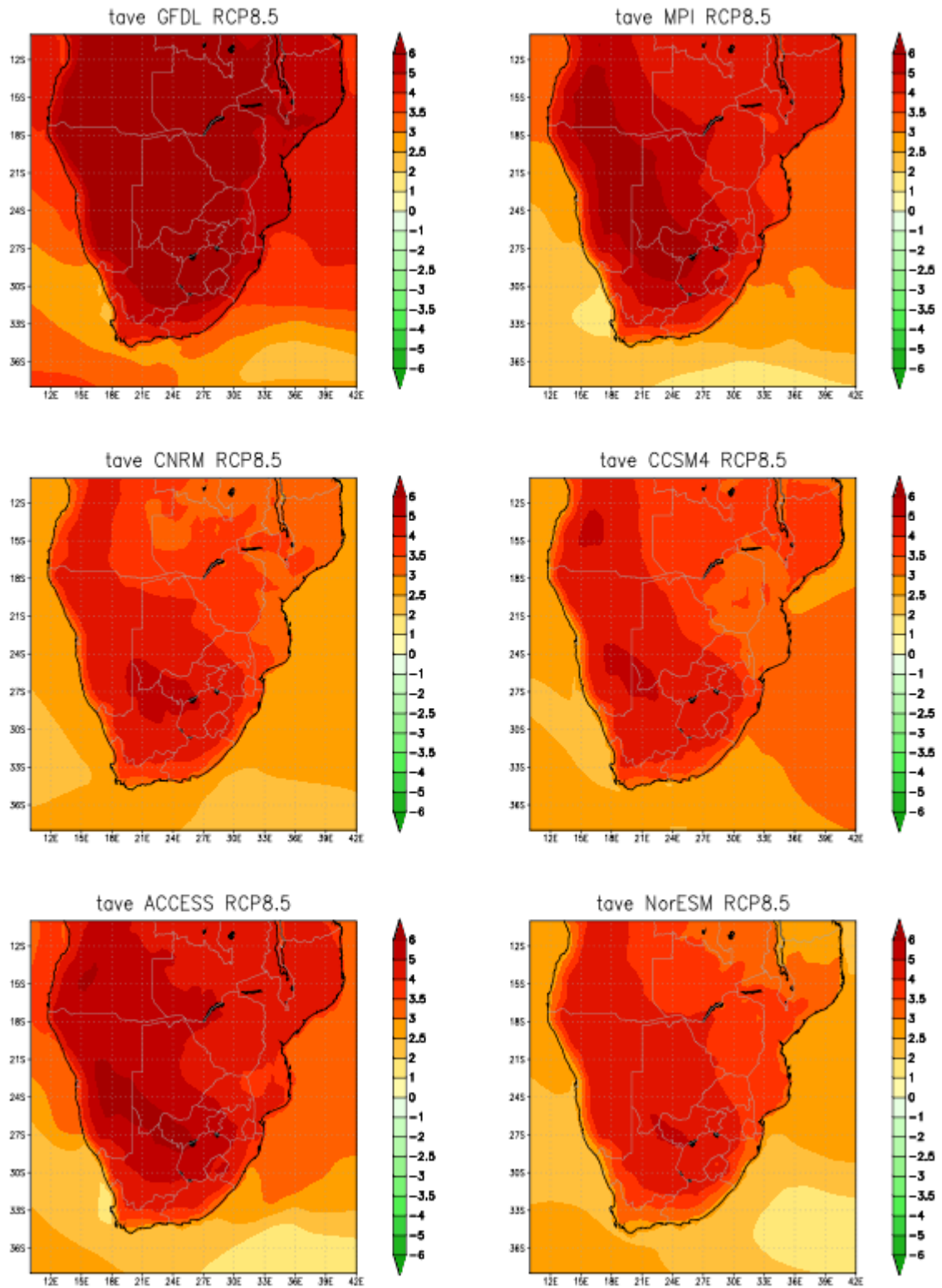


**Figure 2.4:** CCAM-CABLE projected changes in annual mean temperature (°C) under RCP 8.5 for the period 2070-2099 relative to 1961-1990.

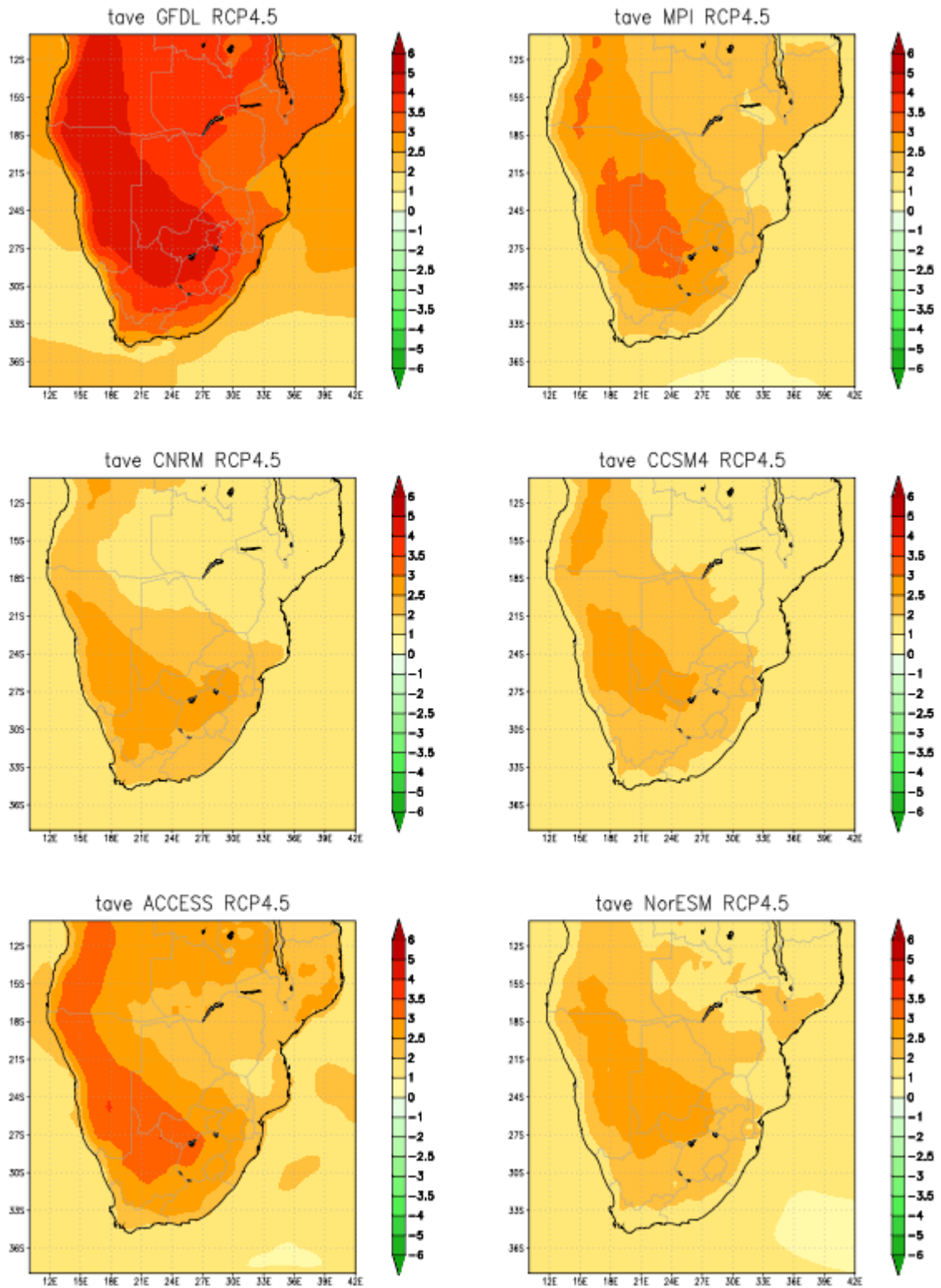


**Figure 2.5:** CCAM-CABLE projected changes in annual mean temperature (°C) under RCP 4.5 for the period 2070-2099 relative to 1961-1990.

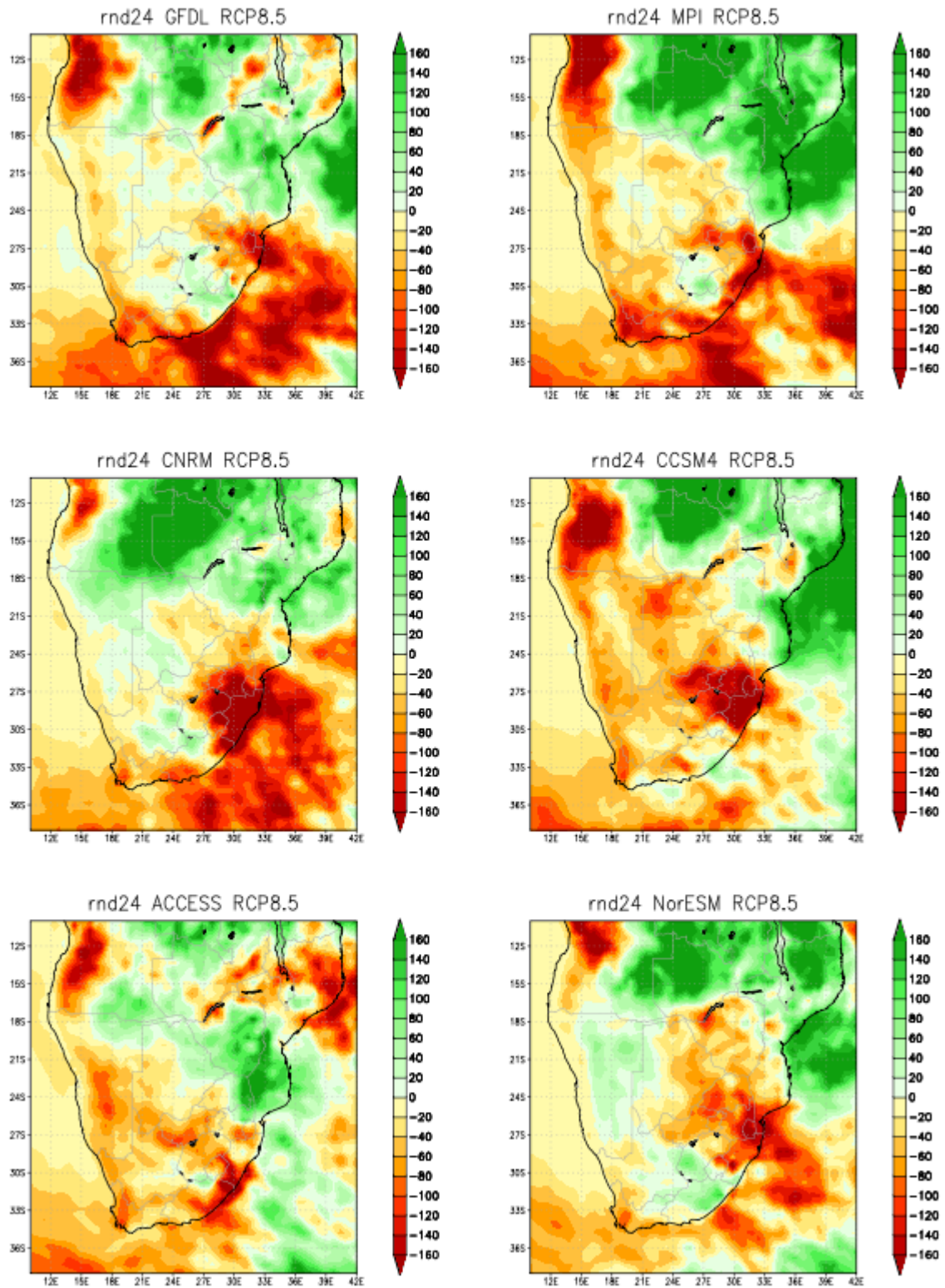


**Figure 2.6:** CCAM-CABLE projected changes in annual rainfall (mm) under RCP 8.5 for the period 2046-2065 relative to 1961-1990.

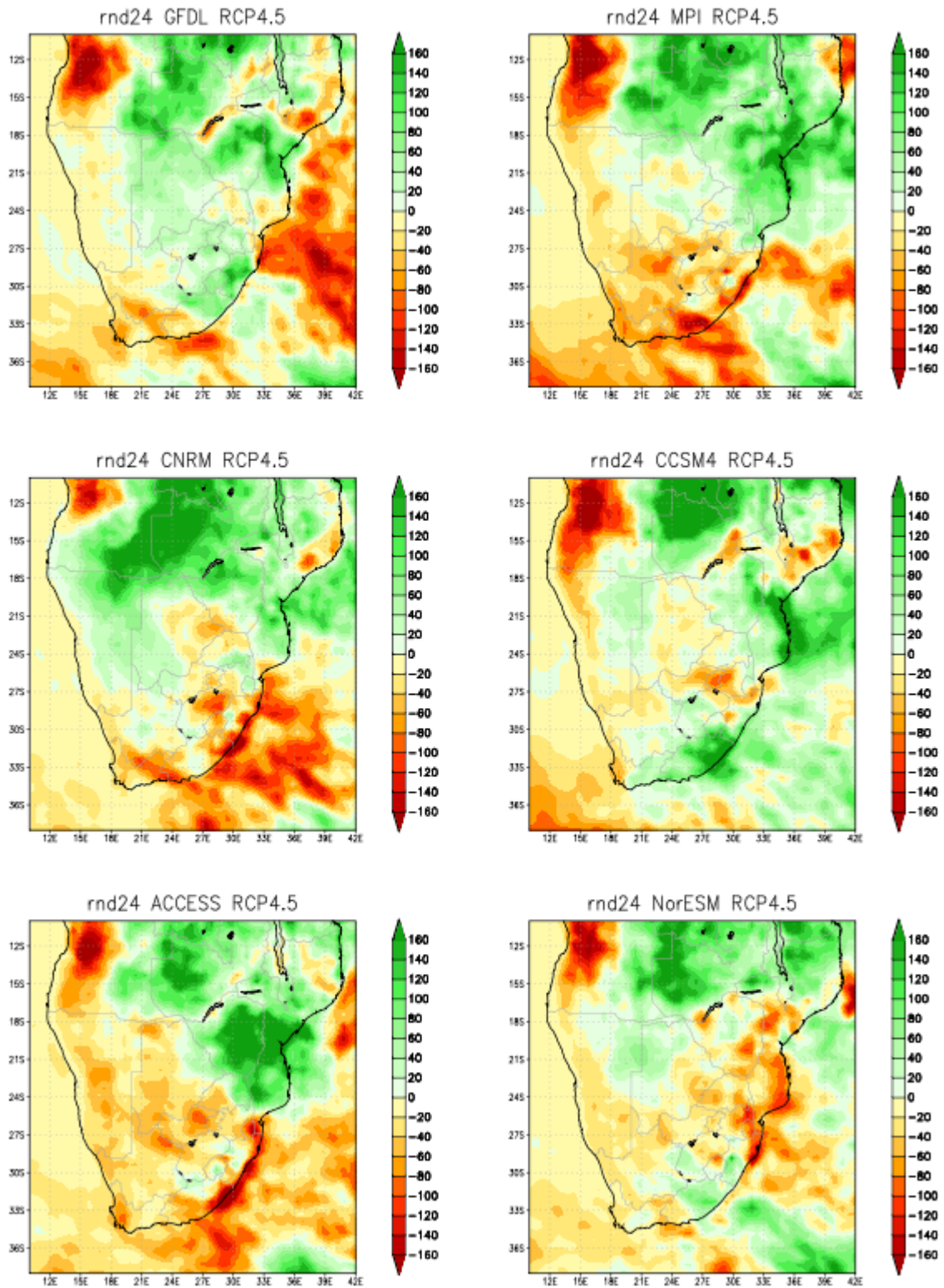


**Figure 2.7:** CCAM-CABLE projected changes in annual rainfall (mm) under RCP 4.5 for the period 2046-2065 relative to 1961-1990.

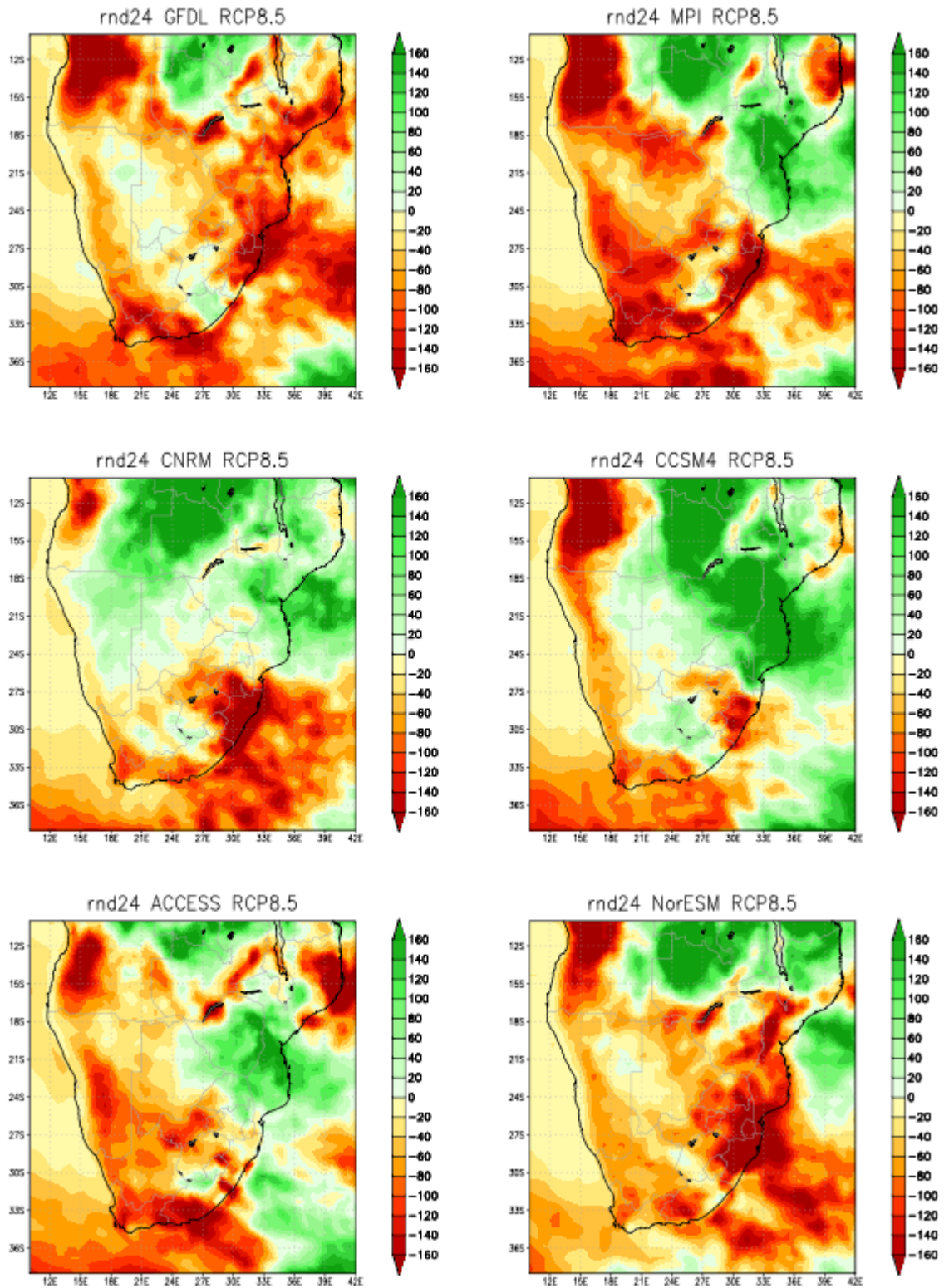


**Figure 2.8:** CCAM-CABLE projected changes in annual rainfall (mm) under RCP 8.5 for the period 2070-2099 relative to 1961-1990.

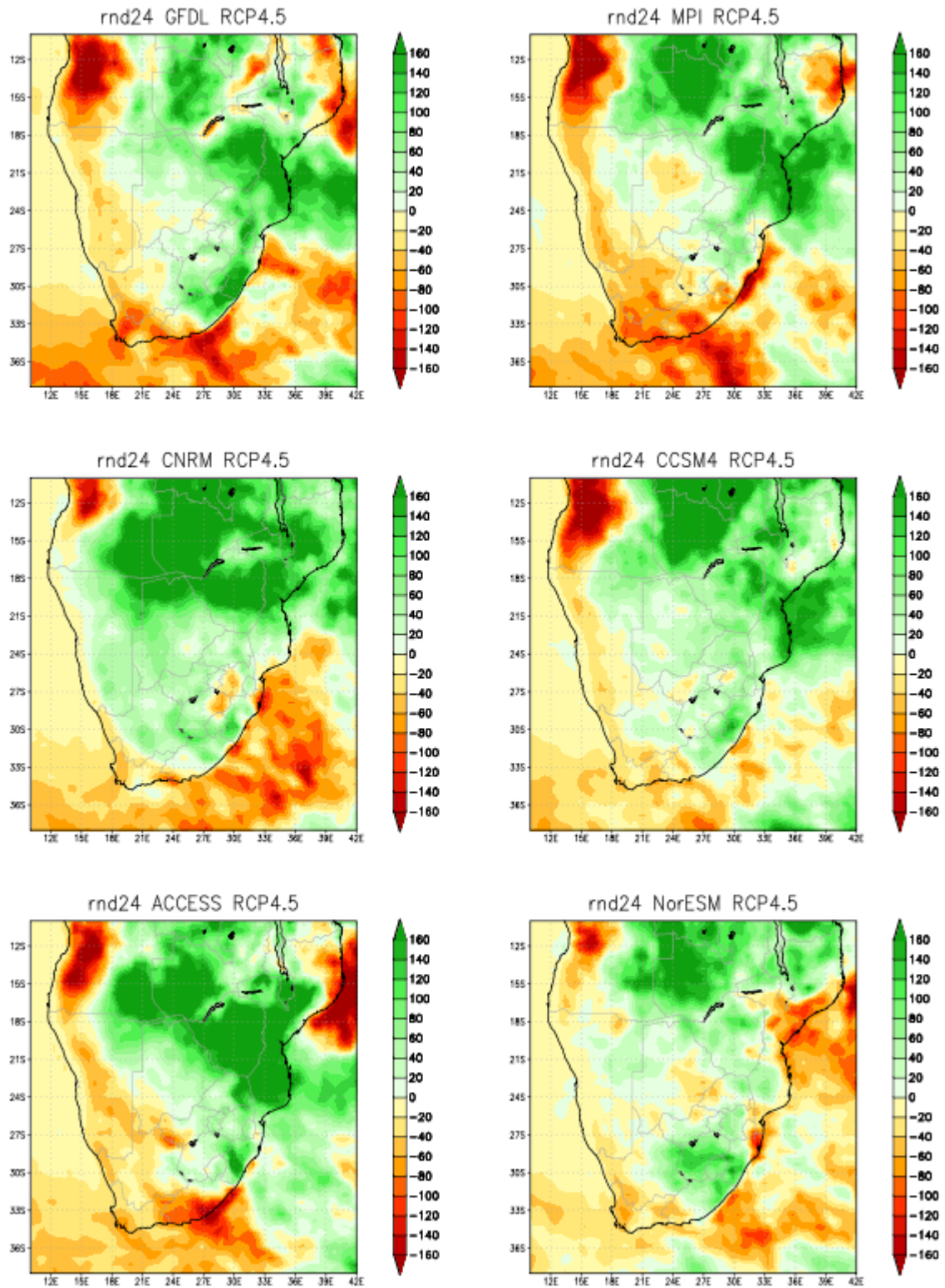


**Figure 2.9:** CCAM-CABLE projected changes in annual rainfall (mm) under RCP 8.5 for the period 2070-2099 relative to 1961-1990.

As is evident from the discussion in sections 2.3.1 and 2.3.2, a significant shift in the climate regime of eastern South Africa is projected under low mitigation futures. This is demonstrated by Figure 2.10, which shows the CCAM ensemble simulated annual rainfall and temperature anomalies over Lesotho for the period 1971-2099. The blue dots (representative of the period 1971-2000) are indicative of the pronounced present-day climate variability of the region. Systematic drying is projected for Lesotho over time. Annual temperature anomalies are projected to range between 3 and 6°C during the period 2080-2099, with most years being drier than the present-day climate.

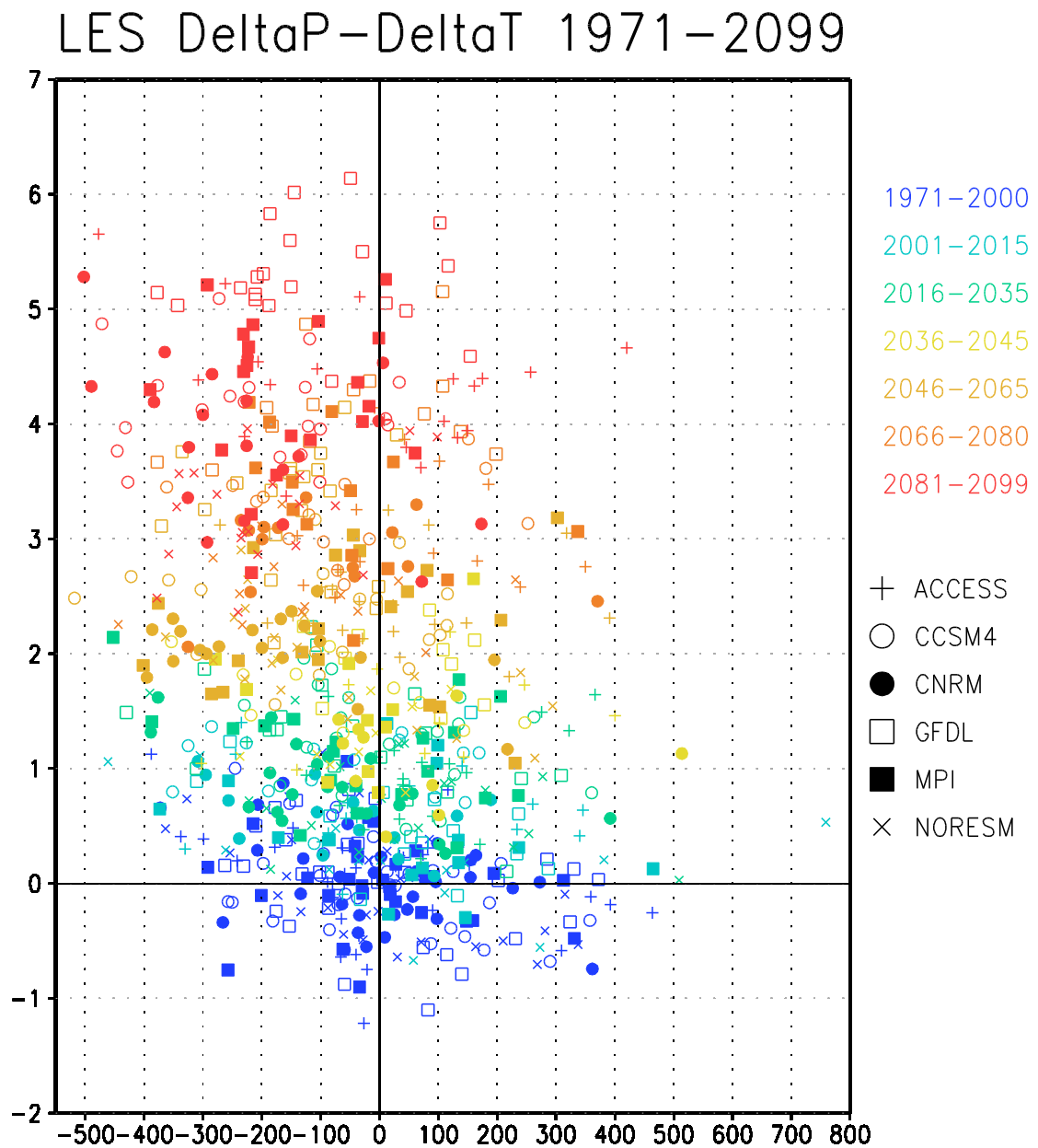


**Figure 2.10:** CCAM simulated annual temperature anomalies (°C, y-axis) and corresponding rainfall anomalies (mm, x-axis) over Lesotho for the period 1971-2099.

It is important to note from the Figure 2.10 that years of unprecedented drought over Lesotho may occur as early as during the period 2016-2035. Moreover, the emergence of frequently occurring multi-year droughts, at least as measured in terms of present-day rainfall, is projected to occur as early as the mid-future period of 2046-2065.

### 2.3.3 Projected changes in wetness and dryness over southern Africa

To further explore the changing rainfall attributes over southern Africa under low mitigation, future changes in dryness and wetness over Africa are estimated through the calculation of the standardized precipitation index (SPI).

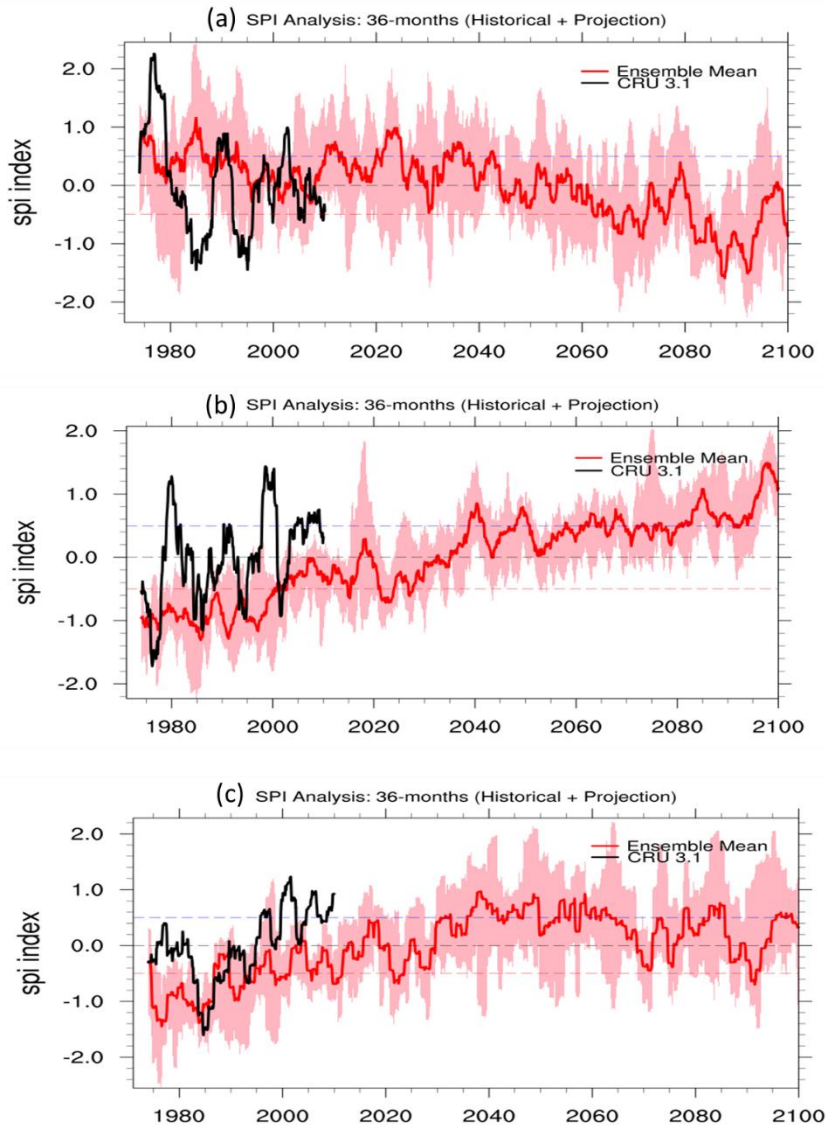


**Figure 2.11:** SPI evolution over the period 1971-2099, for (a) southern Africa, (b) West Africa and (c) East Africa. The light-pink shade represents the CCAM ensemble spread; red and black lines are the CCAM ensemble mean and observations, respectively.

The SPI (McKee et al., 1993, 1995) is used to characterize the trends and intensity of drought and flooding over an area of interest. The SPI indices were computed using a 2-parameter gamma distribution fit where the shape and scale parameters are maximum likelihood estimates on monthly averaged daily rainfall totals for a 36-month base period. The SPI severity index is interpreted as indicating drought (flooding) for negative (positive) values when the index exceeds 0.5 in absolute value. Exceptionally dry values are associated with the index assuming values  $< -2.0$  and exceptionally wet conditions are associated with values  $> 2.0$ .

The SPI calculations were performed for each of the CCAM projections under RCP8.5 and were also applied for the present-day period to CRU 3.10 data (Harries et al., 2013). Results are presented in Figure 2.11 for the southern African region, the Sahel of West Africa and the Horn of Africa region in East Africa. The downscalings present a mixed signal of change over the 1971-2009 period for the Horn of Africa region, a robust message of wetting over the Sahel and a clear trend towards drying over southern Africa. The latter positive and negative trends are also present in the CRU 3.10 data. The CRU 3.10 data is also indicative of increased wetness over the coastal areas of Somalia and Kenya (Figure 2.11). It should be noted, however, that the CRU 3.10 data time-series may be heterogeneous over some regions and not suitable for trend analysis. The time-series analysis indicates that under a low mitigation future, southern Africa may experience increasing frequencies of drought occurrence and systematically become drier. For West Africa and the western Sahel, conditions of increased wetness are projected. This change may well be caused by an increase in the West African monsoon system, which would also likely result in the more frequent occurrence of flood events. Trends projected for the East African region are also generally positive, although pronounced multi-decadal variability remains a key feature of this region's climate under low mitigation.

## 2.4 Summary

This chapter provides an analysis and review of the regional climate change futures of southern Africa, with a focus on eastern South Africa, and in particular the eastern escarpment, Lesotho and the mega-dam region. It should firstly be noted that both AR4 and AR5 of the IPCC have concluded that the southern African region is likely to become generally drier under low mitigation. Against this background, regional projections of future climate change over Africa were generated by the project as a contribution to CORDEX of the WCRP. These simulations spanned the period 1961-2100, and downscaled six CMIP5 GCMs for both low and high mitigation scenarios to a horizontal resolution of 50 km across the globe. The simulations are the first projections of future climate change contributed by an African institute to CORDEX, and thus represent an important outcome of the project. The downscalings performed are largely consistent with those of the GCMs described in AR4 and AR5 in terms of their climate change signals, indicating that the southern African region is likely to become generally drier under climate change. Moreover, the projections are indicative that rainfall decreases over the eastern escarpment of South Africa, including Lesotho, may well be substantial under low mitigation by the end of the century. In fact, under low mitigation unprecedented dry years may occur as early as the period 2016-2035, and by the mid-future period of 2046-2065 multi-year droughts may be frequently occurring over eastern South Africa. Such changes may seriously compromise South Africa's water security, including that of Gauteng, and may significantly hamper future industrial development in the country. Further to the north, rainfall increases are projected over much of Mozambique, a signal of change that is likely the result of more landfalling tropical cyclones. Some of the downscalings are indicative of this pattern of change extending southwards into northeastern South Africa. Under modest-high mitigation, a generally drier climate remains likely over eastern South Africa by the mid-future, although the amplitudes of rainfall reductions are reduced. However, by the end of the century under modest-high mitigation, the pattern of stronger easterlies over Mozambique is projected to be displaced southwards, extending into eastern South Africa, with generally wetter conditions projected for much of the region. It should also be noted that drastic increases in temperature are projected for South Africa under low mitigation, and that even under modest-high mitigation the country is committed to significant increases in temperature. Rising temperatures are projected to have a range of negative impacts on southern Africa, including reductions in crop yield and live-stock production, but may also directly impact on water security through inducing enhanced evaporation and land-use change. These aspects are explored further in the remaining chapters of the report.

# Chapter 3 Detailed projections of future climate change over the eastern escarpment and mega-dam regions of South Africa

## 3.1 Introduction

Steep gradients in orography are known to induce steep gradients in climate, and the realistic simulation of these gradients require the use of high resolution regional climate models (e.g. McGregor, 1997; Engelbrecht et al., 2002). The orography of southern Africa exhibits some particularly steep gradients, which require careful consideration in the design of climate simulations over the region. The country has a pronounced upwelling system along its west coast, generally known as the Benguela current e.g. (Andrews and Hutchings, 1980), whilst the fast-flowing, narrow Agulhas current has a pronounced influence on the climate of the east coast (e.g. Rouault *et al.*, 2002). The coastal plain is generally narrow, with an elevated escarpment (reaching altitudes of 1000-2000 m or even higher) separating the coastal regions from the interior plateau (e.g. Van der Beek et. al, 2002). The eastern escarpment of South Africa (the Drakensberg Mountains) is particularly steep and high, with the Maluti Mountains in Lesotho peaking at altitudes of more than 3000 m. The high altitude eastern escarpment influences the local weather and cloud development that produces rainfall. Generally, there exists a positive correlation between altitude and rainfall specifically along the eastern slopes of the eastern mountain ranges in north east Lesotho (Tyson et al., 1976). However, this relationship seems to break down at altitudes higher than 2100 m (Nel and Sumner, 2006).

Understanding the rainfall producing mechanisms and weather systems of the eastern escarpment of South Africa is critical to generating reliable projections of future climate change over this region. Meso-scale convective systems are typically hundreds of kilometres in horizontal dimension at the advanced stages of development and have lifespans in the order of 10 hours. Convective cells, convective lines, gust fronts, meso-lows, meso-highs and tornados are substructures, ranging from 1 to 50 km in horizontal scales, that are embedded within these large systems (e.g. Houze *et al.*, 1989). Variations in topography often trigger meso-scale convective systems as already existing convective systems have the potential to create meso-scale convective vortices on the eastern escarpment of southern Africa (Blamey and Reason, 2009). The two prominent rainfall producing systems over the Drakensberg during summer are organised line thunderstorms and orographically induced thunderstorms (Tyson et al., 1976). Stations in the Drakensberg record 16 to 18 rain days on average during December and January. The extended summer period from November to March yield 70% of the annual rainfall (Tyson et al., 1976). The effects of the eastern escarpment are not limited to localised rainfall effects, however. This region is the primary cause of the well-defined west-east gradient in rainfall totals across South Africa (e.g. Jury, 2012; Engelbrecht *et al.*, 2009). North of the northern Drakensberg of the Mpumalanga province of South Africa, this strong west-east gradient disappears where a dry slot in rainfall extends from Namibia over Botswana and Zimbabwe into the Limpopo basin of South Africa (e.g. Engelbrecht et al., 2002).

Cumulus convection is the rain producing process leading to most of the rainfall occurring over South Africa. Convective rainfall occurs as a result of the complex interactions between cloud dynamics, cloud microphysical processes, mesoscale forcing, diurnal heating and synoptic-scale conditions. The occurrence of thunderstorms over the eastern escarpment is mostly later in the day, from mid to late afternoon over the continental interior and with a night-time maximum in mountainous regions (Schulze, 1965; Rouault et al., 2013). Nel and Sumner (2006) showed that the total rainfall measured at Sani Pas and Sentinel, 40.1% and 30.8% occurred between 15h00 and 20h00, respectively. The diurnal cycle of rainfall is an expression land surface response to solar radiation and made more complex by a number of dynamical and physical processes (Rouault et al., 2013). A significantly larger amplitude in the diurnal cycle is experienced by the land compared to the ocean. This is the consequence of surface heating of the land masses, the convergence of sea breezes in coastal areas and anabatic flows in valleys and highland areas (McGregor and Nieuwolt, 1998). Moreover, the interaction between topography and convection

lead to more pronounced diurnal cycles in rainfall over land (Rouault et al., 2013; Machado et al., 1993).

In fact, only a few studies where regional climate models have been applied beyond the hydrostatic limit (~ 10 km resolution in the horizontal; Engelbrecht et al., 2007) have been performed for the southern African region to date (e.g. Engelbrecht et al., 2011). At the CSIR, CCAM has been applied at resolutions of 1 km to simulate the transport of carbon dioxide over the Cape Peninsula (Nickless et al., 2015), and to simulate land-atmosphere feedback processes in the Kruger National Park. In these simulations, the domain sizes were relatively small, in the order of 150 x 150 km<sup>2</sup>, and the simulations were nudged in 8 km resolution CCAM simulations performed over a larger area. The simulations performed spanned only a few years for each of these studies, and were nudged within ERA reanalysis data. At both the South African Weather Service (SAWS) routine weather forecast systems also exist where numerical weather prediction models are applied at resolutions finer than 10 km. No study has to date, however, verified model simulations beyond the nonhydrostatic limit within the context of the representation of convective rainfall over the region. It is thought that such simulations, that may partially resolve storm dynamics, may provide a substantial improvement over typical simulations performed at hydrostatic resolutions, where convection is parameterised.

Of particular interest with regards to model simulations over southern Africa, is the representation of the diurnal cycle in convection and convective rainfall. Generally, the simulation of the amplitude and phase of the diurnal cycle provides a valuable test for model parameterizations and for the representation of land-atmosphere feedbacks (e.g. Yang and Slingo, 2001). The verification of model simulations performed at hydrostatic resolutions have indeed revealed systematic errors over the summer rainfall region. In the simulations of Hernandez-Diaz et al. (2012), rainfall peaks too early in the day over the eastern parts of South Africa. General overestimations of rainfall over eastern South Africa has also been reported in the modelling studies of Engelbrecht et al. (2002), Engelbrecht et al. (2009) and Engelbrecht et al. (2011). Along the eastern escarpment of South Africa, the diurnal amplitude of surface moisture fluxes has been shown to be important for the diurnal cycle in rainfall as daytime surface latent heat fluxes increase steeply toward the east compared to the almost non-existent night time fluxes that exhibit little east-west gradient (Jury, 2012). Correctly simulating all the variables that contribute to the diurnal cycle is of utmost importance because it influences rainfall on a variety of time scales such as monthly, seasonal, annual, intra-annual and inter-annual rainfall scales.

The main purpose of this chapter is to analyse the most extensive model simulations performed to date beyond the hydrostatic limit over eastern South Africa. The first set of model simulations presented is a downscaling of ERA reanalysis data over the steep topography region of the eastern South Africa. The model simulations of a range of convective rainfall attributes, including the diurnal cycle, are verified against observations. The second set of high resolution simulations presented are downscalings of the 50 km resolution CCAM CORDEX simulations described in Chapter 2, to 8 km resolution over South Africa. These simulations are analysed in terms of the projected climate change signal over eastern southern Africa.

### **3.2 Data and design of the model simulations of present-day climate**

The dynamic regional climate model applied in this chapter to perform the high resolution downscalings is the CCAM-CABLE system, which was described in some detail in section 2.2. The 50 km resolution simulations performed globally as a contribution to CORDEX were obtained solving the hydrostatic primitive equations. However, since the 8 km resolution simulations performed in this chapter are beyond the hydrostatic limit, the model in this case solves a set of nonhydrostatic equations, specifically the quasi-elastic equations cast in a  $\sigma$ -coordinate based on the full pressure field (e.g. Engelbrecht et al., 2007). Towards obtaining the high resolution (8 km resolution in the horizontal) simulations over Lesotho, CCAM was applied in stretched-grid mode using a Schmidt transformation factor of 0.133. Each panel of the cube projected onto the sphere contained 160 x 160 grid points. The 8 km resolution simulations were nudged within ERA

reanalysis, using a digital filter technique to preserve large-scale patterns of the ERA data (Thatcher and McGregor, 2009; 2010). The model simulations were performed for the period 1979-2005. At its lower boundary, the model was forced with sea-surface temperatures and sea-ice from the ERA reanalysis data.

Rainfall station data from around Lesotho were selected based on completeness of the records. The rainfall stations acquired from the South African Weather Service (SAWS) were required to have more than 80% of their entries to be complete (hourly and daily data, for the case of automatic stations for the period 1993-2012) and manual stations (data record for 1979-2012). Additionally, extreme and missing value tests were performed using 14 daily rainfall stations and 5 hourly rainfall stations (Table 3.1 and Table 3.2). The hourly station records were used to create the 6-hourly datasets ranging from 02-08h, 08-14h, 14-20h and 20-02h. This insight into the diurnal cycle is used to evaluate the 6-hourly CCAM simulations, to see if the convection scheme used in CCAM is robust and can describe the diurnal rainfall cycle.

The spatial patterns and magnitude of the simulated monthly and seasonal rainfall totals were verified against observations of the Climatic Research Unit (CRU) for the period 1979-2004 and against data of the Tropical Rainfall Measuring Mission (TRMM) at a resolution of 0.5 degrees for the period 1998-2011. The simulations are analysed in the following way:

- 1) The simulations are subtracted from the TRMM and CRU data to detect systematic over and under estimations of rainfall as a function of space (that is, the model's spatial rainfall biases are identified).
- 2) The pattern correlation is calculated between the simulations and observed fields after the simulations were interpolated to the TRMM and CRU fields respectively, to inspect the models ability to the spatial distribution of rainfall. The pattern correlation is a correlation of two spatial fields,  $x_i$  and  $o_i$ , at specific time interval as  $i$  ranges from 1 to  $N$ , where  $N$  is the number of grid points in the model domain:

$$\rho = \frac{\sum(x_i - \bar{x})(o_i - \bar{o})}{\sqrt{(\sum(x_i - \bar{x})^2)(\sum(o_i - \bar{o})^2)}} \dots\dots\dots(1)$$

Here  $\bar{x}$  and  $\bar{o}$  are the domain averages of  $x_i$  and  $o_i$ .

- 3) The Root Mean Square Error (RMSE) is a measure of the accuracy between a specific forecasted variable from a model and the same observed variable since it is scale dependent (Hyndman and Koehler, 2006).
- 4) The standard deviation is calculated as the measurements for the simulations and observed fields as an estimate of average uncertainty of those measured values.
- 5) SAWS station rainfall is analysed against the simulations as a direct measure of rainfall at a particular point on a monthly, seasonal and annual time-scale.
- 6) The diurnal cycle is calculated and verified on a 6 hour basis against SAWS rainfall stations that measured hourly rainfall.

### 3.3 Results: simulations of present-day climate

#### 3.3.1 Verification of the CCAM simulations against station data

The eastern escarpment of South Africa exhibits steep topographic gradients (Figure 3.1), especially around the Lesotho region. These can induce very large differences in rainfall occurrence over relatively small areas when a weather system moves over the area. For this reason, stations were divided into three groups, based on location (south, north-west and east of Lesotho). Large differences in annual, seasonal and monthly rainfall totals are evident for the three groups of stations (Figure 3.1 and Table 3.1). Stations to the east have annual rainfall totals well

above 900 mm, which are severely over estimated in the CCAM simulations. At the Cathedral Peak and Royal National Park Hotels locations rainfall totals are over estimated by factors of almost 4 times and 2.5, respectively (Table 3.1). Over this region, the lower tropospheric flow is upslope and surface moisture is advected from the east when ridging anti-cyclones are present to the east of South Africa (Joubert et al., 1999). It is possible that this orographic lift and the rainfall it induces are overestimated in the CCAM simulations. Observed rainfall totals are lower in the south and west of Lesotho. This is partially due to the rain-shadow effect and blocking of low-level moisture by the eastern escarpment. Low clouds advected in from the east often remains trapped east of and along the escarpment. Convective clouds that occur in association with the easterly winds in the presence of an upper-air disturbance also largely rain out to the east of the Lesotho mountains. This situation is reflected in the lower rainfall amounts, between 600-700 mm, recorded over the eastern Free State showing a strong west-east rainfall gradient over the domain. CCAM correctly simulates the west-east gradient in rainfall, but also overestimates rainfall totals in the west, by a factor of two for some locations. The model correctly simulates the highest rainfall totals for the region to occur during mid-summer (DJF), with lower totals simulated for November compared to December.

**Table 3.1:** Daily SAWS station rainfall compared to rainfall from CCAM at the points of the SAWS stations. Highlighted blocks show large over estimations (larger than 2x the observed rainfall).

	Station	CCAM						SR					
		Annual	DJF	Nov	Dec	Jan	Feb	Annual	DJF	Nov	Dec	Jan	Feb
	Cathedral Peak	4237.7	2225.4	460.8	650.6	795.5	761.4	1152.3	586.4	130.6	152.3	209.6	224.4
	Royal National Park	3127.9	1681.6	331.0	477.6	623.0	566.7	1225.7	628.2	145.7	167.7	212.5	235.7
	Ficksburg	1010.5	490.4	127.7	181.6	172.7	139.5	661.0	273.0	81.5	82.2	102.9	89.5
	Giants Castle	2044.4	1163.4	242.8	369.2	410.7	381.9	984.1	498.3	114.8	163.0	179.8	162.8
	Kommissiepoort	937.7	458.4	116.9	159.2	171.7	125.6	642.0	274.9	77.8	81.1	96.4	90.9
	HighMoore	1725.1	937.8	204.4	300.8	337.5	300.4	1233.3	628.8	164.3	196.0	220.6	205.1
	HobHouse	973.0	475.9	119.9	171.2	175.0	128.7	604.1	251.1	80.8	79.6	89.3	89.1
	SaniPass	2030.8	1127.7	227.2	332.2	413.1	390.9	1122.4	571.8	126.9	164.7	208.0	189.4
	FunnyStone	1413.0	591.3	176.5	227.1	216.8	150.1	835.8	329.8	107.0	111.9	111.9	111.9
	BarkleyEast	1236.3	557.9	153.9	218.3	210.2	139.4	601.9	254.1	79.6	81.7	83.7	95.5
	Lille	1030.0	491.9	116.9	186.7	173.7	131.3	698.1	306.7	82.1	98.4	99.5	106.8
	Matatiele	1206.8	589.2	152.6	208.0	203.6	177.0	683.4	318.7	85.0	102.2	119.8	101.2
	HighLands	984.1	468.8	128.3	164.7	170.8	139.1	641.4	281.3	92.0	97.8	92.2	86.6
	Kestell	1043.3	531.7	139.7	179.8	194.4	157.6	684.6	318.4	93.1	103.3	108.9	102.8

**Table 3.2:** The diurnal cycle from SAWS station data compared to CCAM data at the location of the particular station. The location from the stations is marked in Figure 3.1.

	SAWS					CCAM				
		02-08h	08-14h	14-20h	20-02h		02-08h	08-14h	14-20h	20-02h
Ficksburg	Dec	7.6	14.1	36.9	19.5	Dec	37.2	24.7	72.1	53.2
▲	Jan	14.8	13.4	29.4	20.9	Jan	30.8	22.5	65.1	64.3
	Feb	10.7	13.8	26.6	22.4	Feb	27.1	17.8	51.1	51.5
	DJF	33.0	41.3	92.9	62.8	DJF	95.2	64.9	188.3	169.0
	Annual	89.6	93.4	192.9	142.8	Annual	194.9	209.4	422.3	426.6
Ladysmith	Dec	14.7	6.8	57.3	36.6	Dec	88.0	18.3	39.3	95.9
▣	Jan	14.1	9.7	57.3	69.7	Jan	119.2	15.1	31.9	117.2
	Feb	7.9	7.1	38.2	38.3	Feb	80.5	19.1	23.3	63.3
	DJF	36.6	23.6	152.8	144.5	DJF	199.7	34.3	55.2	180.5
	Annual	86.5	68.0	283.1	279.0	Annual	551.9	99.4	228.2	386.7
Mooi Rivier	Dec	8.2	8.5	46.2	38.8	Dec	68.6	14.8	33.4	132.9
★	Jan	9.5	9.4	50.3	23.4	Jan	60.8	14.2	25.1	142.2
	Feb	6.3	5.0	38.6	14.1	Feb	58.5	16.6	27.6	87.0
	DJF	24.0	22.9	135.0	76.3	DJF	187.9	45.5	86.0	362.1
	Annual	64.3	71.6	294.0	176.7	Annual	593.7	127.9	195.6	730.1
Van Reenen	Dec	19.7	13.4	71.0	51.0	Dec	100.5	31.5	39.4	123.8
=	Jan	27.4	21.7	73.7	78.2	Jan	116.6	24.0	40.0	134.1
	Feb	18.2	13.9	66.8	53.0	Feb	99.7	27.5	28.8	118.4
	DJF	65.2	49.0	211.5	182.1	DJF	316.8	83.0	108.2	376.3
	Annual	141.5	111.3	360.1	339.7	Annual	706.9	289.4	241.2	601.2
Wepener	Dec	9.6	10.9	42.2	20.5	Dec	29.5	23.5	61.9	60.1
⊘	Jan	13.1	12.0	42.1	22.1	Jan	21.4	21.7	69.4	56.7
	Feb	13.4	20.4	27.4	23.1	Feb	19.1	11.2	57.8	62.4
	DJF	36.2	43.4	111.7	65.8	DJF	70.0	56.5	189.0	179.2
	Annual	94.9	119.2	226.4	146.3	Annual	104.3	178.6	467.2	495.2

### 3.3.2 Annual rainfall totals

There is a distinct west-east rainfall gradient over much of the research domain with CCAM (CRU) annual rainfall totals in the west being in the order of 800 mm (500 mm) increasing to well over 2000 mm (800 mm) in the east (Figure 3.2). The largest amount of rainfall in the vertical cross-section at 29.25°S occurs on the eastern side of the Maluti Mountains between altitudes of 1450 and 1650 m (Figure. 3.2a). On the western side of the mountains between 26°E and 27.5°E the 8 km CCAM simulations show prominent features of orographic uplift that are not clearly seen in the CRU or TRMM data. These high totals are simulated for a region which is not covered by the weather station data available for this study. It is plausible that this local maximum simulated by the model is a real physical feature that is not present in the 0.5 degree resolution CRU data, due to

the absence of underlying station data for this region. . There is indeed some indication of the existence of a western rainfall maximum in the FEWS data, although this remotely sensed precipitation data sets are known to have biases in the presence of topography.

CCAM generally overestimates rainfall totals across the domain, particularly so over KwaZulu-Natal (KZN) and the Lesotho border (Figures 2b, 2c and 2d). These overestimations on the Lesotho border are as large as 800 mm. At the SAWS stations High Moore (2019 m) and Giants Castle (1981 m) on the eastern side of the escarpment, the rainfall is over estimated by 40% and 107%, respectively. From the stations on the eastern side of the escarpment there is no clear correlation that depicts an increase in rainfall with altitude below 2100 m above sea level. In fact, CCAM simulates a strong increase in rainfall with altitude below 1500 m before severely decreasing rainfall with altitude, as the altitude increases to above 2500 m (Figure 2a). The pattern correlation between the TRMM and CCAM rainfall data is weak, probably because there is no well-defined west-east rainfall gradient present in the TRMM data (Figure 2f). The spatial patterns of rainfall simulated by CCAM compares better to those depicted by the SAWS station data and CRU gridded station data (Figure 2e).

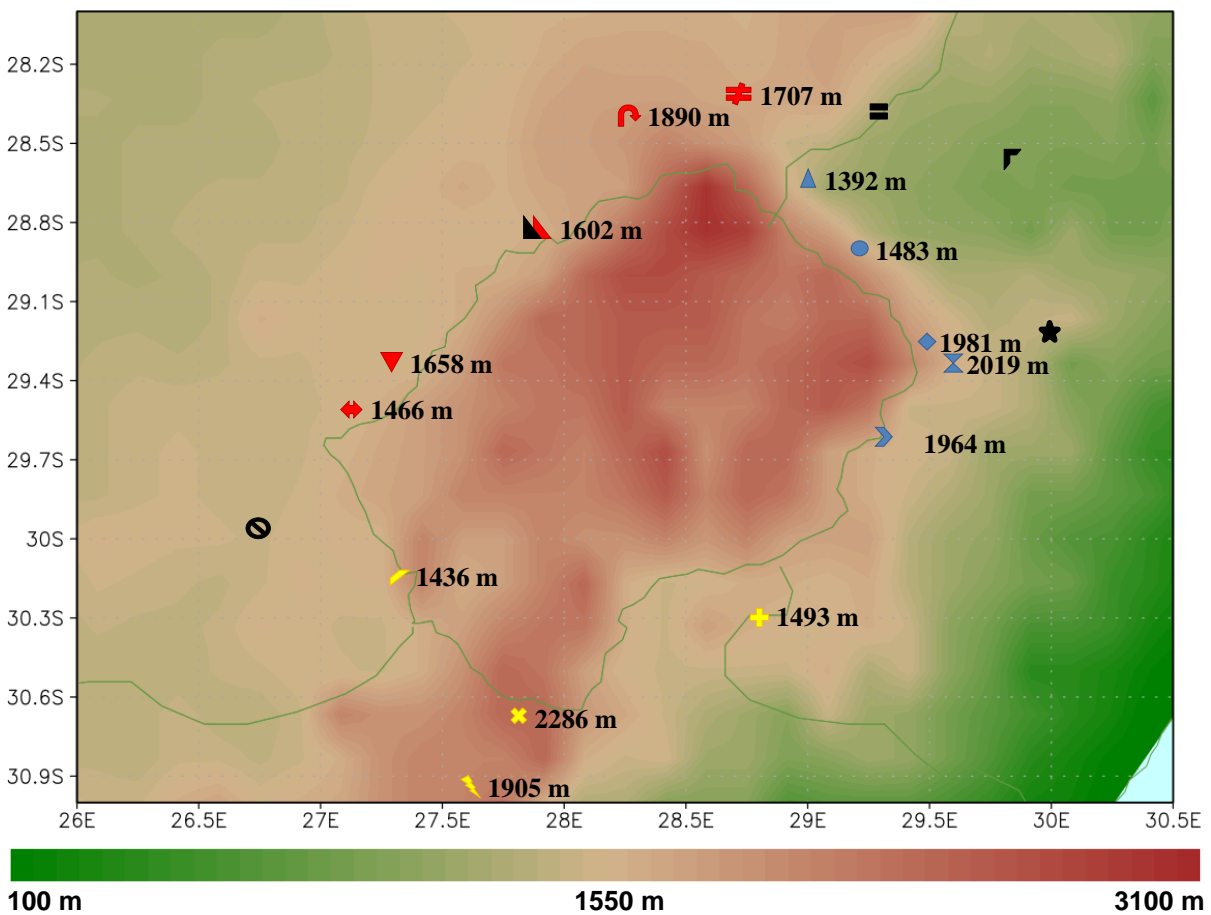


**Figure 3.1:** Location of South African Weather Service (SAWS) stations around Lesotho measuring at daily (coloured) and hourly (black) time intervals.

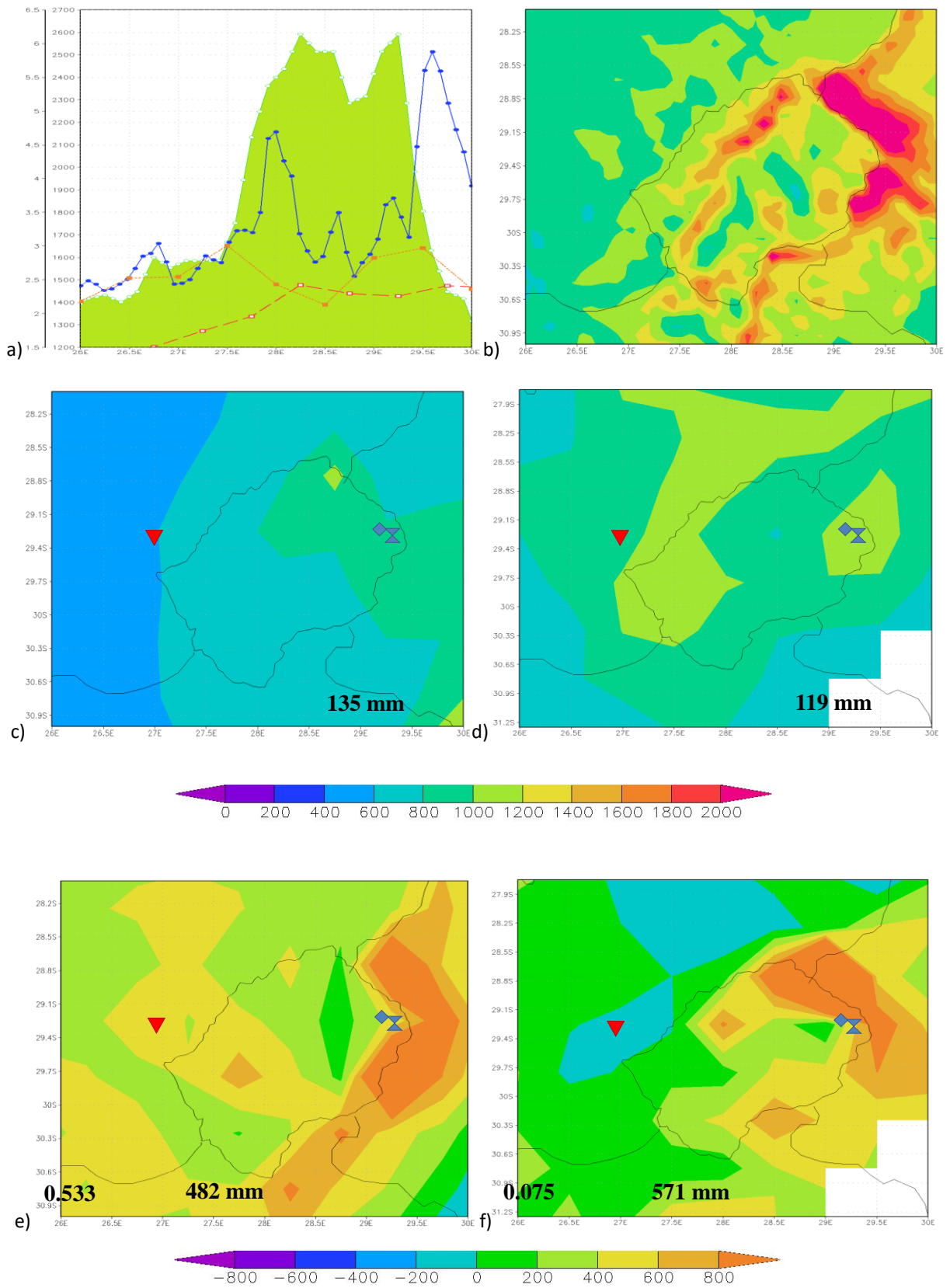


**Figure 3.2:** a) Vertical cross-section at 29.25°S for annual rainfall in mm/day (solid line – CCAM; long stripes – CRU; short stripes – TRMM). Annual rainfall totals (mm) for b) CCAM (1979-2004), c) CRU (1979-2007) and d) TRMM (1998-2010). Bias (mm) for e) CCAM-CRU and f) CCAM-TRMM.

### 3.3.3 Seasonal rainfall totals

The observed summer rainfall pattern over the region closely resembles the annual rainfall pattern, given that the region is a summer rainfall region. During summer moisture-laden easterly winds frequent the eastern escarpment as low-level high-pressure systems ridge along the South African east coast, thereby inducing high rainfall totals east of the escarpment. In the CCAM simulations large overestimations of summer rainfall totals are evident over KZN and along the Lesotho border. The model rainfall correlates well with that with CRU in space (Figure 3.3), more so than in the case of the TRMM data. CCAM simulates a western rainfall maximum similar to TRMM at 27.5°E, but then extends this feature to 28°E (at 2400 m) as the topography increases on the western side of the mountain. This feature is not present in the TRMM data and implies a wet bias in the model simulations. During the summer season the altitude and rainfall correlation does not exist. CCAM shows an increase in rainfall with altitude up to 1800 m, before totals start to decrease with the rising slope (Figure 3.3a).

### 3.3.4 Monthly rainfall totals

The month by month analysis is important as previous versions of CCAM incorrectly simulated November as the month of maximum rainfall during summer (Dedekind et al., 2016). The early onslaught of the season was a result of the model simulating too strong temperate-trough linkages in November rather than the observed January rainfall maximum (also see Tozuka et al., 2013). The newer version of CCAM applied here shows a more realistic seasonal cycle in rainfall with the simulated rainfall peaking during mid-summer rather than in November (Figure 3.4). TRMM shows relatively large amounts of rainfall on the western side of the Maluti Mountain when compared to SAWS stations in that vicinity (Figure 3.4d and Table 3.1). Kommissiepoort (27°E) has an average rainfall of 2.59 mm/day compared to TRMM having 5.25 mm/day. This suggests some apparent biases in the TRMM data in terms of rainfall totals in regions of steep topography (at least when compared to the station data available). CCAM overestimates rainfall totals with respect to both the TRMM and CRU data, with these overestimations most severe on both the western and eastern sides of the mountains (Figures 3.4a-f).

The model displays a wet bias for December over the KwaZulu-Natal and the Lesotho border. This is most evident for verification with respect to the TRMM data (Figures 5e and 5f). CCAM simulates relatively lower amounts of rainfall above 2200 m (Figures 5a and 5b). At Kommissiepoort the rainfall is 2.7 mm/day, a factor of two less than in the CCAM simulations. The Giants Castle (1981 m) and High Moore (2019 m) stations, which are approximately on the same latitude as Kommissiepoort, have simulated (SAWS station) rainfall of 369.2 mm (163 mm) and 300.8 mm (196 mm), respectively. The CCAM rainfall for January increases over the largest part of the domain with respect to the December totals, especially on the Eastern Cape-Lesotho border and the KZN-Lesotho border (Figure 3.6b). These local rainfall increases occur consistently with January being the month of highest rainfall over eastern South Africa. The increase occurs in response to a strengthening of the heat low over the central interior and the frequent occurrence of tropical-temperate troughs over the region. The largest increases from the SAWS station are on the eastern side of the Maluti Mountains, with the exception of Kommissiepoort that has an increase of 17% on the western side of Lesotho. The TRMM exhibits large increases in rainfall (for January with respect to December) over the Free State that does not correspond to the SAWS data or CCAM simulations (Figure 3.6d). The CRU data displays increased rainfall on the eastern side the escarpment that is similar to CCAM (Figures 3.6c and 3.6e). At Kommissiepoort the station rainfall total is well represented by CRU (gridded station data), but TRMM and CCAM over estimates the rainfall by a factor of 2. The CCAM simulates the west-east rainfall gradient well and captures the increase in rainfall that is caused by the steeper topography at 26.75°E (Figure 6a).

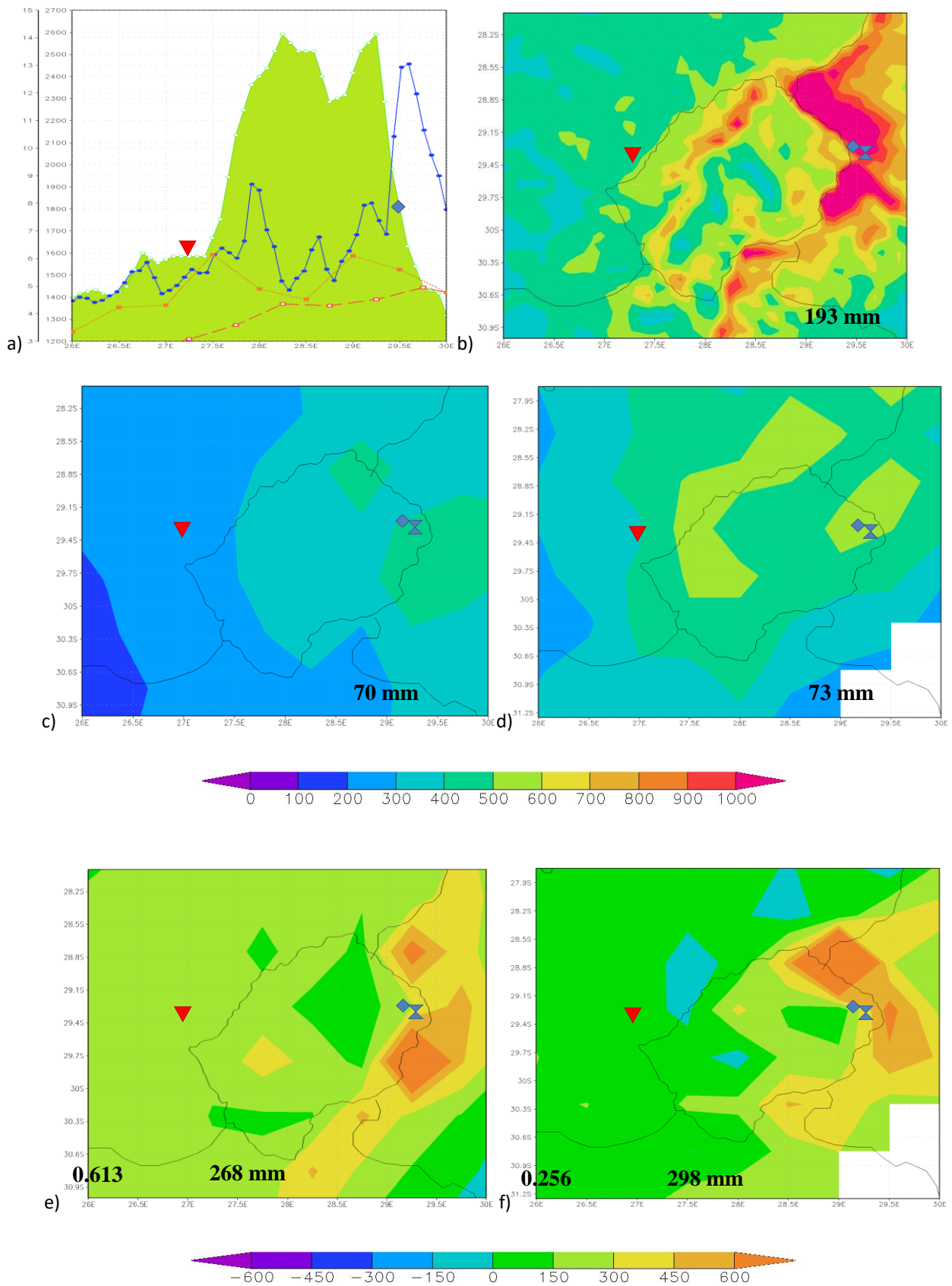


**Figure 3.3:** a) Vertical cross-section at 29.25°S for DJF rainfall in mm/day (solid line – CCAM; long stripes – CRU; short stripes – TRMM). DJF rainfall totals (mm) for b) CCAM (1979-2004), c) CRU (1979-2007) and d) TRMM (1998-2010). Bias (mm) for e) CCAM-CRU and and f) CCAM-TRMM.

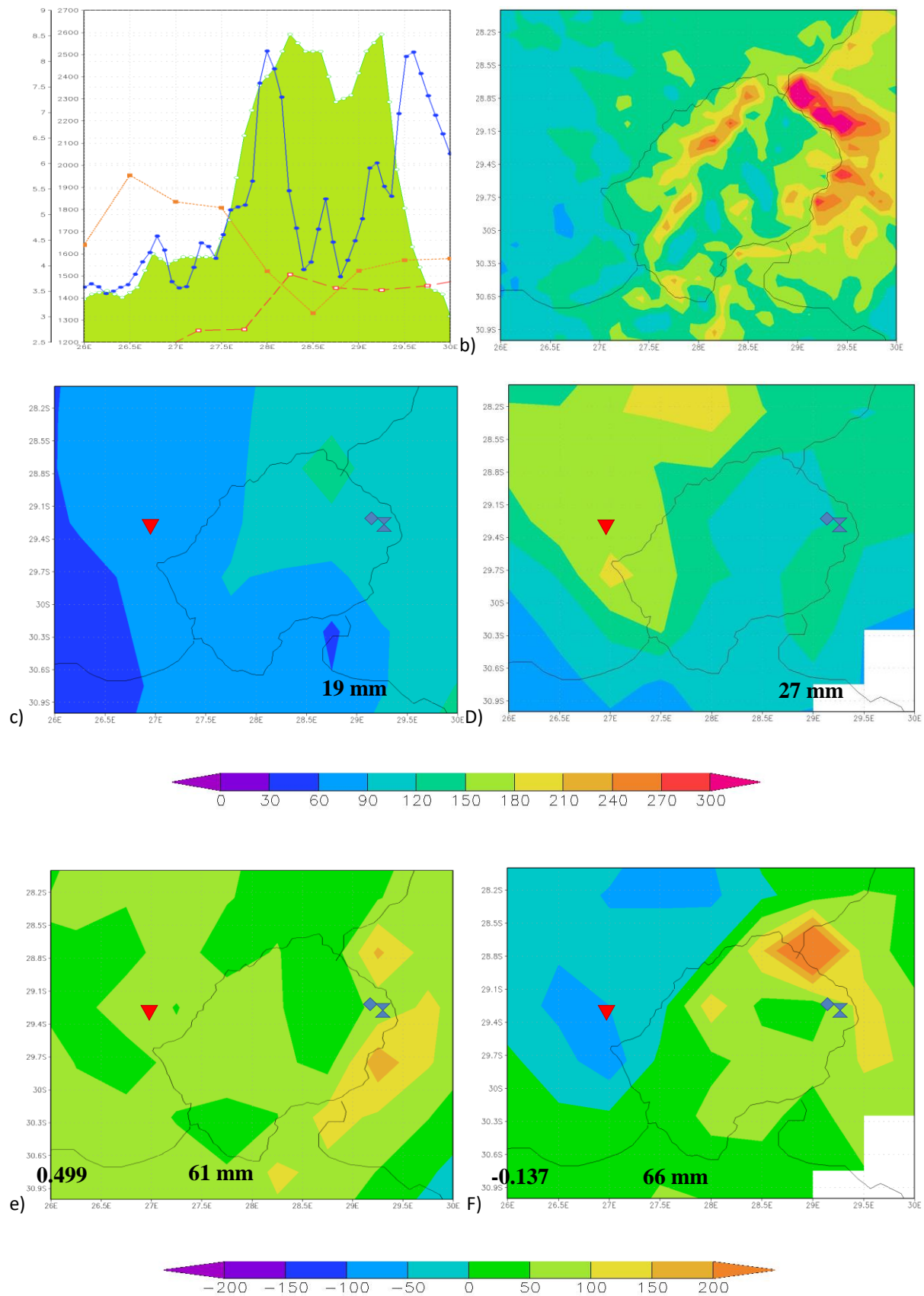


**Figure 3.4:** a) Vertical cross-section at 29.25°S for November rainfall in mm/day (solid line – CCAM; long stripes – CRU; short stripes – TRMM). November rainfall totals (mm) for b) CCAM (1979-2004), c) CRU (1979-2007) and d) TRMM (1998-2010). Bias (mm) for e) CCAM-CRU and f) CCAM-TRMM.

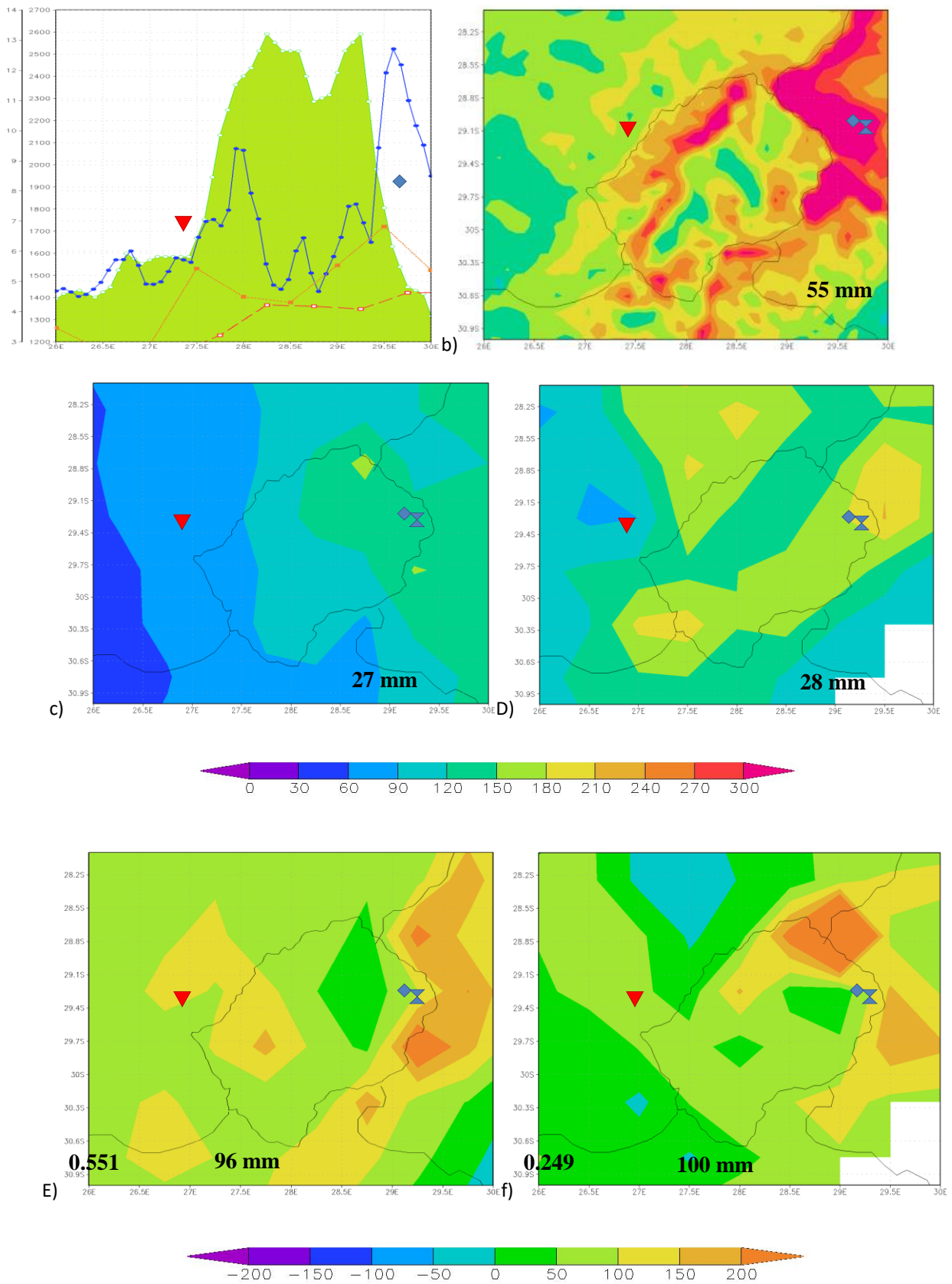


**Figure 3.5:** a) Vertical cross-section at 29.25°S for December rainfall in mm/day (solid line – CCAM; long stripes – CRU; short stripes – TRMM). December rainfall totals (mm) for b) CCAM (1979-2004), c) CRU (1979-2007) and d) TRMM (1998-2010). Bias (mm) for e) CCAM-CRU and f) CCAM-TRMM.

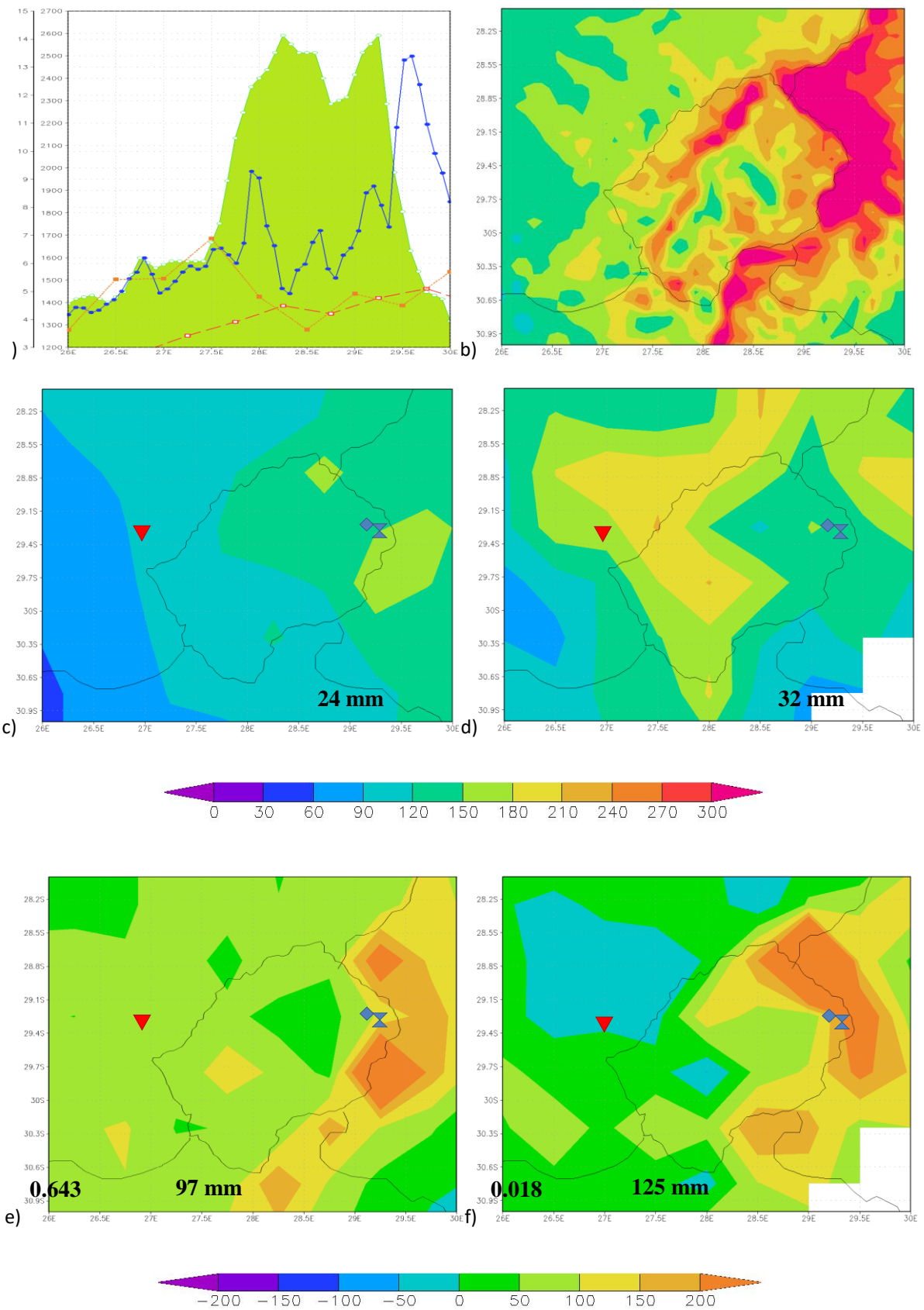


**Figure 3.6:** a) Vertical cross-section at 29.25°S for January rainfall in mm/day (solid line – CCAM; long stripes – CRU; short stripes – TRMM). January rainfall totals (mm) for b) CCAM (1979-2004), c) CRU (1979-2007) and d) TRMM (1998-2010). Bias (mm) for e) CCAM-CRU and f) CCAM-TRIMM.

### *3.3.5 Diurnal rainfall cycle*

Representation of the diurnal cycle in convection is known to be problematic in dynamic climate models, with most models simulating the peak in rainfall to early in the day. Here the 6-hourly simulated totals of CCAM are analysed to investigate how the model deals with changes in the daily heat balance and the effects that orographic lift has on the diurnal cycle. The Agulhas current also plays an important role in the diurnal cycle of adjacent coastal areas (Rouault et al., 2013). The rainfall producing systems occurring over the area vary from ridging high-pressure systems, cut-off lows, heat thunderstorms (that mainly occur late in the afternoon and evenings), cold fronts and tropical-temperate troughs.

The CCAM simulated diurnal cycle of rainfall is compared to 6-hourly SAWS station data over the domain to analyse the ability to simulate convection and rainfall. The pronounced feature seen in the CCAM simulations on the western side of the escarpment is rainfall peaking between 14h and 20h (Figure 3.7a-e). Annually the combined afternoon and evening rainfall make up 65% (68% according to CCAM) and 64% (77% according to CCAM) of the total diurnal rainfall cycle at Ficksburg and Wepener respectively (Figures 3.7a and Table 3.2). However, CCAM is not representative of the annual and February diurnal rainfall maximum period between 14-20h for both the stations. During summer months the afternoon rainfall occurs more frequently than evening showers (fig. 7b-e). CCAM does well in capturing the diurnal cycle on the western side of the escarpment. On the eastern side of the escarpment most weather stations report the diurnal rainfall cycle to peak between 14-20h. Over most of this region, CCAM simulates rainfall to peak either in the early morning or evening. 75% of the SAWS station rainfall occurs in the second half of the day with the peak between 14-20h for most stations. Rouault et al. (2013) found that for stations to the north-east and east of Lesotho (within 150 km) rainfall varied between 18h and 21h for austral summer months (November to March). It is clear that CCAM simulates rainfall too late during the day on the eastern side of the escarpment. This is especially true for Lady Smith where the early morning rainfall amount to more than 40% of the diurnal cycle that is not comparable to the 10% from SAWS stations (Table 3.2). The largest and most unrealistic rainfall station simulations comes from stations on the eastern side of the Drakensberg with Lady Smith, Mooi Rivier and Van Reenen showing as little as 5 times, 6 times and 5 times more than the SAWS station rainfall. The reason for this is most likely that CCAM simulates too much convection in conjunction with the steep topography that creates uplift.

### *3.3.6 Intra-annual rainfall*

The modelled monthly rainfall totals from the eastern escarpment are compared to the corresponding observed values. The curves are obtained by merely taking rainfall values month to month and plotting it next to each other. Rainfall values are severely overestimated for almost every month except from May-July when rainfall subsides during winter. CCAM simulates the onset of rainfall in September, comparable to onset as described by the TRMM and CRU data. The peak of the rainfall season is simulated in January that compares well with the observations. The average rainfall over the domain is 75 mm and 93 mm higher than TRMM and CRU respectively indicating severe overestimations that is unrealistic (Figure 3.8). From January the rainfall reduces gradually until March at which point CCAM simulates the dry conditions that prevail from May to September.

### *3.3.7 Inter-annual rainfall*

The inter-annual rainfall variability for the summer rainfall is analysed for the region over the eastern escarpment of southern Africa (26-30°E and 28-31°S). The simulated over estimation prevail on a yearly basis with the largest rainfall over estimations occurring between 1985 to 1989 and 1997-2003. Dedekind et al. (2016) showed that the same region, at a simulated 50 km resolution, has a Spearman Rank Correlation (SRC) of 0.57 that is significant at 99.9%. The high resolution 8 km simulations, with a newer version of CCAM, performed better obtaining a SRC of 0.69 that is significant at 99.9% (Figure 3.9) CCAM captures the severe decrease in rainfall that is

associated with the 1982-1983 droughts over southern Africa. The simulated rainfall trends from 1979 to 2004 shows a greater slope indicative of higher rainfall totals over the region in the future, but this is unlikely as this strong positive trend can be explained by the severe droughts that significantly influence the rainfall variability at the start of the period.

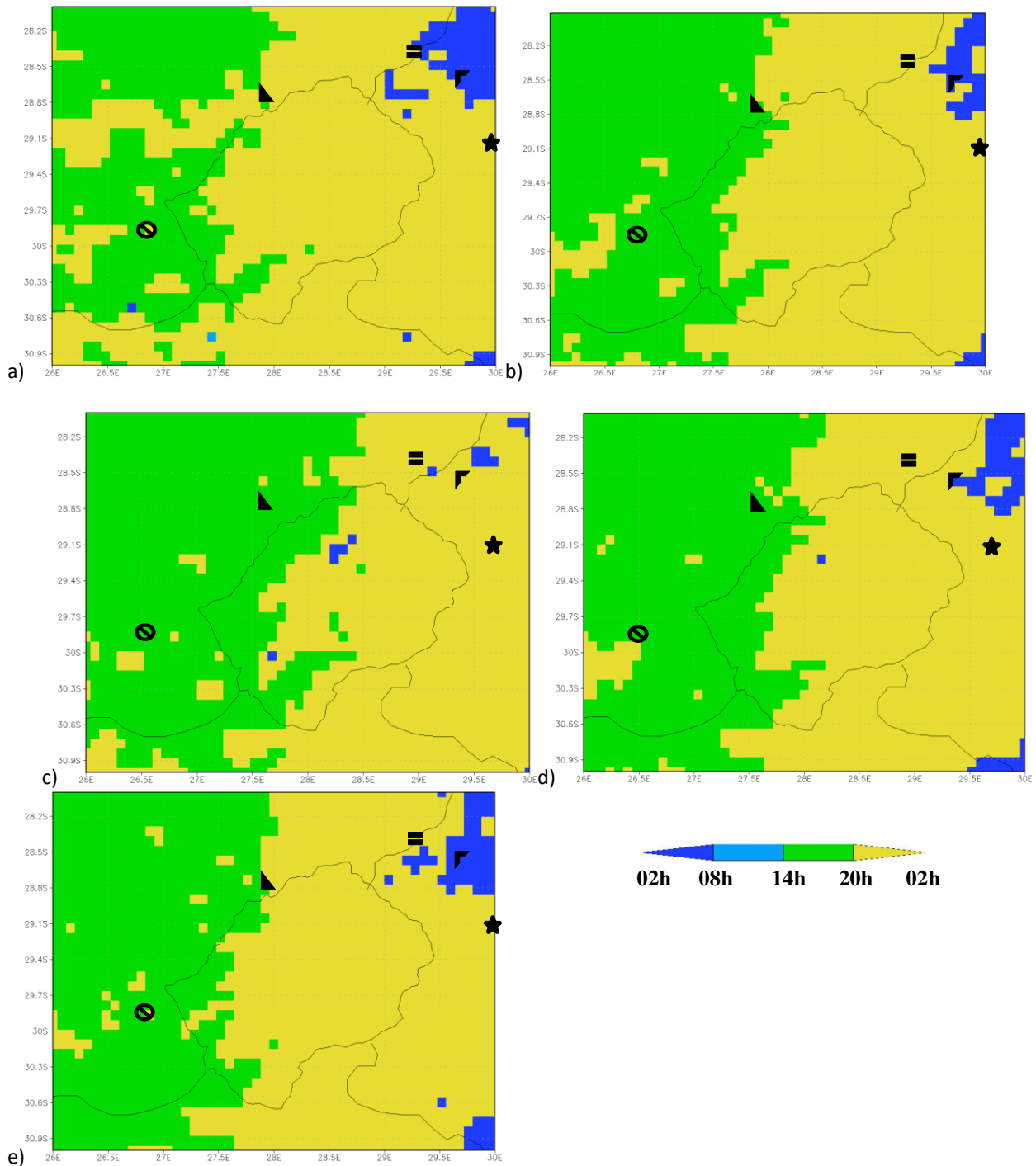


**Figure 3.7:** 6-Hourly diurnal cycle for CCAM a) annually, b) DJF, c) November, d) December and e) January. Intervals are 00h to 06h (dark blue), 06h-12h (light blue), 12h-18h (green) and 18h-24h (yellow).

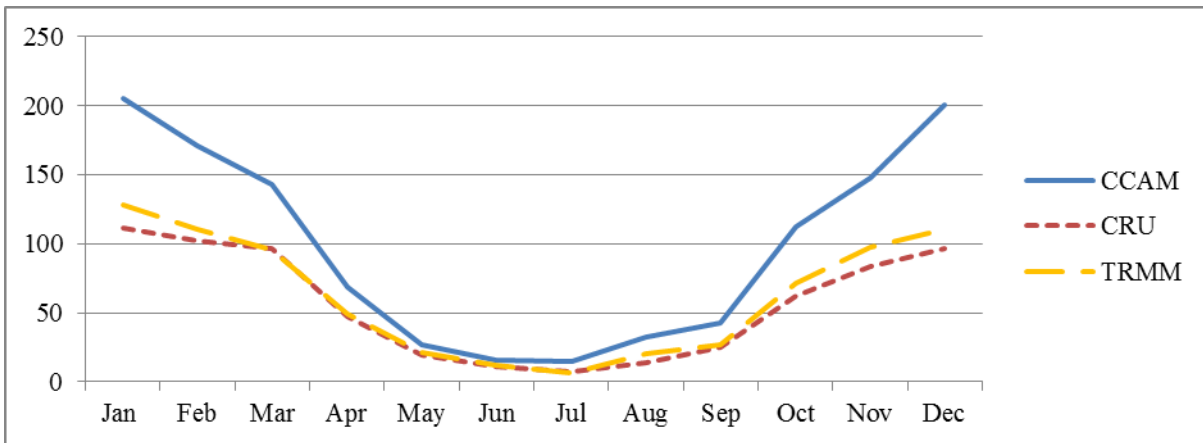


**Figure 3.8:** Intra-annual rainfall totals (mm) for CCAM AMIP (1979-2004), NCEP reanalysis (1979-2009), CRU (1979-2004) and TRMM (1998-2010) over the regions of a) LES, b) NESa and c) ESA.

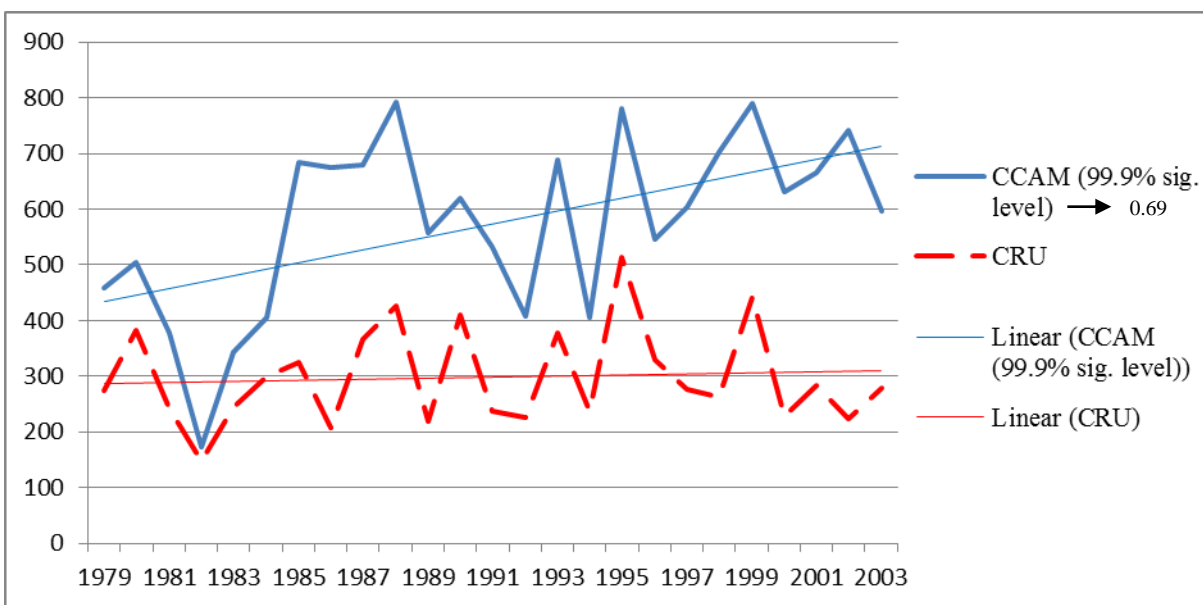


**Figure 3.9:** Inter-annual DJF rainfall totals (mm) for CCAM (1979-2004) and CRU (1979-2004) over the regions of LES. In brackets is the Spearman Rank Correlation level of significance.

### 3.4 Summary – detailed simulations of present-day climate

The detailed simulations of present-day (8 km resolution in the horizontal) have been performed over the eastern escarpment of South Africa, and verified against observations from CRU, TRMM and SAWS. Rainfall features around Lesotho such as the wetter eastern parts of KwaZulu-Natal and the drier western parts in the Free State and Eastern Cape are captured well in the CCAM simulations. However, the model simulations exhibit very large wet biases north east of Lesotho that are at some stations up to 3 times the rainfall observed at SAWS stations. CCAM is able to simulate the well-defined west-east gradient in rainfall over the eastern escarpment of southern Africa (e.g. Engelbrecht et al., 2009). However, this strong gradient is not shown in the TRMM rainfall data and this results in a relatively low pattern correlation with the CCAM simulations. The CRU and SAWS data show an increase in rainfall as the longitude increase over the domain. The SAWS data does not show a clear correlation between increases in rainfall as the altitude increase below 2100 m on the eastern side of the escarpment, but CCAM does simulate a large increase in rainfall with elevation in topography below about 1700 m depending on whether annual, seasonal or monthly rainfall were analysed. The intra-annual cycle is also captured well by the model,

especially the annual rainfall maximum that occurs during January as previous research by Dedekind et al. (2014) showed that a previous version of CCAM erroneously simulated an annual rainfall maximum during November. It is important that CCAM can capture the whole cycle with the onset of the season starting in October until January when rainfall subsides for winter months. Significant Spearman Rank Correlation between CCAM rainfall simulations and observations is indicative of skilfully simulating the inter-annual rainfall variability, but the trend and wet bias are problematic. Simulating the diurnal cycle is a robust test of how well the dynamics and physics in a model works. CCAM simulates two distinct regions where rainfall occurs between 14-20h on the western side of the steep Maluti Mountains and between 20-02h over Lesotho and the eastern side of the Maluti Mountains that is not present at the SAWS stations. The observations show that CCAM simulates rainfall too late during the day on the eastern side of the escarpment. Extreme wet biases are also present at Lady Smith, Van Reenen and Mooi Rivier locations. The diurnal cycle for the stations on the western side is reasonably well captured by CCAM. Further investigation is needed to analyse these extreme wet biases occurring over the largest parts of the domain.

### **3.5 Experimental design of the detailed downscalings of future climate change**

Following on the verification of the detailed CCAM downscalings of present-day climate over eastern South Africa, similarly detailed projections of future climate change were obtained for the region. The projections were performed for the period 1961-2100 and for both low and high mitigation emission scenarios. For each mitigation scenario, six GCMs were downscaled to 8 km resolution over eastern South Africa, through a multiple-nudging procedure. The first step in the downscaling procedure involved obtaining the 50 km resolution global simulations for CORDEX, as described in Chapter 2. The CORDEX simulations then subsequently provided the boundary conditions for the 8 km resolution downscalings to be obtained.

The resulting set of projections is the most detailed ever obtained for the mega-dam region of eastern South Africa, and a potentially important contribution towards understanding the range of potential climate change impacts over this region. As for the present-day climate downscalings of ERA data described in section 3.2, CCAM was integrated in stretched-grid mode over eastern South Africa, at a resolution of about 8 km (0.08° degrees in latitude and longitude). The high resolution part of the model domain was about 2000 x 2000 km<sup>2</sup> in size – somewhat larger than the domain used in the ERA reanalysis downscalings. The higher resolution simulations were nudged within the quasi-uniform global CORDEX simulations, through the application of a digital filter using a 600 km length scale. The filter was applied at six-hourly intervals and from 900 hPa upwards.

In the remainder of this chapter we select for analysis a domain covering the mega-dam region of the South Africa – all graphics shown represent averages taken over the domain 22°E to 33°E and 35°S to 27°S. As before, to this region will be referred to in the chapter as the “mega-dam domain” or the “mega-dam region”.

### **3.6 Results: detailed projections of future climate change**

The model integrations performed at a resolution of 8 km over eastern South Africa offer a number of advantages over the 50 km resolution simulations. Firstly, convective rainfall is partially resolved in the 8 km simulations, implying that the model is less dependent on statistics to simulate this intricate aspect of the atmospheric dynamics and physics. Secondly, important topographic features such as the eastern escarpments (in particular the Drakensberg mountains) are much better resolved in the 8 km resolution simulations, implying that the topographic forcing of temperatures, wind patterns and convective rainfall can be simulated more realistically. The 8 km resolution results represented here may therefore be regarded as providing a most informative, novel view on the futures of extreme weather events over eastern South Africa under climate change. In this section the projected changes in a number of climatological variables, including extreme weather-events metrics, are presented. For each of the metrics under consideration, the simulated baseline (climatological) state over eastern Africa calculated for the period 1961-1990 is shown in a first

figure (note that the median of the six downscalings is shown in this case). The projected changes in the metric are subsequently shown, for the time-slab 2021-2050 relative to the baseline period 1961-2000, first for RCP8.5 (low mitigation) and then for RCP4.5 (high mitigation). Three figures are presented for each metric for each RCP, for the 10th, 50th (median) and 90th percentiles of the ensemble of projected changes under the RCP. In this way, it is possible to gain some understanding of the uncertainty range that is associated with the projections. A list of the climate metrics analyzed is provided in Table 3.3.

**Table 3.3:** Relevant climate variables

Variable	Description and/or units
Average temperature	°C
Minimum temperature	°C
Maximum temperature	°C
Rainfall	Mm
Extreme rainfall (also a proxy for lightning)	More than 20 mm of rain falling within 24 hrs over an area of 64 km <sup>2</sup> . Units are number of events per grid point per year.

### 3.6.1 Average temperature

The model-simulated annual average temperatures (°C) are displayed in Figure 3.10a for the baseline period 1961-1990. The coolest conditions occur over the eastern escarpment regions of the domain. The hottest regions are simulated to occur along the east coast of KwaZulu-Natal.

- Rapid rises in the annual-average near-surface temperatures are projected to occur over southern Africa during the 21st century – temperatures over the South African interior are projected to rise at about 1.5 to 2 times the global rate of temperature increase (Engelbrecht et al., 2015).
- For the period 2021-2050 relative to the period 1961-1990, under low mitigation, temperature increases of 1 to 2.5°C may plausibly occur over the southern coastal regions. Over the interior regions larger temperature increases are likely, which may well exceed 3°C over the northern parts (Figure 3.10b).
- Under modest-high mitigation, temperature increases over eastern South Africa will be somewhat less, but may still reach 3°C over the northern interior (Figure 3.10b).
- For the period 2070-2099 relative to the period 1961-1990 under low mitigation, temperature increases of 2-3°C are plausible to occur over the southern coastal regions (Figure 3.10a). Over the interior temperature increases of more than 4°C are likely, and may well exceed 7°C over the northern interior. Such drastic temperature increases would have significant impacts on numerous sectors, including agriculture, water and energy. Under modest-high mitigation, temperature increases may still be significantly reduced, plausibly to less than 2-4°C even over the interior – with only a minority of downscalings indicative of temperature increases exceeding 4°C over the northern interior.
- Increasing average temperatures over eastern South Africa may plausibly increase evaporation from South Africa’s mega-dams.

tave 50 perc

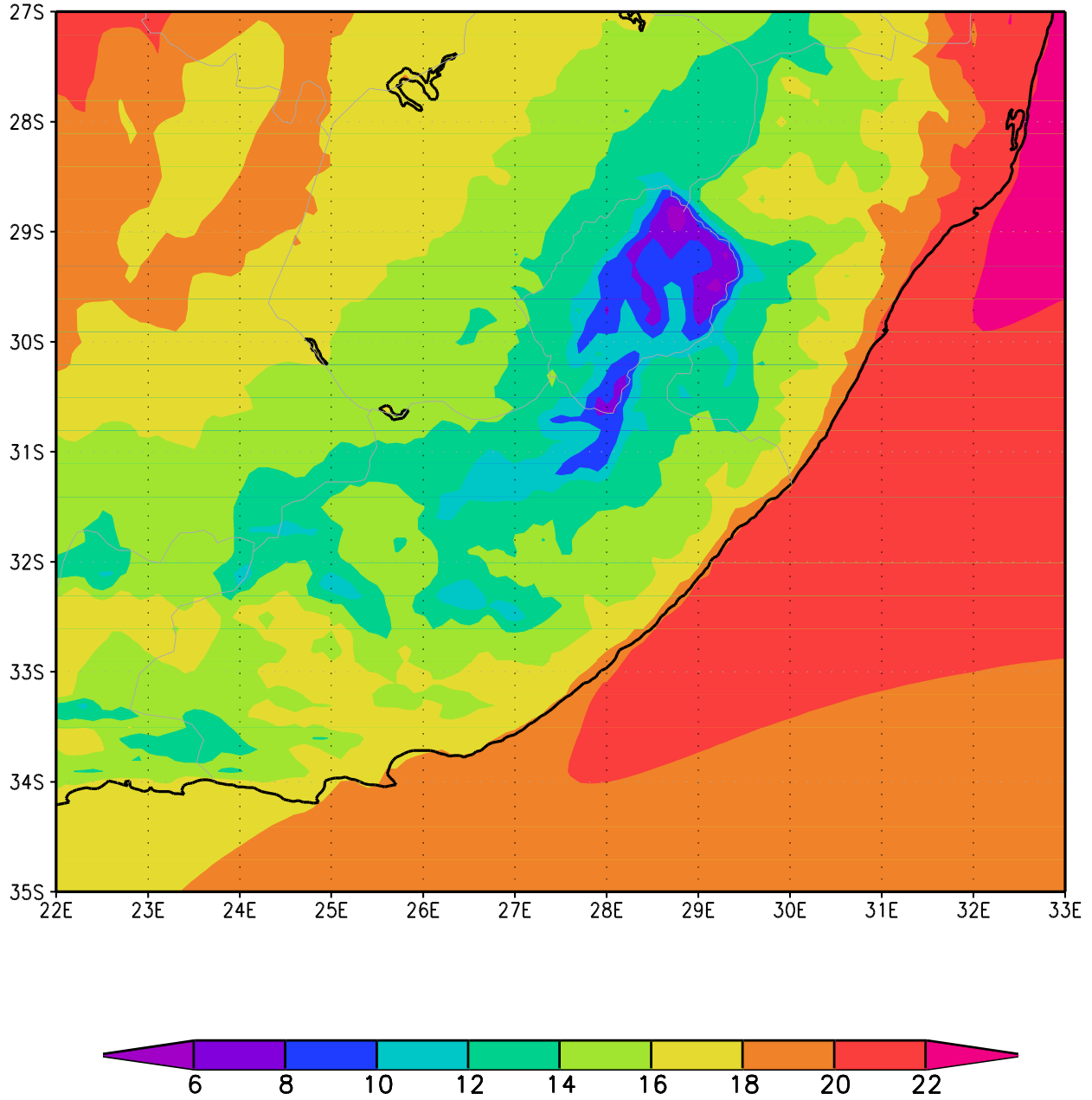


**Figure 3.10a:** CCAM simulated annual average temperature (°C) over eastern South Africa at 8 km resolution, for the baseline period 1961-1990. The median of simulations is shown for the ensemble of downscalings of six GCM simulations.

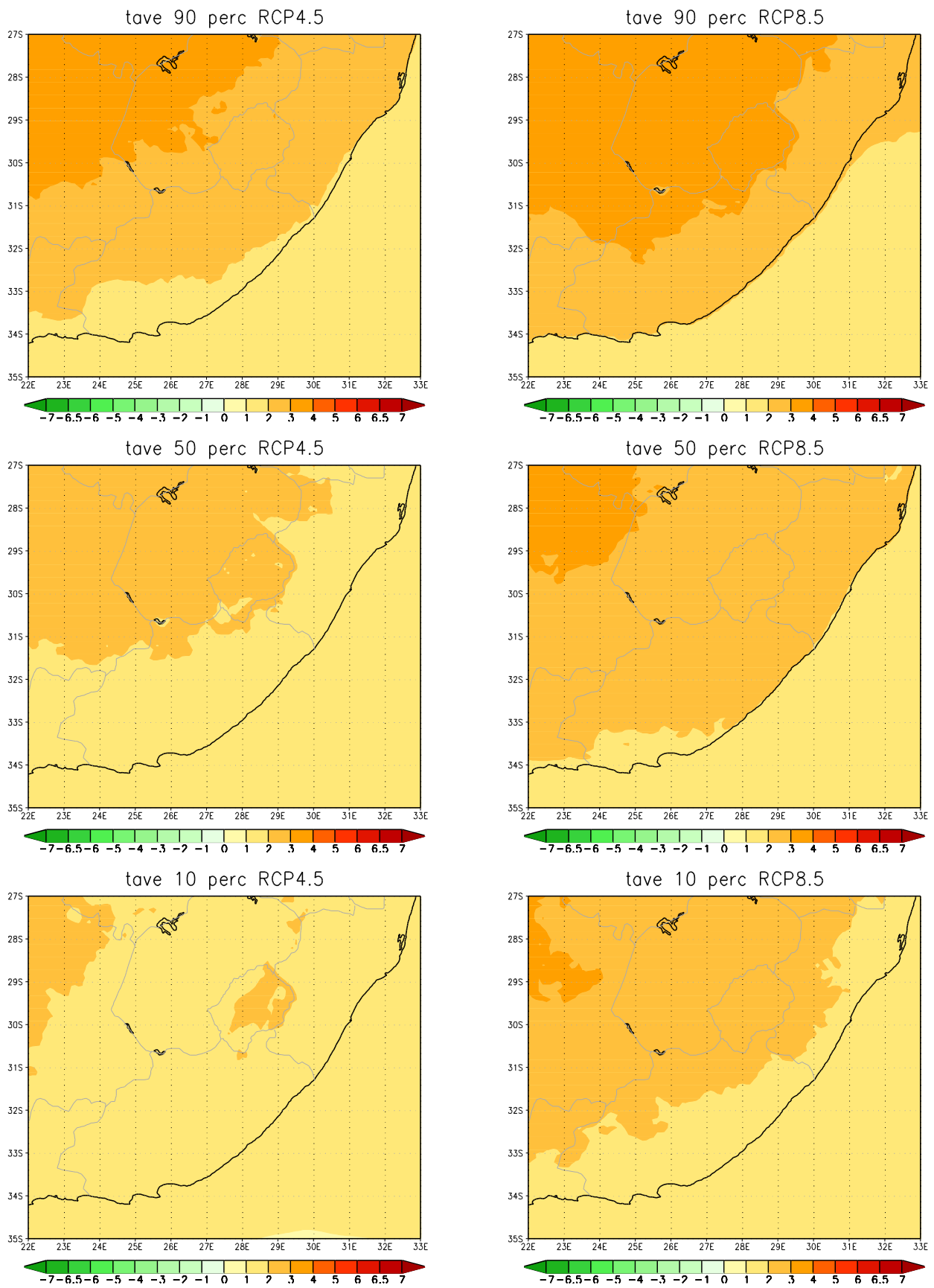


**Figure 3.10b** CCAM projected change in the annual average temperature ( $^{\circ}\text{C}$ ) over eastern South Africa at 8 km resolution, for the time-slab 2021-2050 relative to 1961-1990. The 10th, 50th and 90th percentiles are shown for the ensemble of downscalings of six GCM projections under RCP4.5 (left) and RCP8.5 (right).

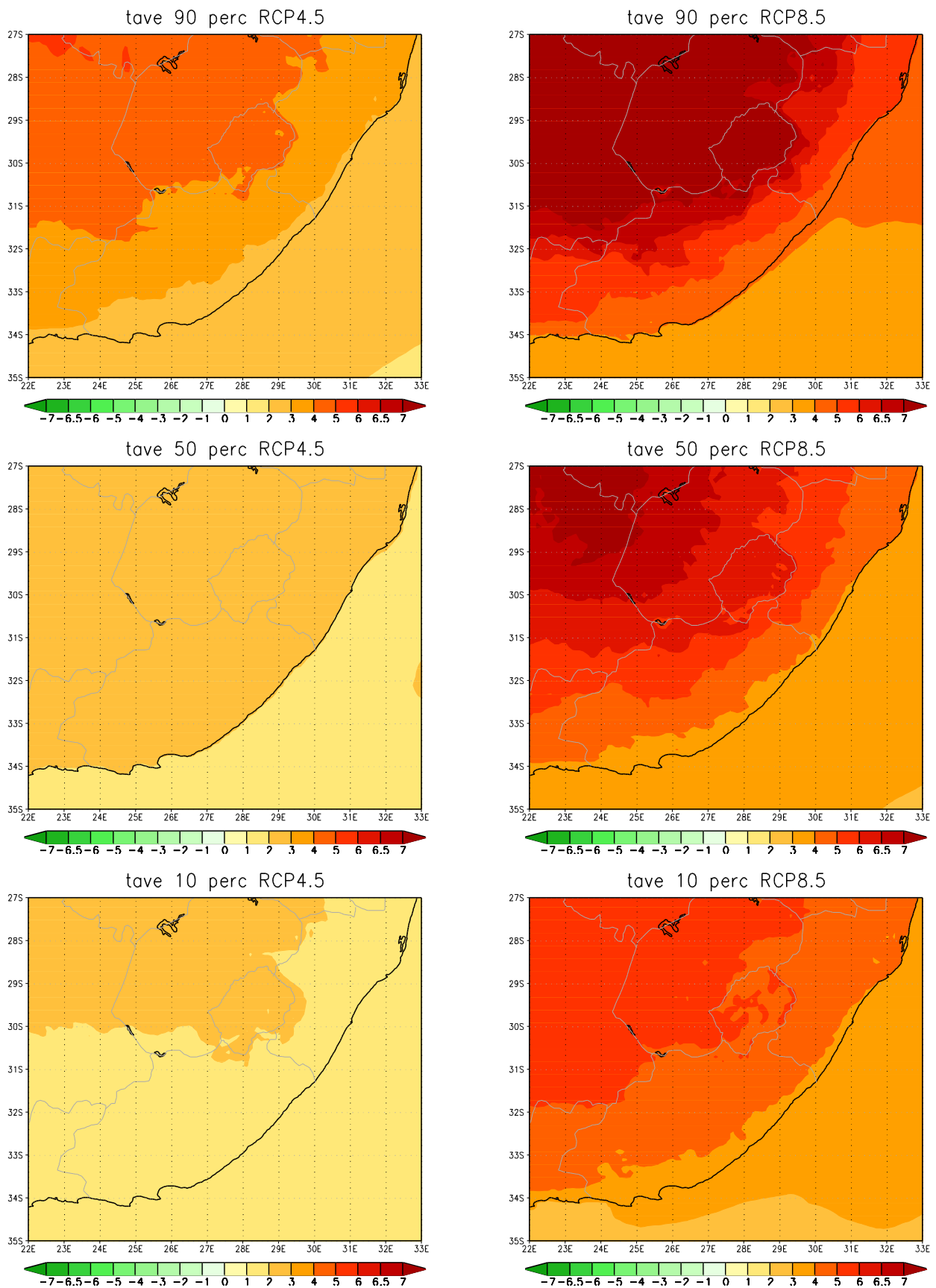


**Figure 3.10c:** CCAM projected change in the annual average temperature ( $^{\circ}\text{C}$ ) over eastern South Africa at 8 km resolution, for the time-slab 2070-2099 relative to 1961-1990. The 10th, 50th and 90th percentiles are shown for the ensemble of downscalings of six GCM projections under RCP4.5 (left) and RCP8.5 (right).

### 3.6.2 Maximum temperature

The model-simulated and bias-corrected annual average maximum temperatures (°C) are displayed in Figure 3.11a for the baseline period 1961-1990. The lowest maximum temperatures occur over Lesotho. The hottest regions are occur over the western part of the domain, in the Northern Cape.

- Rapid rises in the annual average maximum temperature are projected to occur over southern Africa during the 21<sup>st</sup> century – temperatures over the South African interior are projected to rise at about twice the global rate of temperature increase.

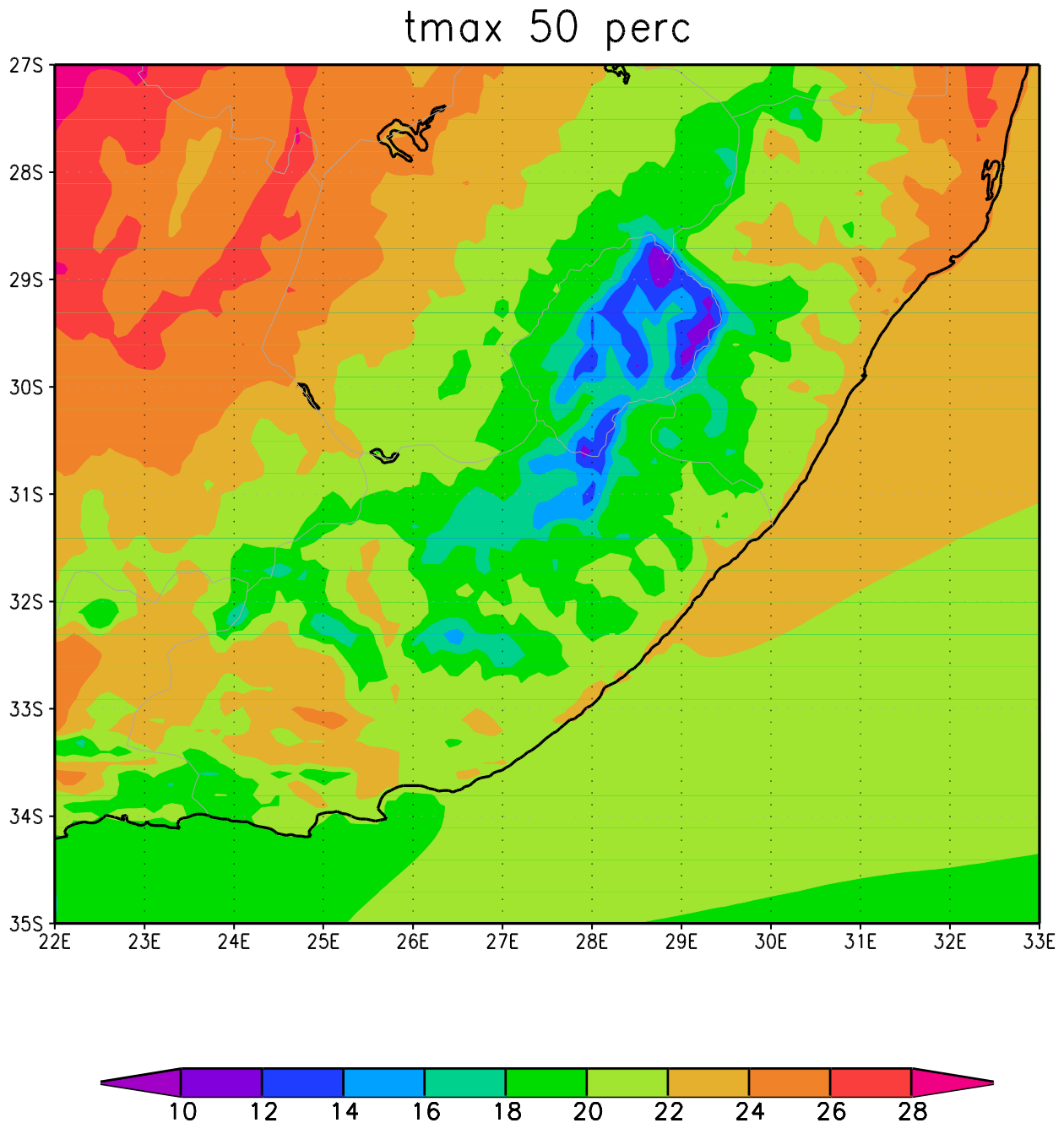


**Figure 3.11a:** CCAM simulated annual average maximum temperature (°C) over eastern South Africa at 8 km resolution, for the baseline period 1961-1990. The median of simulations is shown for the ensemble of downscalings of six GCM simulations.

- For the period 2021-2050 relative to the period 1961-1990, maximum temperature increases may 3°C over much of the northern interior of eastern South Africa (Figure 3.10b), with smaller increases plausible over the southern parts (less than 2°C over the Cape south coast).

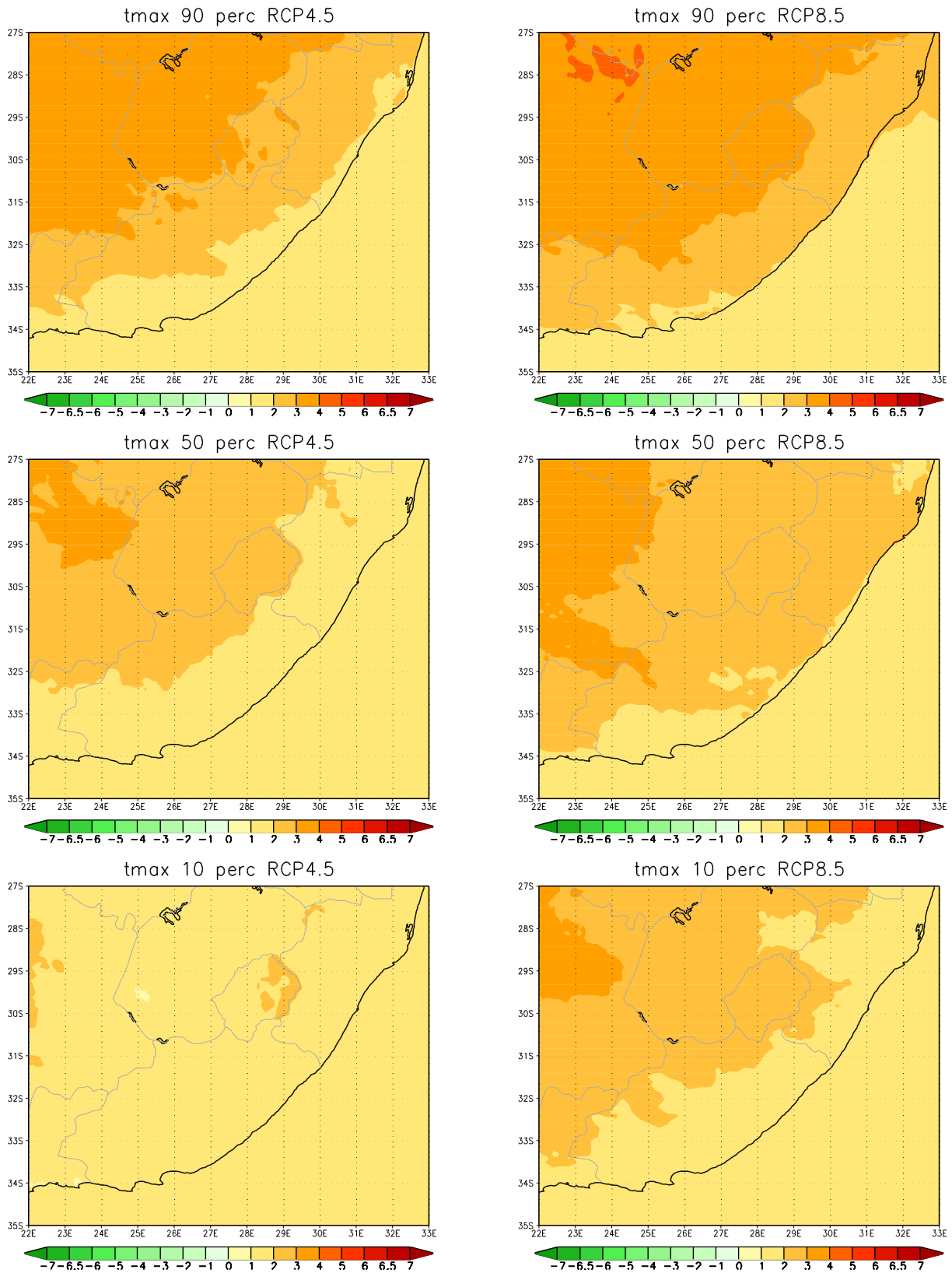


**Figure 3.11b:** CCAM projected change in the annual average maximum temperature (°C) over eastern South Africa at 8 km resolution, for the time-slab 2021-2050 relative to 1961-1990. The 10<sup>th</sup>, 50<sup>th</sup> and 90<sup>th</sup> percentiles are shown for the ensemble of downscalings of six GCM projections under RCP4.5 (left) and RCP8.5 (right).

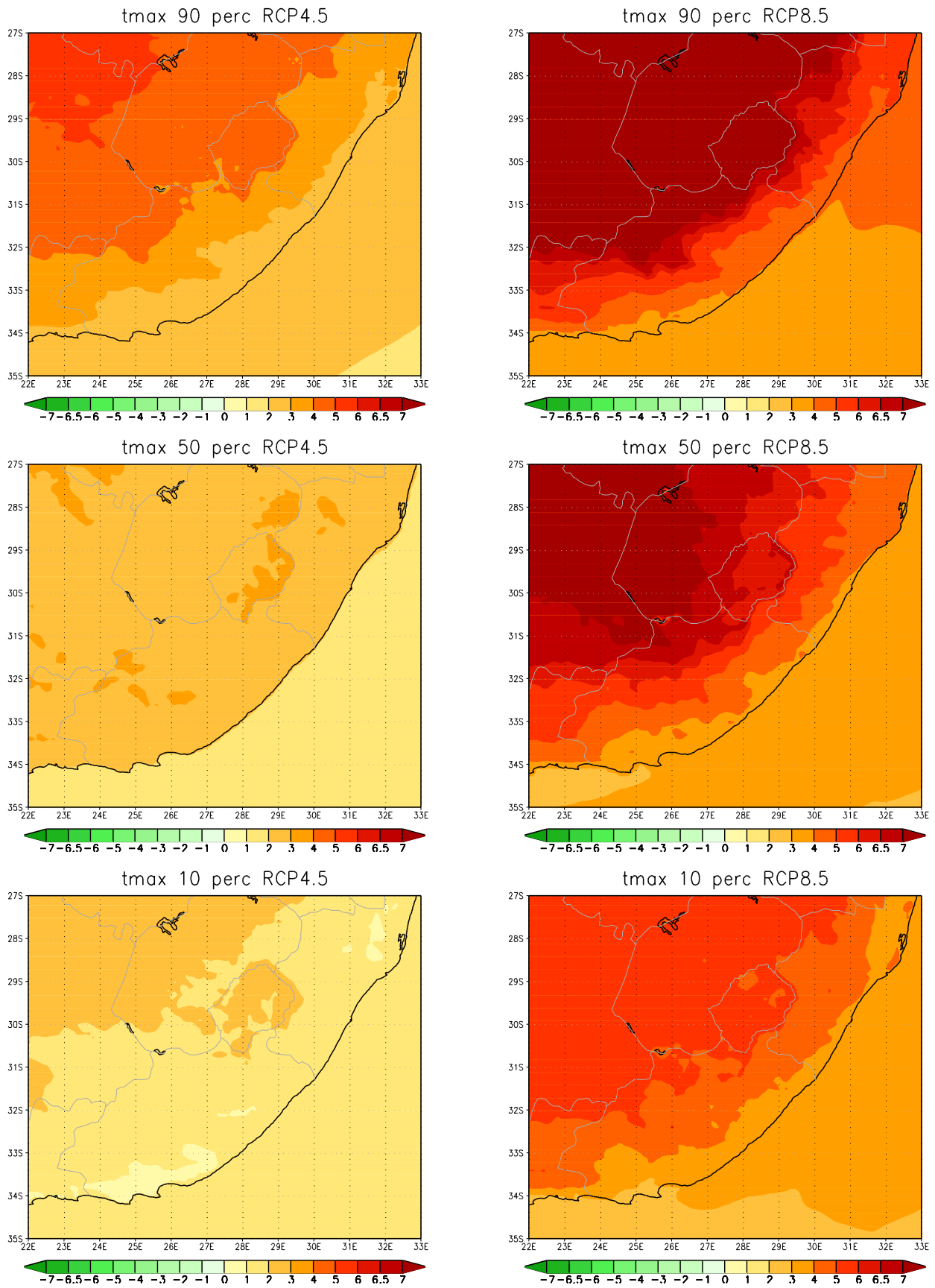


**Figure 3.11c:** CCAM projected change in the annual average maximum temperature (°C) over eastern South Africa at 8 km resolution, for the time-slab 2021-2050 relative to 1961-1990. The 10<sup>th</sup>, 50<sup>th</sup> and 90<sup>th</sup> percentiles are shown for the ensemble of downscalings of six GCM projections *under RCP4.5 (left) and RCP8.5 (right)*.

- Under modest-high mitigation, maximum temperature increases over South Africa will be very similar for the mid-future compared to the low mitigation case (Figure 3.11b).
- For the period 2070-2099 relative to the period 1961-1990, maximum temperature increases are projected to exceed 4°C over most of the interior (Figure 3.11c), and may indeed exceed 7°C over parts of the northern interior. Under modest-high mitigation maximum temperature increases may still reach 4°C over parts of the northern interior (Figure 3.11c), but the temperature increases are in general significant less than for the low mitigation case.
- Under both low and high mitigation, maximum temperatures are projected to rise faster than minimum temperatures.
- The projected drastic temperature increases under particularly low mitigation may have significant impacts on many sectors, including agriculture (e.g. crop yield and livestock mortality rates), energy demand (an increased need for cooling to achieve human comfort is plausible, particularly in summer) and possibly also on water security (through increased evaporation rates in the mega-dam region).

### 3.6.3 Minimum temperature

The model-simulated and bias-corrected annual average minimum temperatures (°C) are displayed in Figure 3.12a for the baseline period 1961-1990. The coolest conditions occur over the escarpment regions of eastern South Africa. The regions with the highest minimum temperatures are the east coast of KwaZulu-Natal.

- Rapid rises in the annual average minimum temperature are projected to occur over southern Africa during the 21<sup>st</sup> century – minimum temperatures over the South African interior are projected to rise at about 1.5 to 2 times the global rate of temperature increase.
- For the period 2021-2050 relative to the period 1961-1990, minimum temperature increases of 2 to 3°C are projected to occur over eastern South Africa under low mitigation (Figure 3.12b).
- Under high mitigation, minimum temperature increases over eastern South Africa are projected to be very similar than for the low mitigation case, except along the south and east coast regions where smaller increases are plausible (Figure 3.12b).
- For the period 2071-2099 relative to the period 1961-1990, minimum temperature increases of more than 4°C are projected to occur over much of the interior under low mitigation (Figure 3.12c). These increases may well exceed 7°C over parts of the northern interior. Smaller changes are projected only for the southern coastal regions. Under modest-high mitigation, minimum temperature increases may likely be reduced to less than 3°C over much of eastern South Africa, although a minority of downscalings still indicating increases as high as 4°C over the northern interior (Figure 3.12c).
- The projected minimum temperature increases may have significant impacts on energy demand – that is, the household demand for energy during winter (warming need) may be expected to decrease. Rising minimum temperatures are also associated with a decrease in a number of days with frost, with implications for agriculture and bush encroachment.

### 3.6.4 Rainfall

The model-simulated annual average rainfall totals (mm) are displayed in Figure 3.13a, for the baseline period 1961-2000. There is a pronounced west-east rainfall gradient over the country. Over the eastern escarpment and east coast the simulated annual rainfall totals exceed 1000 mm.

- A general decrease in rainfall is plausible over southern Africa under enhanced anthropogenic forcing (e.g. Christensen et al., 2007; Engelbrecht et al., 2009).
- For the period 2021-2050 relative to the period 1971-2000, under low mitigation, rainfall is projected to increase over the central interior and east coast. A minority of ensemble members project general rainfall increases over eastern South Africa (Figure 3.13b). The western interior, is projected to become generally drier by most ensemble members.
- The projected changes in rainfall patterns under high mitigation are very similar to the patterns projected under low mitigation (Figure 3.13b).

## tmin 50 perc

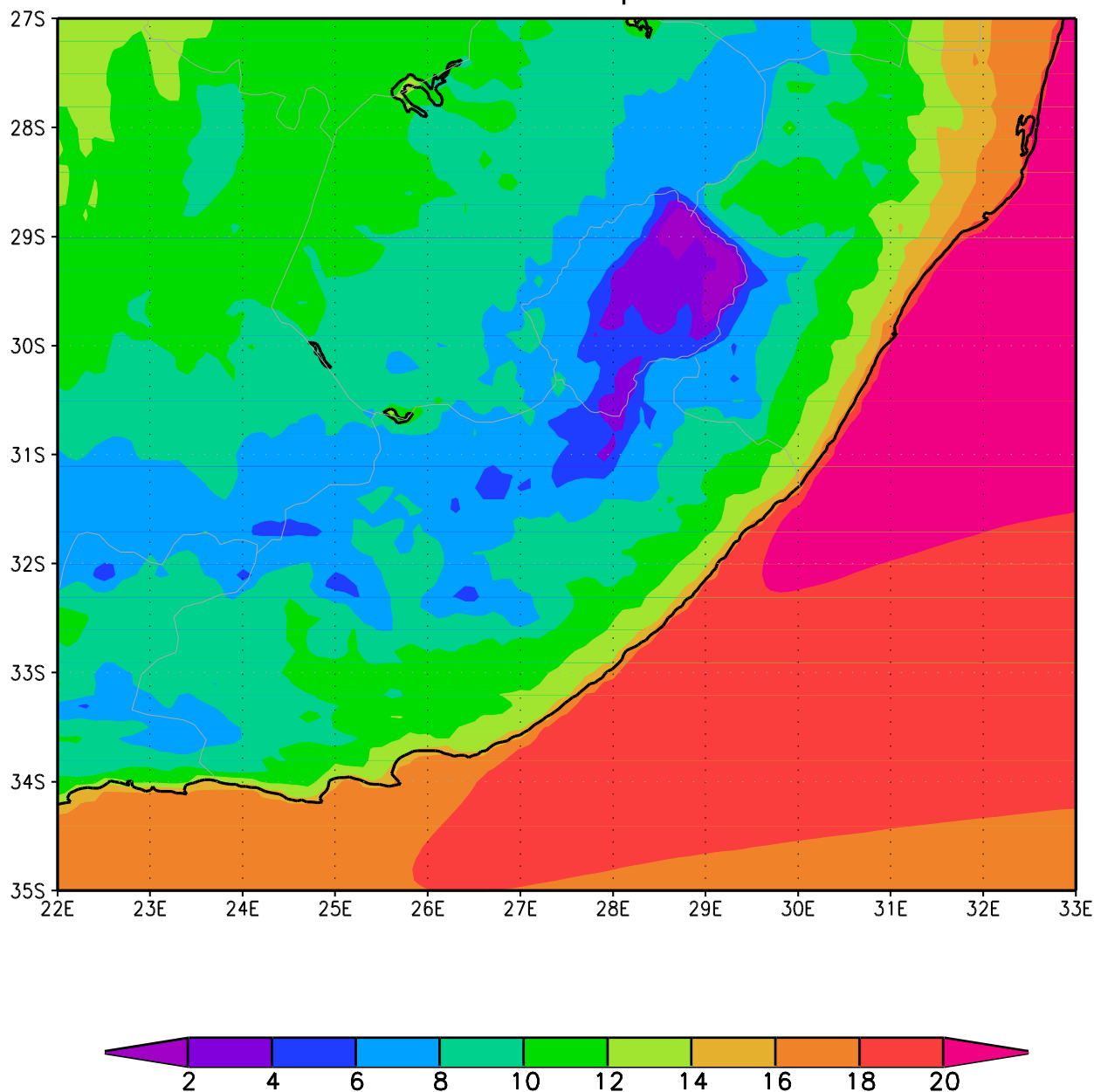


**Figure 3.12a:** CCAM simulated annual average minimum temperature ( $^{\circ}\text{C}$ ) over eastern South Africa at 8 km resolution, for the baseline period 1961-1990. The median of simulations is shown for the ensemble of downscalings of six GCM simulations.

- For the period 2070-2099 relative to the period 1961-1990, under low mitigation, rainfall is projected to decrease over the central interior and east coast of eastern South Africa by most ensemble members (Figure 3.13c). In fact, the pattern of change closely resembles that of the 202-2050 period. A minority of ensemble members project general rainfall increases over eastern South Africa, but most ensemble members project rainfall decreases over the western parts of the region (Figure 3.13c). The projected changes in rainfall patterns for 2070-2099 under high mitigation is very similar to the patterns projected under low mitigation (Figure 3.13c).
- The projected changes in rainfall patterns over eastern South Africa in the ensemble of downscalings described here, and more generally in AR4 and AR5 projections, display more uncertainty than in the case of projected changes in temperature. This implies that adaptation policy makers need to take into account a range of different rainfall futures, often of different signal (i.e. drier and wetter) during the decision making process.

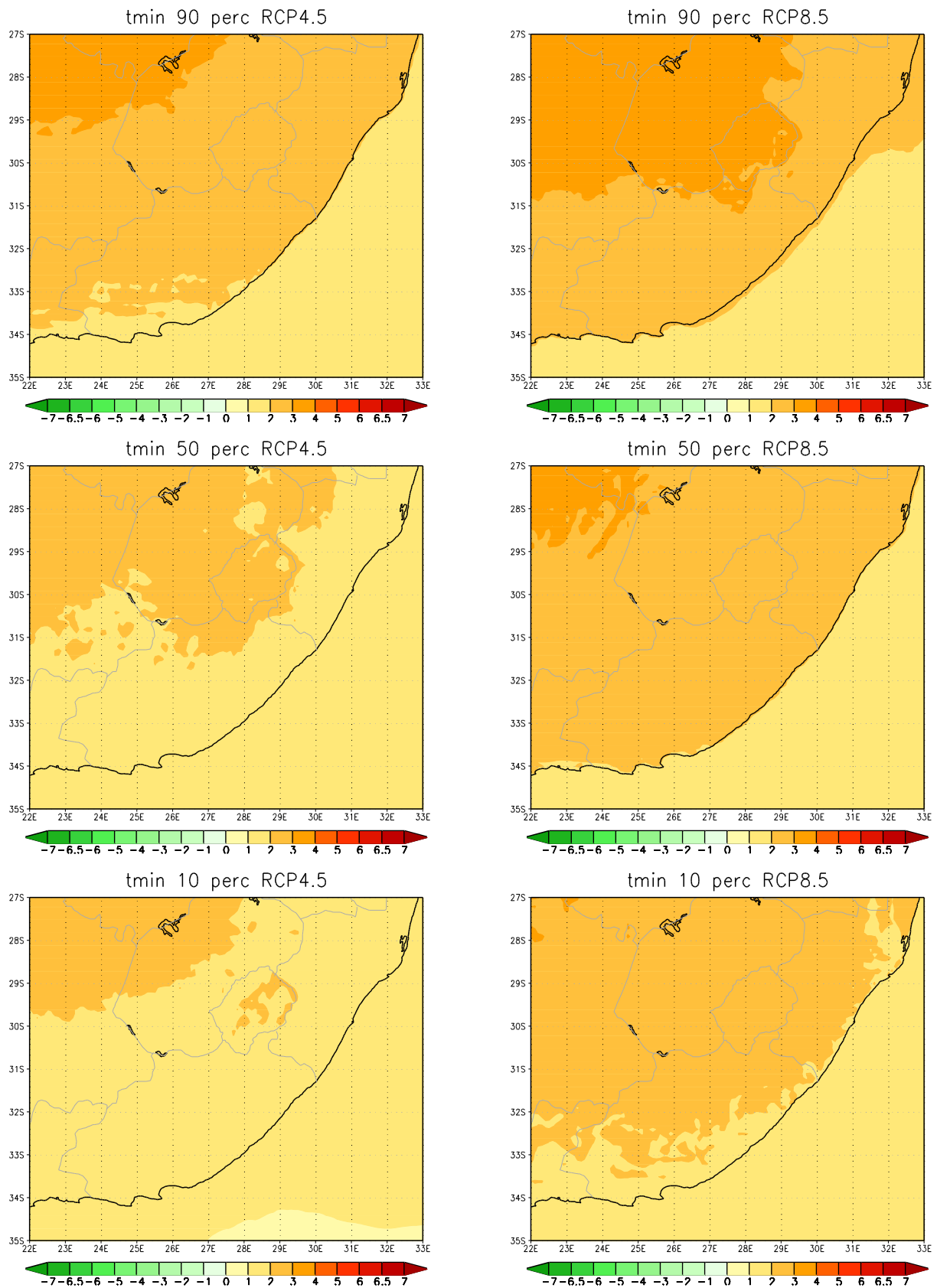


**Figure 3.12b:** CCAM projected change in the annual average minimum temperature (°C) over eastern South Africa at 8 km resolution, for the time-slab 2021-2050 relative to 1961-1990. The 10<sup>th</sup>, 50<sup>th</sup> and 90<sup>th</sup> percentiles are shown for the ensemble of downscalings of six GCM projections under RCP4.5 (left) and RCP8.5 (right).

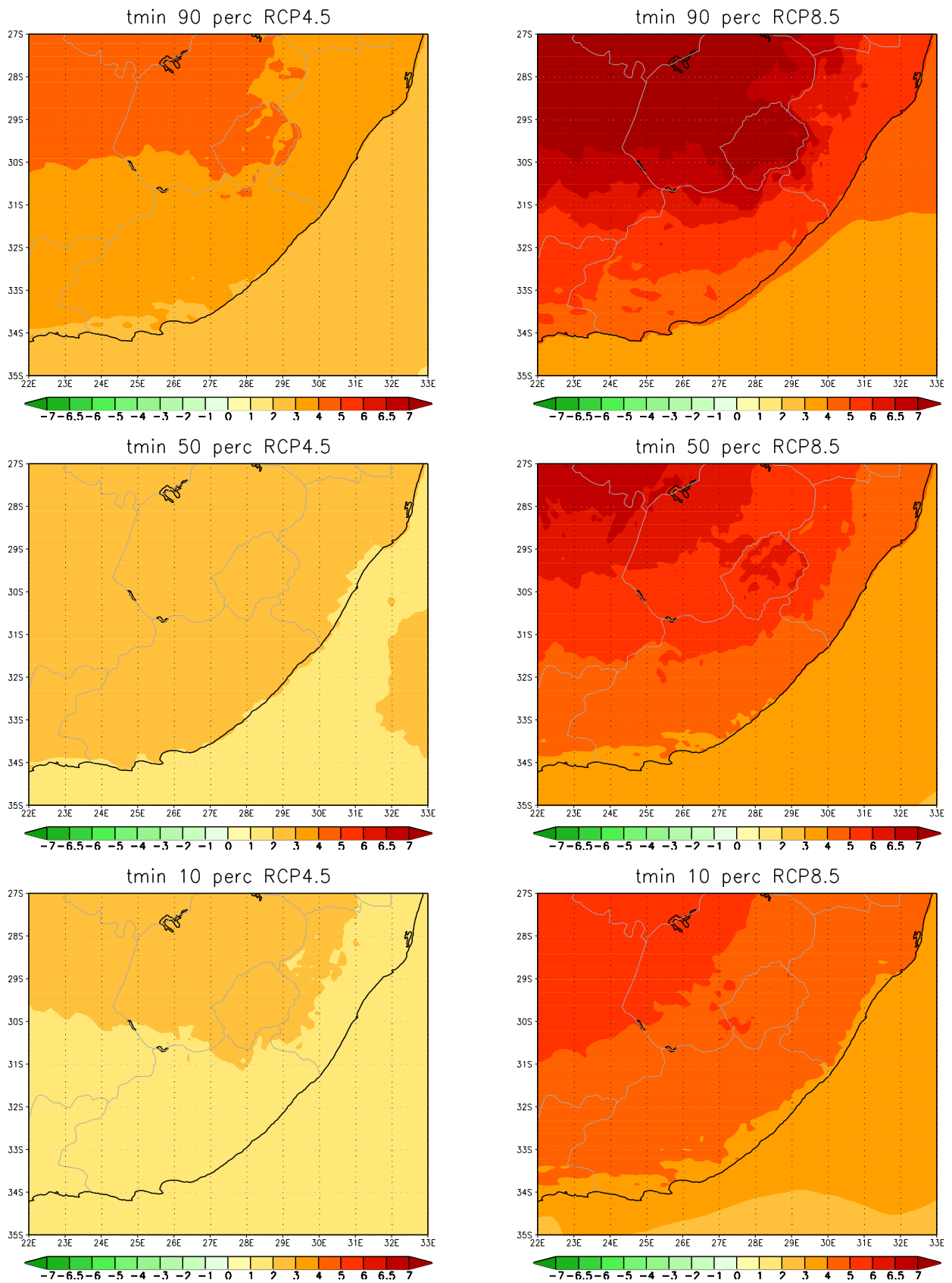


**Figure 3.12c:** CCAM projected change in the annual average minimum temperature ( $^{\circ}\text{C}$ ) over eastern South Africa at 8 km resolution, for the time-slab 2070-2099 relative to 1961-1990. The 10<sup>th</sup>, 50<sup>th</sup> and 90<sup>th</sup> percentiles are shown for the ensemble of downscalings of six GCM projections under RCP4.5 (left) and RCP8.5 (right).

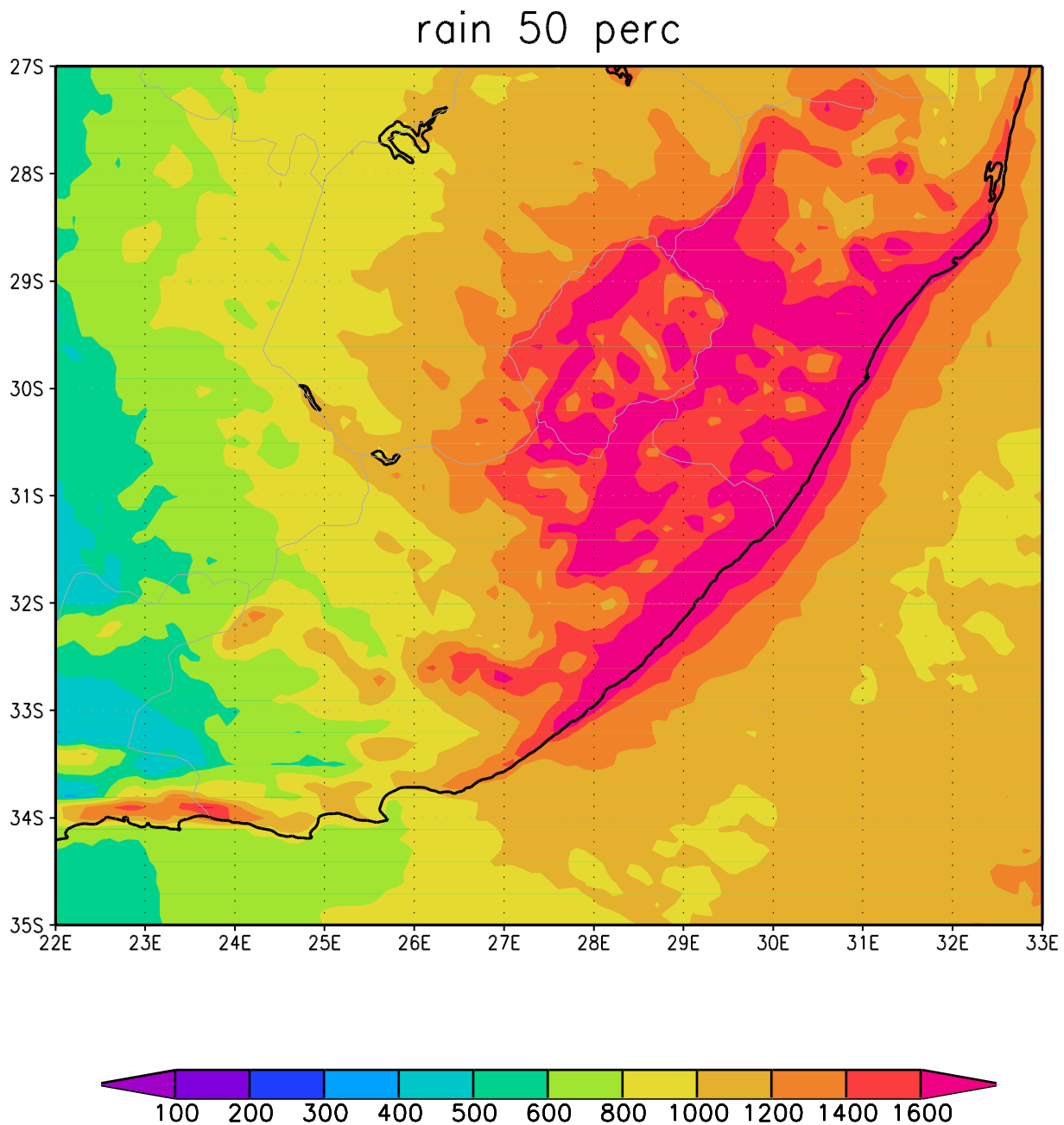


**Figure 3.13a:** CCAM simulated annual average rainfall totals (mm) over eastern South Africa, for the baseline period 1961-1990 at 8 km resolution. The median of simulations is shown for the ensemble of downscalings of six GCM simulations.

### 3.6.5 Extreme rainfall events

The model-simulated annual average extreme rainfall event frequencies (units are number of events per model grid box per year) are displayed in Figure 3.14a, for the baseline period 1971-2000. Here an extreme rainfall event is defined as 20 mm of rain occurring within 24 hours over an area of 64 km<sup>2</sup>). Over the east coast and eastern escarpment regions more than 10 extreme rainfall events are simulated occur annually, on the average.

- Consistent with the projected decreases in rainfall, extreme rainfall events are projected to increase in frequency over most of the central interior and east coast of eastern South Africa under low mitigation, for the period 2021-2050 relative to 1961-1990, by most ensemble members (Figure 3.14b). A minority of ensemble members project increases in extreme rainfall events over most of eastern South Africa (Figure 3.14b).

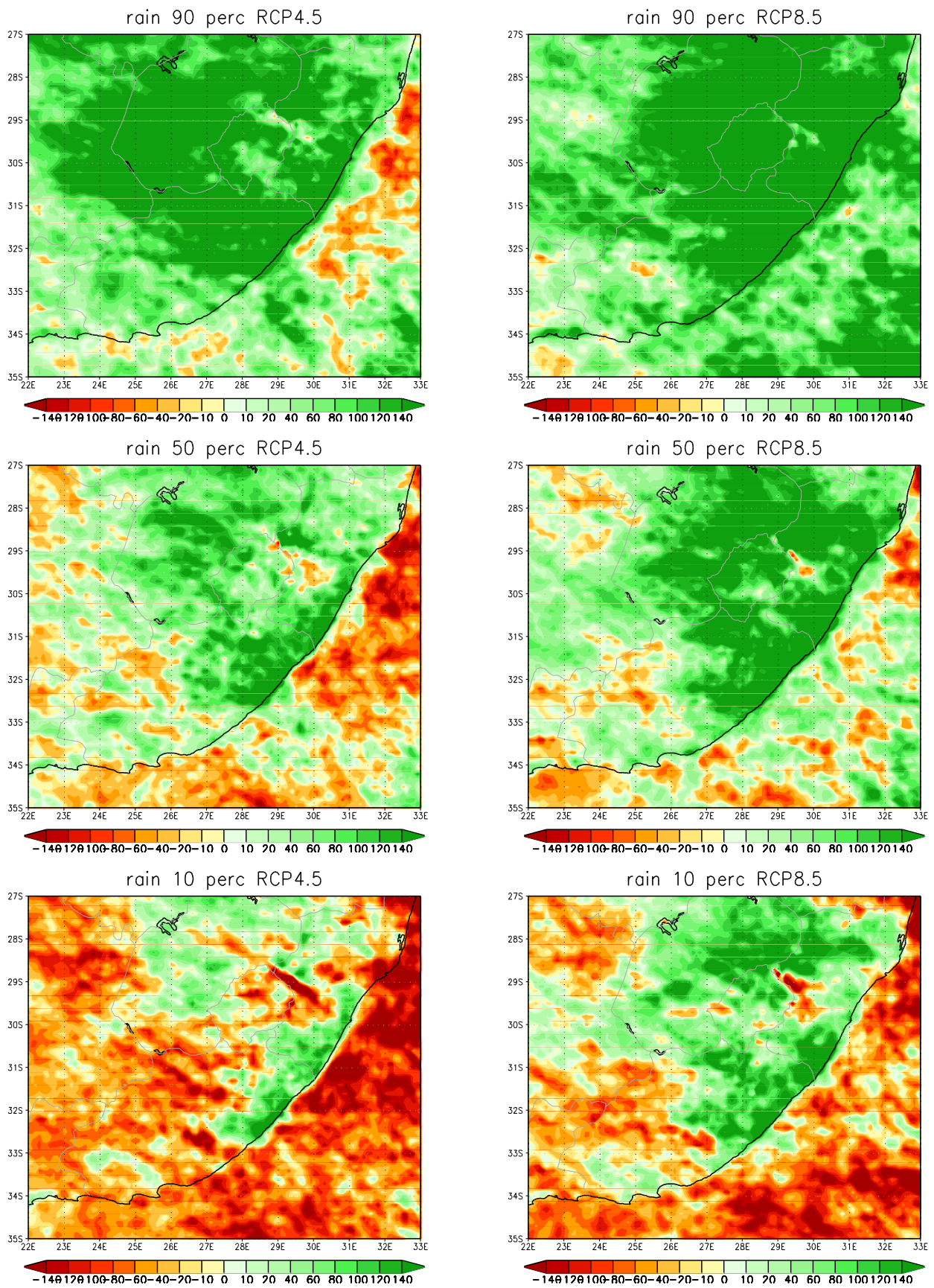


**Figure 3.13b:** CCAM projected change in the annual average rainfall totals (mm) over eastern South Africa at 8 km resolution, for the time-slab 2021-2050 relative to 1961-1990. The 10<sup>th</sup>, 50<sup>th</sup> and 90<sup>th</sup> percentiles are shown for the ensemble of downscalings of six GCM projections under RCP4.5 (left) and RCP8.5 (right).

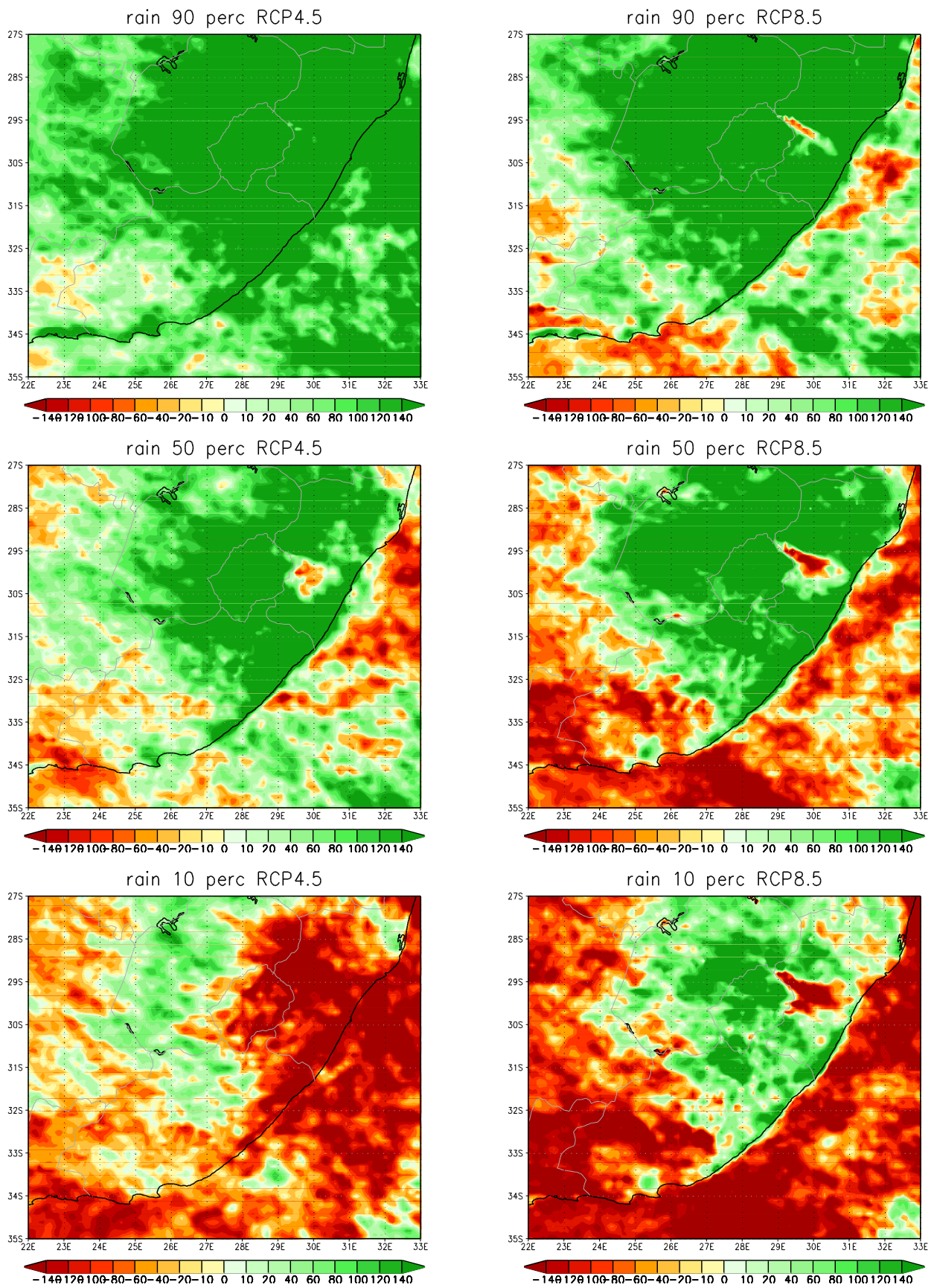


**Figure 3.13c:** CCAM projected change in the annual average rainfall totals (mm) over eastern South Africa, for the time-slab 2071-2100 relative to 1961-1990. The 10<sup>th</sup>, 50<sup>th</sup> and 90<sup>th</sup> percentiles are shown for the ensemble of downscalings of six GCM projections under RCP4.5 (left) and RCP8.5 (right).

## rn de 50 perc

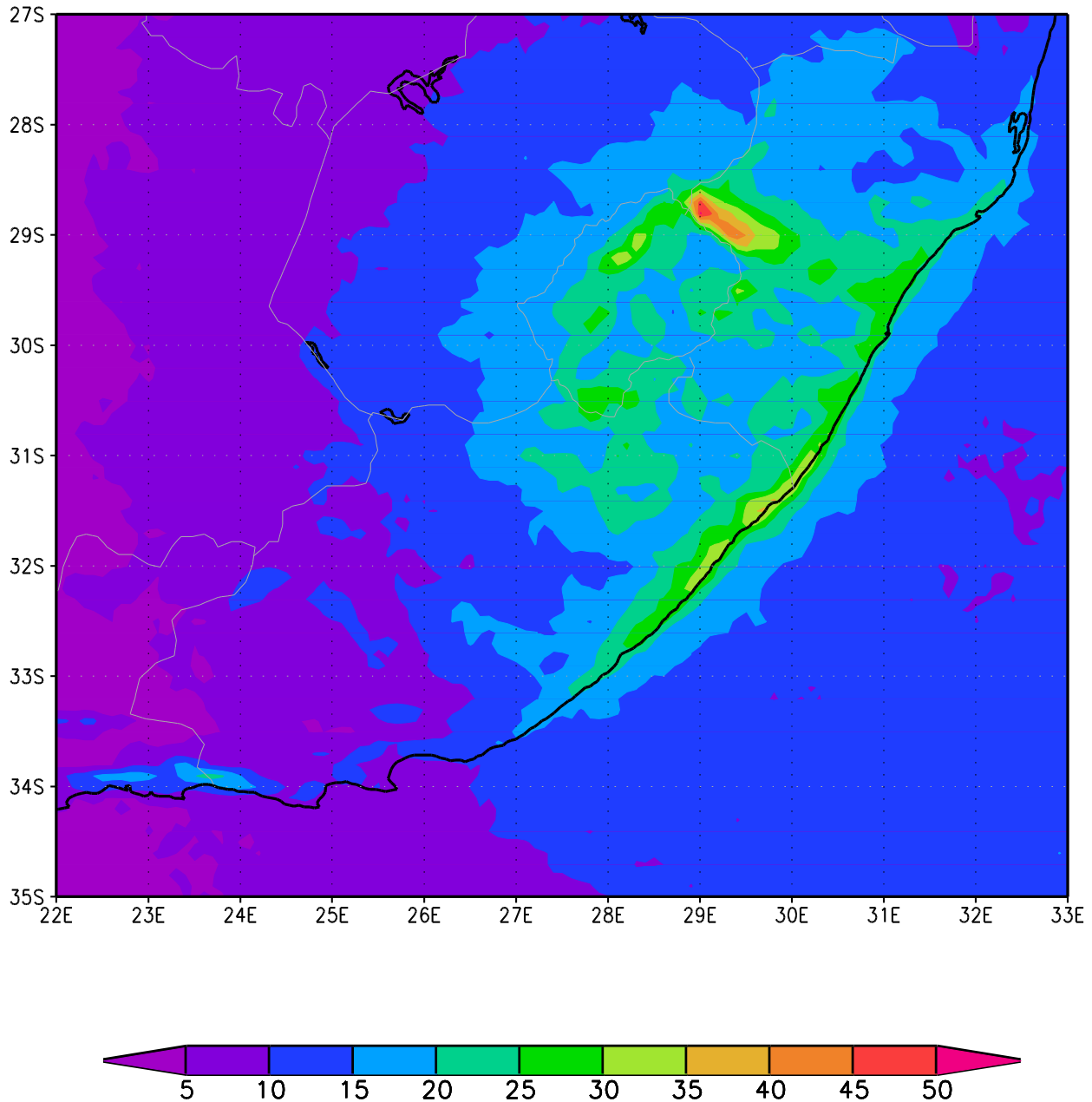


**Figure 3.14a:** CCAM simulated annual average number of extreme rainfall days (units are number of days per grid point per year) over eastern South Africa, for the baseline period 1961-1990. The median of simulations is shown for the ensemble of downscalings of six GCM simulations.

- Extreme rainfall events are also projected to decrease in frequency over most of eastern South Africa for the period 2070-2099, with the patterns of change very similar for the cases of low and high mitigation (Figure 3.14c). A minority of ensemble members project increases in extreme rainfall events over most of eastern South Africa (Figure 3.14c) for 2070-2099. The relatively large decreases in extreme rainfall events projected for Lesotho and the KwaZulu-Natal midlands may be important from the perspectives of run-off and water security.
- The projected changes in extreme rainfall events under high mitigation are very similar to the patterns projected under low mitigation (Figure 3.14c).
- Extreme rainfall events are mostly caused by intense thunderstorms, which are often also the cause of lightning, hail, damaging winds and flash floods. That is, the climate change

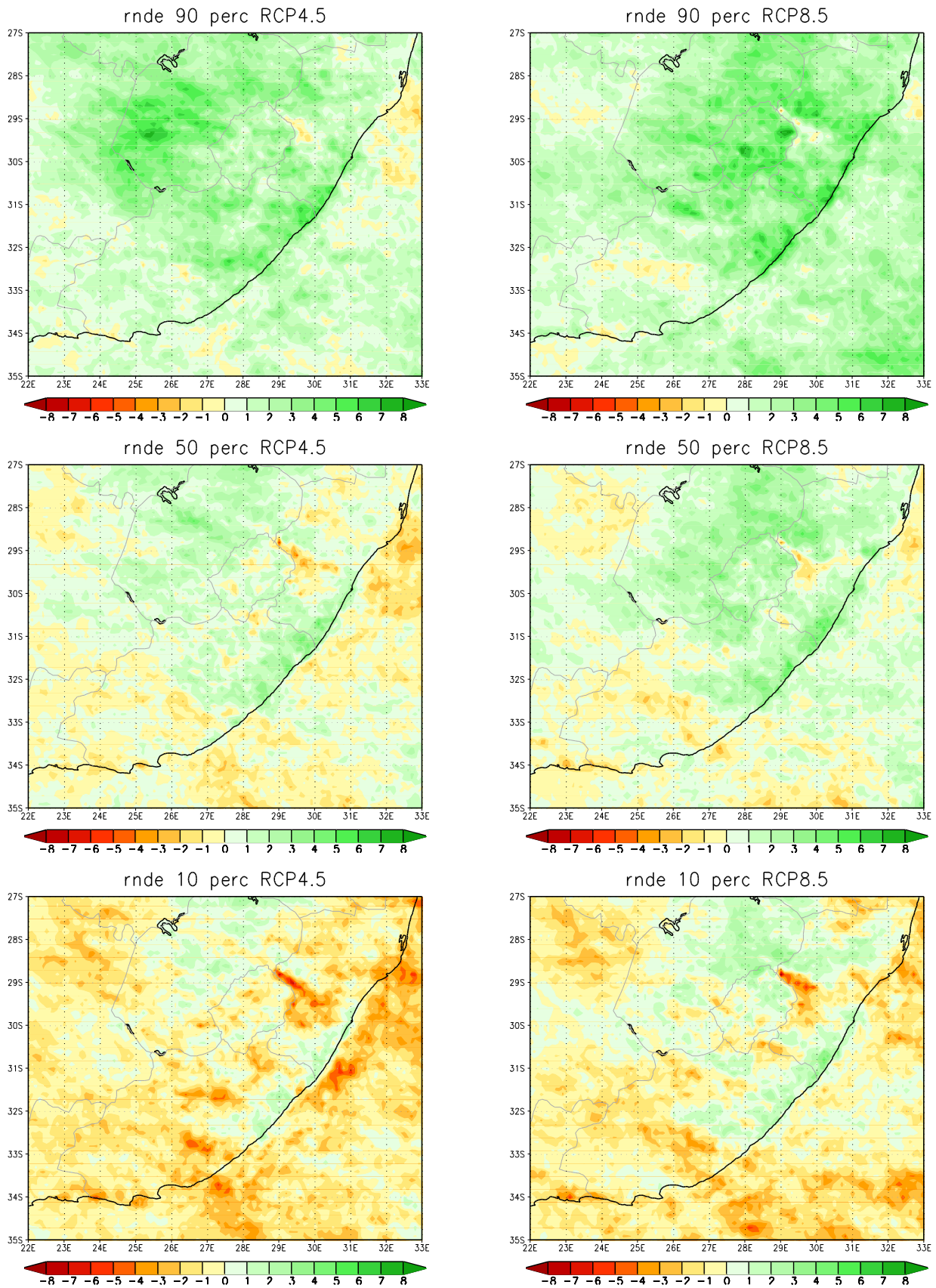


**Figure 3.14b:** CCAM projected change in the annual average number of extreme rainfall days (units are numbers of grid points per year) over eastern South Africa at 8 km resolution, for the time-slab 2021-2050 relative to 1961-1990. The 10<sup>th</sup>, 50<sup>th</sup> and 90<sup>th</sup> percentiles are shown for the ensemble of downscalings of six GCM projections under RCP4.5 and RCP8.5.

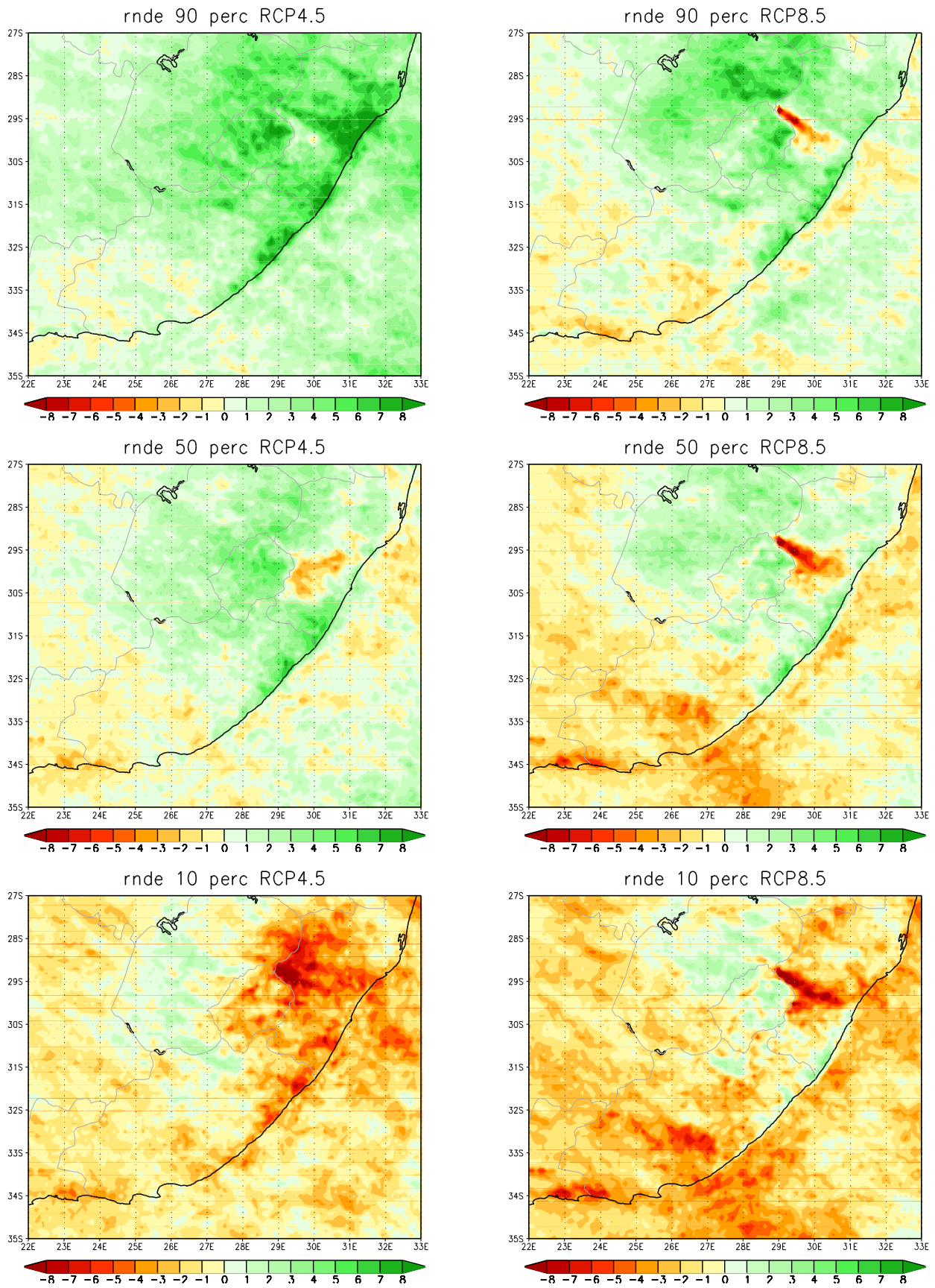


**Figure 3.14c:** CCAM projected change in the annual average number of extreme rainfall days (units are numbers of grid points per year) over eastern South Africa, for the time-slab 2071-2100 relative to 1961-1990. The 10<sup>th</sup>, 50<sup>th</sup> and 90<sup>th</sup> percentiles are shown for the ensemble of downscalings of six GCM projections under RCP4.5 (left) and RCP8.5 (right).

Projections analysed here are indicative that decreases in these hazardous storms are plausible over most of eastern South Africa, however, a minority of ensemble members are indicative of increases in such events. That is, adaptation policies need to take into account the possibility that extreme rainfall events over eastern South Africa may increase in their frequency of occurrence.

### **3.7 Summary of the detailed projections of future climate change**

This report is based on an ensemble of high-resolution projections of future climate change over eastern South Africa, obtained by using the regional climate model CCAM to downscale the output of a number of CMIP5 (AR5) GCMs over Africa. The projections downscaled represent both high (RCP4.5) and low (RCP8.5) mitigation scenarios. CCAM was applied at 50 km resolution globally, and the experimental design of the simulations is consistent with that of CORDEX. The 50 km resolution global simulations were subsequently downscaled to a resolution of 8 km over South Africa. These projections are the most detailed ever obtained for eastern South Africa. Many regional climate features, such as the high precipitation totals induced by the eastern escarpment, are well resolved in the 8 km resolution simulations.

The 8 km resolution projections are indicative of drastic temperature increases in near-surface temperatures and related extreme events over the mega-dam region. Already for the mid-future period of 2021-2050, high fire-danger days, heat-wave days and very hot days are likely to occur at unprecedented frequencies. The projected changes are similar for low (RCP8.5) and modest-high (RCP4.5) mitigation futures. The changes may reach devastating proportions by the far-future period (2071-2099) under low mitigation futures, at least in terms of impacts on agriculture. However, the modelling indicates that under modest-high mitigation, changes in temperature and related extremes are significantly mitigated for the far-future period. The projections also provide evidence of a plausible increase in extreme convective rainfall events over the central interior regions under climate change. Associated increases in streamflow may benefit water yield in the mega-dam region, although increases sedimentation may also result from the enhanced run-off. These aspects are explored in more detail in Chapter 5 of the report.

## Chapter 4 Climate variability and predictability over eastern South Africa under climate change

### 4.1 Introduction

Chapters 2 and 3 have explored the projected climate change futures of eastern South Africa under low and high mitigation futures. Such changes may occur through changes in precipitation and temperature as well as through their extremes including drought, heavy rainfall events, very hot days, heat-wave days and high fire-danger days. An important consideration implicit to the above, is how climate variability may change over eastern South Africa under climate change. The analysis in previous chapters have already revealed some insights into this question, most importantly perhaps the plausibility that multi-year droughts may occur more frequently over eastern South Africa by the mid-future period of 2046-2065. In this context, it is important to note that super El Niño events may occur more frequently under climate change, with a doubling of events plausible to occur even under 1.5°C of global warming (Wang et al., 2017). This is likely one of the reasons why most climate models are projecting the more frequent occurrence of drought over southern Africa (see Chapter 2). Moreover, despite the general decreases projected in average rainfall totals, increases in heavy rainfall events may occur over eastern South Africa under climate change (see Chapter 3). The changes, which may be described as plausible or likely in the case of drought, suggest that the skilful prediction of extreme events over eastern South Africa may become increasingly important as an adaptation tool to climate change (e.g. Winsemius, 2014; Bett et al., 2017; Clark et al., 2017). This in turn, raised the question whether climate change may change the predictability of anomalous weather events, at both short-range to seasonal time-scales. For example, with seasonal predictive skill over southern Africa depending largely on the ENSO signal (Landman and Beraki, 2012), any decreases in the strength or stability of the ENSO teleconnection to the region may impact negatively on the seasonal forecast skill. At shorter time-scales, more intense thunderstorms may occur more frequently in a changing climate, with detrimental effects on the skill of short-range deterministic forecasts if weather forecast models do not properly represent convection. This chapter thus explore whether the climate over eastern South Africa will become more variable under climate change, and how this may impact on short-range to seasonal predictability over the region.

It may be noted that the seasonal forecasting effort in South Africa goes back as early as the 1990s. Already then, a number of local institutions developed objective seasonal forecast techniques which were based entirely on statistical methods. A variety of forecasting systems were subsequently developed over the years, including systems that incorporated GCMs (e.g. Beraki et al., 2014, 2016) and statistical downscaling models (Landman and Beraki, 2012). Local seasonal forecasting efforts have recently been reviewed by Landman (2014). The seasonal forecasting effort in South Africa is motivated primarily by the fact that numerous observational and numerical studies have conclusively shown the existence of potential predictability over the region (e.g. Klopfer et al., 1998; Landman and Goddard, 2002; Tennant and Hewitson, 2002; Reason and Rouault, 2005). Most importantly, is that southern African climate variability is to some extent driven by the slowly evolving components of the climate system (Palmer and Anderson, 1994; Barnston et al., 1999). Most of the signature of these slowly evolving systems is thought to originate from the ocean and thus the interaction between the ocean and the atmosphere is of paramount importance in the context of seasonal predictions (Goddard et al., 2001).

This chapter also strives to further the seasonal prediction of climate variability over eastern South Africa, through the process of high-resolution dynamic downscaling. Dynamical downscaling from a seasonal forecast perspective over southern Africa was first attempted locally by Kgatuke et al. (2008) and more recently by Ratnam et al. (2016). As opposed to these previous studies, which used Limited Area Models (LAMs), our study employs the stretched-grid model CCAM (see Chapter 2 for the model description). Short-range predictability aspects is also explored using CCAM, implying that the same modelling system is applied seamlessly across the time-scales of short-range to seasonal prediction in the project.

## 4.2 Methodology

### 4.2.1 AMIP-style simulations as an upper boundary for seasonal forecast skill

This chapter relies heavily in the CSIR CORDEX simulations described in Chapter 2, as a baseline data set to explore climate variability over southern Africa under climate change. A second set of simulations was performed towards directly quantifying the predictability of streamflow over the mega-dam region. These simulations are Atmospheric Model Intercomparison Project (AMIP) style simulations. Here CCAM was forced at its lower boundary with observed monthly SST and sea-ice fields over the period 1978-2005. An ensemble of simulations was obtained, using a lagged-average forecasting approach, with each ensemble member initialised during a different day of February 1978. AMIP-simulations are thought to provide an estimation of the upper boundary of predictability of seasonal forecasts, since these simulations are forced with observed rather than predicted SSTs.

### 4.2.2 High-resolution CCAM seasonal forecasts

CCAM-CABLE was forced with predicted sea-ice concentration (SIC) and SSTs as acquired from the outputs of the SINTEX-F2v ensemble seasonal prediction system (Doi et al., 2014, 2016), based on the SINTEX-F2 CGCM (Sasaki et al., 2013, 2014, 2015). The atmospheric component is ECHAM5 (Roeckner et al., 2003), and the oceanic component is the Nucleus for European Modelling of the Ocean (NEMO) system (Madec 2006). We refer the reader to Doi et al. (2016) for complete description of the CGCM experimental design. The CCAM-CABLE retroactive experiment consists of 18 ensembles integrations of 6 months in length, which are built as a function of both atmospheric states (ICs) and boundary forcing (BCs; Beraki et al., 2016). This model configuration offers a better description of uncertainties that may arise from the initial and boundary forcings. The uncertainties that arise from the ICs are accounted for by taking 6 consecutive daily realistic atmospheric states back from the forecast date in each month and year. For the November hindcasts, for instance the atmospheric ICs cover the period from November 1 to 6 for 15 years starting from 2000 to 2014. To minimize potential climate drift, the CCAM-CABLE is nudged at its surface to the SINTEX-F2 CGCM SSTs, using the spectral nudging method of Thatcher and McGregor (2009, 2010). Furthermore, all climate simulations are forced by the time-varying CO<sub>2</sub> and ozone fields provided through the CMIP5 archive for the period 1870-2100. The atmospheric ICs are acquired from the NCEP (National Centers for Environmental Prediction), Department of Energy (DOE) Atmospheric Model Intercomparison Project (AMIP) II Reanalysis (R2) data set (Kanamitsu *et al.*, 2002). The NCEP/DOE atmospheric states are transformed to the CCAM CABLE quasi-uniform (C96) horizontal resolution (approximately 105 km<sup>2</sup>) and 25 vertical sigma layers similarly to Beraki et al. (2014).

Forcing CCAM-CABLE with all ensemble realizations of the SINTEX-F2 CGCM is computationally inhibiting. This is due to a double fold increase in the AGCM integrations by the size of atmospheric ICs as it is also important to account for uncertainties arising from the atmospheric states. Hence, the prescription of the SST scenarios follows a manner that optimizes the representation of the uncertainty envelope whilst also taking into account computational constraints. The background error here is estimated from the standard deviation of the 6 CGCM ensemble integrations and subsequently added/subtracted to the ensemble mean anomalies. It is also worth noting that the SIC and SST anomalies are superimposed to the AMIP observed climatology to minimize the biases in the boundary forcings (Beraki *et al.*, 2016; Ratnam *et al.*, 2017). In the CGCM experiment, as noted in Doi et al. (2016), uncertainties in ocean vertical mixing estimations, ocean physics is perturbed in two different ways by considering or neglecting ocean vertical mixing induced by small vertical-scale structures (SVSs) within and above the equatorial thermocline (Sasaki *et al.*, 2012). This similar paradigm also ensures the quantification of uncertainties of both initial conditions and model physics for forecasts.

The most striking advantage of the CCAM is that, as noted earlier, it embraces a dynamic kernel and physics all cast on a cube-based grid and can be applied either at quasi-uniform horizontal resolution to function as a global climate model, (here we use C96 resolution approximately corresponds 105 km<sup>2</sup>), or in stretched-grid mode to function as a high-resolution regional climate model (RCM). In the current ultra-high resolution experiment, the CCAM uses C192 stretched-grid configuration which is a resolution approximately about 8 km<sup>2</sup> over the Southern Africa where the centre of the panel is placed, while it has coarse resolution elsewhere. To arrive at this high-resolution, the C192 experiment is constrained with the C96 integration of the AGCM in order to maintain numerical stability and achieve a balanced simulation consistent with the driving AGCM reinforced with spectral nudging technique of Thatcher and McGregor (2010) while the RCM is allowed to freely develop self-dynamics coherent to the expected regional details.

The CCAM forecasts are verified using the Climate Hazards Group InfraRed Precipitation (CHIRP) quasi-global rainfall dataset. Spanning 50°S-50°N (and all longitudes), starting in 1981 to near-present, CHIRP(S) incorporates 0.05° resolution satellite imagery without (with) in-situ station data to create gridded rainfall time series for trend analysis and seasonal drought monitoring (Funk *et al.*, 2015). We use the version that doesn't include station data (due to the quality concern and lack of homogeneity in in-situ observation coverage over the southern Africa sub-continent).

#### *4.2.3 Short-range predictability under climate change*

The simulations performed here have been designed to explore how short-range weather predictability may change over southern Africa under climate change, with a focus on the key metric of rainfall. Towards finding an upper boundary for the short-range predictive skill of rainfall, a reanalysis-style simulation was performed for the period 1979-2014. This simulation mirrors the CCAM 50 km short-range weather forecast system of the CSIR, with the exception that the reanalysis simulations are nudged every 6 hours towards ERA reanalysis data. A scale-selective filter was applied for this purpose at 4000 km length scale and from 900 hPa upwards, at six hourly intervals. Nudging was performed towards the three-dimensional temperature and velocity fields of the reanalysis data. This procedure ensured that the synoptic-scale fields in the model resemble reality, and allows the model's ability to predict rainfall occurring in association with a specific synoptic weather-scale pattern to be assessed. By mapping the daily synoptic weather patterns on a Self-Organising Map (SOM) that identifies 35 dominant synoptic types for the period 1979-2014, the predictive skill of the model in terms of associating rainfall with each of these synoptic types was subsequently explored.

From this baseline analysis, the study then proceeds to project how synoptic types may change under climate change. For this purpose the projections of future climate change from a global circulation model (GCM), the Community Climate System Model (CCSM4), was downscaled to 50 km resolution globally (this is one of the six CORDEX projections generated in Chapter 2). The synoptic-type frequencies as projected in this CCAM downscaling for the periods 1961-1990 and 2070-2099 were subsequently explored. By examining the projected change in synoptic-type frequencies from the present-day period to the future, and by relating these changes to the predictive skill in associating rainfall with each synoptic type, it is possible to deduce how predictive skill may be affected by climate change.

### **4.3 Results**

#### *4.3.1 Projected changes in climate variability over eastern South Africa*

Figure 2 (top) shows the projected increase in temperature (11-year moving average) over the mega-dam area of South Africa for the austral summer (the December to February (DJF) period). The projection was obtained by downscaling the simulations of the ACCESS1-0 GCM to a 50 km resolution global grid using the regional model CCAM, following the experimental design described in Chapter 2 (CSIR CORDEX simulations). The downscalings were obtained for the period 1960-

2100, and here 11-year moving averages of temperature for the period 1976-2094 are considered. To investigate the potential impacts of climate change on variability, the standard deviation of the detrended temperature time-series for each 11-year moving period was calculated (Figure 4.1a, bottom). The trends were calculated using simple linear regression. This approach provides a better representation of natural variability as depicted by the standard deviation, than the standard deviation calculated for the raw (not detrended) data. In the latter case, the standard deviation is strongly influenced by temperatures trending around the mean value, so that it is a depiction of the trend rather than the underlying variability. Figures 4.1b to 4.1f are exactly the same as Figure 4.1a, but for the downscaled GFDL-CM3, MPI-ESM-LR, NorESM1M, CCSM4 and CNRM-CM5 models, respectively.

The ensemble of downscalings depicts drastic temperature increases over the mega-dam area under the low mitigation future. By the end of the 21st century temperature increases of 5°C to 7°C are projected for the region. It is interesting that many of the models project a short hiatus (about a decade long) in near to mid-21st century during which regional warming will slow down, or even be replaced by regional cooling. This is followed by a prolonged period of accelerated warming. Such drastic temperature increases (5-7°C) may impact directly on South Africa's water security, by introducing enhanced evaporation in the mega-dam area. Water quality may also be affected negatively in a significantly warmer regional environment. These are factors that require further investigation through the application of hydrological models.

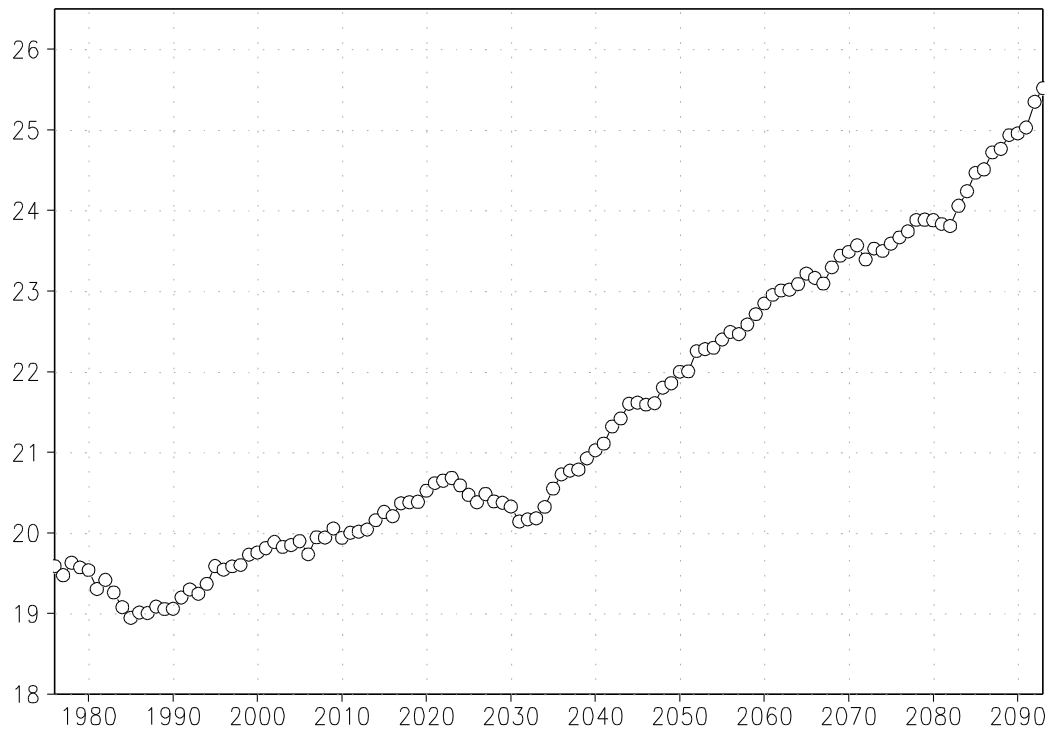
Decadal and multi-decadal climate variability in temperature over the mega-dam area is evident from the standard deviations calculated for the detrended 11-year moving averages of temperature (averaged over the mega-dam area) (Figures 4.1a to 4.1f). Some of the downscalings (GFDL, NorESM1M, MPI-ESM-LR, CNRM) are indicative of decreased variability towards the end of the century, whilst the ACCESS1-0, MPI-ESM-LR and CCSM downscalings are indicative of increased variability.

Figure 4.2a (top) shows the projected increase in rainfall (11-year moving average) over the mega-dam area of South Africa for the austral summer obtained by downscaling the simulations of the ACCESS1-0 GCM. The associated standard deviation of rainfall, calculated using the same methodology as for temperature, is depicted in Figure 4.2a (bottom). Figures 4.2b to 4.2f are exactly the same as Figure 4.2a, except that they are for the GFDL-CM3, MPI-ESM-LR, NorESM1M, CCSM4 and CNRM-CM5 models, respectively.

The downscaled MPI-ESM-LR, NorESM1M, CCSM4 and CNRM GCM projections are all indicative of a generally drier future over the mega-dam area, whilst the ACCESS1-0 and GFDL models are not indicative of significant drying or wetting. Earlier studies (Christensen et al., 2007; Engelbrecht et al., 2009; Niang et al., 2014 and Engelbrecht et al., 2015) have indeed concluded that the larger southern African region is likely to become generally drier under climate change. Three of the downscaled models (NorESM1M, CCSM4 and CNRM) are indicative of increased rainfall variability, whilst the remaining models do not exhibit a clear signal in this regard. Rainfall is simulated to vary pronouncedly at decadal to multi-decadal time scales by most of the downscalings.

The results of Figures 4.1a to 4.1f and 4.2a to 4.2f can also be presented spatially. Figure 4.3 describes the projected changes in climate variability over southern Africa under enhanced anthropogenic forcing, for the austral summer (DJF). The projections are shown for the same 6 CSIR CORDEX downscalings described before. Note again that the standard deviation of the detrended temperature time-series for each 11-year moving period was calculated using simple linear regression. This approach provides a better representation of natural variability as depicted by the standard deviation, than the standard deviation calculated for the raw (not detrended) data.

tave mov ave 1976–2094 ACCESS



tave stand dev 1976–2094 ACCESS

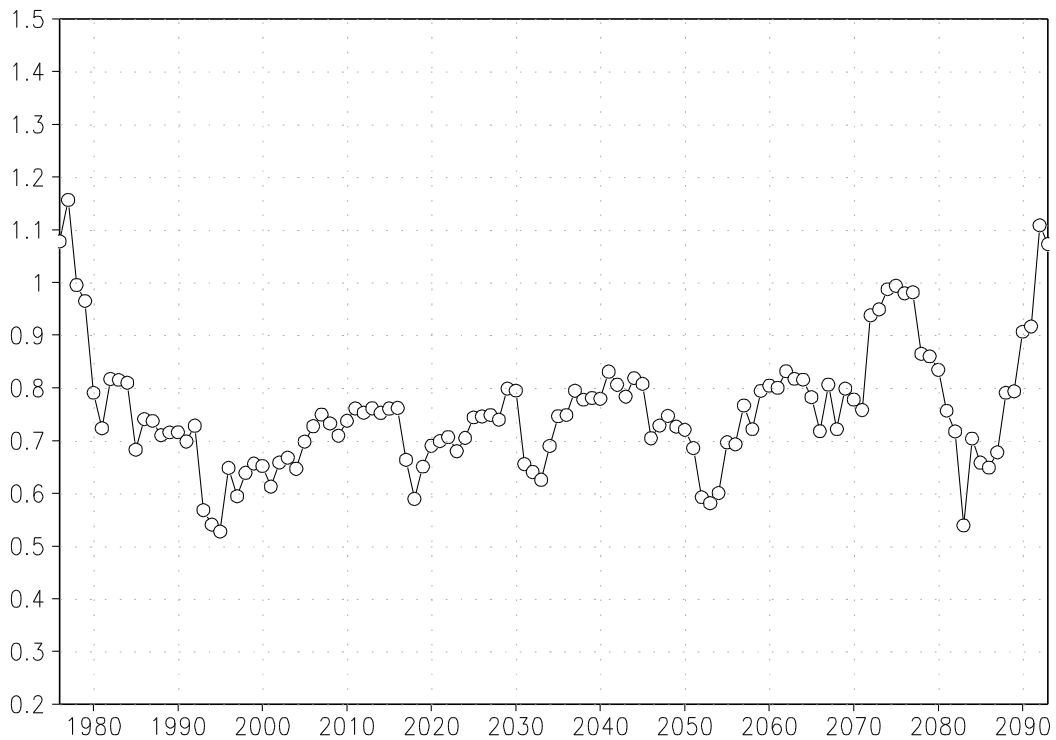
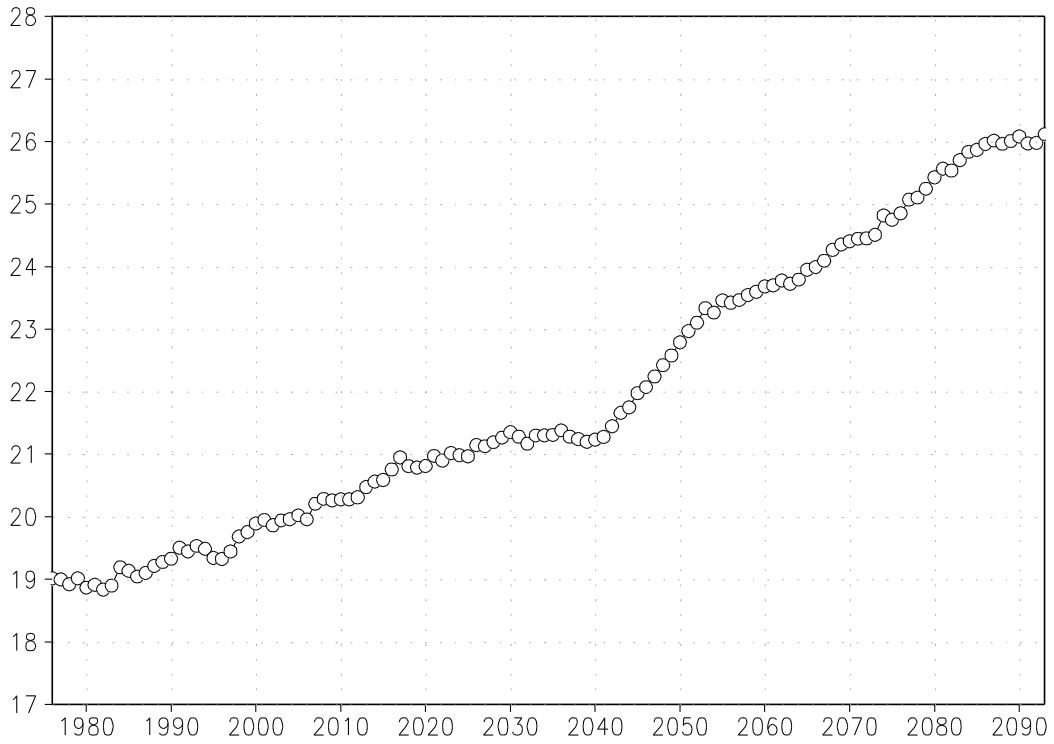


**Figure 4.1a:** 11-year moving average of projected summer temperature (°C) over the mega-dam area, obtained through downscaling of the ACCESS1-0 GCM using CCAM (top). Standard deviation of the detrended 11-year moving time series, depicting summer temperature variability (°C) over the mega-dam area.

tave mov ave 1976–2094 GFDL



tave stand dev 1976–2094 GFDL

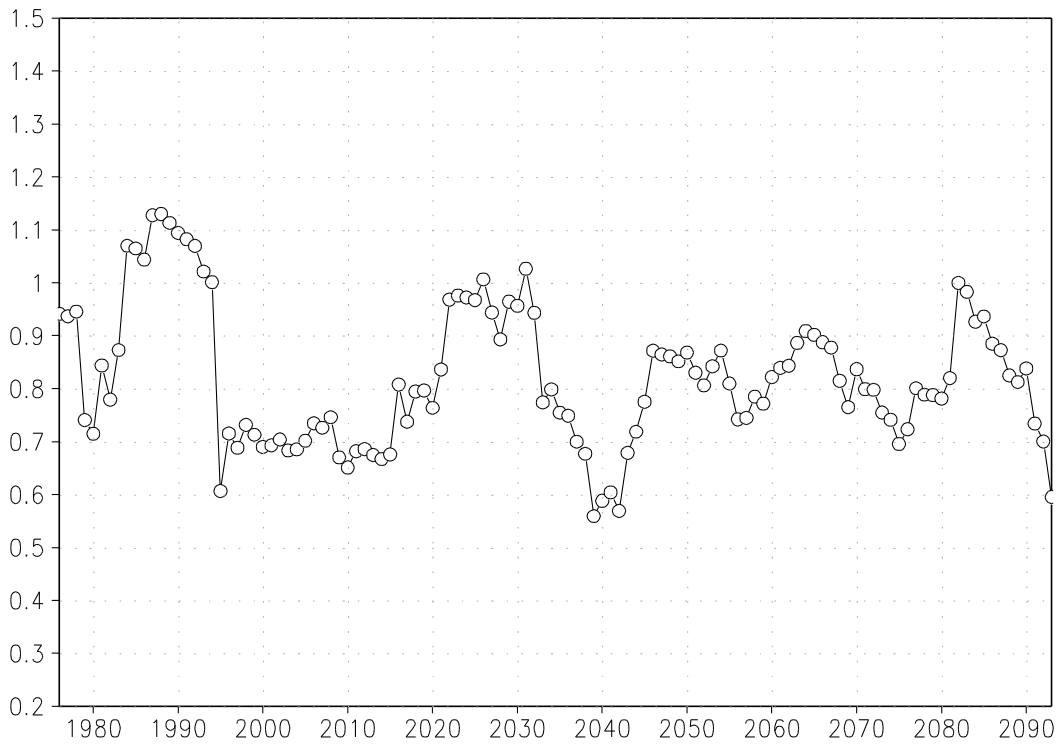
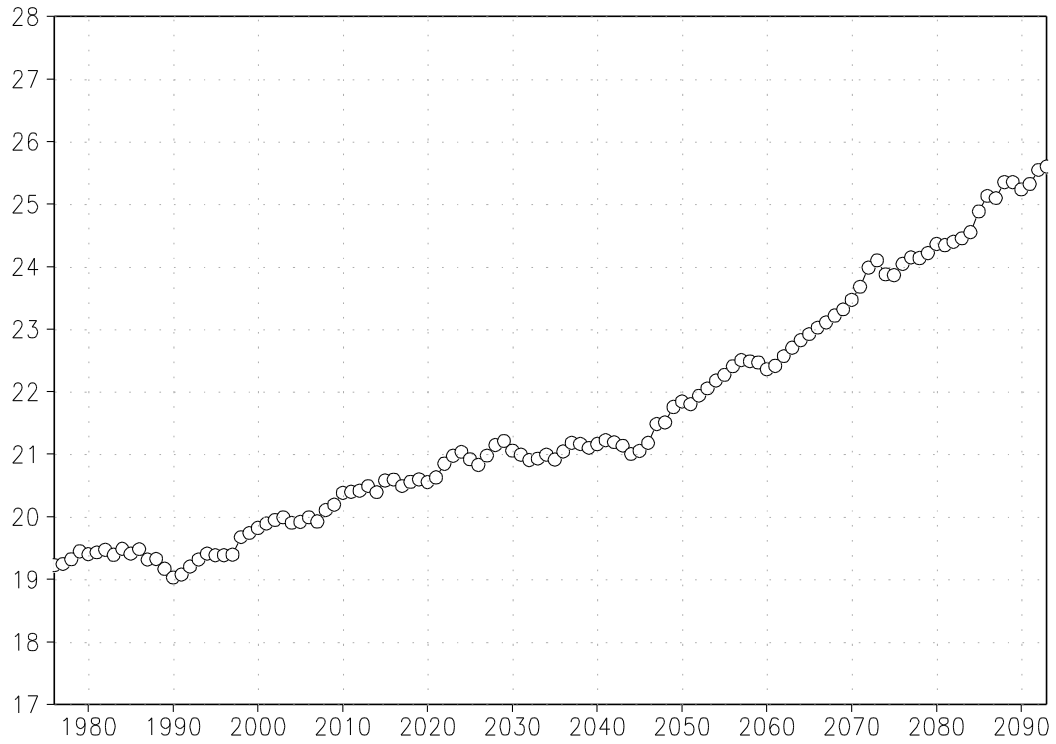


**Figure 4.1b:** 11-year moving average of projected summer temperature (°C) over the mega-dam area, obtained through downscaling of the GFDL-CM3 GCM using CCAM (top). Standard deviation of the detrended 11-year moving time series, depicting summer temperature variability (°C) over the mega-dam area.

tave mov ave 1976–2094 MPI



tave stand dev 1976–2094 MPI

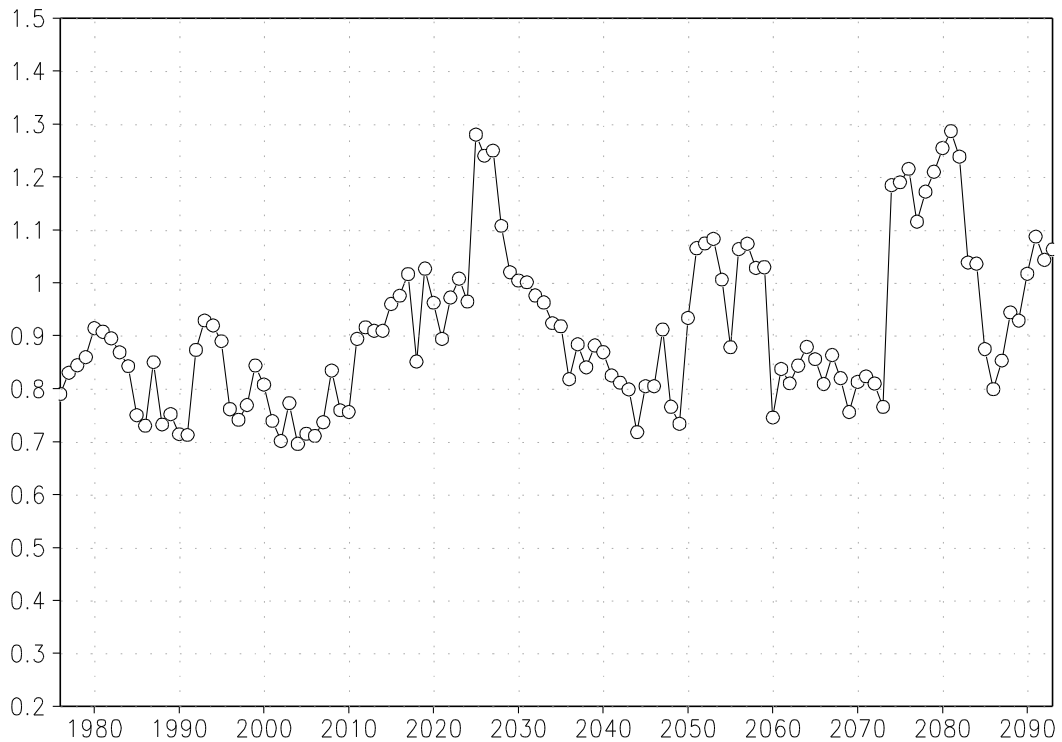
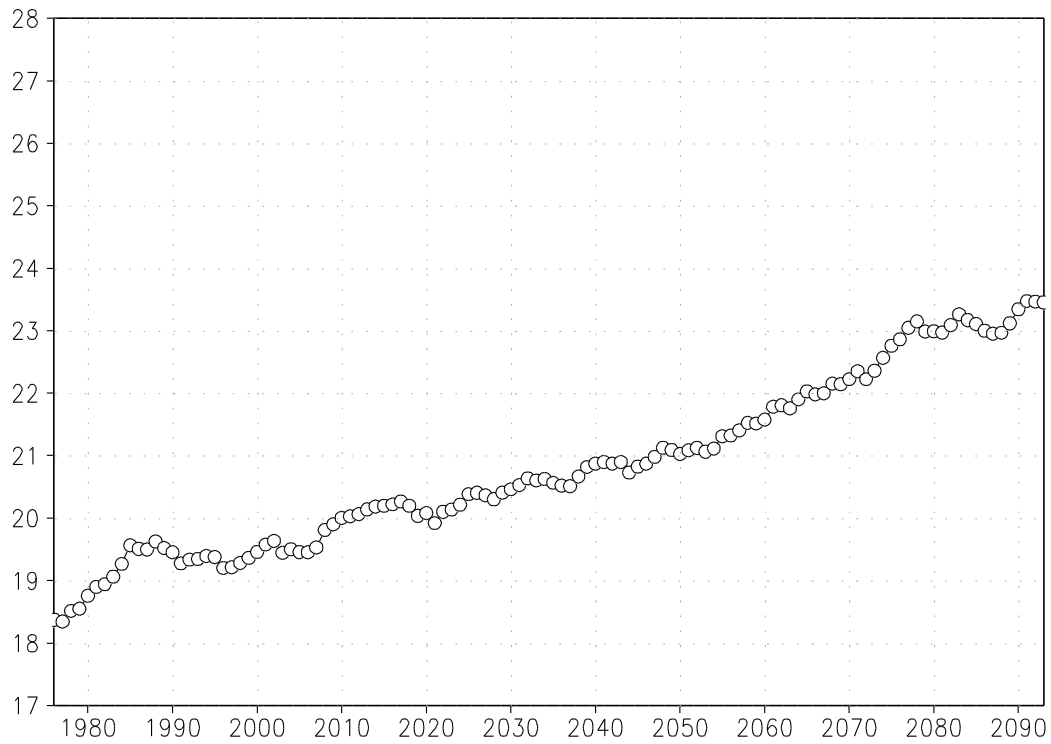


**Figure 4.1c:** 11-year moving average of projected summer temperature (°C) over the mega-dam area, obtained through downscaling of the MPI-ESM-LR GCM using CCAM (top). Standard deviation of the detrended 11-year moving time series, depicting summer temperature variability (°C) over the mega-dam area.

tave mov ave 1976–2094 NorESM1M



tave stand dev 1976–2094 NorESM1M

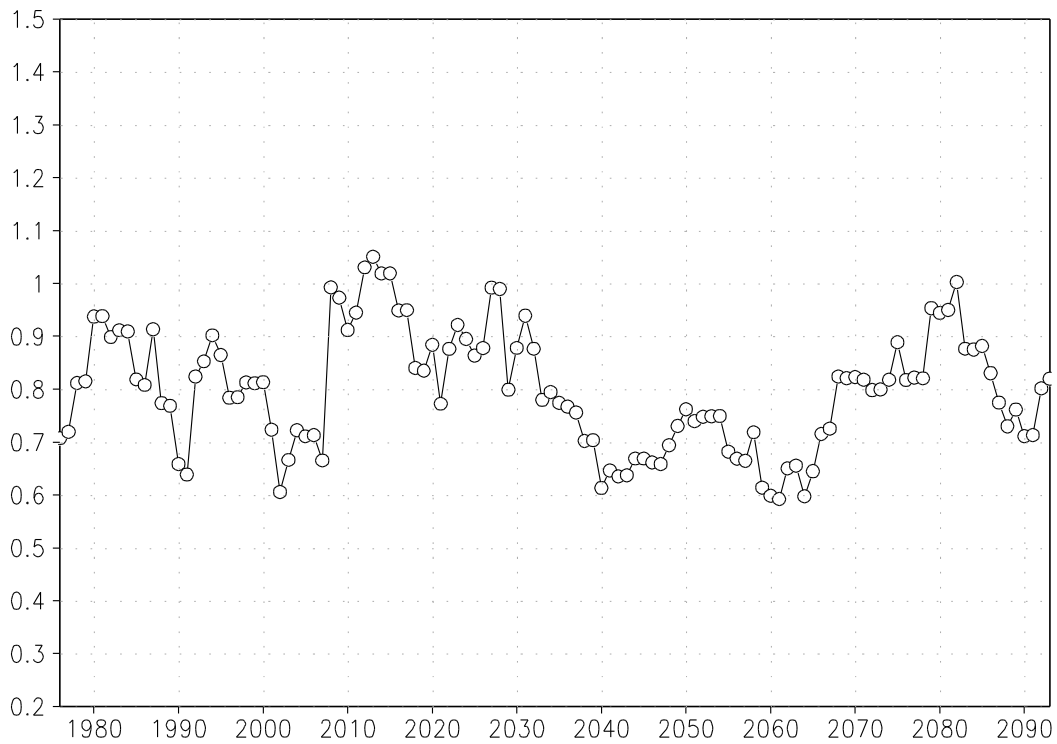
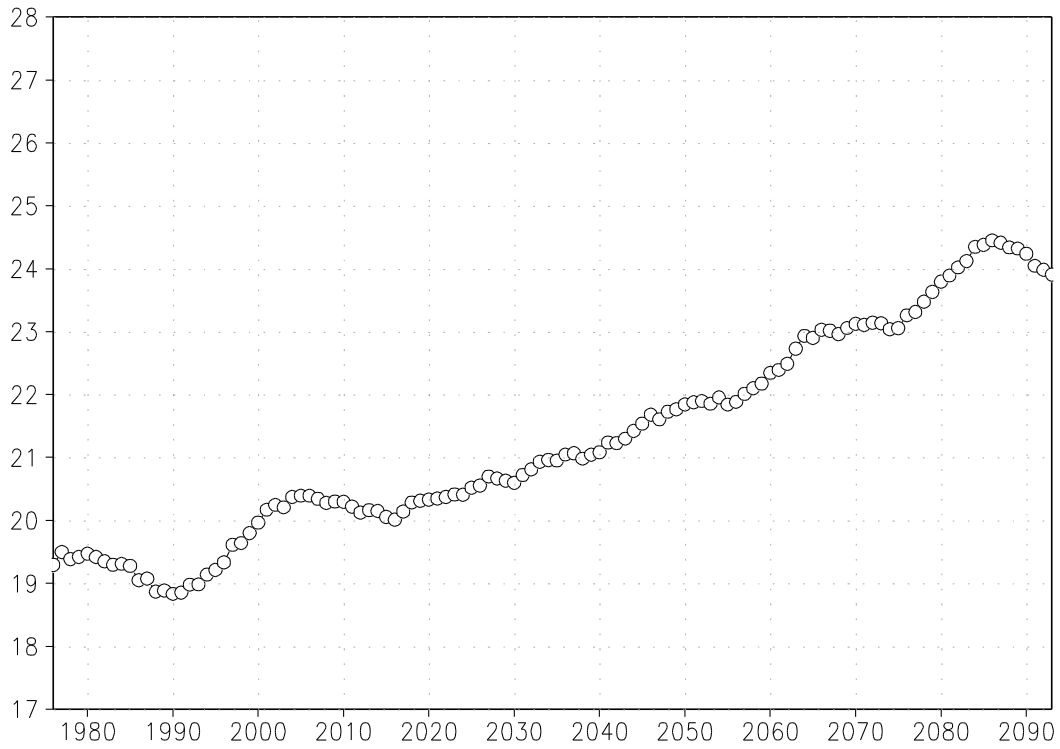


**Figure 4.1d:** 11-year moving average of projected summer temperature (°C) over the mega-dam area, obtained through downscaling of the NorESM1M GCM using CCAM (top). Standard deviation of the detrended 11-year moving time series, depicting summer temperature variability (°C) over the mega-dam area.

tave mov ave 1976–2094 CCSM4

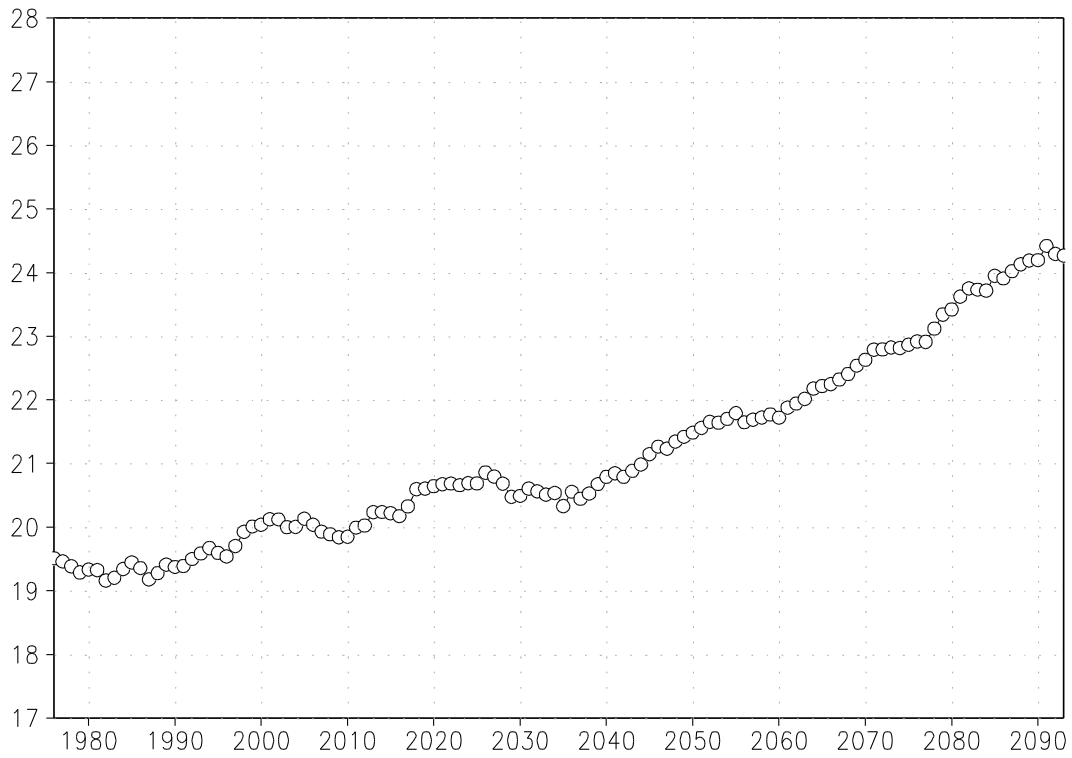


tave stand dev 1976–2094 CCSM4



**Figure 4.1e:** 11-year moving average of projected summer temperature (°C) over the mega-dam area, obtained through downscaling of the CCSM4 GCM using CCAM (top). Standard deviation of the detrended 11-year moving time series, depicting summer temperature variability (°C) over the mega-dam area.

tave mov ave 1976–2094 CNRM



tave stand dev 1976–2094 CNRM

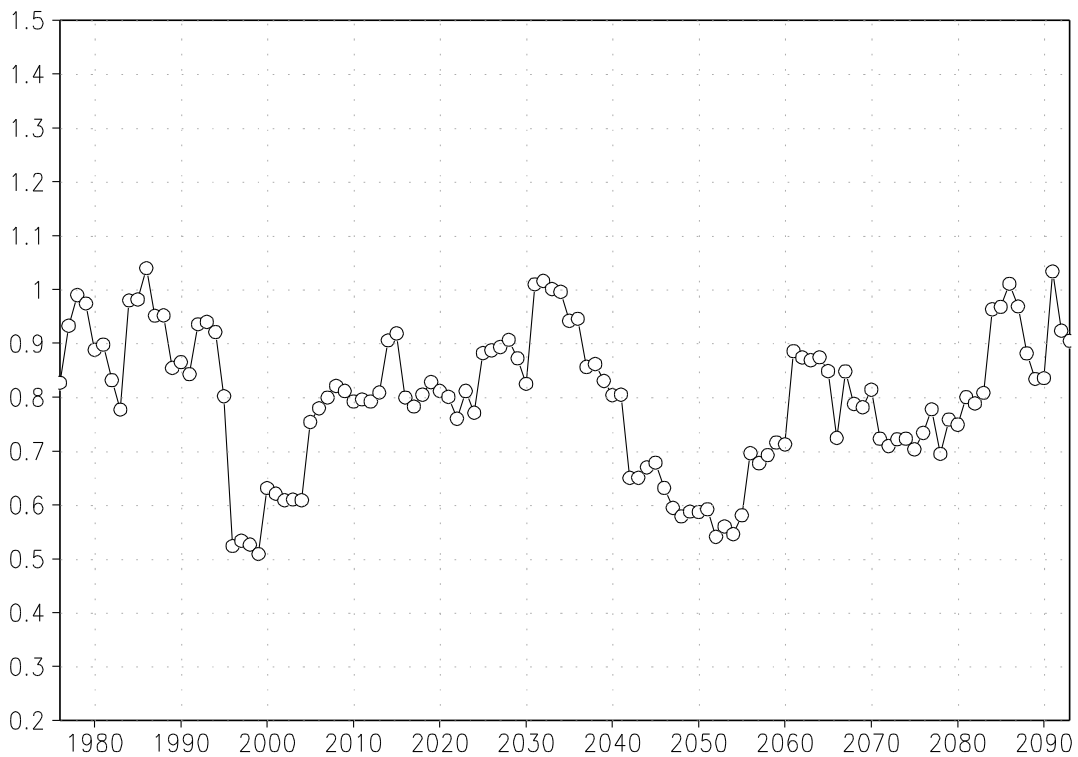
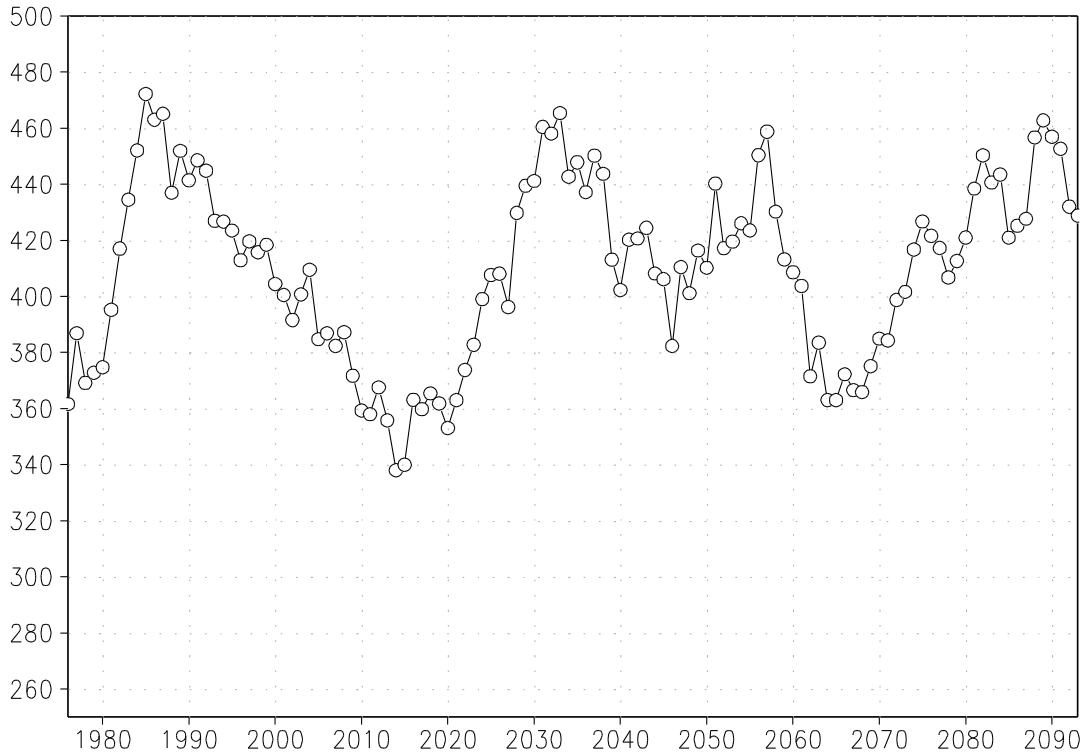


**Figure 4.1f:** 11-year moving average of projected summer temperature (°C) over the mega-dam area, obtained through downscaling of the CNRM GCM using CCAM (top). Standard deviation of the detrended 11-year moving time series, depicting summer temperature variability (°C) over the mega-dam area.

### rnd mov ave 1976–2094 ACCESS



### rnd stand dev 1976–2094 ACCESS

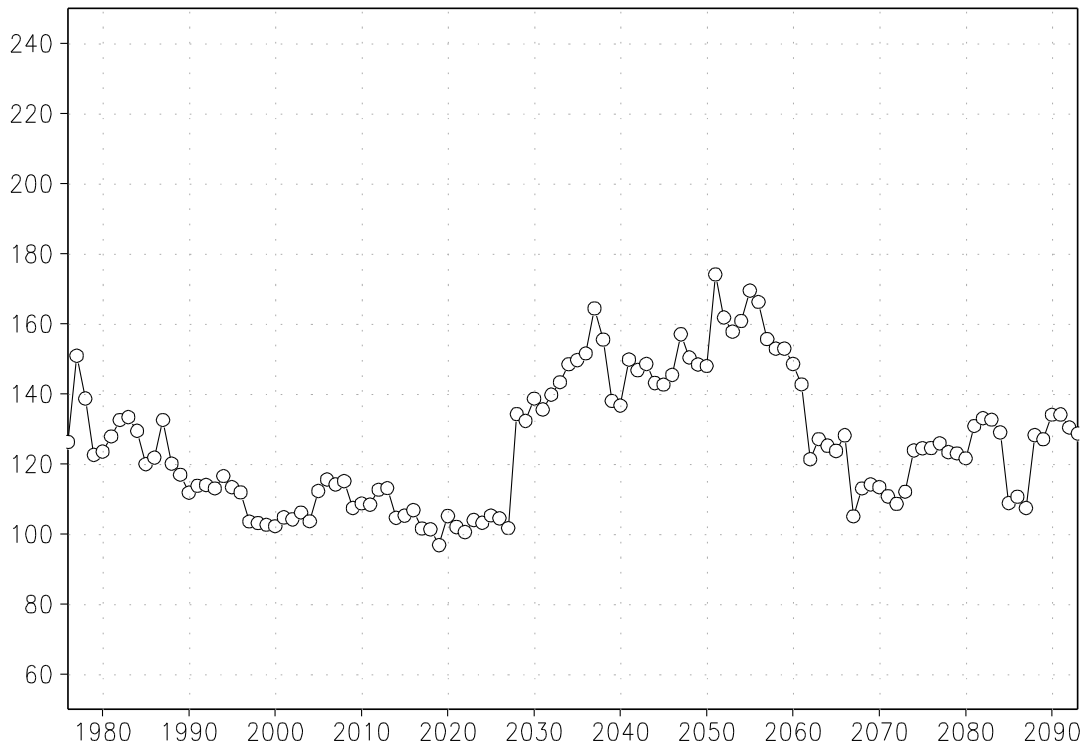
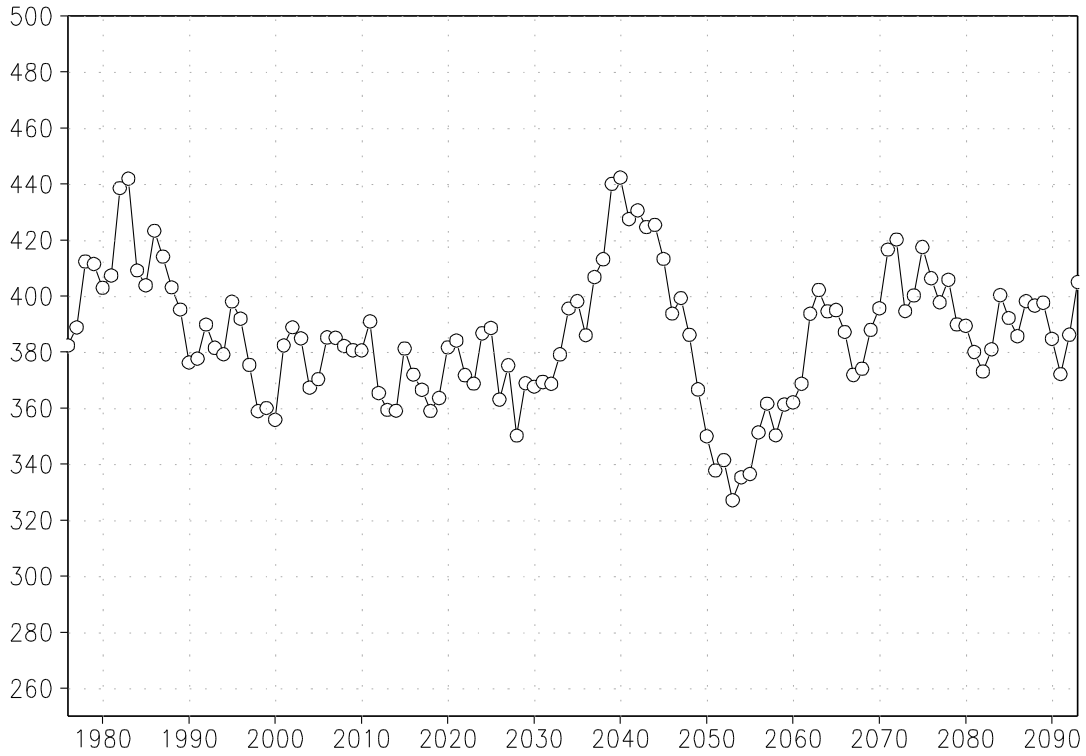


**Figure 4.2a:** 11-year moving average of projected summer rainfall (mm) over the mega-dam area, obtained through downscaling of the ACCESS1-0 GCM using CCAM (top). Standard deviation of the detrended 11-year moving time series, depicting summer rainfall variability (mm) over the mega-dam area.

rnd mov ave 1976–2094 GFDL



rnd stand dev 1976–2094 GFDL

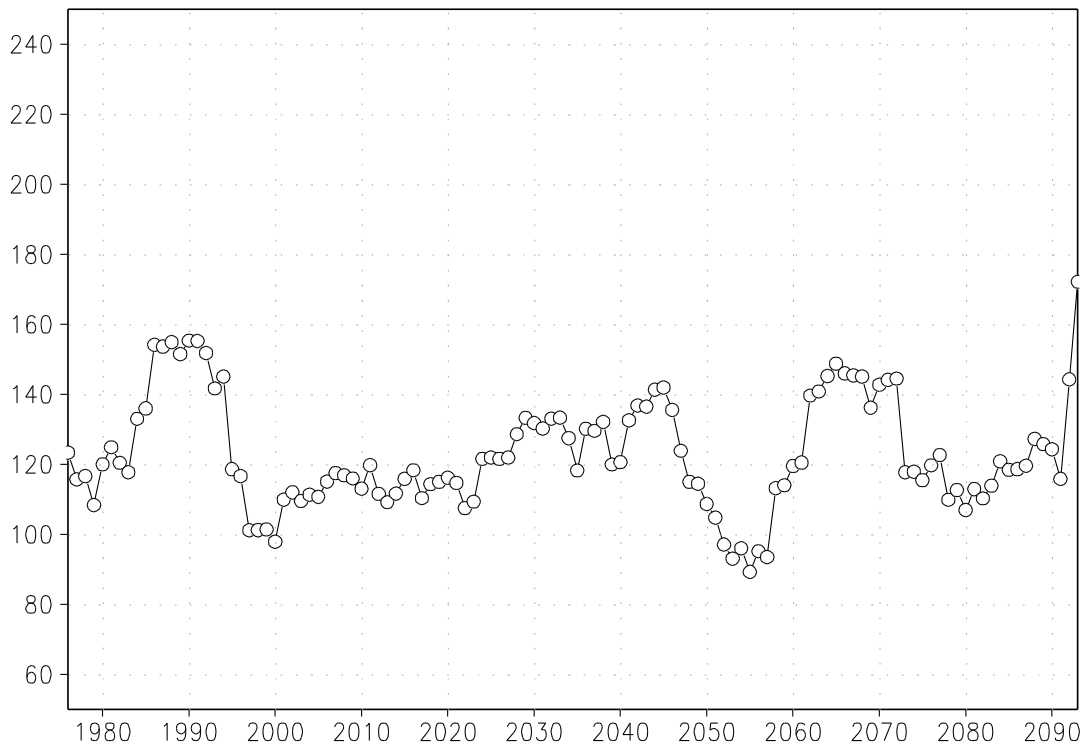
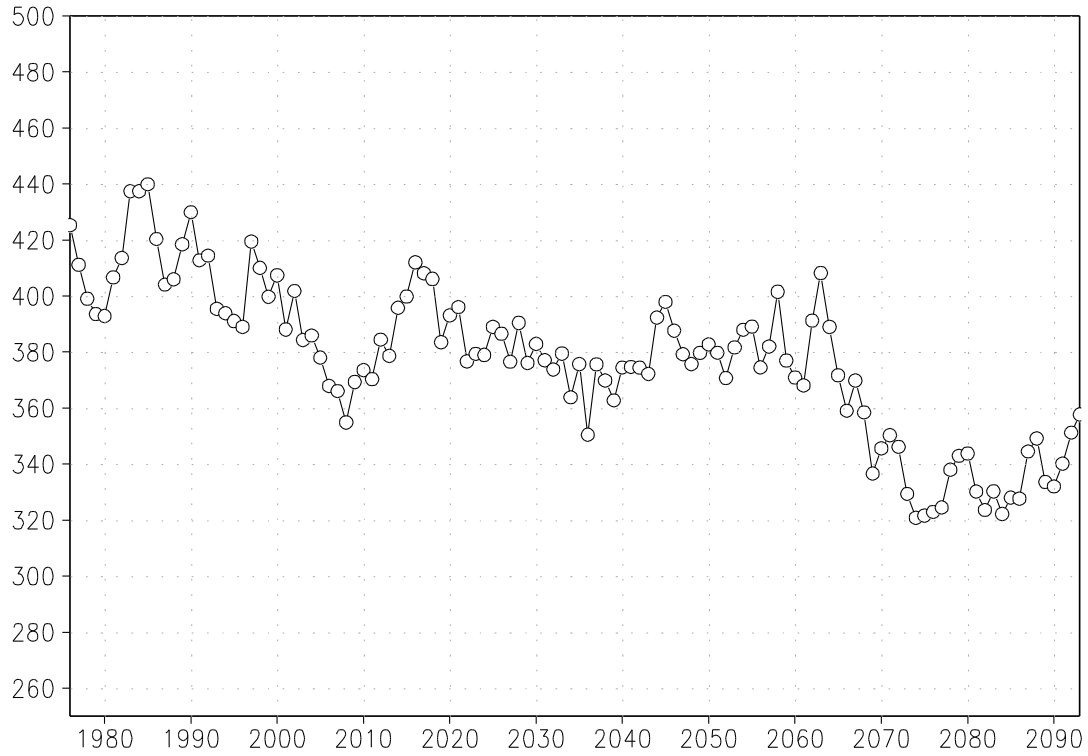


**Figure 4.2b:** 11-year moving average of projected summer rainfall (mm) over the mega-dam area, obtained through downscaling of the GFDL-CM3 GCM using CCAM (top). Standard deviation of the detrended 11-year moving time series, depicting summer rainfall variability (mm) over the mega-dam area.

rnd mov ave 1976–2094 MPI



rnd stand dev 1976–2094 MPI

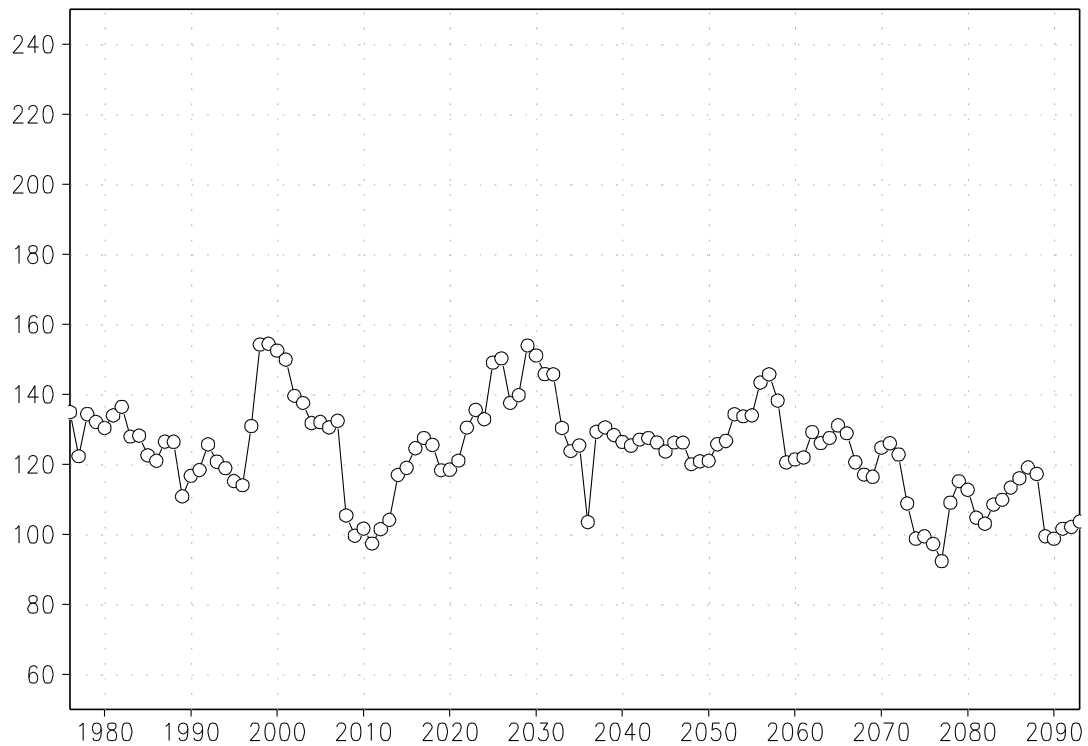
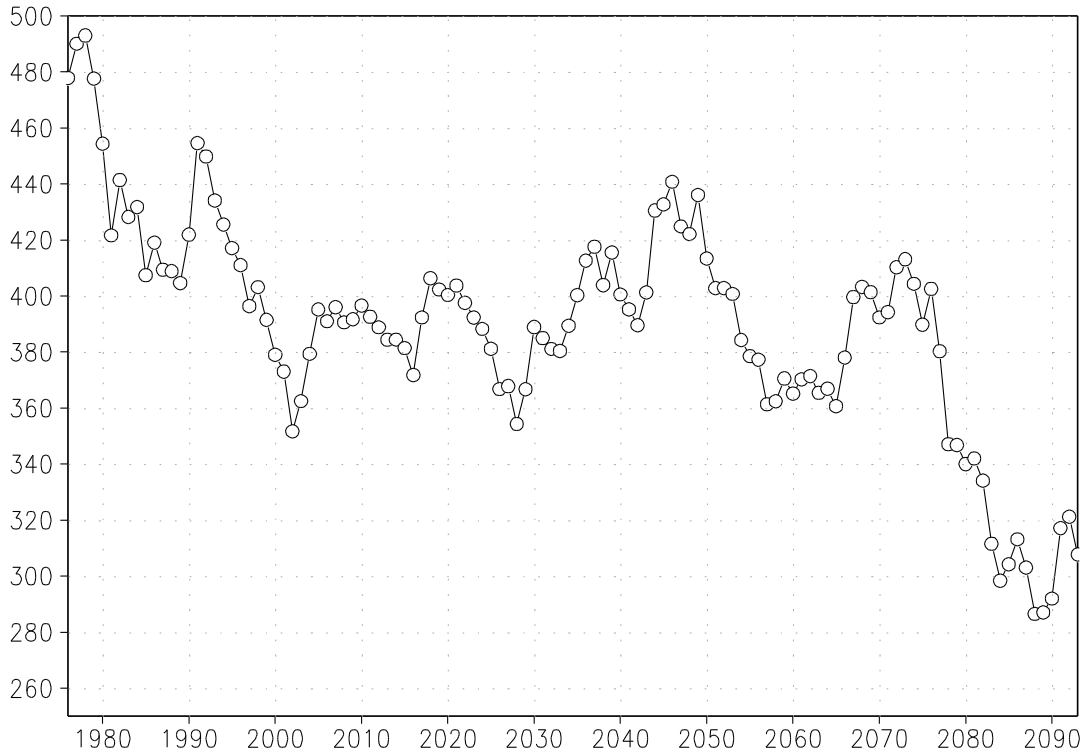


**Figure 4.2c:** 11-year moving average of projected summer rainfall (mm) over the mega-dam area, obtained through downscaling of the MPI-ESM-LR GCM using CCAM (top). Standard deviation of the detrended 11-year moving time series, depicting summer rainfall variability (mm) over the mega-dam area.

rnd mov ave 1976–2094 NorESM1M



rnd stand dev 1976–2094 NorESM1M

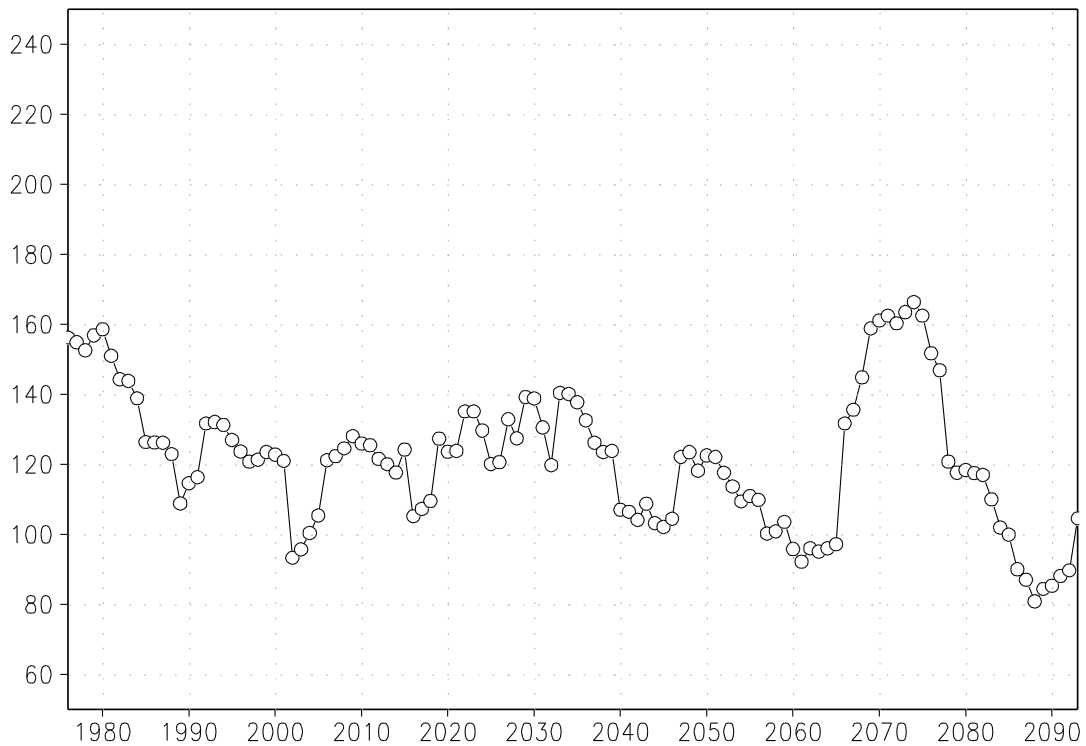


**Figure 4.2d:** 11-year moving average of projected summer rainfall (mm) over the mega-dam area, obtained through downscaling of the NorESM1M GCM using CCAM (top). Standard deviation of the detrended 11-year moving time series, depicting summer rainfall variability (mm) over the mega-dam area.

rnd mov ave 1976–2094 CCSM4



rnd stand dev 1976–2094 CCSM4

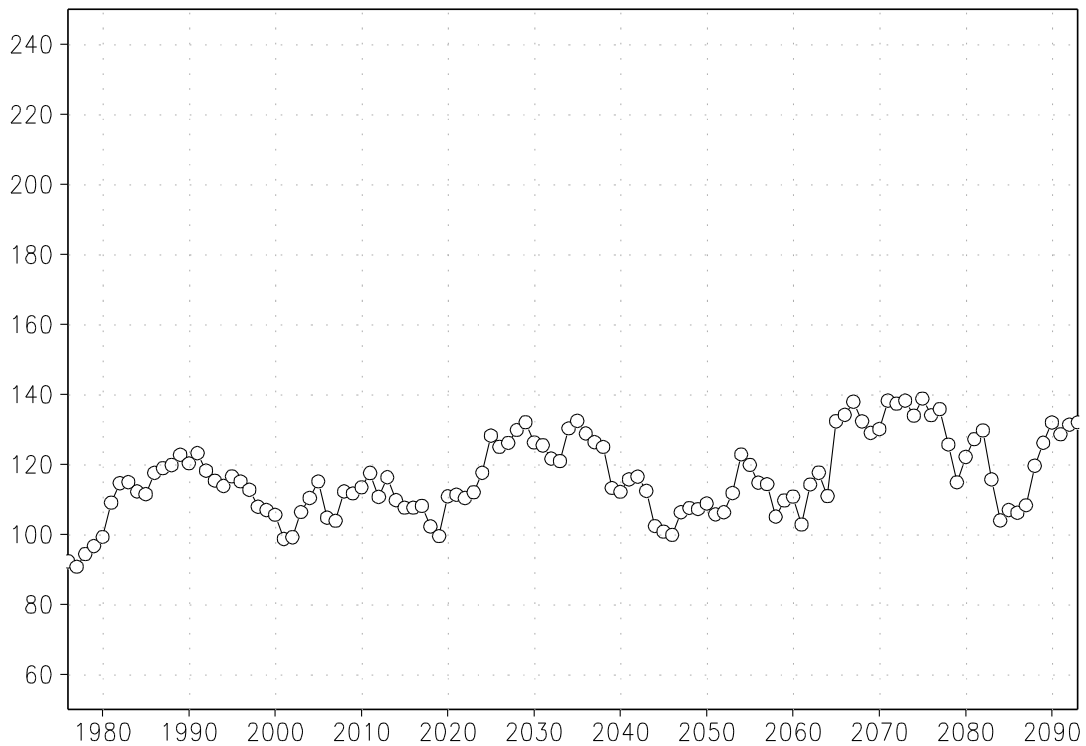
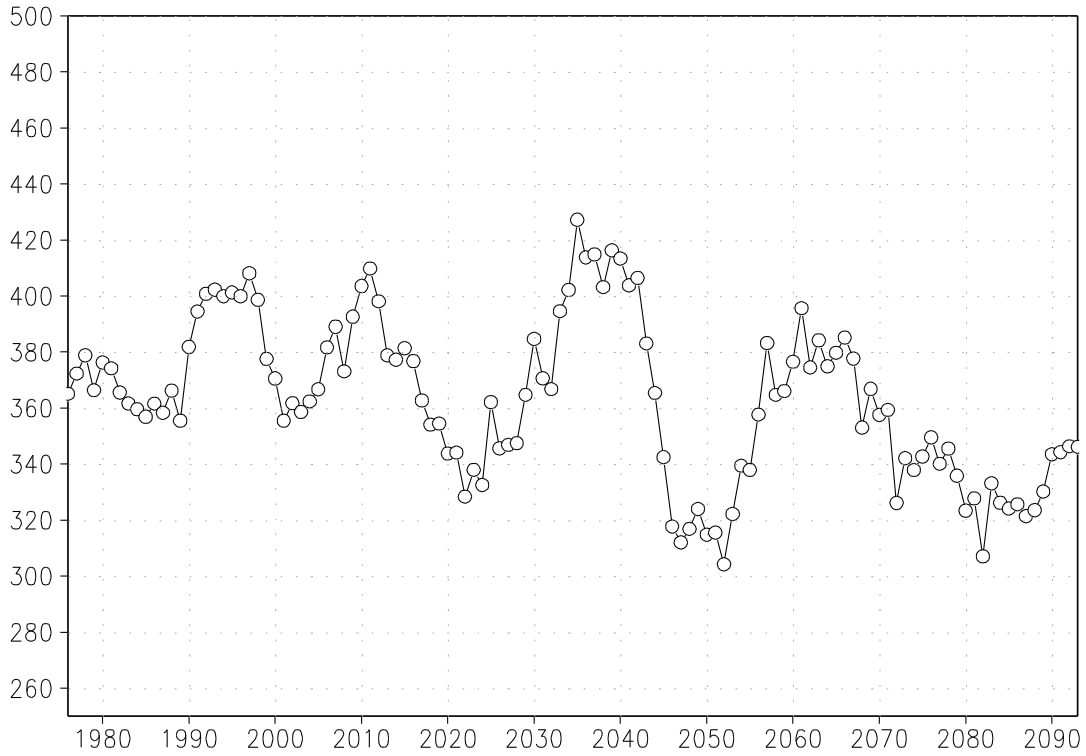


**Figure 4.2e:** 11-year moving average of projected summer rainfall (mm) over the mega-dam area, obtained through downscaling of the CCSM4 GCM using CCAM (top). Standard deviation of the detrended 11-year moving time series, depicting summer rainfall variability (mm) over the mega-dam area.

rnd mov ave 1976–2094 CNRM



rnd stand dev 1976–2094 CNRM

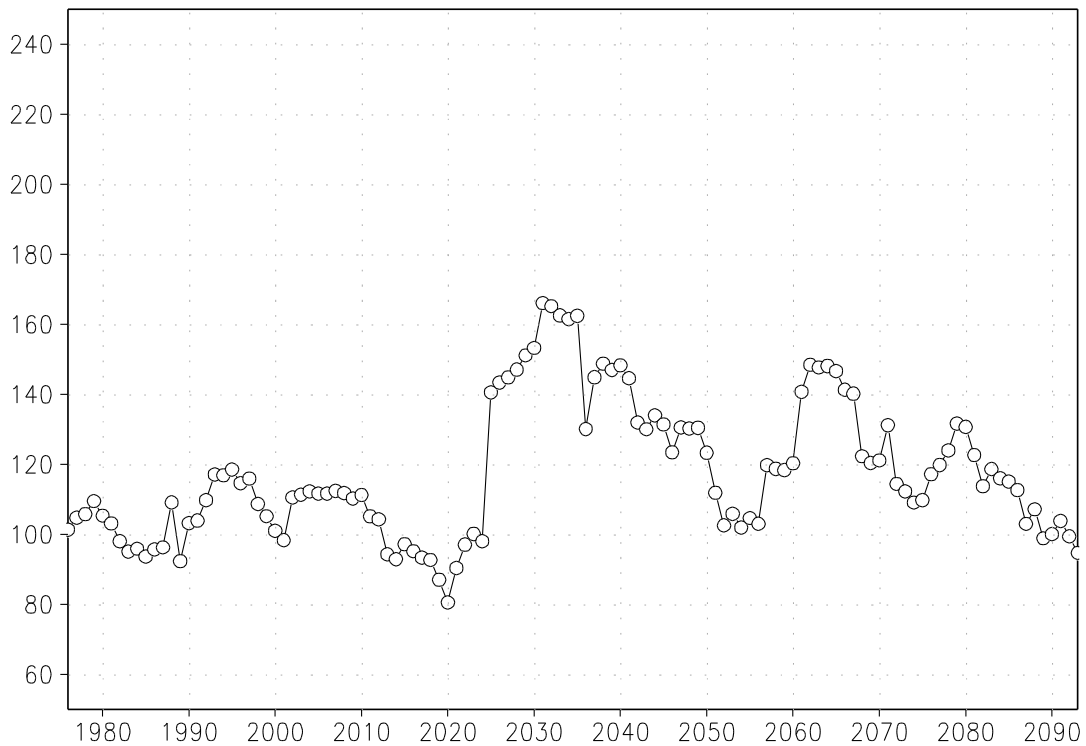


**Figure 4.2f:** 11-year moving average of projected summer rainfall (mm) over the mega-dam area, obtained through downscaling of the GFDL-CM3 GCM using CCAM (top). Standard deviation of the detrended 11-year moving time series, depicting summer rainfall variability (mm) over the mega-dam area.

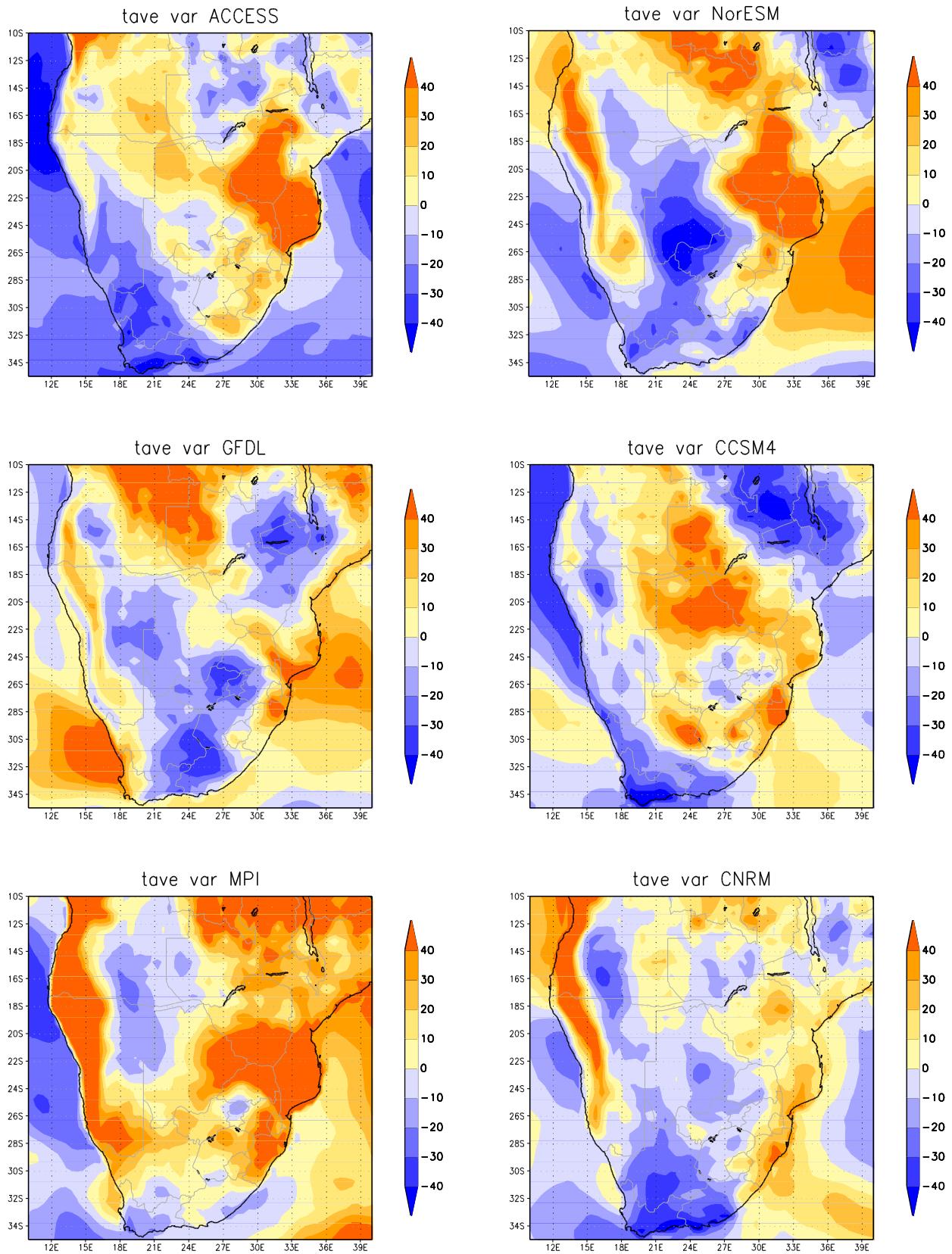


**Figure 4.3:** Projected changes in the standard deviation of austral summer near-surface atmospheric temperature ( $^{\circ}\text{C}$ ) over southern Africa for the period 2071-2100 relative to 1971-2000. The projections were obtained by downscaling the simulations of six different GCMs integrated under RCP8.5 to a high resolution global grid, using the variable-resolution atmospheric model CCAM.

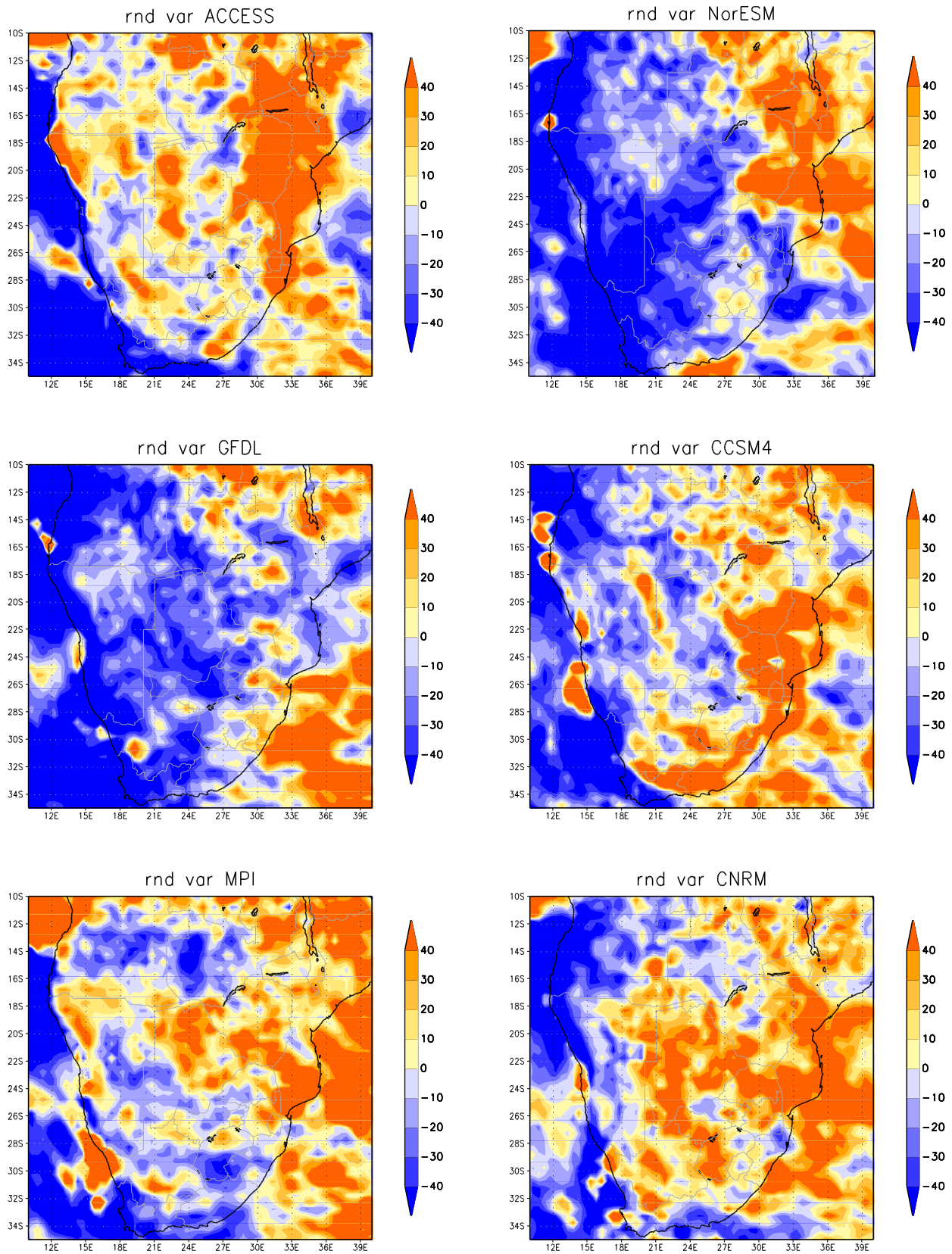


**Figure 4.4:** Projected changes in the standard deviation of austral summer rainfall (mm) over southern Africa for the period 2071-2100 relative to 1971-2000. The projections were obtained by downscaling the simulations of six different GCMs integrated under RCP8.5 to a high resolution global grid, using the variable-resolution atmospheric model CCAM.

In the latter case, the standard deviation is strongly influenced by temperatures trending around the mean value, so that it is a depiction of the trend rather than the underlying variability. Figure 2 shows the projected change in the standard deviation calculated using this methodology, for the period 2070-2099 (moving averages 2075-2094) relative to 1971-2000 (moving averages 1976-2005).

The projections are indicative of increasing temperature variability increasing over the eastern parts of southern Africa under climate change, and particularly so over the Limpopo river basin of southern Africa and southern Mozambique. This region has a pronounced ENSO signal under present-day climate, so that the enhanced variability may imply a more pronounced cycle of ENSO events, or possibly a strengthening of the ENSO teleconnection to southern Africa. Temperature variability is projected to decrease over the southwestern Cape and Cape south coast by most projections, and there are also indications of decreased variability over the western and central interior. Over the mega-dam area of eastern South Africa a mixed signal is present, although the majority of projections are indicative of increased variability.

The projected changes in rainfall variability are depicted in Fig. 4.4, as before for the period 2070-2099 relative to 1971-2000. The projected changes in variability are qualitatively similar than for the case of temperature. Variability is projected to increase over the eastern escarpment, particularly so over the Limpopo river basin and also over the mega-dam area of eastern South Africa. A robust pattern of decreasing variability is projected for the western parts of southern Africa.

The pattern of increasing variability over the eastern parts of southern Africa, the parts of the subcontinent that receive most rainfall and are most important from the perspective of water and food security, is important. It is often assumed that increased variability implies decreased predictability – but this is not necessarily always the case. This hypothesis may be explored further through the objective analysis of the AMIP-style simulations described in section 4.2. Figure 4.5 shows the skill of the CCAM AMIP-style control simulation in representing austral summer inter-annual climate variability over southern Africa, using the rank-probability skill score (RPSS) with climate as the reference forecast. Predictability is highest over the eastern parts of the subcontinent, where the ENSO teleconnection is known to be the strongest. Under enhanced greenhouse gas warming (as present in the second AMIP-style simulation that was obtained using realistically increasing greenhouse gas concentrations rather than the climatological values) the model skill in representing inter-annual variability is projected to increase across the model domain – but particularly so in the east and over the Limpopo river basin (where the ENSO signal is strongest). Since AMIP simulations are regarded as providing an upper boundary to seasonal forecast skill, these findings may be interpreted as enhanced greenhouse gas warming providing additional predictability over the southern African region. This result does make sense intuitively. An increase in the frequency of occurrence of strong El Niño and La Niña events are projected to occur under climate change (Wang et al., 2017), and indeed the projected climate change signal over southern Africa exhibits a pronounced ENSO signal (Chapter 2). This, in conjunction with the fact that seasons of strong ENSO forcing are the most predictable over southern Africa (e.g. Landman and Beraki, 2012) strongly suggests that predictability of southern African climate variability may increase over the summer rainfall region under climate change.

#### *4.3.2 Seasonal forecast skill in rainfall and streamflow over eastern South Africa*

Given the predictive skill that exists in the seasonal forecasting of circulation patterns over the summer rainfall in southern Africa (Figure 4.5; Engelbrecht et al., 2015; Landman and Beraki, 2012), and the prospect that this predictability may strengthen under climate change (Figure 4.5), it is worthwhile to explore whether this predictability extends to the predictability of streamflow over eastern South Africa. Although the coarse resolution CCAM-AMIP simulations or equivalent CCAM seasonal forecasts can't adequately represent local sub-grid features such as stream-flow, semi-empirical relationships exist between observed large-scale circulation and rainfall.

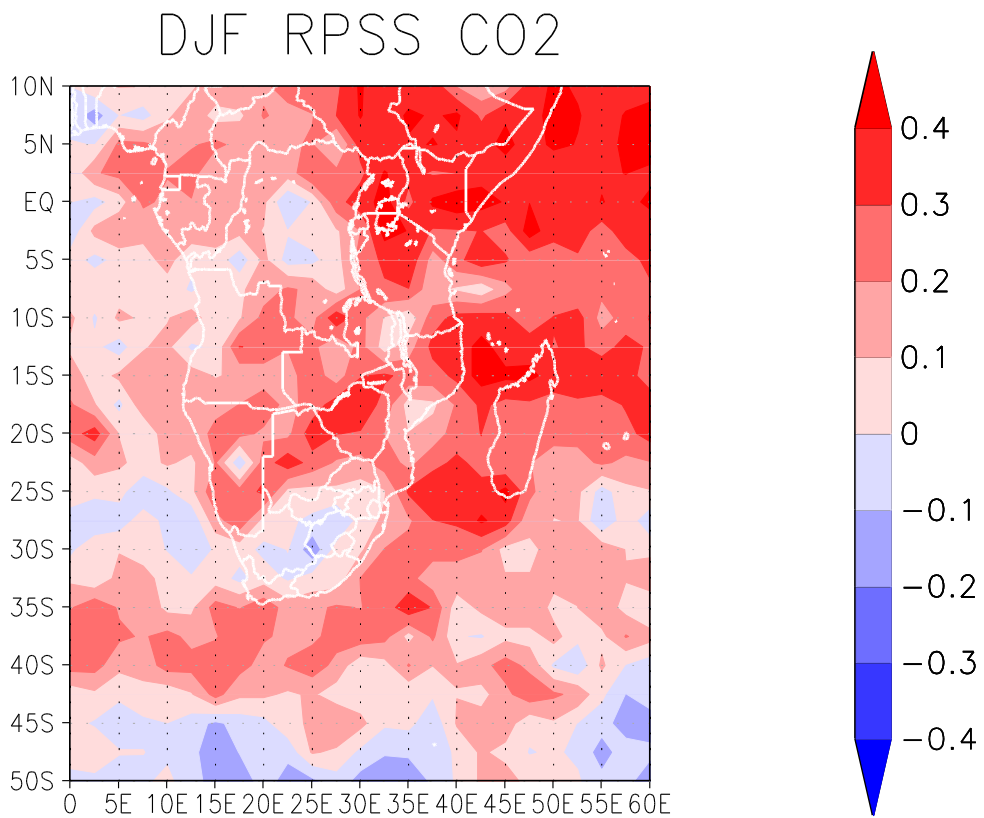
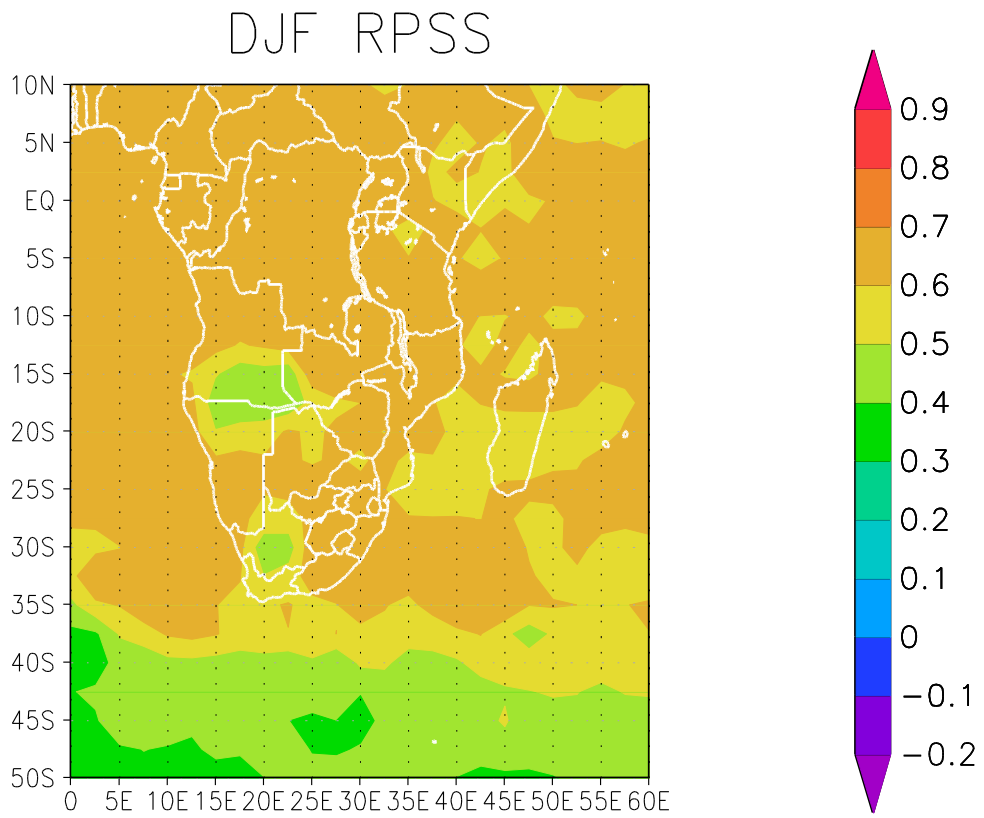


**Figure 4.5:** Rank probability skill score of the CCAM AMIP-style simulations in representing 850 hPa inter-annual circulation variability over southern Africa, for the austral summers of 1978-2004 (top). The effects of enhanced greenhouse gas forcing on changing this predictability are depicted in the bottom figure.

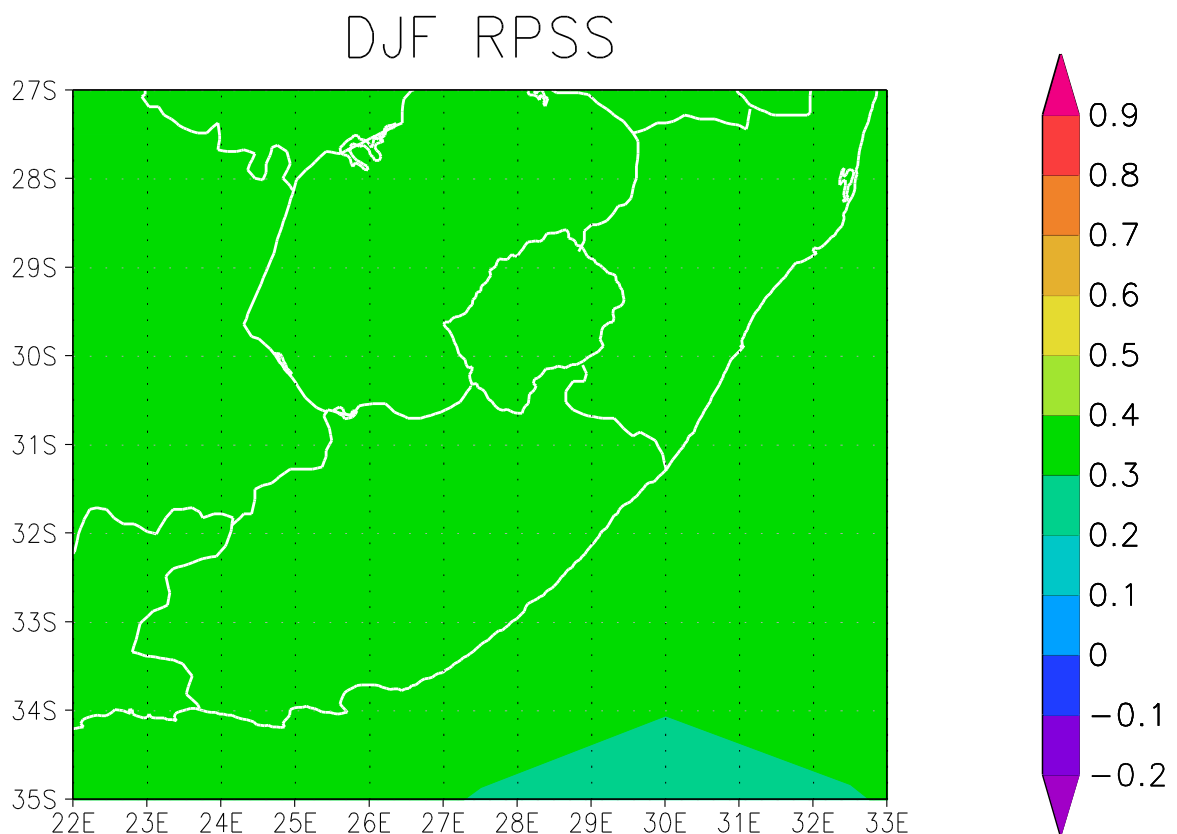
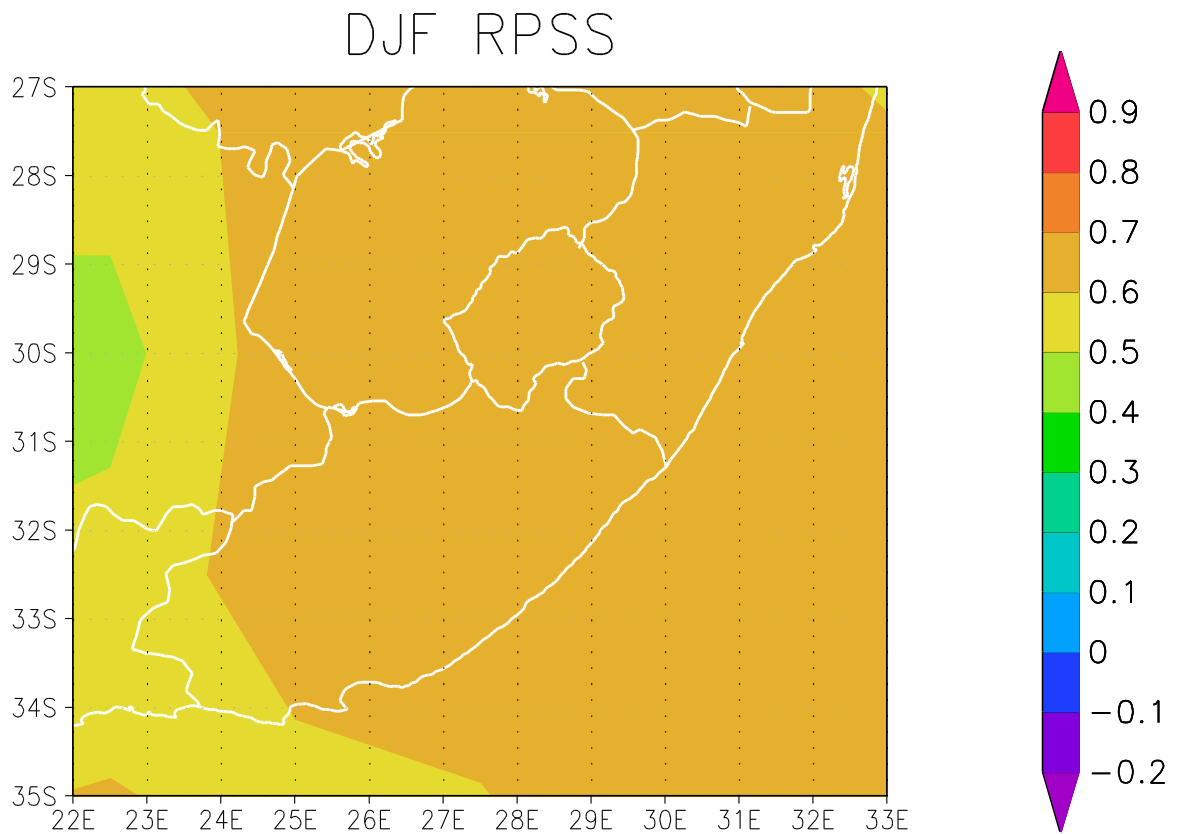


**Figure 4.6:** Rank probability skill-score for the CCAM-AMIP simulations in predicting summer (top) and winter (bottom) inter-annual circulation variability over southern Africa, for the period 1979-2005.

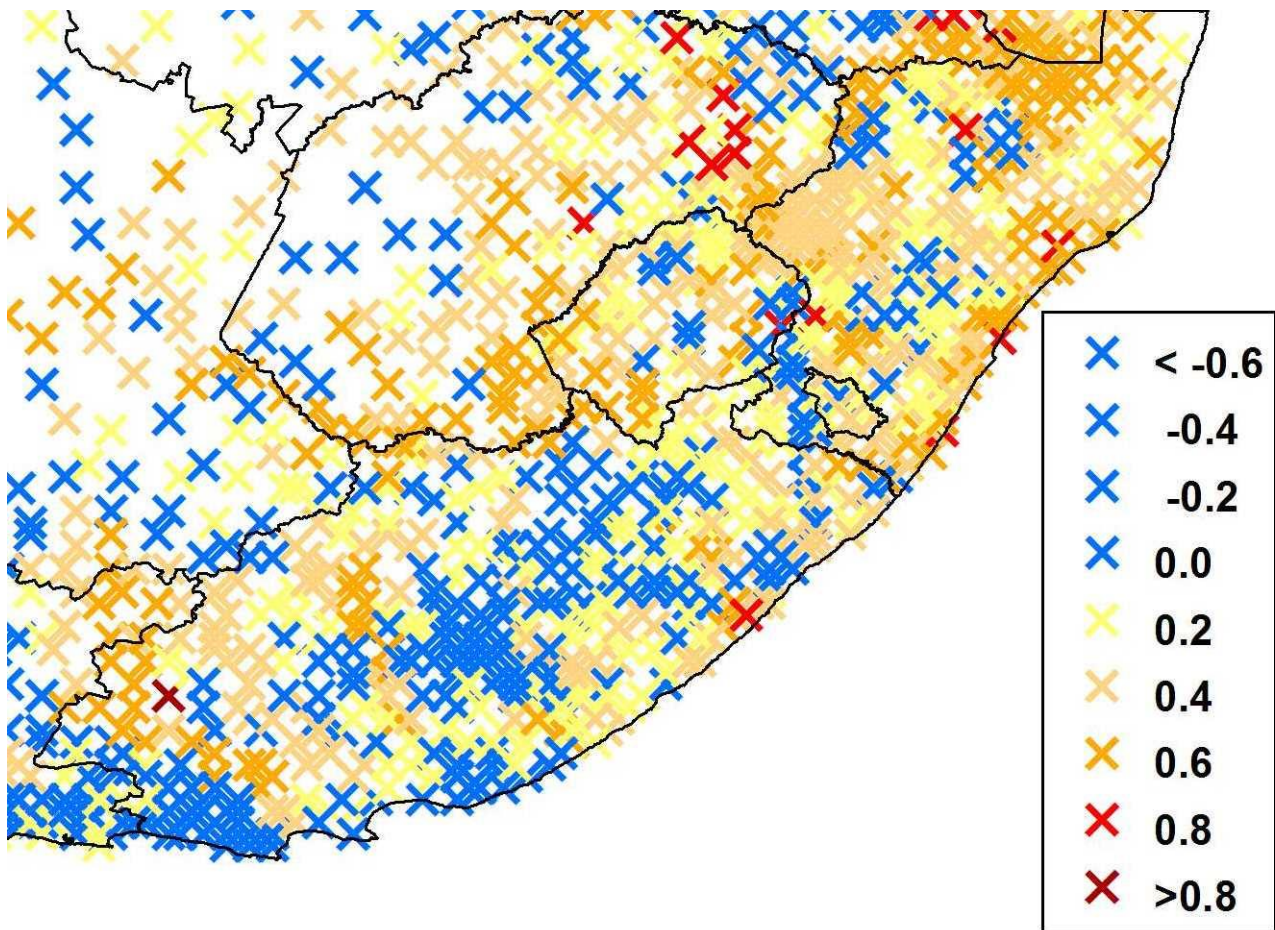


**Figure 4.7:** Kendal Tau correlation between the CCAM-AMIP predictions of summer season streamflow over the mega-dam area and observed natural streamflow, over the period 1979-2005.

From these relationships, mathematical equations can be constructed to predict local streamflow from the forecast large-scale circulation. Empirical remapping of atmospheric model fields to regional rainfall and streamflow has been demonstrated successfully over southern Africa. Here, the Climate Predictability Tool (CPT; <http://iri.columbia.edu>) was used to downscale the coarse resolution 850 hPa geopotential height fields of the CCAM AMIP simulations for summer (DJF) to streamflows at quaternary catchments across the mega-dam area by using catchment data produced by the University of KwaZulu-Natal. The skill in forecasting DJF and winter (July to August, JJA) rainfall over eastern South Africa is depicted in Figure 4.6. The skill is particularly high for the summer season, and this translates to high positive Kendal Tau correlations between predicted and observed streamflow (Figure 4.7) which demonstrates the skill of the statistically downscaled forecasts in representing observed streamflow over the mega-dam area.

#### 4.3.3 High-resolution seasonal forecasting over southern Africa

The results presented in this section are taken from the November initialized C96 (quasi-uniform resolution) global and C192 regional (8 km resolution over southern Africa) CCAM hindcast simulations for the 15 years from 2000 to 2014. In this study, the lead time is defined from the starting month when the model is initialized. For example, hindcasts from November ICs for NDJ (November-December-January) are referred to as zero month lead time hindcasts, while hindcasts for December-January-February (DJF), with the same initial conditions, are made at a 1 month lead and so forth. However, we only focus on the mid-summer (DJF) to assess the performance of the model simulations since the region has profound tropical influence via ENSO.

Figure 4.8 compares the model climatological simulation and corresponding observation. It is shown that the model C192 stretched-grid configuration tends to show a more realistic

climatological representation on the southern Africa region (Figure 1(b)) relative to the C96 CCAM configuration Figure 1(c). The latter particularly extends the rainfall regime to southern Namibia and western South Africa. Both model configurations overestimate rainfall over Indian Ocean and its surroundings, noticeably over Mozambique Channel while underestimating precipitation climatology over the central part of the model domain (eastern-Angola, southern-Zambia, northern-Zimbabwe and Mozambique). Nonetheless, the model global precipitation pattern reasonably resembles the Climate Research Unit (CRU 4.1; Harris et al., 2013).

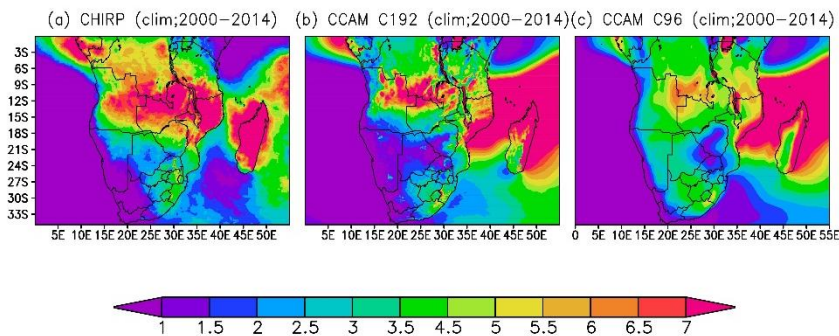


**Figure 4.8:** Daily Precipitation (mm/day) averaged over the period from DJF 2000/01 to DJF 2012/13. (a) CHIRP satellite estimates, (b) ensemble mean CCAM-CABLE C192, and (c) ensemble mean CCAM-CABLE C96.

The CCAM 8 km resolution seasonal forecast skill was investigated for the mid-austral summer at a one-month lead. The verification is based on 270 (15 years  $\times$  18 ensemble members) model retroactive forecasts each consisting of 6-month integrations in order to establish forecast lead-times of up to 4 months. Each ensemble set emulates a set of operational forecasts issued on the 6 of November each year starting from 2000 to 2014. The model bias in the mean annual cycle was removed from the model forecasts prior to comparing the statistics, i.e. computing the anomalies of the model about its own drifted climatology as a function of different initialization time and lead-months (e.g. Beraki et al., 2014, 2016). The model evaluation is done probabilistically because seasonal climate prediction is inherently probabilistic and applicably judges the model's ability or weakness in an operational context. Figure 4.9 presents the ability of the model to discriminate events from non-events using the relative operating characteristic area (ROC). It is noticeable that the model is skilful in discriminating below- and above-normal rainfall conditions over the southern Africa region where the tropical rainfall bearing system apparently associated with the seasonal migration of the ITZS (Inter Tropical Convergence Zone) and tropical temperate trough (TTT). However, the C96 probabilistic skill is marginal (not shown) which suggests that the dynamical downscaling may be able to further augment the quality of forecast (Figure 4.10) and potentially offer a better climate prediction strategy despite its computational cost. ROC applied to probabilistic forecasts indicates whether the forecast probability was higher when an event such as a flood or drought season occurred compared to when it did not occur. ROC scores for the rainfall categories for example represent the respective areas beneath the ROC curve that is produced by plotting the forecast hit rates against the false alarm rates. If the area would be  $\leq 0.5$ , the forecasts have no skill, and for a maximum ROC score of 1.0, perfect discrimination has been obtained. As in Beraki et al. (2014), the significance test is conducted using a variant of the Mann-Whitney non-parametric procedure that explicitly accounts for variance adjustment caused by incidents of ties.

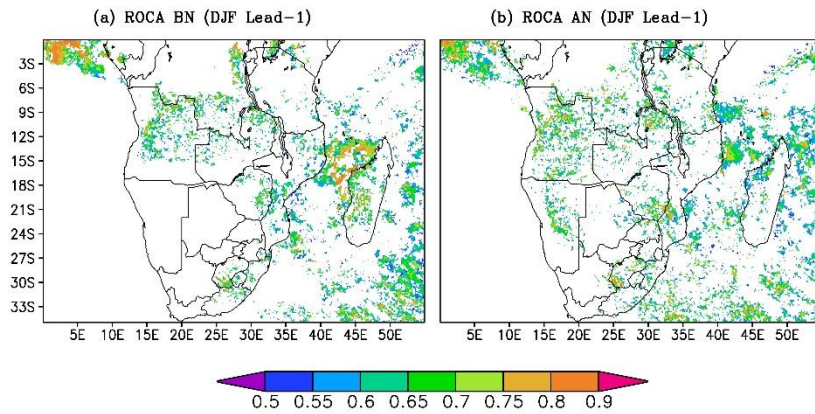


**Figure 4.9:** Southern Africa kill distribution as measured with ROC area daily accumulated rainfall (mm/day) the CCAM 8 km horizontal resolution mid-austral summer (DJF) one month lead for (a) below- and (b) above-normal categories. Only statistically significant values at the 95% level shades are shown

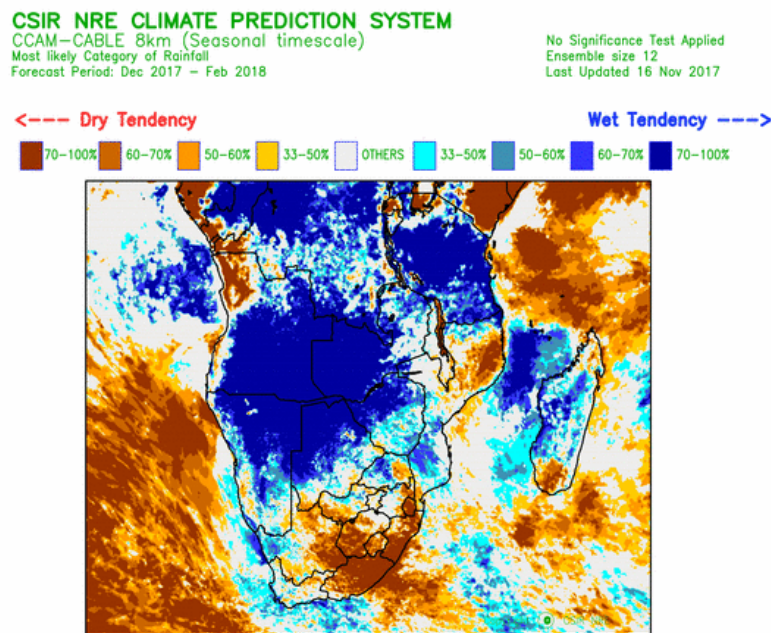


**Figure 4.10:** First ever probabilistic seasonal rainfall forecast release of the CCAM-CABLE operation ensemble prediction system (C192 stretched grid with 8 km zoom in over the southern Africa region). The forecast is based on the November initialization consist of 12 ensembles built as a function of 12 slightly different NCEP Environmental Modelling Center's (EMC) Global Forecasting System (GFS) atmospheric states and forced with multi-model SSTs (Landman et al., 2014). Worth noting is that the probabilities shown here were computed from the AMIP2 style climatology and the skill presented here is not the true reflection of this forecast.

#### 4.3.4 Changes in short-range predictability over southern Africa

Towards the objective analysis of synoptic types over southern Africa, a SOM was applied to National Centers for Environmental Prediction (NCEP) data for the period 1979-2014. The SOM was set-up to characterise 35 dominant synoptic types occurring over the region, specifically for the austral summer half-year months of October to March. The analysis was performed for 850 hPa geopotential data, given that circulation at this level resembles circulation over the southern African interior regions. The SOM obtained is shown in Figure 4.11. The bottom-left part of the SOM shows the case of a mid-latitude trough to the east of South Africa, with a ridging high-pressure system moving eastwards behind the trough. As is typical of a SOM analysis, the top-right

part of the SOM shows the “opposite” situation, namely an approaching trough in the western part of the domain, with a high ridging over eastern South Africa.

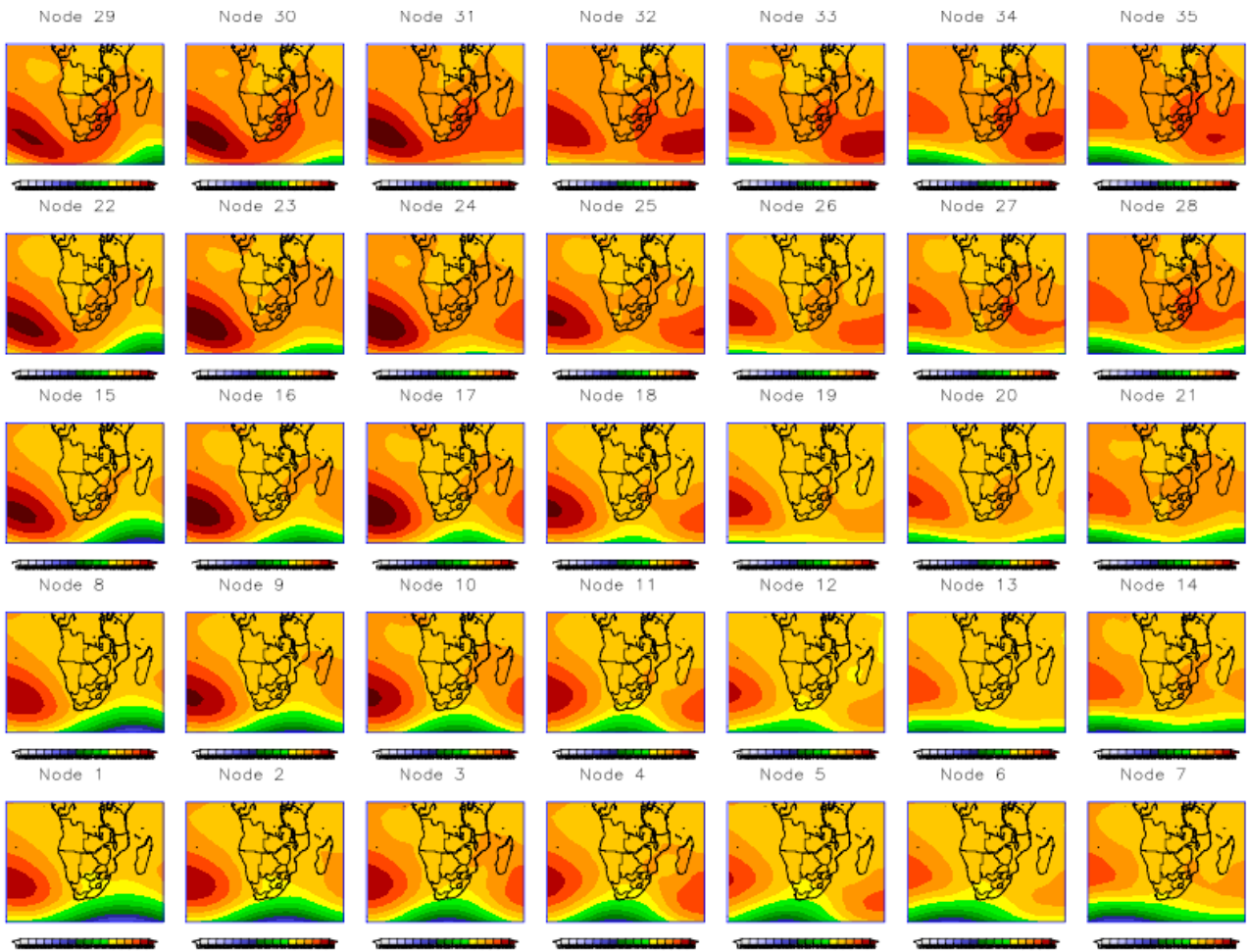


**Figure 4.11:** SOM characterisation of 35 dominant synoptic types over southern Africa based on NCEP reanalysis data for the period 1979-2014.

As a next step in the analysis, the rainfall pattern associated with each mode in the SOM was obtained by a mapping of Global Precipitation Climatology Project data onto the SOM, for the period 1997-2014. The results obtained are displayed in Fig. 4.12. For example, the bottom-left part of the SOM shows a meridional cloud band over the eastern part of the country, which occurs in association with the mid-latitude trough present in the south-eastern part of the domain (Fig. 4.11). The top-right part of the SOM shows an approaching band of rainfall in the southwestern part of the domain, which is also consistent with the corresponding synoptic-scale pattern of Fig. 4.11. The same procedure was subsequently applied to the CCAM predicted rainfall fields, also for the period 1997-2014. The result obtained is shown in Fig. 4.13. There is a close correspondence between the CCAM simulated rainfall patterns for each synoptic mode, and the corresponding GPCP patterns.

*To quantify how the CCAM predictions differ from one synoptic type to the next, the pattern correlation was calculated between the observed (Fig. 4.12) and predicted (Fig. 4.13) rainfall maps, for each of the 35 synoptic types. The result obtained is presented in Fig. 4.14. Rainfall is most predictable for the synoptic types occurring in the bottom-left part of the domain – these include in particular tropical-temperature troughs (Fig. 4.11) with well-defined meridional cloud bands connecting tropical Africa to mid-latitudes south of South Africa (Fig. 4.12). The synoptic types for which rainfall is predicted the least skilfully occur in the bottom-right part of the SOM. These include flow patterns indicative of easterly waves (Fig. 4.11), which are associated with*

zonal bands of high rainfall patterns stretching from Madagascar over the Indian Ocean to Mozambique. Such weather systems include landfalling tropical lows and tropical cyclones.

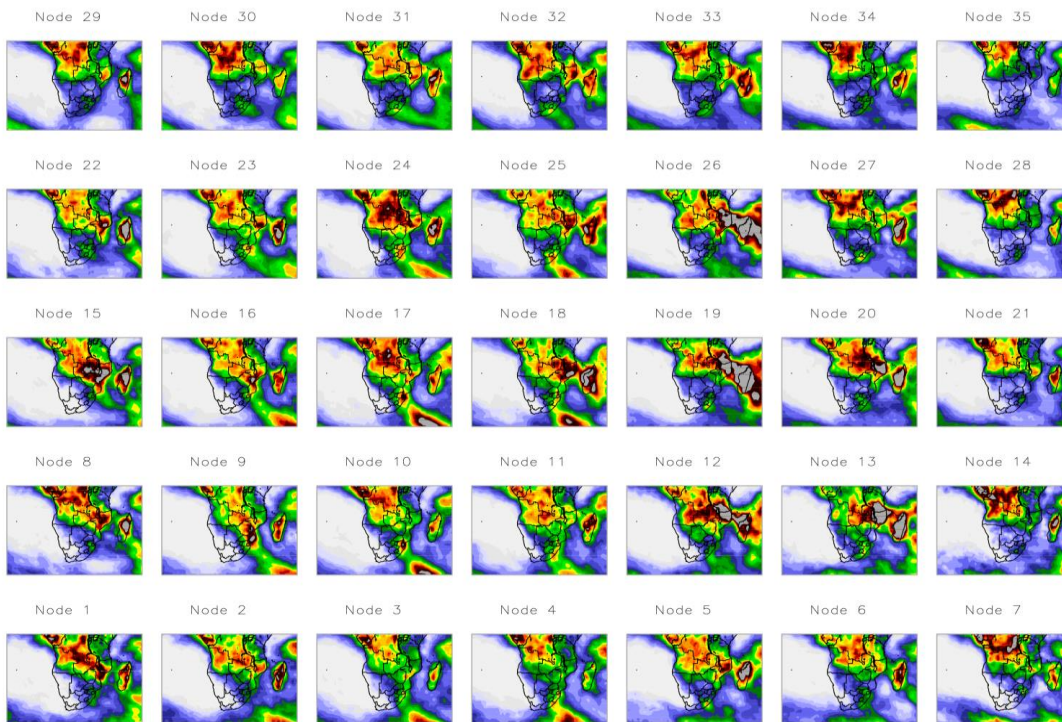


**Figure 4.12:** Rainfall patterns associated with each of the synoptic types, as deduced from GPCP data for the period 1997-2014.

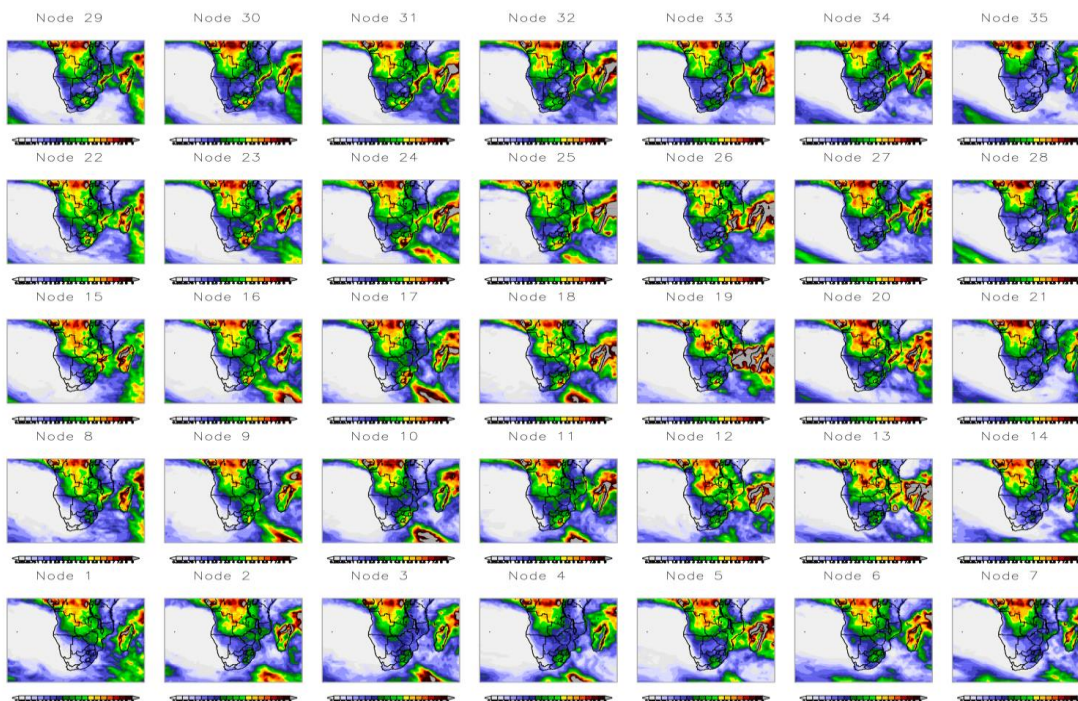


**Figure 4.13:** Rainfall patterns associated with each of the synoptic types, as deduced from the CCAM predictions for the period 1997-2014.

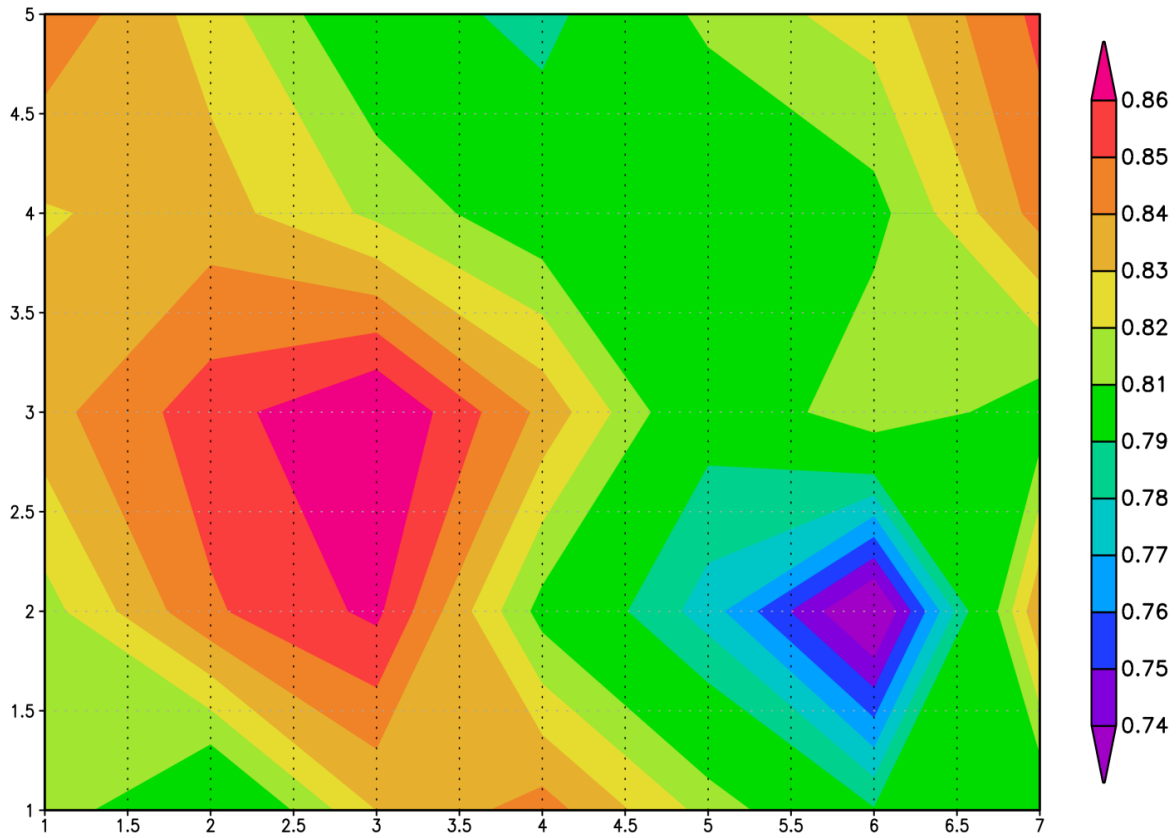


**Figure 4.14:** Pattern correlations between the CCAM (predicted) and GPCP (observed) rainfall fields for each of the 35 synoptic types

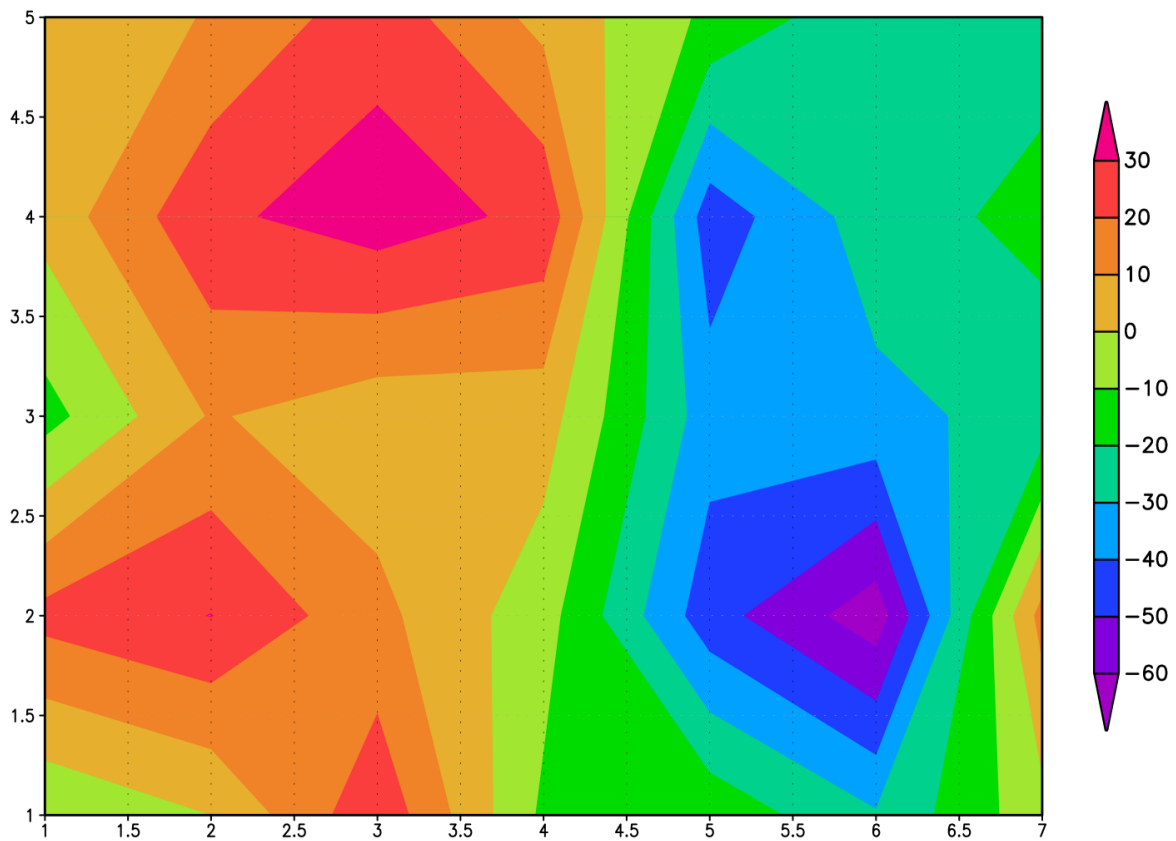


**Figure 4.15:** Projected changes in the frequency of occurrence of synoptic types over southern Africa (% change) for the far-future period (2070-2099) relative to the present-day (1961-1990).

In the final step of the analysis, CCAM was used to downscale the projections of the CCSM4 GCM to a resolution of 50 km globally, for the period 1961-2100. The CCAM simulations of the daily 850 hPa geopotential heights were subsequently mapped onto the SOM of NCEP-reanalysis derived synoptic types. This mapping was performed for the period 1961-1990 (present-day climate) and 2070-2099 (future climate), and the frequencies of occurrence of the different synoptic types for both periods were subsequently obtained. The results obtained are shown in Fig. 4.15. A clear pattern is projected, of synoptic types occurring in the left part of the SOM occurring more frequently under climate change, with synoptic types occurring in the right part of the SOM occurring less frequently under climate change. The synoptic types of the left part of the SOM are clearly (Fig. 4.11) defined by well-defined westerly troughs in the south-eastern part of the domain, including westerly waves occurring in association with well-defined tropical-temperate, meridional rainfall bands. Such weather systems are the most-predictable (Fig. 4.14) and are projected to increase in frequency under climate change (Fig. 4.15). The synoptic types on the right part of the SOM are associated with much weaker westerly wind circulation patterns, but with stronger easterly waves and patterns of moisture advection from the east. That is, the systems in the east exhibit more tropical characteristics and are less predictable in terms of rainfall (Fig. 4.14). Such systems are projected to occur less frequently under climate change (Fig. 4.15).

#### **4.4 Summary**

In response to a generally warmer global climate under low mitigation, the austral summer inter-annual variability of both temperature and rainfall are projected to increase over the eastern parts of southern Africa. This is the case in particular for the Limpopo river basin, which exhibits the strongest ENSO signal in southern Africa under present-day climate. Most projections are also indicative of increased variability over the mega-dam area of eastern South Africa, but variability is projected to decrease over the Cape south coast region and also over the central and western interior regions. However, increasing variability does not necessarily imply decreasing predictability. In fact, the research is indicative that the inter-annual variability of austral summer circulation may become more predictable over the eastern parts of southern Africa under enhanced greenhouse gas warming – and specifically over the Limpopo river basin. This may be due to a stronger ENSO cycle and teleconnection to southern Africa under climate change, a signal already well captured and simulated by climate models, thereby yielding increased predictability.

The present-day predictability of streamflow over the mega-dam region was also investigated through a typical statistical downscaling approach. Predictability of circulation (predictor) is high for summer, due to the strong influence of the El Niño Southern Oscillation (ENSO) on atmospheric circulation over southern Africa during this season. With summer also the most important season in terms of streamflow and the replenishment of dams, this is an important result. The predictability of winter-time circulation over the mega-dam area is significantly less, however. This is due to the ENSO signal being weak in winter, which in combination with an equatorward displacement of the westerly wind regime results in a more chaotic circulation regime over the southern parts of southern Africa. It follows that the skill in predicting circulation as streamflow predictor for DJF, the predictions for the predictant (streamflow) is also skilful. This is an important finding, implying that water managers responsible for decision making around flows and dam-levels in the mega-dam area can with confidence make use of seasonal forecasts of streamflow as an aid in decision making.

The chapter also explored the potential advantages of downscaling typical low-resolution CCAM seasonal forecasts, such as those used to generate the seasonal predictions of streamflow, to very high resolution (8 km in the horizontal) to South Africa. The primary motivation for pursuing this computational expensive model configuration, lies on the fact that this level of detail (if rigorously skilful) is vital for various climate applications. There is also the possibility that higher resolution may result in increased skill in predicting rainfall over regions of steep topography such as the eastern escarpment. The high-resolution probabilistic forecasts for the austral summer season for daily accumulated rainfall were found to be fairly skilful. The model was able to discriminate significantly wet and dry summers over southern Africa. Climatologically, the dynamical downscaling was also found to further improve the rainfall pattern simulated by its driving GCM.

Short-range predictability over southern Africa was explored for the present-day climate, followed by an analysis of how this predictability may be altered by climate change. A SOM-based analysis revealed that rainfall is predicted best for synoptic-types associated with well-defined westerly wave characteristics, including well defined tropical-temperate troughs occurring over southern Africa. Such weather patterns are projected to occur more frequently under climate change, implying that rainfall over southern Africa may become more predictable. Conversely, synoptic types associated with moisture fluxes from the east, including easterly wave systems, are projected to occur less frequently under climate change. Such systems, although the least predictable, are also the most important in terms of the occurrence of rainfall over southern Africa. Qualitatively, therefore, the results are indicative of a generally drier climate over southern Africa under climate change, but in which individual rainfall events may be more predictable.

## Chapter 5 Projected changes in hydrology over the eastern escarpment and mega-dam region of South Africa

### 5.1 Introduction

The research performed in previous chapters has demonstrated that pronounced changes in rainfall and temperature may occur over the mega-dam region under climate change. In terms of potential impacts on hydrology, there are three main messages of change that may be considered to be most important: 1) Multi-year droughts may occur frequently over the mega-dam region as early as the mid-future period of 1946-2065, presumably in response to the more frequent occurrence of El Niño events; 2) it is nevertheless that extreme convective rainfall events may occur more frequently over the mega-dam region, which may result in increases in run-off and 3) drastic increases in temperature may result in increases in evaporation in the mega-dam region.

In this chapter the potential effects of climate change on dam levels and streamflow in the mega-dam region is explored, through the use of both statistical downscaling procedures and fully dynamic (mechanistic) hydrological models. An analysis of variability and trends in dam levels as observed over the last few decades is also presented, for each of the major dams in the mega-dam region.

### 5.2 Methodology

#### *5.2.1 Time-series analysis of dam levels*

A time-series analysis is performed on the dam-levels recorded for each of the largest dams in the mega-dam area as recorded over the last several decades. The purpose of this analysis is to gain insight into the inter-annual to decadal to multi-decadal variability as well as trends in dam levels, and to investigate how these variabilities and trends correlate to rainfall. It is acknowledged though, that while the estimate of observed rainfall as calculated for each catchment relevant to a particular mega dam represents the output of a natural system, levels of dams are determined both by the characteristics of the climate system, particularly inter-annual variability, and management decisions. While management decisions are taken with consideration of user needs and climate variability, the overall effect of large/severe climatological anomalies may still be expected to be reflected in the year-to-year variation of dam levels. Moreover, the cumulative effect of prolonged climate anomalies – such as hydrological droughts – is reflected more significantly in the deviation of dam levels, especially as capacity increases. The investigation of the characteristics of the levels of mega dams in the summer rainfall region of eastern South Africa therefore aims to explore this broad association and also the characteristics of the time series of rainfall and fluctuations in the dam levels.

The global updated gridded climate dataset at 0.05° spatial resolution and monthly temporal resolution (CRU TS3.10 – Harris et al., 2014) was used to calculate the spatial average total yearly rainfall per relevant catchment for each of the dams. This climate dataset is an interpolation of monthly observations at meteorological stations across the world's land areas. A time series of weekly levels of storage for each of the relevant storage dams was obtained from the Department of Water Affairs and Sanitation (DWS). The dataset for each dam spans the entire operational period. The statistical properties of annual rainfall and percentage of storage for each of the dams was calculated. The dams considered are listed in Table 5.1.

**Table 5.1:** Location of Dams

	<b>Dam Name</b>	<b>latitude</b>	<b>Longitude</b>	<b>Dam Record</b>
<b>1</b>	<b>Gariep</b>	<b>-30.6237</b>	<b>25.5064</b>	<b>1971-2014</b>
<b>2</b>	<b>Vaal</b>	<b>-26.8947</b>	<b>28.1455</b>	<b>1936-2014</b>
<b>3</b>	<b>Sterkfontein</b>	<b>-28.4484</b>	<b>29.0228</b>	<b>1974-2014</b>
<b>4</b>	<b>Katse</b>	<b>-29.3369</b>	<b>28.5060</b>	<b>1996-2014</b>
<b>5</b>	<b>Vanderkloof</b>	<b>-29.9922</b>	<b>24.7317</b>	<b>1977-2014</b>

### *5.2.2 Dynamic hydrological modelling*

The core input to the dynamic hydrological modelling performed in the project are the 8 km resolution projections of future climate change over eastern South Africa, performed for the period 1961-2100 through the downscaling of 6 different GCMs for two different mitigation scenarios (see Chapter 3). Simulations of present-day hydrology and its projected futures under climate change are presented for the mega dam area – based on the simulations of state of the art dynamic hydrological model (river routing model) which runs fully coupled to the CCAM-CABLE modelling system. This system has recently been further developed to include the river runoff scheme previously used within the Commonwealth Scientific and Industrial Research Organisation (CSIRO) Mk3.5 coupled global climate model. The river runoff is directed, using the local topography for river direction, down to coastal points. A time delay method is applied to transfer water to the oceans, with river flow being processed via “river-reservoirs” per model land point using flow velocities to adjacent grid points (CSIRO Atmospheric research Technical Paper). Due to the complexity of river systems in reality, with the actual terrain not being adequately resolved by typical climate model simulations, there is an option of a pre-computation stage using a high resolution surface topography data set, together with manual intervention, to help define realistic surface flow directions for the river runoff on the model grid. The river routing scheme is fairly simple with no meandering term, although there are options for allowing moisture to seep into the surrounding soil. Also, the local slope is used to estimate the water flux leaving the four sides of each model grid, whereas more advanced river models allow water to leave in 8 directions. Nevertheless, the application of this system lays the foundation for a more advanced river routing scheme within the new CSIR fully coupled climate model, and potentially provides the foundation for a step-up in hydrological modelling over southern Africa.

### *5.2.3 Observed streamflow data and statistical projections of stream-flow*

The projections of future streamflow and its variability under climate change as described in this deliverable were obtained through a Self-Organising Map (SOM) approach. The first step involved the clustering of the summer half-year (October to March; ONDJFM) rainfall anomalies as obtained from Climatic Research Unit (CRU) data (CRU-TS3.2) for the period 1920/21 to 2008/09 into 12 representative nodes using SOMs. The anomalies were obtained by subtracting from each of the ONDJFM rainfall totals the ONDJFM climatology for the period 1961-1990. Streamflow data for the same period were subsequently mapped onto the SOM, thereby statistically defining a spatial relationship between rainfall and streamflow. The streamflow data used was naturalised as constructed by the Royal HaskoningDHV for the Water Research Commission project of 2012 (WR2012) and it is available online ([www.waterresourceswr2012.co.za](http://www.waterresourceswr2012.co.za)). Naturalised flow is obtained by removing man-made influences such as dams, irrigation schemes, abstractions for mines, industry and towns, the return flows from treatment works, etc. The WR2012 streamflow data consist of monthly flows in million cubic meters per month and span the period 1920 to 2009. For the purpose of this report, data for each ONDJFM period was accumulated from the relative individual months.

The model projections of future rainfall anomalies for the summer season were subsequently mapped onto the SOM, season by season, which enabled the projection of future streamflow patterns, by using the previously determined statistical relationship between rainfall and streamflow.

### 5.3 Results – variability, trends and projected changes in dam levels

#### 5.3.1 Present-day variability

Climate variability at the decadal time scale is prevalent in South Africa, especially over the summer rainfall region of eastern South Africa and Lesotho. Multi-year dry periods are discernible in extremely low levels of dams associated with these – for all the different dams studied in this report. Such dry periods occurred, in South Africa, in the mid-to late 1940s, early 1950s, mid-to late 1960s, early to mid-1980s, early 1990s, early 2000s (e.g. Malherbe et al., 2016). The clear association between rainfall and dam levels within such periods emphasize the need to study also the tendency for persistent dry or wet conditions to change in their intensity and frequency of occurrence under climate change. Depending on the commissioning dates for the dams, time series lengths differ and vary between 20 and 80 years.

#### Gariep Dam

This storage dam is situated in the Orange River and was completed in 1971. With a total estimated volume of 5 196 000 000 m<sup>3</sup>, this dam is the largest of the mega dams. Its tributaries to the east underline the importance of hydro climatological variability over the escarpment including the Highlands in Lesotho.

Figures 5.1a and 5.1b show the annual rainfall and level (as percentage of full capacity) for the Gariep dam. Multi-year periods of below-normal rainfall are reflected in the level of the dam, resulting in relatively low values by the early 1970s, early 1980s, early 1990s and again the early 2000s.

Table 5.2 shows some of the calculated statistics for the two yearly time series (rainfall and % of full capacity) together with some of the regression statistics.

**Table 5.2:** Statistics for Gariep Dam: Catchment Rainfall and dam fill (%).

<b>CRU Rain Totals</b>		<b>Ave Gariep fill%</b>	
<b>Mean</b>	<b>461.3</b>	<b>Mean</b>	<b>74.1</b>
<b>Standard Error</b>	<b>21.0</b>	<b>Standard Error</b>	<b>2.3</b>
<b>Median</b>	<b>431.8</b>	<b>Median</b>	<b>75.1</b>
<b>Standard Deviation</b>	<b>139.8</b>	<b>Standard Deviation</b>	<b>15.5</b>
<b>Sample Variance</b>	<b>19568.9</b>	<b>Sample Variance</b>	<b>242.3</b>

<b>Regression Statistics</b>	
<b>Correlation coefficient</b>	<b>0.3999</b>
<b>R Square</b>	<b>0.1599</b>
<b>Adjusted R Square</b>	<b>0.1399</b>
<b>Standard Error</b>	<b>14.4365</b>

<b>Coefficients</b>	
<b>Intercept (b)</b>	<b>53.6196</b>
<b>CRU Rain (a)</b>	<b>0.0445</b>

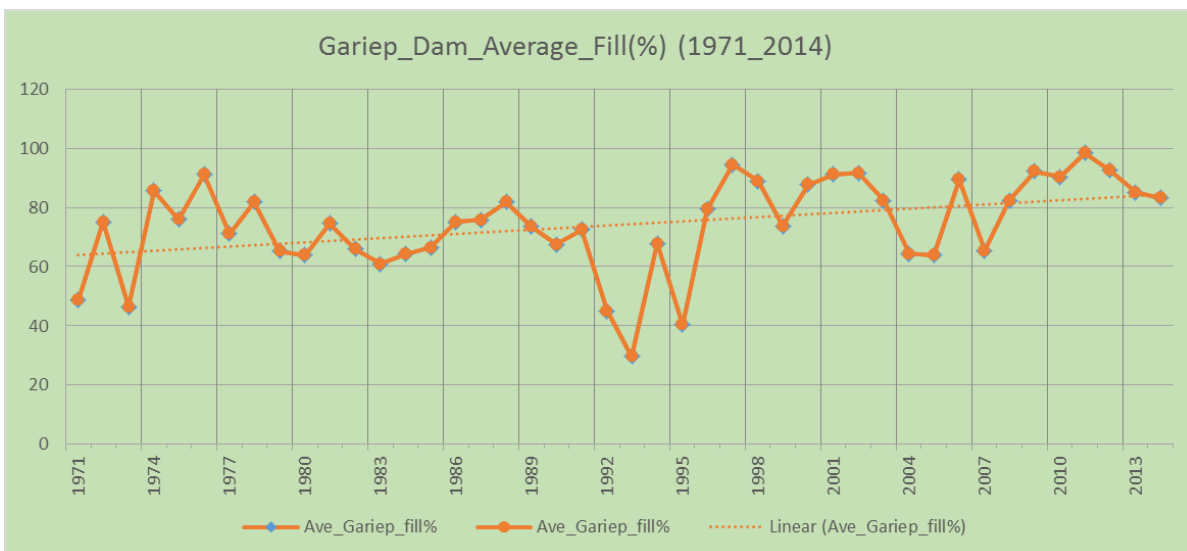
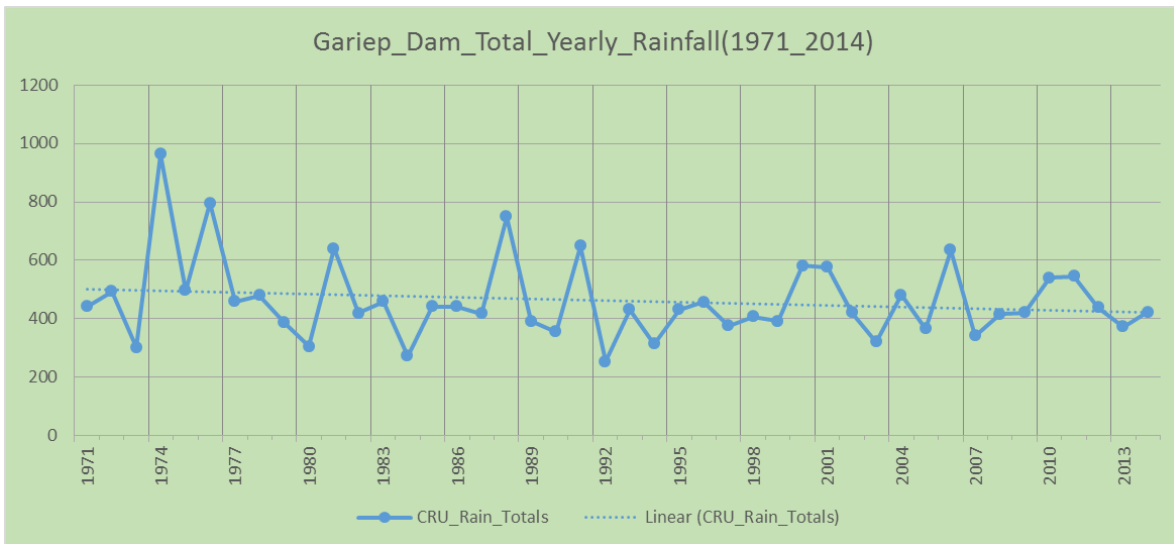


**Figure 5.1:** Gariep dam (a) Rainfall and (b) Dam fill (%).

The Spearman Rank Correlation between the annual rainfall in the catchment and level of the dam is 0.4, and is significant at the 90% level of confidence.

### Vaal Dam

The Vaal Dam lies on the Vaal River and was commissioned in 1938. It has a storage capacity of 2 603 000 000 m<sup>3</sup>. The capacity of the dam was increased in the early 1950s when the wall was raised with 6 m. It is the 4<sup>th</sup> largest dam (by volume) in South Africa.

Figures 5.2a and 5.2b show the annual rainfall and level as percentage of full capacity for the dam. Multi-year periods of below-normal rainfall are reflected in the level of the dam, resulting in relatively low values by the mid-to late 1940s, mid-1960s and the other periods as mentioned for the Gariep. Increased water usage has contributed to the relatively large impacts of the multi-year droughts since the early 1980s.

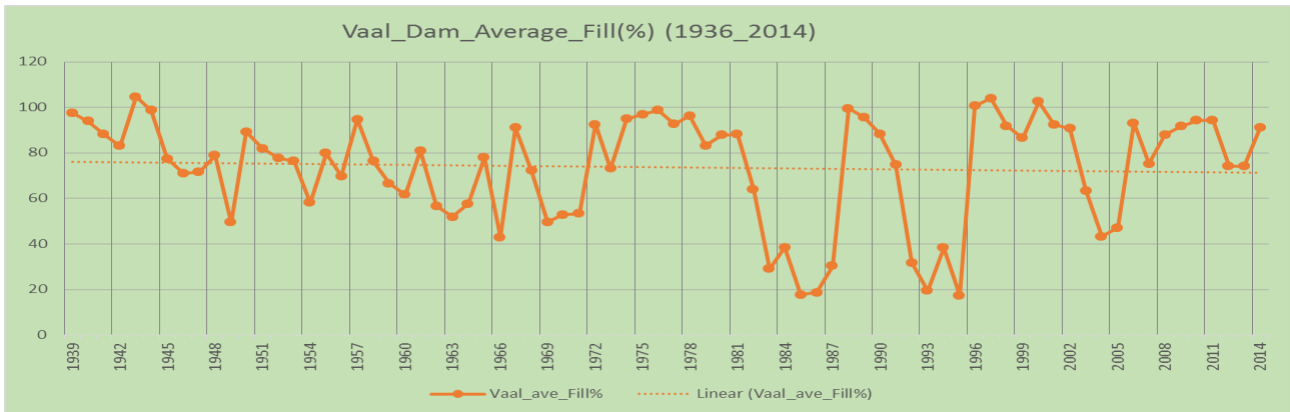
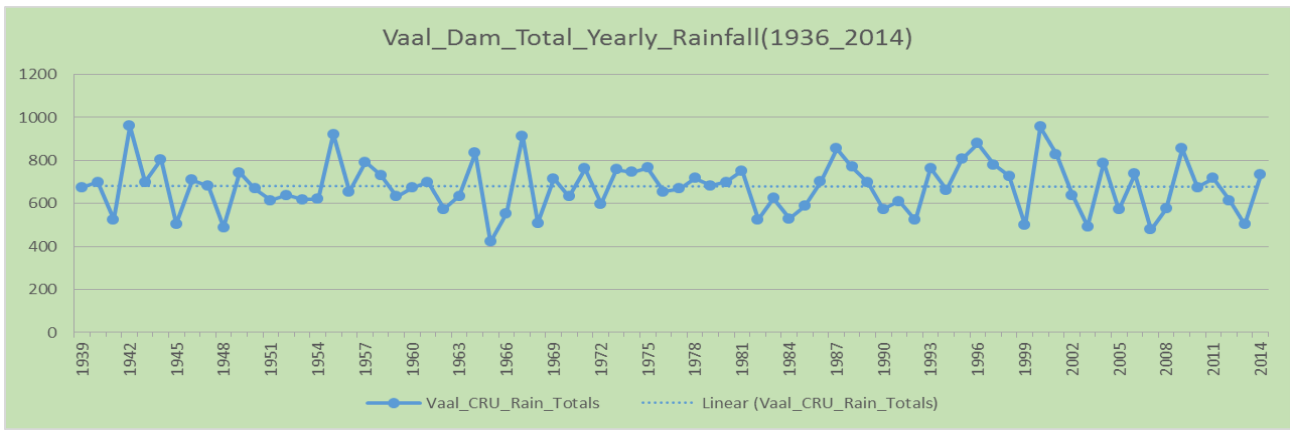


**Figure 5.2:** Vaal dam (a) Rainfall and (b) Dam fill (%).

Table 5.3 shows some of the calculated statistics for the Vaal Dam for the two yearly time series (rainfall and % of full capacity) together with some of the regression statistics.

**Table 5.3: Statistics for Vaal Dam: Catchment Rainfall and Dam fill (%)**

<b>Vaal CRU Rain Totals</b>		<b>Vaal ave Fill%</b>	
<b>Mean</b>	<b>678.6566</b>	<b>Mean</b>	<b>73.7144</b>
<b>Standard Error</b>	<b>13.6197</b>	<b>Standard Error</b>	<b>2.6882</b>
<b>Median</b>	<b>678.0500</b>	<b>Median</b>	<b>78.4680</b>
<b>Standard Deviation</b>	<b>118.7338</b>	<b>Standard Deviation</b>	<b>23.4348</b>
<b>Sample Variance</b>	<b>14097.7078</b>	<b>Sample Variance</b>	<b>549.1889</b>

<b>Regression Statistics</b>	
<b>Correlation coefficient</b>	<b>0.1877</b>
<b>R Square</b>	<b>0.0352</b>
<b>Adjusted R Square</b>	<b>0.0222</b>
<b>Standard Error</b>	<b>23.1732</b>

	<b>Coefficients</b>
<b>Intercept (b)</b>	<b>48.5709</b>
<b>CRU Rain (a)</b>	<b>0.0370</b>

The Spearman Rank Correlation between the annual rainfall in the catchment and level of the dam is 0.3, and is significant at the 90% level of confidence.

## Sterkfontein Dam

The Sterkfontein Dam (commissioned in 1980) is located near Harrismith in the Free State. The dam is part of the Tugela-Vaal Water Project and the Drakensberg Pumped Storage Scheme. It is in a tributary of the Wilge River in the upper catchment area of the Vaal. Full storage capacity is estimated at 2 617 000 000 m<sup>3</sup>.

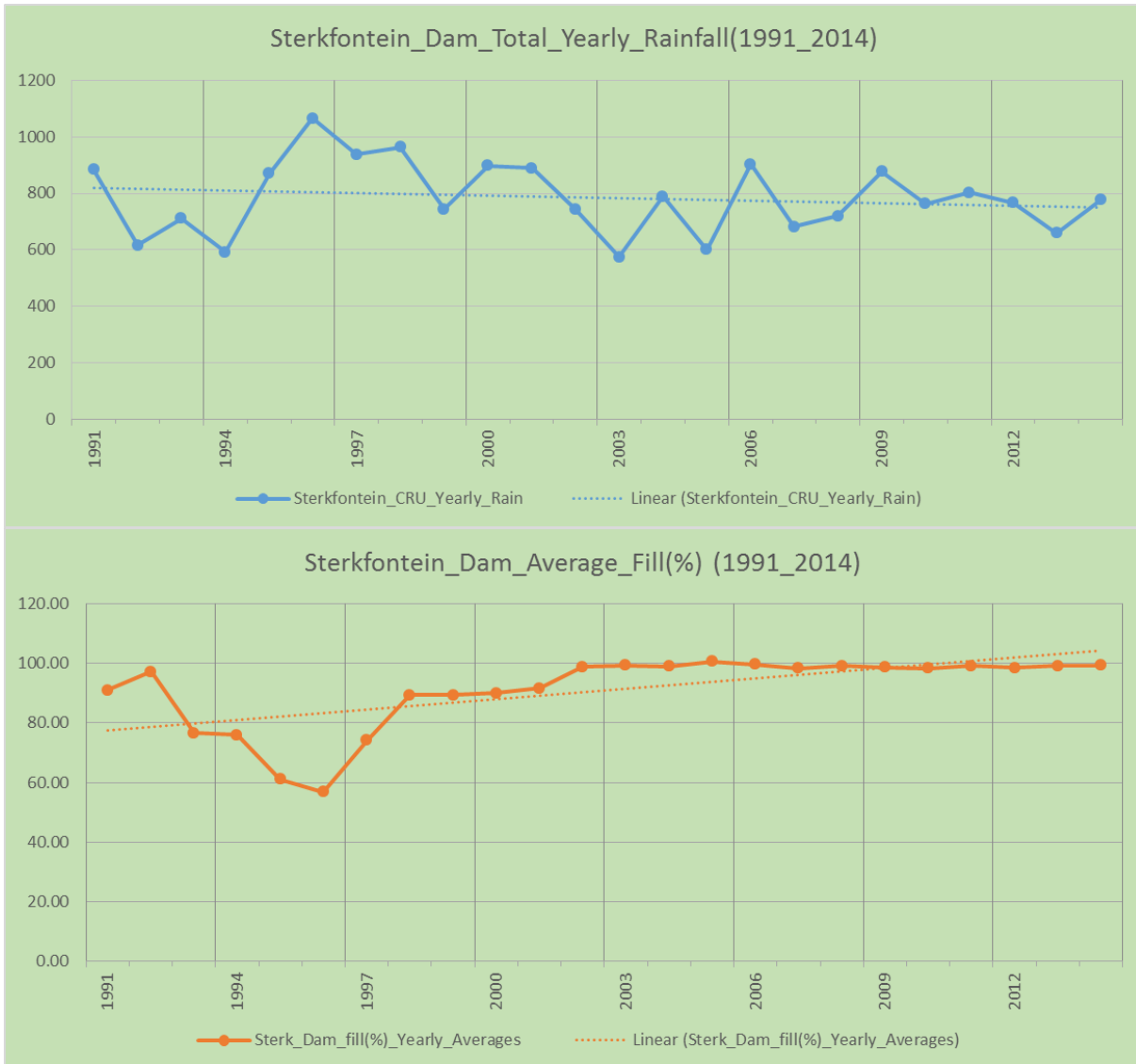


**Figure 5.3:** Sterkfontein dam (a) Rainfall and (b) Dam fill (%).

Table 5.4 shows some of the calculated statistics for the Sterkfontein Dam for the two yearly time series (rainfall and % of full capacity) together with some of the regression statistics.

Figures 5.3a and 5.3b shows the annual rainfall and level as percentage of full capacity for the Sterkfontein dam. Multi-year periods of below-normal rainfall are reflected in the level of the dam, resulting in relatively low values by the early 1990s and the early 2000s. The persistence of below-normal rainfall in the early 1990s had a significant negative impact (whether directly related to climate inputs or indirectly through management responses based on climate input) on the storage.

**Table 5.4:** Statistics for Sterkfontein Dam: Catchment Rainfall and Dam fill (%)

<b><i>Sterkfontein CRU Yearly Rain</i></b>		<b><i>Sterk Dam fill(%) Yearly Averages</i></b>	
<b>Mean</b>	<b>784.3</b>	<b>Mean</b>	<b>90.9</b>
<b>Standard Error</b>	<b>26.2</b>	<b>Standard Error</b>	<b>2.5</b>
<b>Median</b>	<b>771.3000</b>	<b>Median</b>	<b>98.2</b>
<b>Standard Deviation</b>	<b>128.7</b>	<b>Standard Deviation</b>	<b>12.6</b>
<b>Sample Variance</b>	<b>16564.3</b>	<b>Sample Variance</b>	<b>159.9</b>

<b><i>Regression Statistics</i></b>	
<b>Correlation coefficient</b>	<b>0.44</b>
<b>R Square</b>	<b>0.19</b>
<b>Adjusted R Square</b>	<b>0.16</b>
<b>Standard Error</b>	<b>11.57</b>

<b><i>Coefficients</i></b>	
<b>Intercept (b)</b>	<b>125.1491</b>
<b>CRU Rain (a)</b>	<b>-0.0437</b>

*Katse Dam*

The Katse Dam (completed in 1996) is located on the Malibamat'so River in Lesotho. It has a total storage capacity of 1 950 000 000 m<sup>3</sup>. The dam is part of the Lesotho Highlands Water Project. The percentage of storage capacity of the dam shows the strongest correlation with yearly rainfall relative to the other dams considered. Figures 5.4a and 5.4b show the annual rainfall and level as percentage of full capacity for the Katse Dam. The multi-year period during the early 2000s had a profound effect on the level of the dam relative to the rest of the period. Figures 5.4a and 5.4b shows the annual rainfall and level as percentage of full capacity respectively for the dam.

Table 5.5 shows some of the calculated statistics for the Katse Dam for the two yearly time series (rainfall and % of full capacity) together with some of the regression statistics.

**Table 5.5:** Statistics for Katse dam: Catchment Rainfall and Dam fill (%)

<b><i>Katse CRU Rain Aver</i></b>		<b><i>Katse Damfill(%)</i></b>	
<b>Mean</b>	<b>846.6</b>	<b>Mean</b>	<b>86.2</b>
<b>Standard Error</b>	<b>30.3</b>	<b>Standard Error</b>	<b>2.6</b>
<b>Median</b>	<b>839.3</b>	<b>Median</b>	<b>90.1</b>
<b>Standard Deviation</b>	<b>125.0</b>	<b>Standard Deviation</b>	<b>10.9</b>
<b>Sample Variance</b>	<b>15643.8</b>	<b>Sample Variance</b>	<b>120.0</b>

<b><i>Regression Statistics</i></b>	
<b>Correlation coefficient</b>	<b>0.54</b>
<b>R Square</b>	<b>0.29</b>
<b>Adjusted R Square</b>	<b>0.26</b>
<b>Standard Error</b>	<b>9.49</b>

<b>Coefficients</b>	
<b>Intercept (b)</b>	<b>45.8552</b>
<b>CRU Rain (a)</b>	<b>0.0477</b>

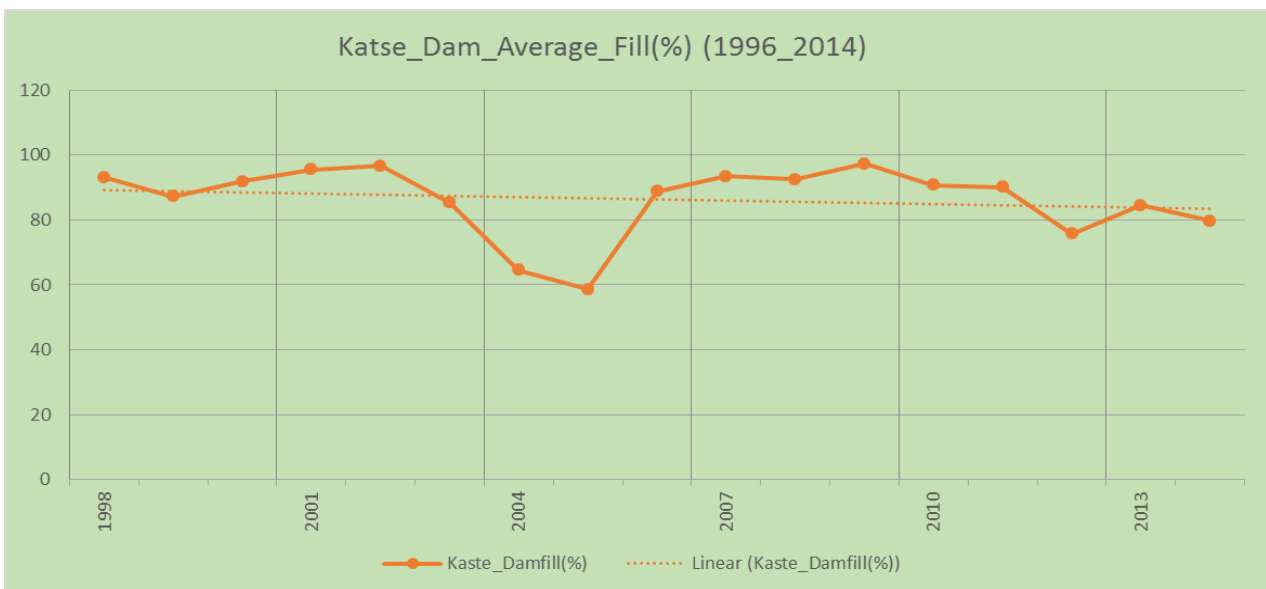
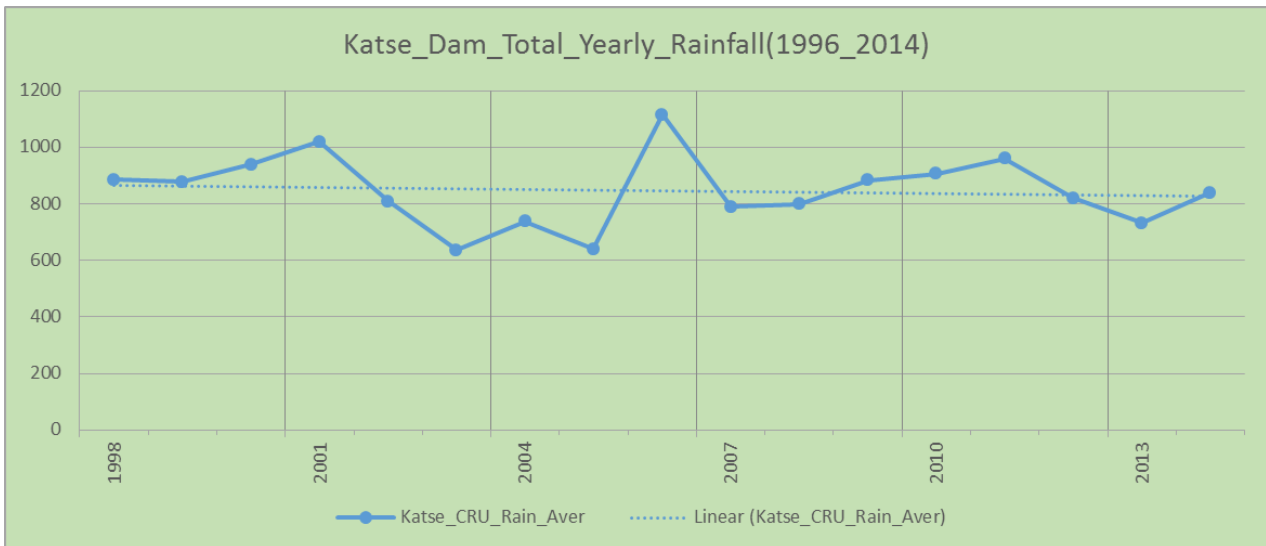


**Figure 5.4:** Katse dam (a) Rainfall and (b) Dam fill (%).

The Spearman Rank Correlation between the annual rainfall in the catchment and level of the dam is 0.4, and is significant at the 90% level of confidence.

#### *Van der Kloof Dam*

The Vanderkloof Dam is situated downstream from Gariep Dam in the Orange River. It is the second-largest dam in South Africa and has a capacity of 3 187 000 000 m<sup>3</sup>. The dam was commissioned in 1977. The multi-year dry periods during the early 1980s, early 1990s and early 2000s had profound impacts on the level of the dam. Figures 5.5a and 5.5b show the annual rainfall and level as percentage of full capacity respectively for the dam.

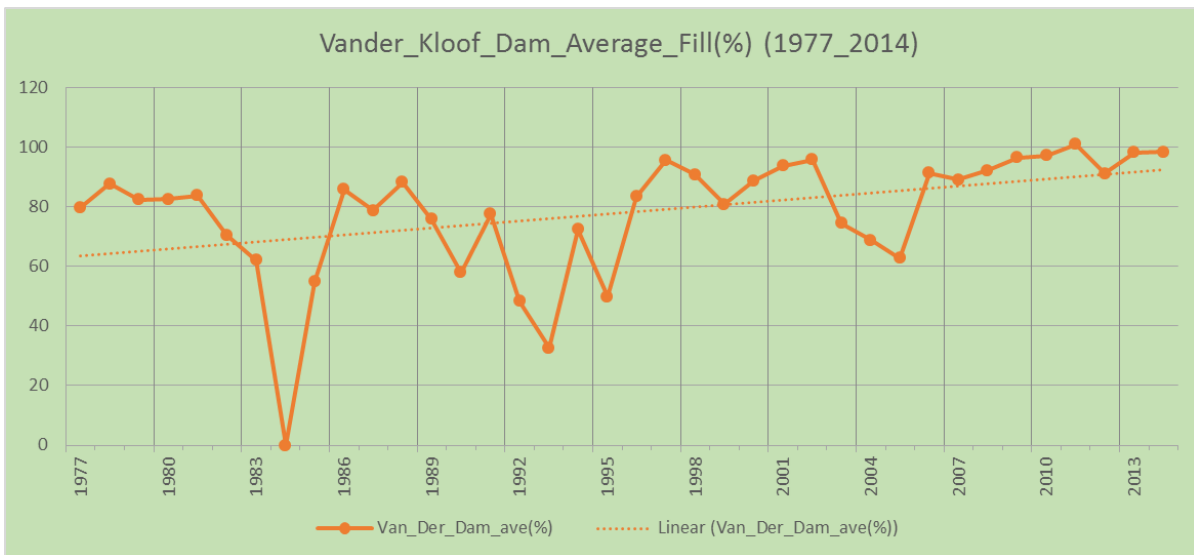
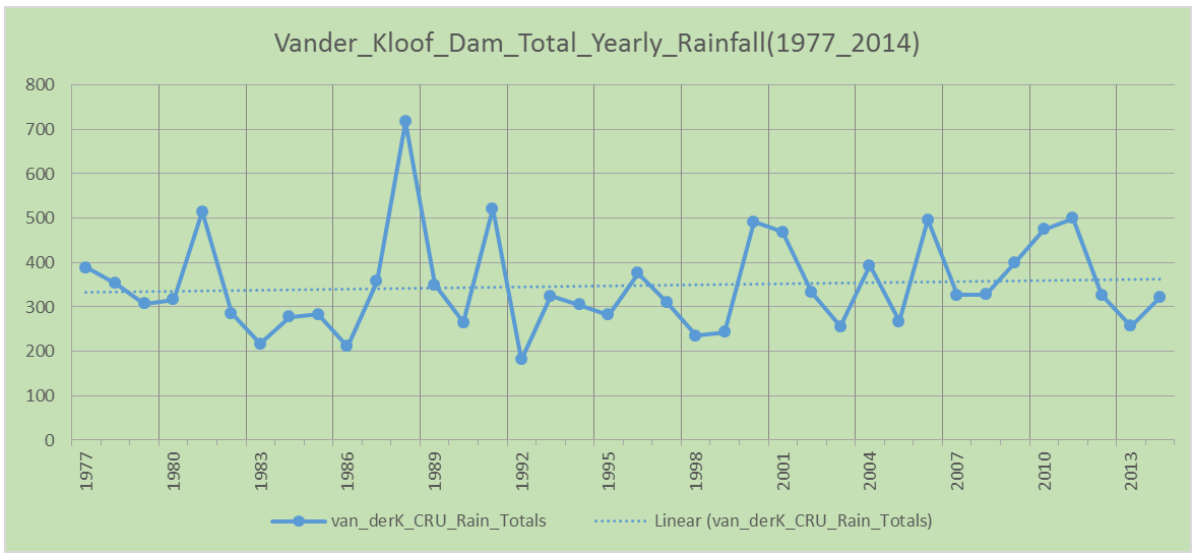


**Figure 5.5:** Van der Kloof dam (a) Rainfall and (b) Dam fill (%).

Table 5.6 shows some of the calculated statistics for the Van der Kloof Dam for the two yearly time series (rainfall and % of full capacity) together with some of the regression statistics.

**Table 5.6:** Statistics for Van der Kloof Dam (a) Rainfall and (b) Dam fill (%) for the climate record in Table 5.1.

<b>Van derK CRU Rain Totals</b>		<b>Van derK Dam ave(%)</b>	
<b>Mean</b>	<b>348.4</b>	<b>Mean</b>	<b>77.8</b>
<b>Standard Error</b>	<b>17.7</b>	<b>Standard Error</b>	<b>3.3</b>
<b>Median</b>	<b>325.0</b>	<b>Median</b>	<b>82.9</b>
<b>Standard Deviation</b>	<b>109.2</b>	<b>Standard Deviation</b>	<b>20.5</b>
<b>Sample Variance</b>	<b>11926.3</b>	<b>Sample Variance</b>	<b>423.7</b>

<b>Regression Statistics</b>	
<b>Correlation coefficient</b>	<b>0.36</b>
<b>R Square</b>	<b>0.13</b>
<b>Adjusted R Square</b>	<b>0.11</b>
<b>Standard Error</b>	<b>19.41</b>

	<b>Coefficients</b>
<b>Intercept (b)</b>	<b>53.7849</b>
<b>CRU Rain (a)</b>	<b>0.0692</b>

The Spearman Rank Correlation between the annual rainfall in the catchment and level of the dam is 0.42, and is significant at the 90% level of confidence.

### *5.3.2 Projections of future climate change – rainfall and dam levels*

In this section the projected changes in rainfall and dam levels are presented for each of the 5 mega-dams considered in this report.

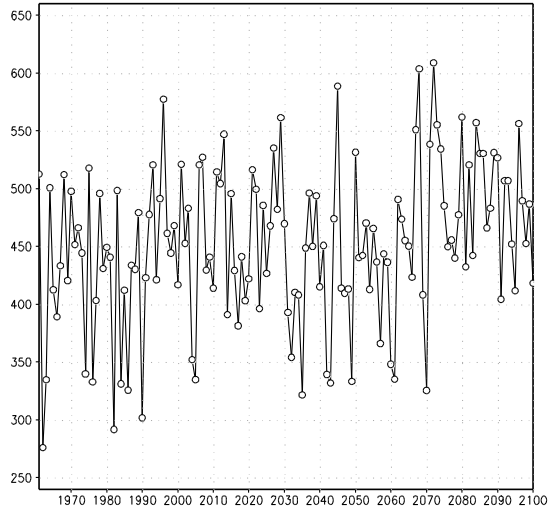
#### *Gariiep Dam*

The rainfall futures for the Gariiep dam catchment (Figure 5.6a) are uncertain. Two of the downscalings are indicative of significant decreases in rainfall, and as a consequence, of associated negative trends in dam levels (Figure 5.6b). However, the remaining downscalings are indicative of rainfall either not changing significantly, or alternatively increasing over time. Dam levels are projected to respond accordingly, under the assumption that the variability in rainfall is the only factor influencing water levels in the dam. Two of the projections are indicative of droughts of unprecedented magnitude starting to occur in the second half the 21<sup>st</sup> century, with three of the projections indicative of wet years of unprecedented magnitude occurring towards the end of the century. For both these diverse futures, dam levels are projected to respond accordingly, reaching all-time low levels during these extreme years of drought. That is, it is plausible for variability in Gariiep dam levels may increase under climate change, and water managers need to prepare in addition to this for the plausible future of larger drought events affecting dam levels.

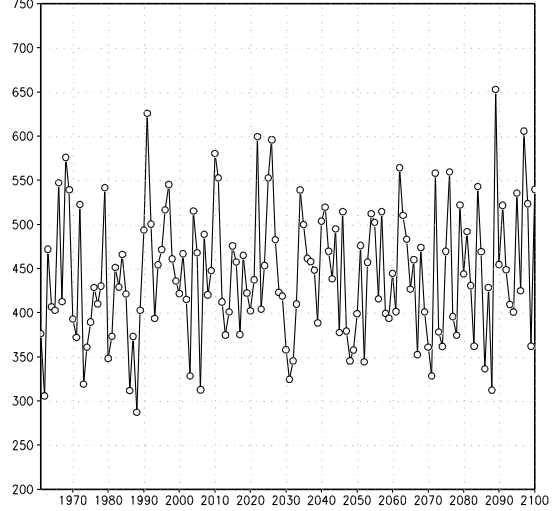
#### *Vaal dam*

The rainfall futures for the Vaal dam catchment (Figure 5.7a) are indicative of a future that may plausibly be drier. Three of the downscalings are indicative of significant decreases in rainfall, and as a consequence, of associated negative trends in dam levels (Figure 5.7b). However, the remaining downscalings are indicative of rainfall either not changing significantly, or alternatively increasing over time. Dam levels are projected to respond accordingly, under the assumption that the variability in rainfall is the only factor influencing water levels in the dam. Two of the projections are indicative of droughts of unprecedented magnitude starting to occur in the second half the 21<sup>st</sup> century, with two of the remaining projections indicative of wet years of unprecedented magnitude occurring towards the end of the century. For both these diverse futures, dam levels are projected to respond accordingly, reaching all-time low levels during the extreme years of drought. That is, it is plausible for variability in Vaal dam levels may increase under climate change, and water managers need to prepare in addition to this for the plausible future of larger drought events affecting dam levels.

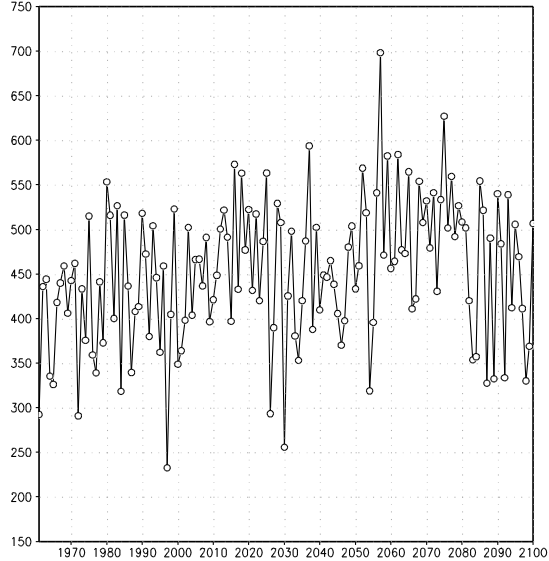
CSIRO Gariep Precipitation [mm/year]



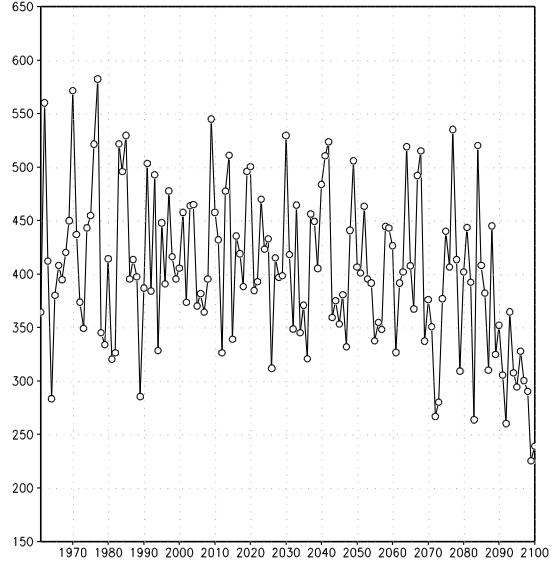
GFDL20 Gariep Precipitation [mm/year]



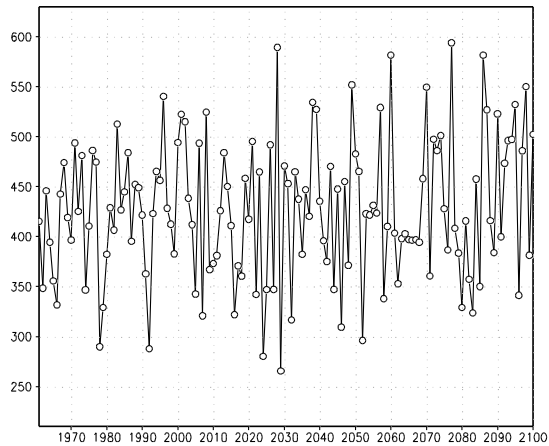
GFDL21 Gariep Precipitation [mm/year]



MIROC Gariep Precipitation [mm/year]



MPI Gariep Precipitation [mm/year]



UKMO Gariep Precipitation [mm/year]

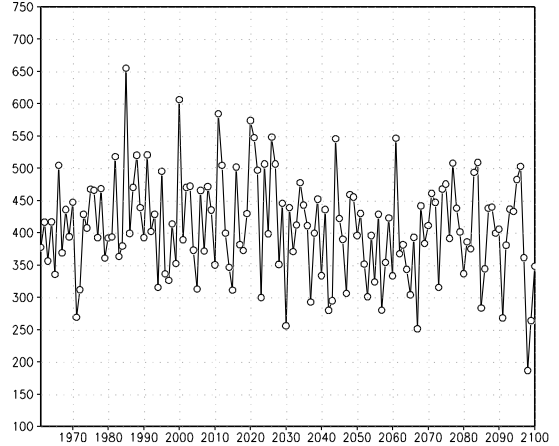


**Figure 5.6a:** Projections of future rainfall patterns (mm) over the Gariep dam catchment region, as obtained from the CCAM dynamic downscalings of six different GCMs.

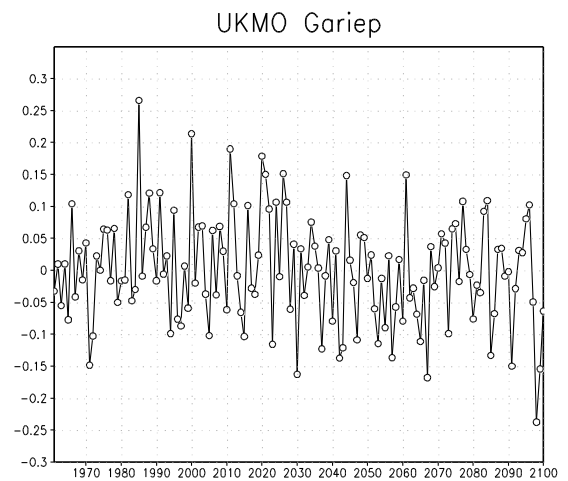
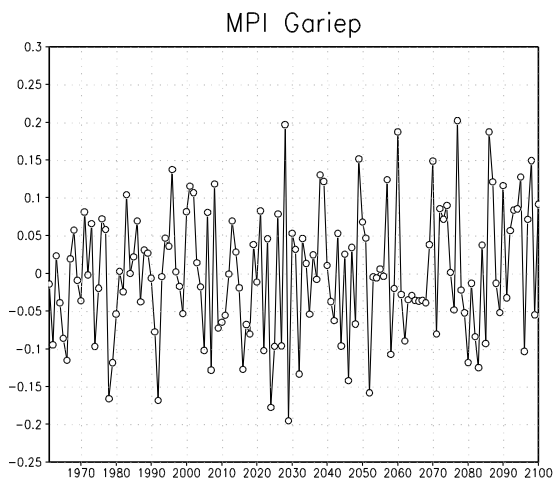
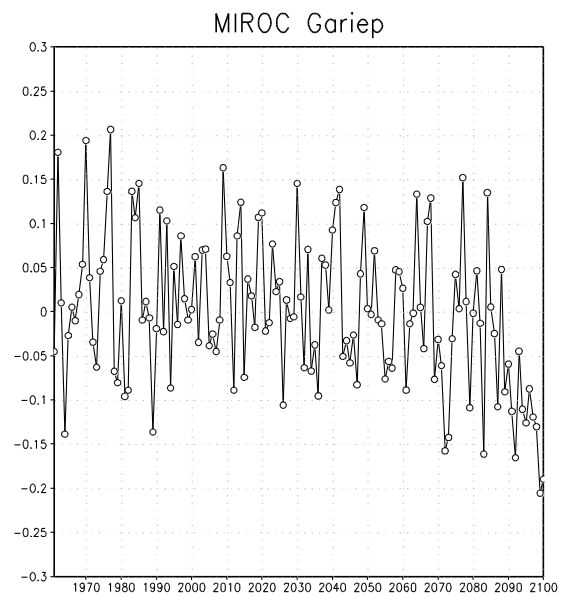
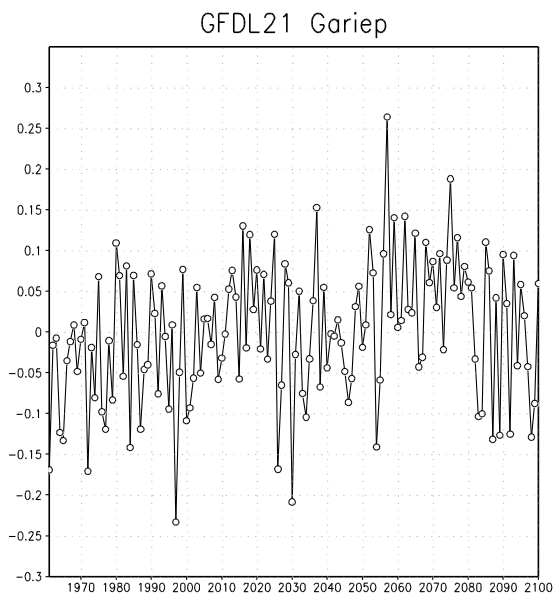
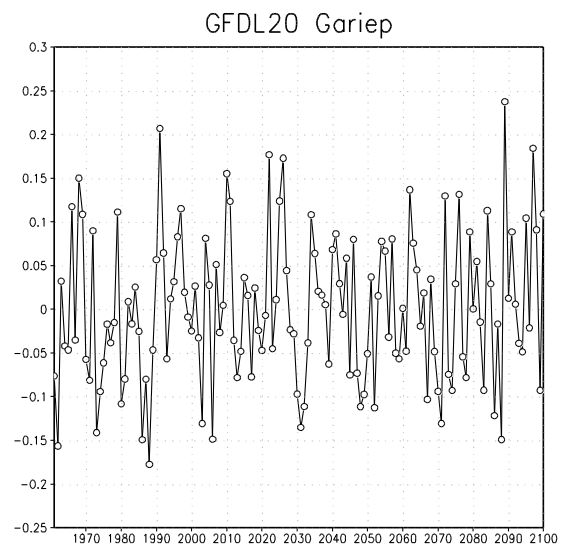
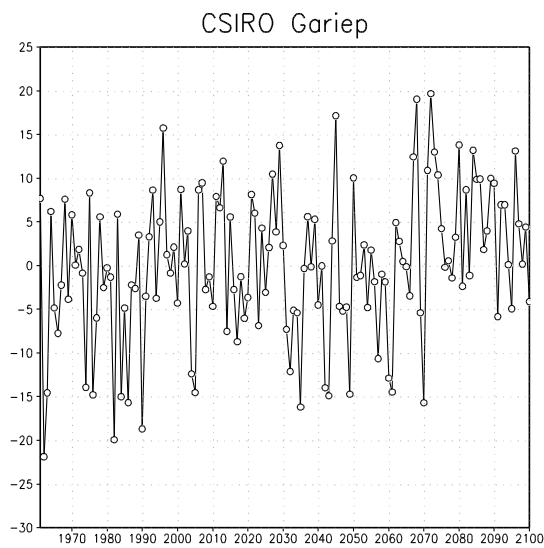


**Figure 5.6b:** Projections of dam levels (standardised % anomalies) over the Gariep dam catchment region, as obtained from the CCAM dynamic downscalings of six different GCMs.

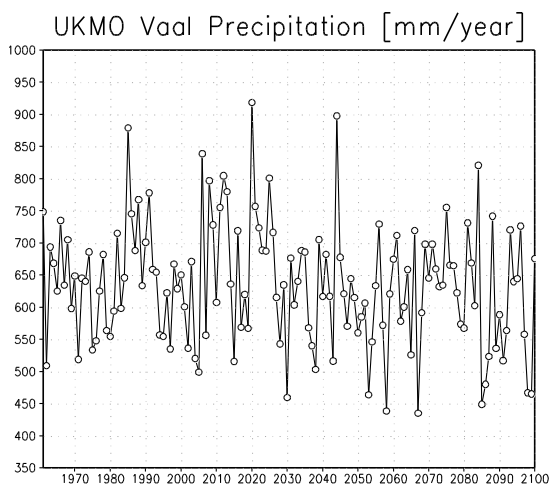
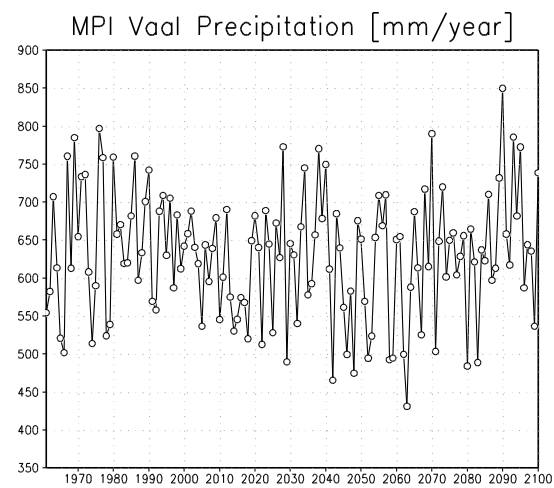
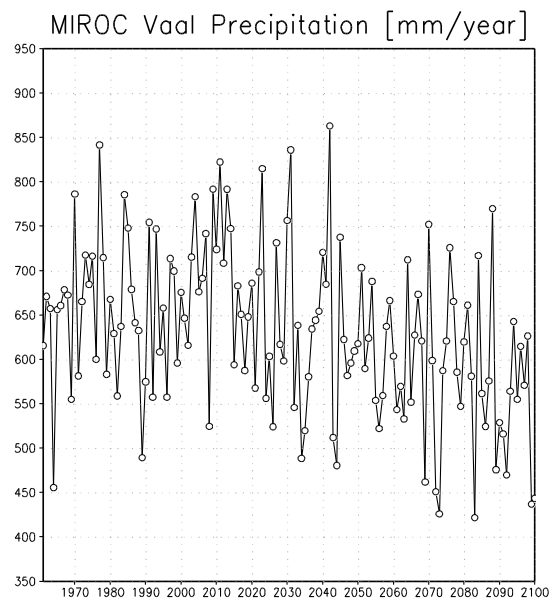
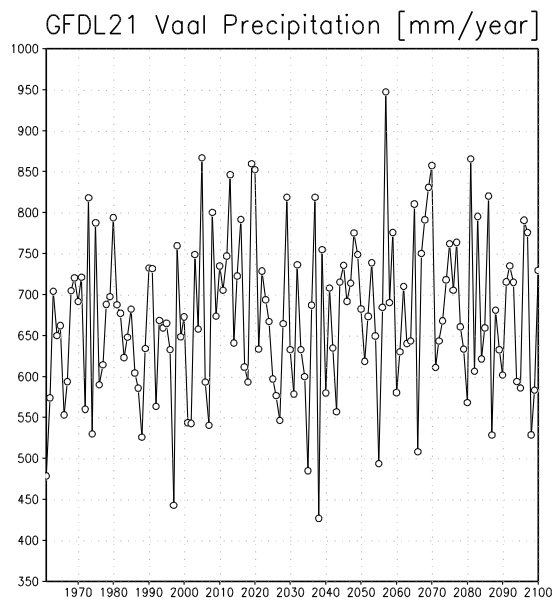
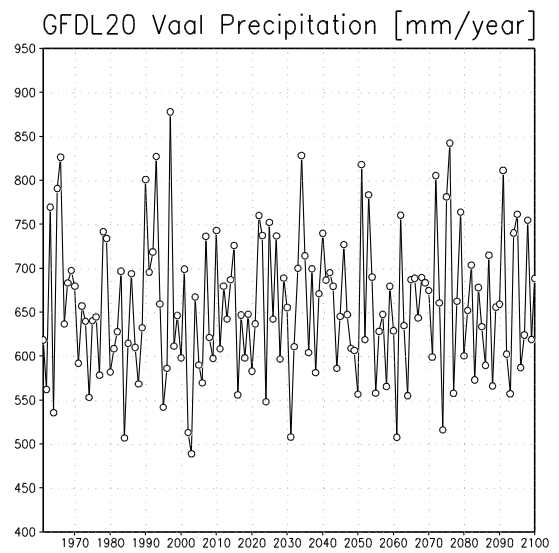
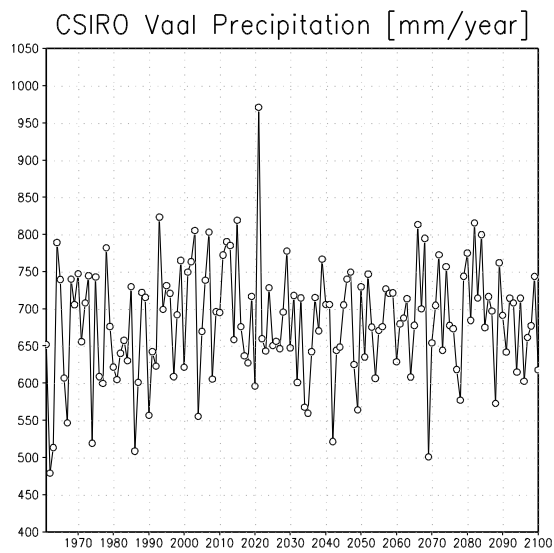


**Figure 5.7a:** Projections of future rainfall patterns (mm) over the Vaal dam catchment region, as obtained from the CCAM dynamic downscalings of six different GCMs.

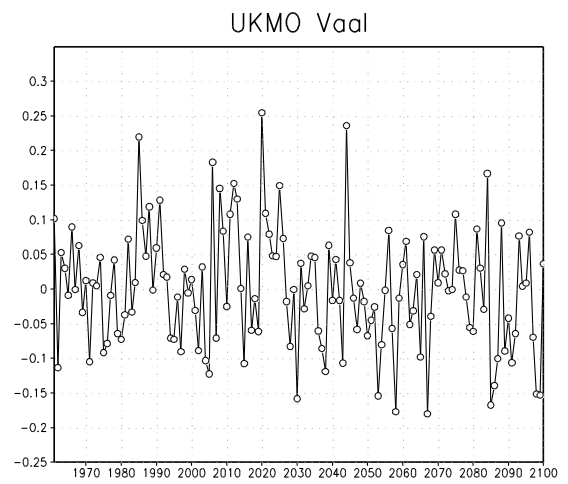
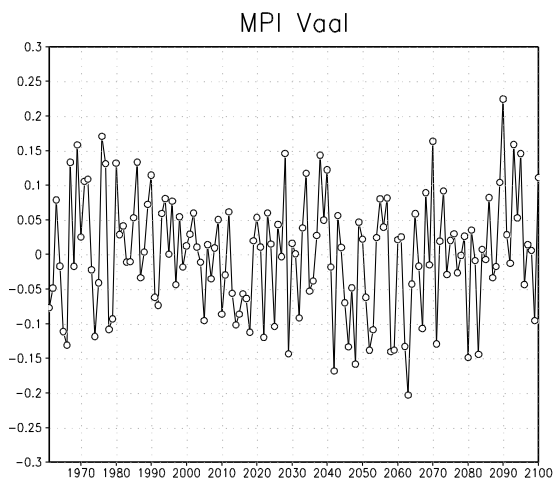
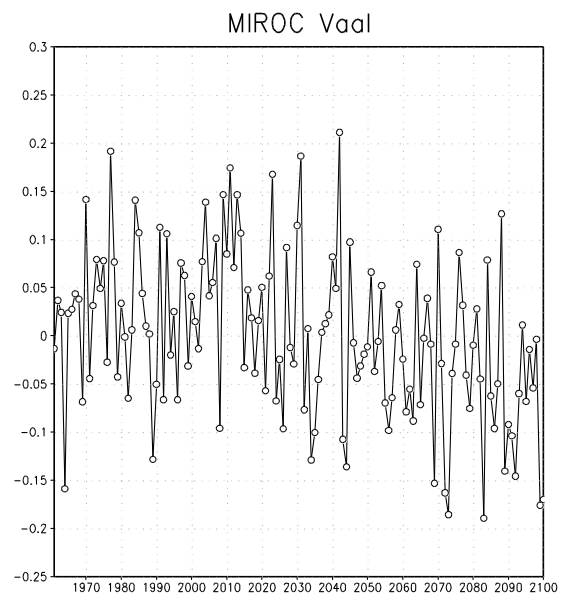
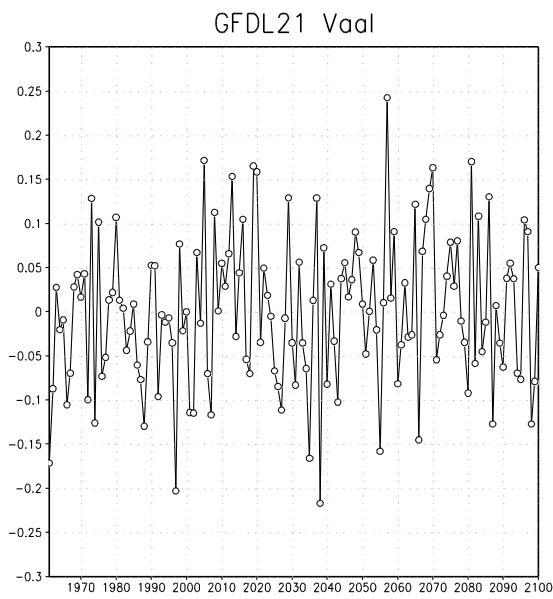
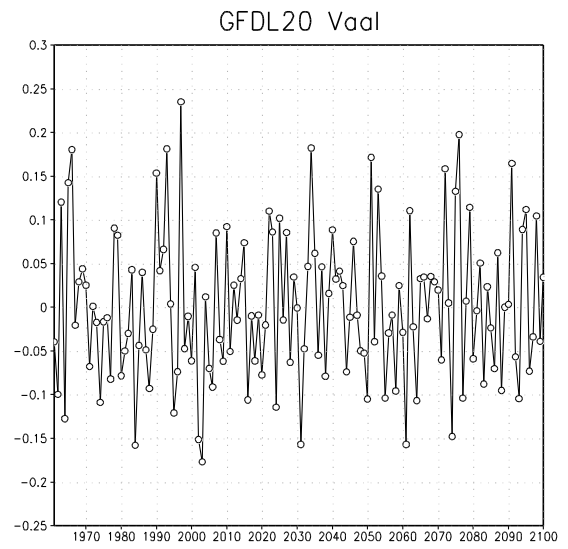
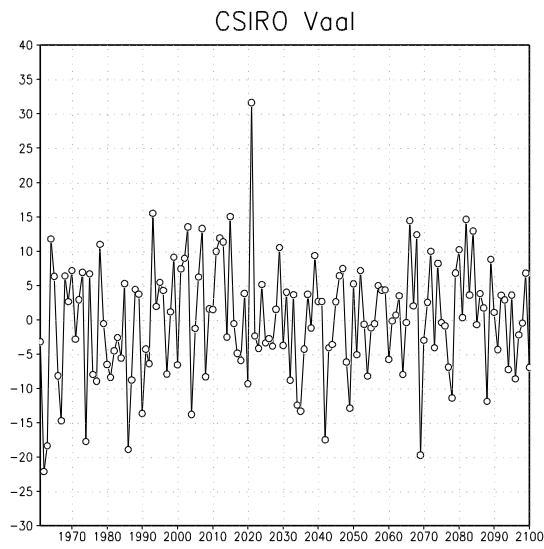
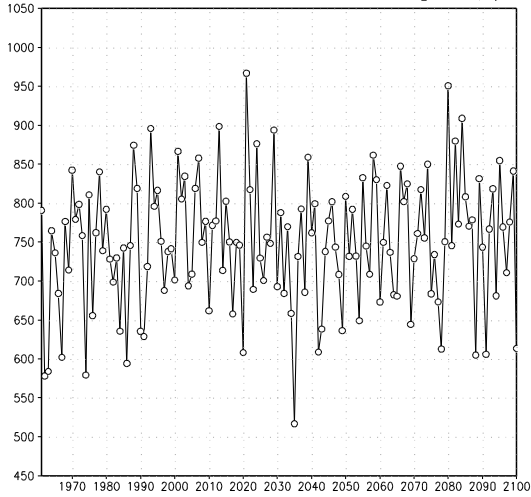
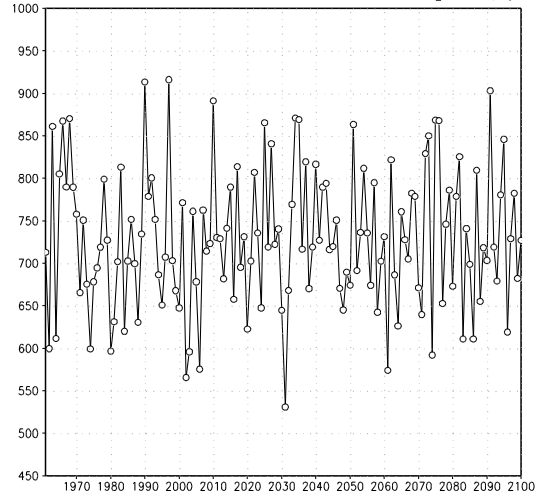


**Figure 5.7b:** Projections of dam levels (standardised % anomalies) over the Vaal dam catchment region, as obtained from the CCAM dynamic downscalings of six different GCMs.

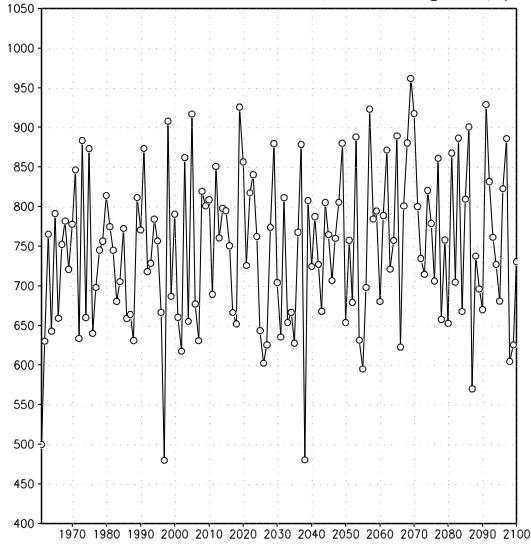
CSIRO Sterkfontein Precipitation [mm/year]



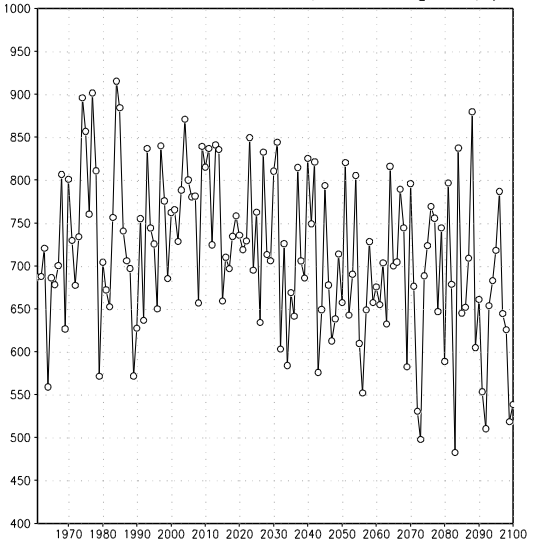
GFDL20 Sterkfontein Precipitation [mm/year]



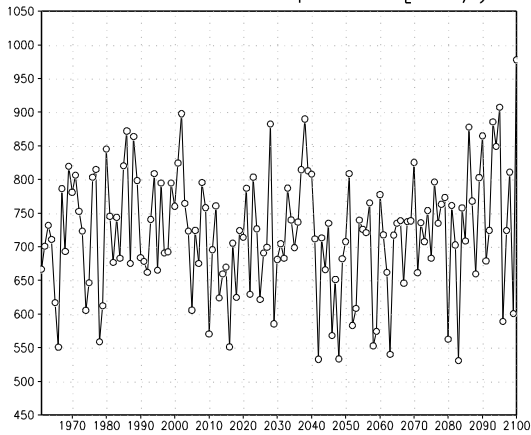
GFDL21 Sterkfontein Precipitation [mm/year]



MIROC Sterkfontein Precipitation [mm/year]



MPI Sterkfontein Precipitation [mm/year]



UKMO Sterkfontein Precipitation [mm/year]

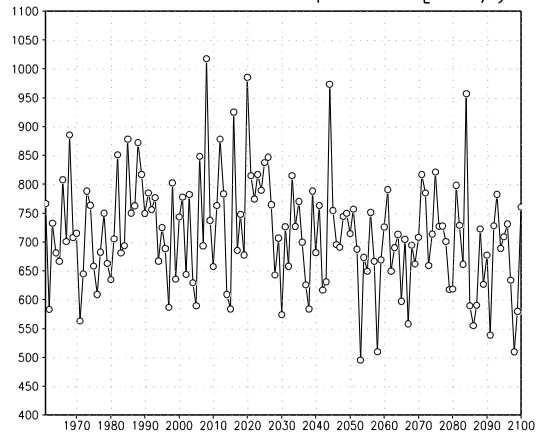


**Figure 5.8a:** Projections of annual rainfall totals (mm) over the Sterkfontein dam catchment region, as obtained from the CCAM dynamic downscalings of six different GCMs.

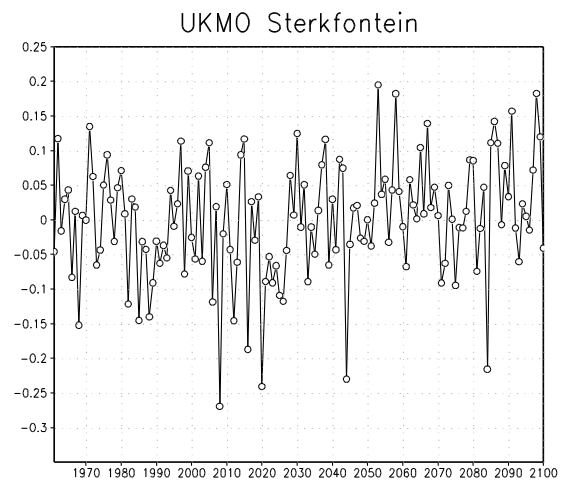
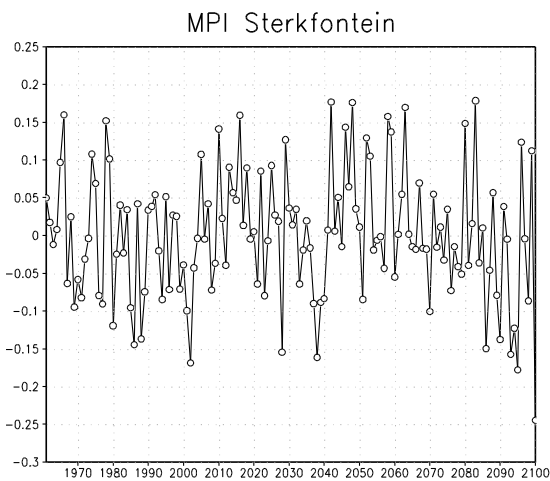
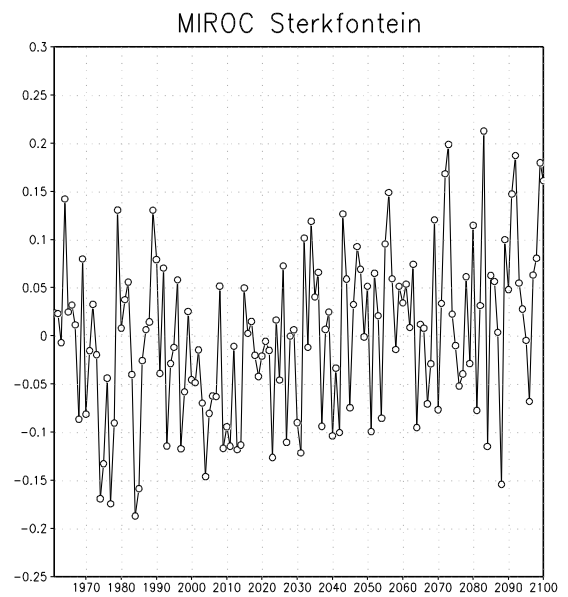
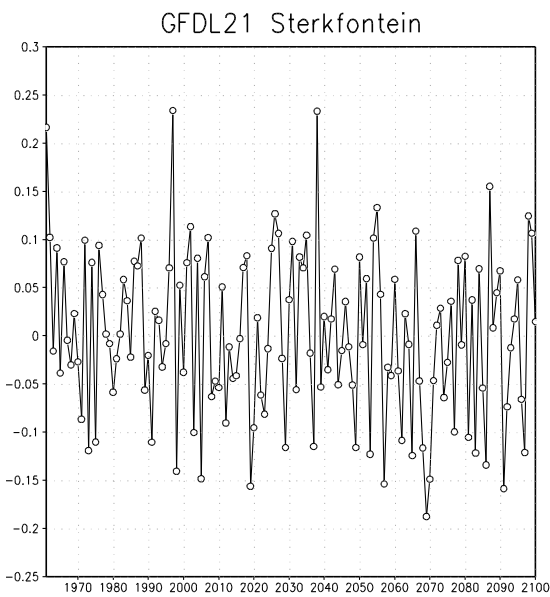
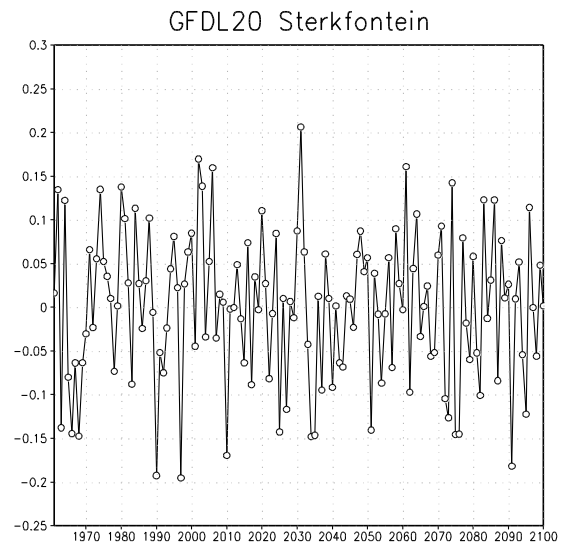
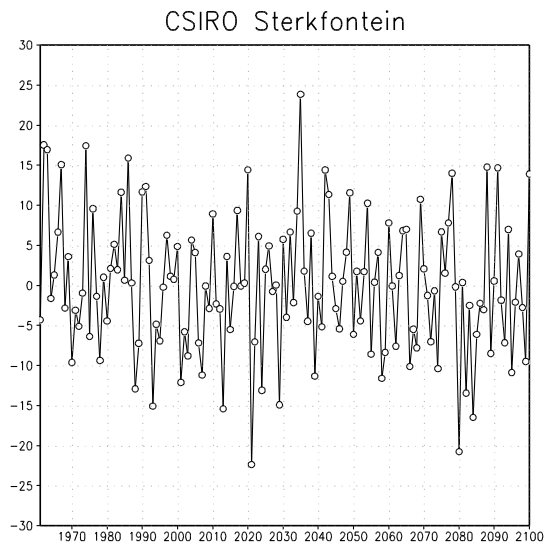


**Figure 5.8b:** Projections of dam levels (standardised % anomalies) over the Sterkfontein dam catchment region, as obtained from the CCAM dynamic downscalings of six different GCMs.

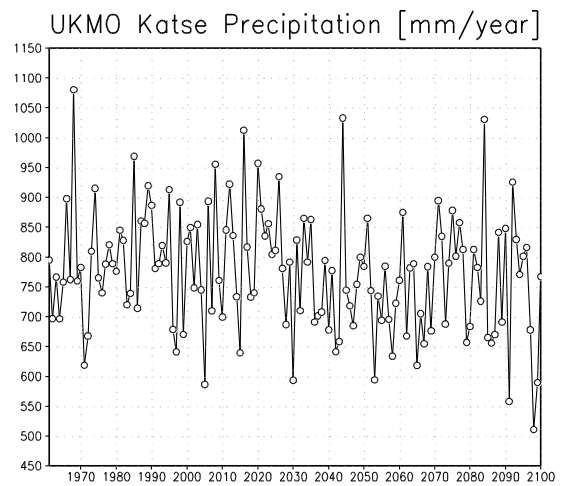
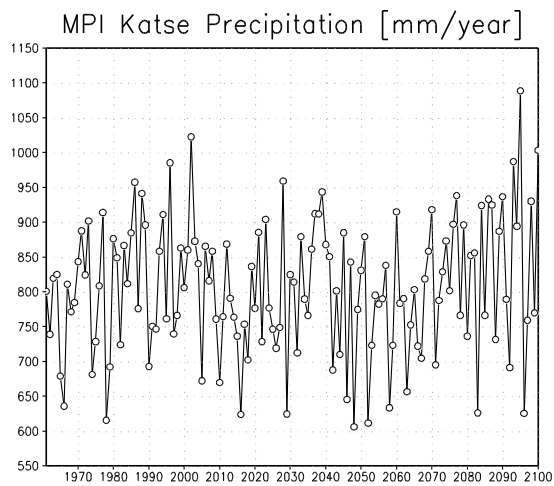
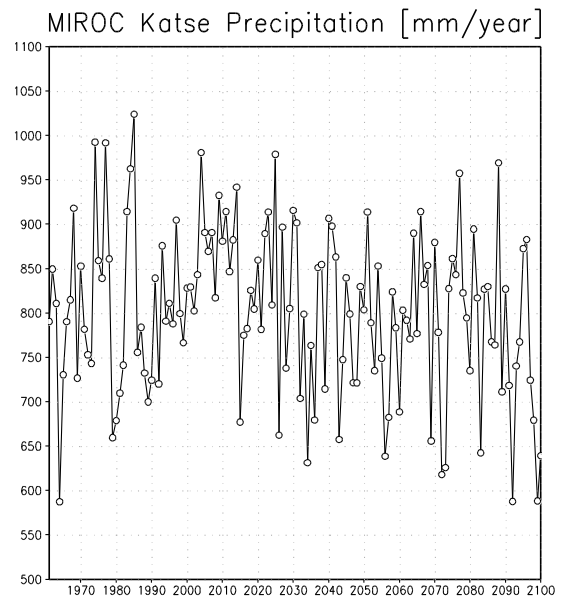
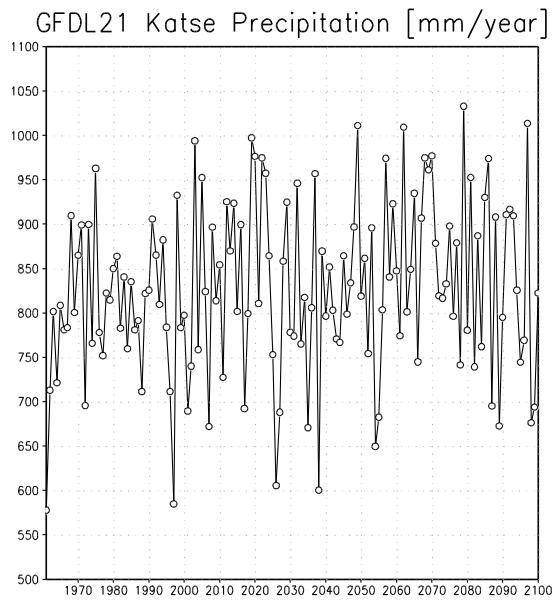
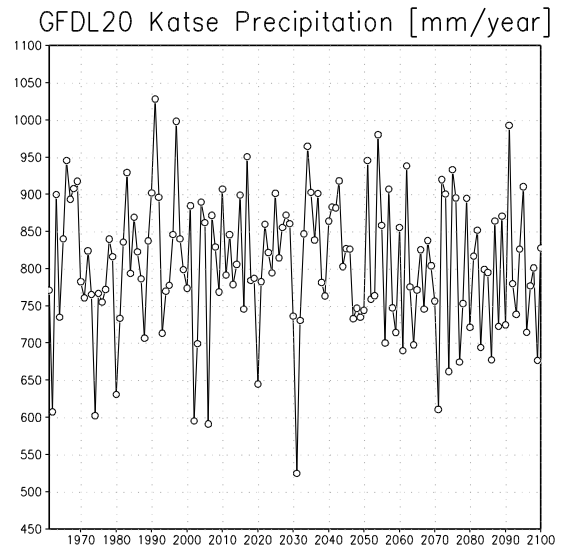
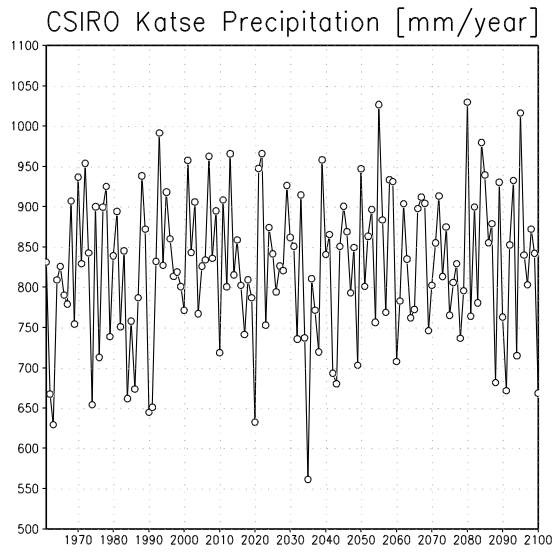


**Figure 5.9a:** Projections of changes in annual rainfall totals (mm) over the Katse am catchment region, as obtained from the CCAM dynamic downscalings of six different GCMs.

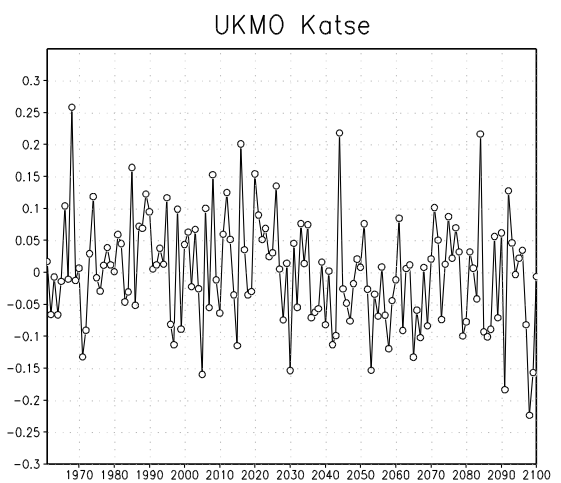
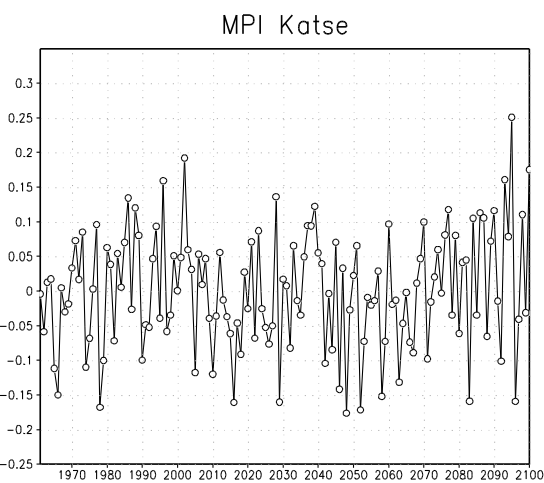
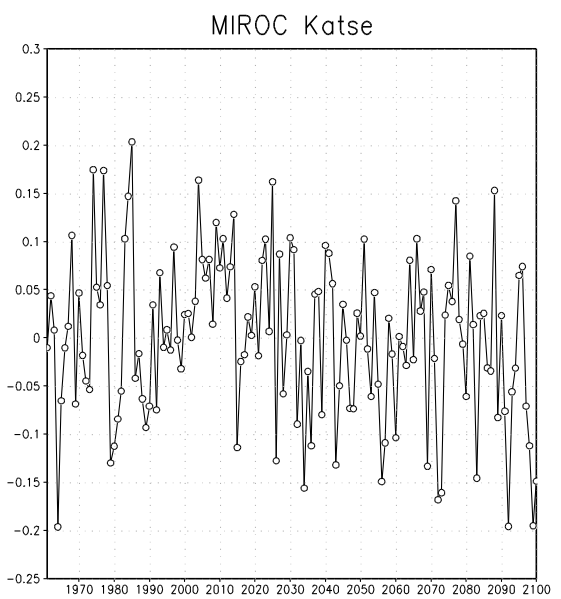
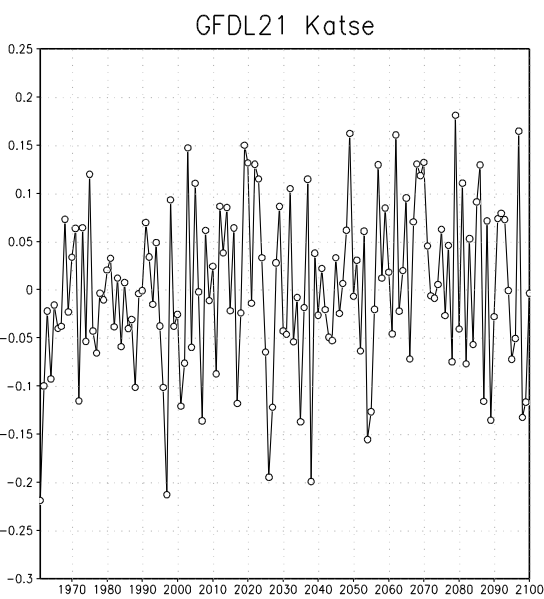
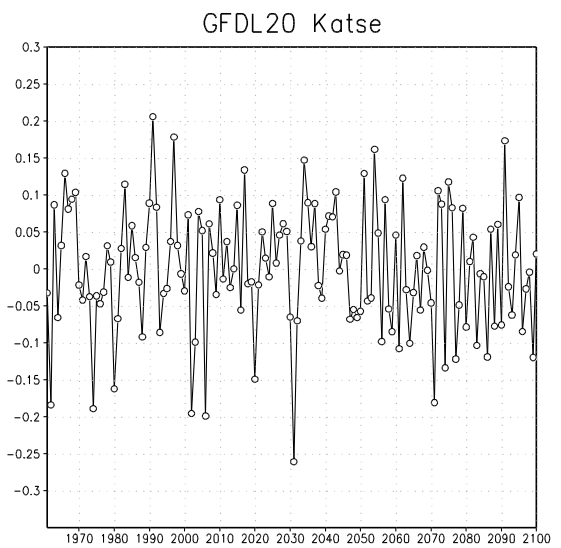
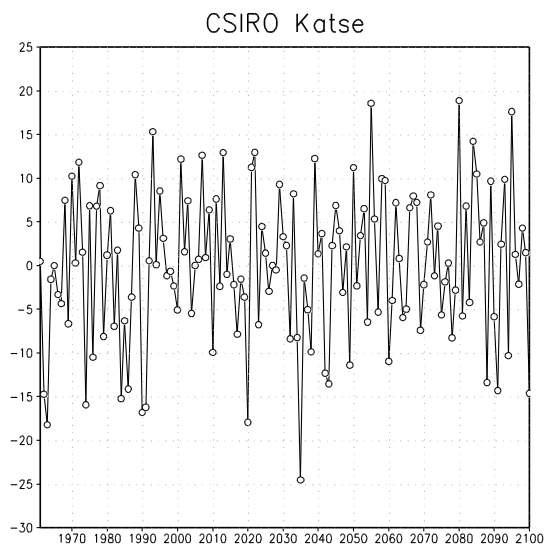
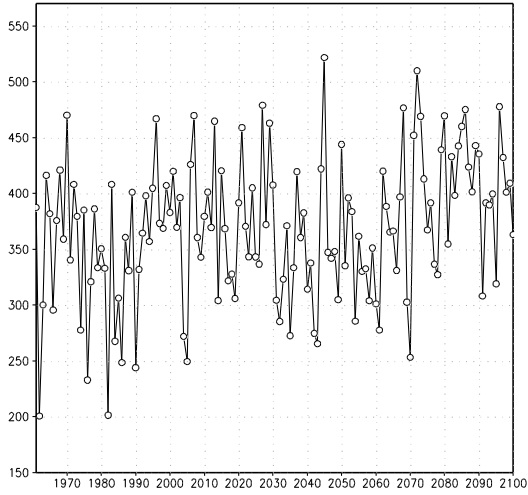
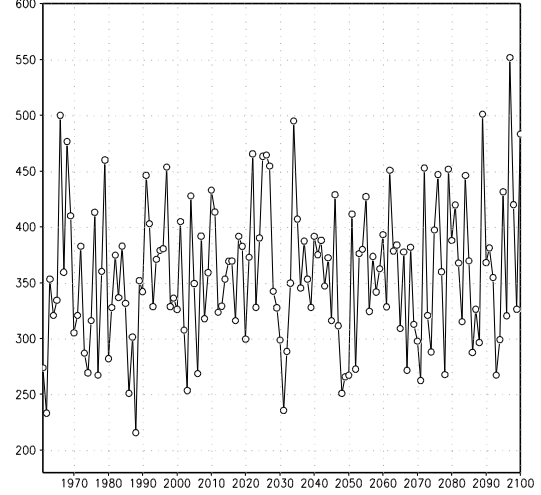


**Figure 5.9b:** Projections of dam levels (standardised % anomalies) over the Katse dam catchment region, as obtained from the CCAM dynamic downscalings of six different GCMs.

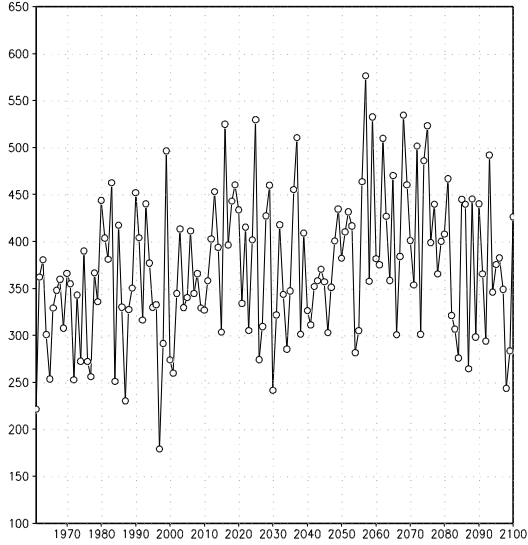
CSIRO Vanderkloof Precipitation [mm/year]



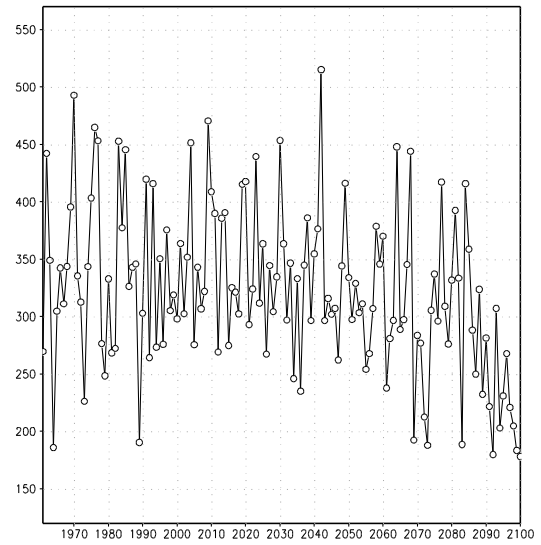
GFDL20 Vanderkloof Precipitation [mm/year]



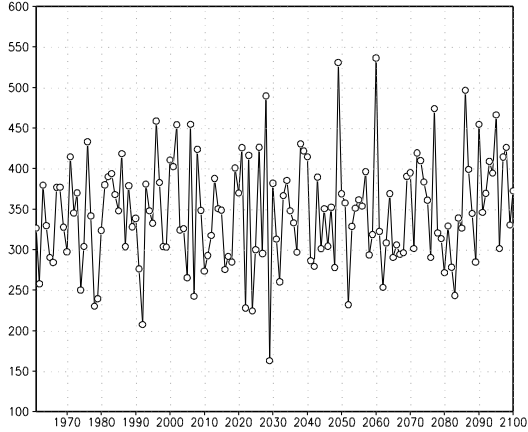
GFDL21 Vanderkloof Precipitation [mm/year]



MIROC Vanderkloof Precipitation [mm/year]



MPI Vanderkloof Precipitation [mm/year]



UKMO Vanderkloof Precipitation [mm/year]

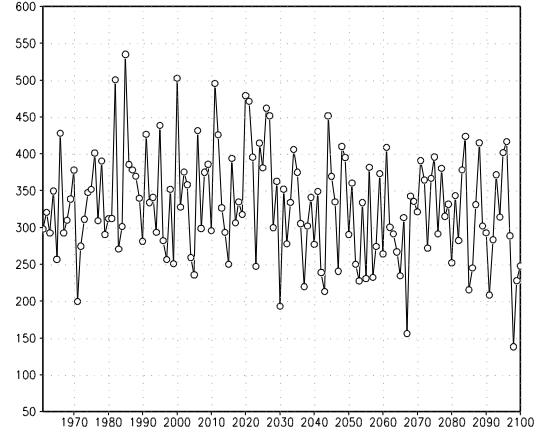


**Figure 5.10a:** Projections of changing rainfall totals over Vanderkloof dam catchment region, as obtained from the CCAM dynamic downscalings of six different GCMs.

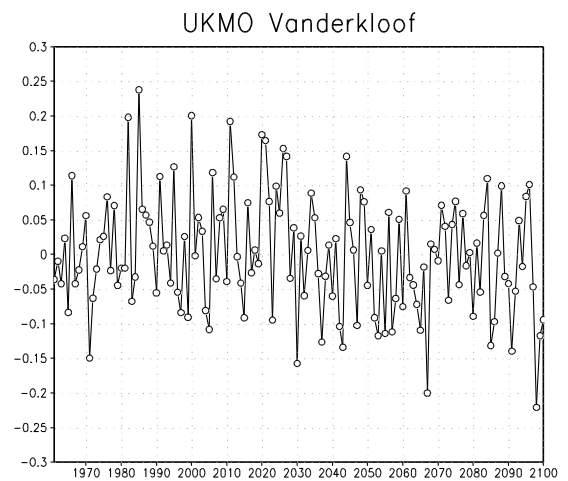
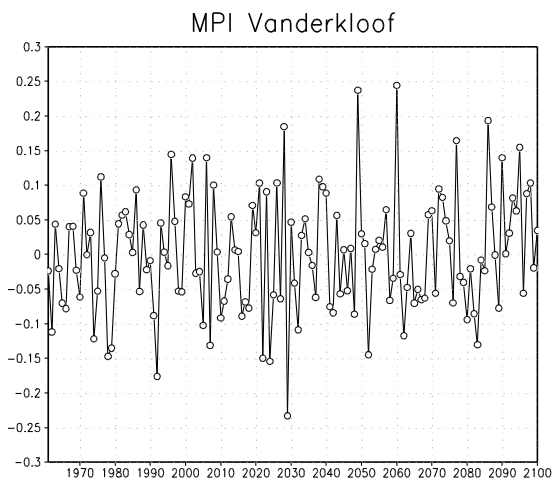
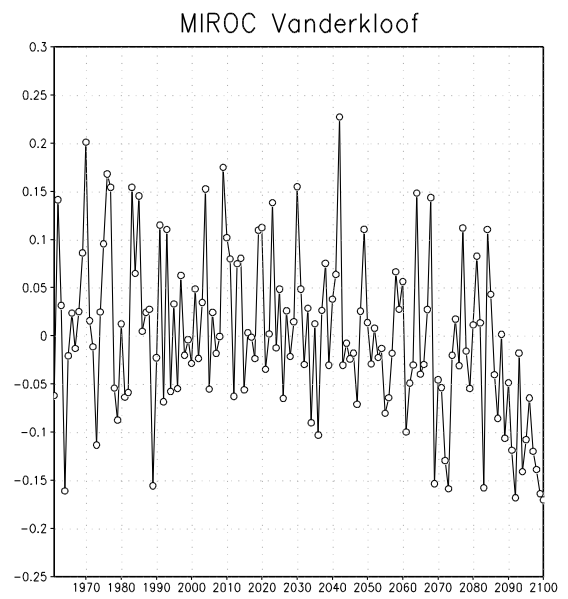
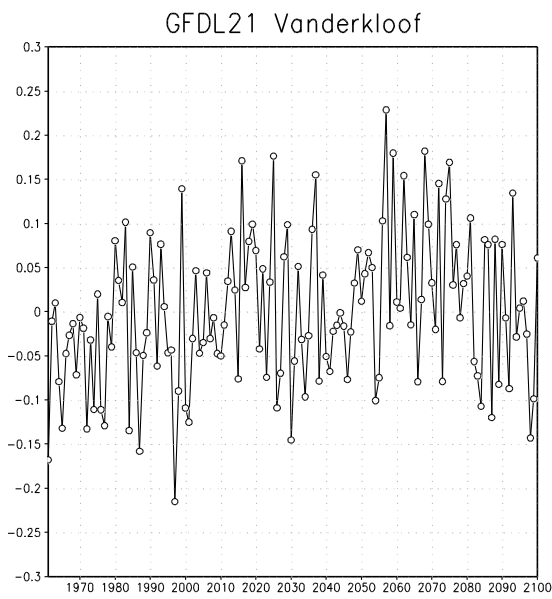
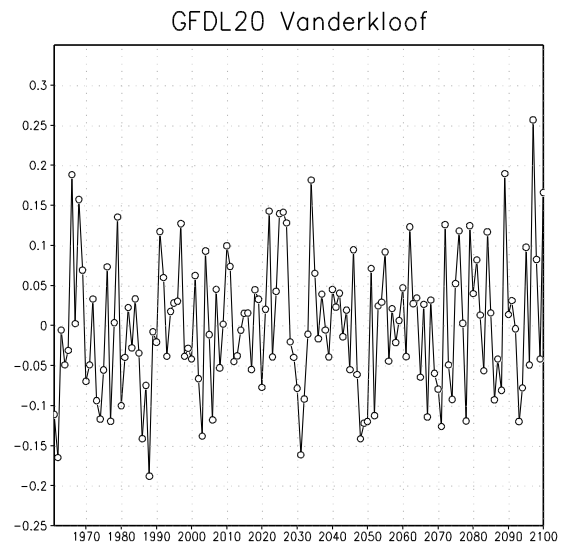
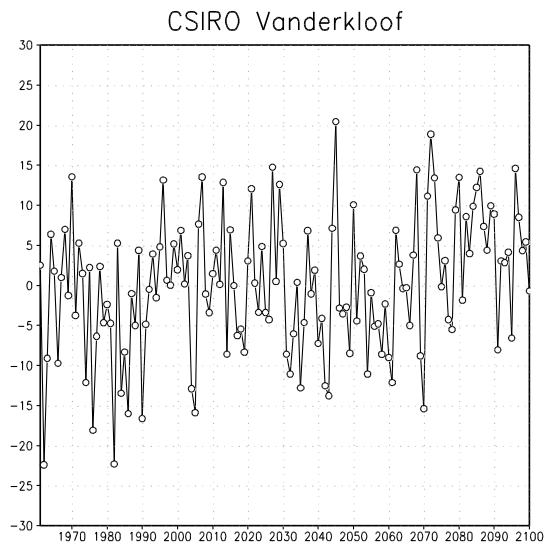


**Figure 5.10b:** Projections of dam levels (standardised % anomalies) over the Vanderkloof dam catchment region, as obtained from the CCAM dynamic downscalings of six different GCMs.

### *Sterkfontein dam*

For the Sterkfontein dam catchment, it is plausible that rainfall may decrease under climate change, with more frequently occurring droughts a feature of most of the downscalings obtained for this region. Dam levels are projected to respond in accordance. Although uncertainty is associated with these projections, in the sense that a minority of projections are indicative of rainfall remaining roughly constant over time, it seems sensible to plan for the possibility of decreasing rainfall and the increased occurrence of drought.

### *Katse dam*

The rainfall futures for the Katse dam catchment (Figure 5.9a) are uncertain – but plausibly drier. Three of the downscalings are indicative of significant decreases in rainfall, and as a consequence, of associated negative trends in dam levels (Figure 5.9b). However, the remaining downscalings are indicative of rainfall either not changing significantly, or alternatively increasing over time. Dam levels are projected to respond accordingly, under the assumption that the variability in rainfall is the only factor influencing water levels in the dam. Two of the projections are indicative of droughts of unprecedented magnitude starting to occur in the second half the 21<sup>st</sup> century, with three of the projections indicative of wet years of unprecedented magnitude occurring towards the end of the century. For both these diverse futures, dam levels are projected to respond accordingly, reaching all-time low levels during these extreme years of drought. That is, it is plausible for variability in Katse dam levels may increase in climate change, and water managers need to prepare in addition to this for the plausible future of larger drought events affecting dam levels.

### *Vanderkloof dam*

Two of the downscalings are indicative of generally drier futures for the Vanderkloof dam catchment, with the remaining projections indicative of rainfall either not changing significantly, or else increasing slightly. Unprecedented wet and dry years are plausible to occur in the second half of the 21<sup>st</sup> century, with dam levels projected to respond accordingly.

## *5.3.3 Dynamic projections of changes in the hydro-climate of eastern South Africa*

The model integrations performed at a resolution of 8 km over eastern South Africa (see Chapter 3) offer a number of advantages over the 50 km resolution simulations. Firstly, convective rainfall is partially resolved in the 8 km simulations, implying that the model is less dependent on statistics to simulate this intricate aspect of the atmospheric dynamics and physics. Secondly, important topographic features such as the eastern escarpments (in particular the Drakensberg mountains) are much better resolved in the 8 km resolution simulations, implying that the topographic forcing of temperatures, wind patterns and convective rainfall can be simulated more realistically. At such high resolution rainfall events at the spatial scales relevant to hydrology are well resolved and important land-surface features such as slopes and land-use type are significantly better resolved than at 50 km resolution. This should contribute to realistic simulations of hydrological features such as run-off in the 8 km resolution simulations. In this section the projected changes in a number of hydrological variables, are presented. For each of the metrics under consideration, the simulated baseline (climatological) state over eastern South Africa calculated for the period 1961-1990 is shown (note that the median of the downscalings is shown in this case). The projected changes in the metric are subsequently shown, for the time-slab 2071-2100 relative to the baseline period 1961-1990, for the case of RCP8.5 (low mitigation). For a discussion of the associated changes in climatological variables such as rainfall, extreme rainfall events and temperature, see Chapter 3.

Output from the CCAM-CABLE coupled hydrology scheme as obtained from the 8 km resolution simulations, as described in Section 5.2.2, are displayed in Figures 3.11 for the present-day period of 1961-1990. The annual average climatologies are shown over the mega-dam area, for the variables of potential pan evaporation ( $W/m^2$ ), evaporation (mm), soil moisture ( $m^3/m^3$ ) and runoff

(mm/day). For the variables of evaporation, runoff and soil moisture a pronounced west-east gradient exists, in response to the west-east gradient in rainfall that exists over South Africa. This gradient is reversed for the case of potential pan evaporation, in response to the east-west gradient in temperatures over the interior regions of South Africa. Note that the dynamic hydrological scheme simulates relatively high values of evaporation over the Vaal Dam and Gariep Dam – these water bodies are sufficiently large to be explicitly resolved by the dynamic hydrology.

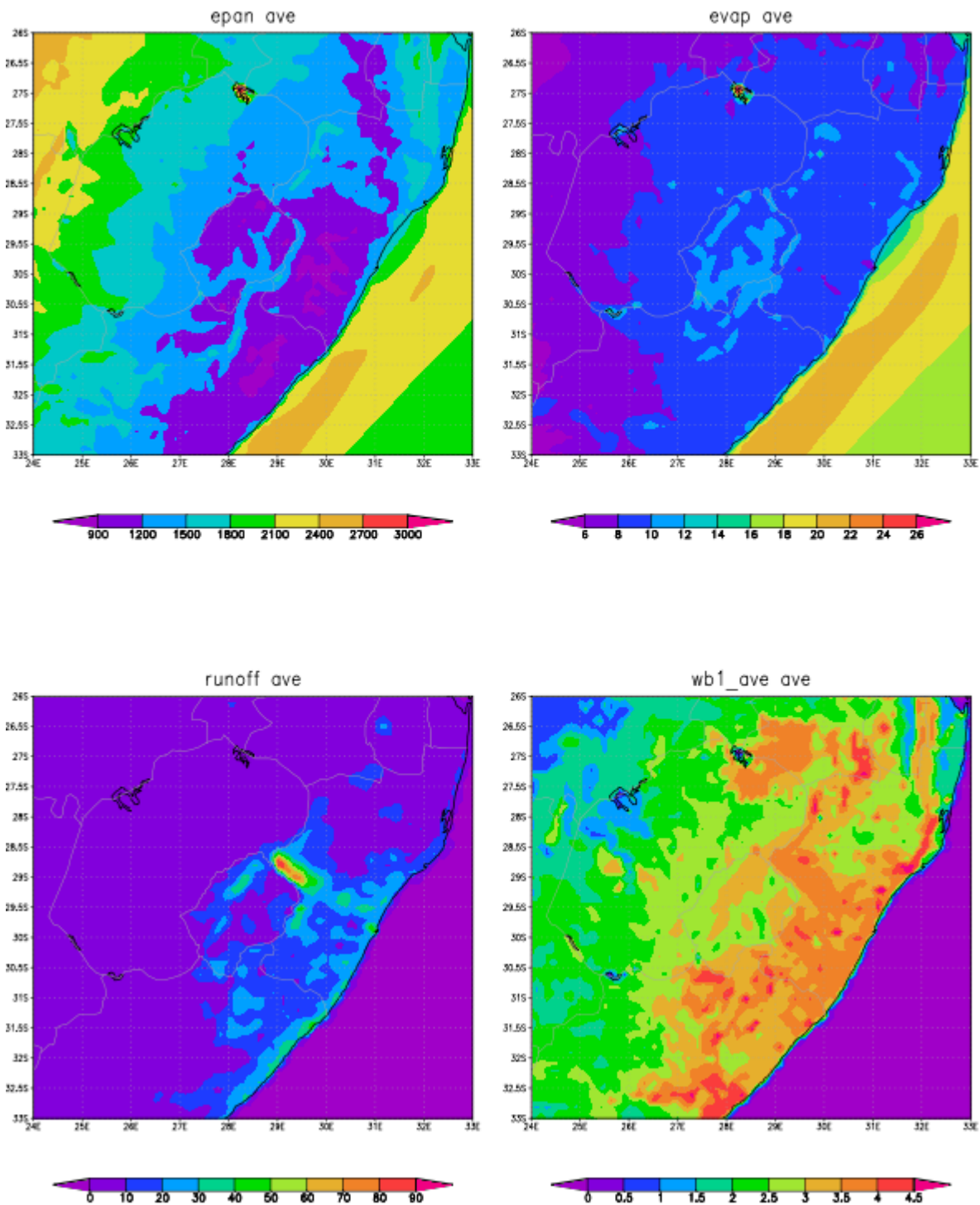


**Figure 5.11:** Annual average climatologies over the mega-dam area, for the variables of potential pan evaporation ( $W/m^2$ ; top left), evaporation (mm; top right), runoff (mm/day; bottom left) and near-surface soil moisture ( $m^3/m^3$ ; bottom right).

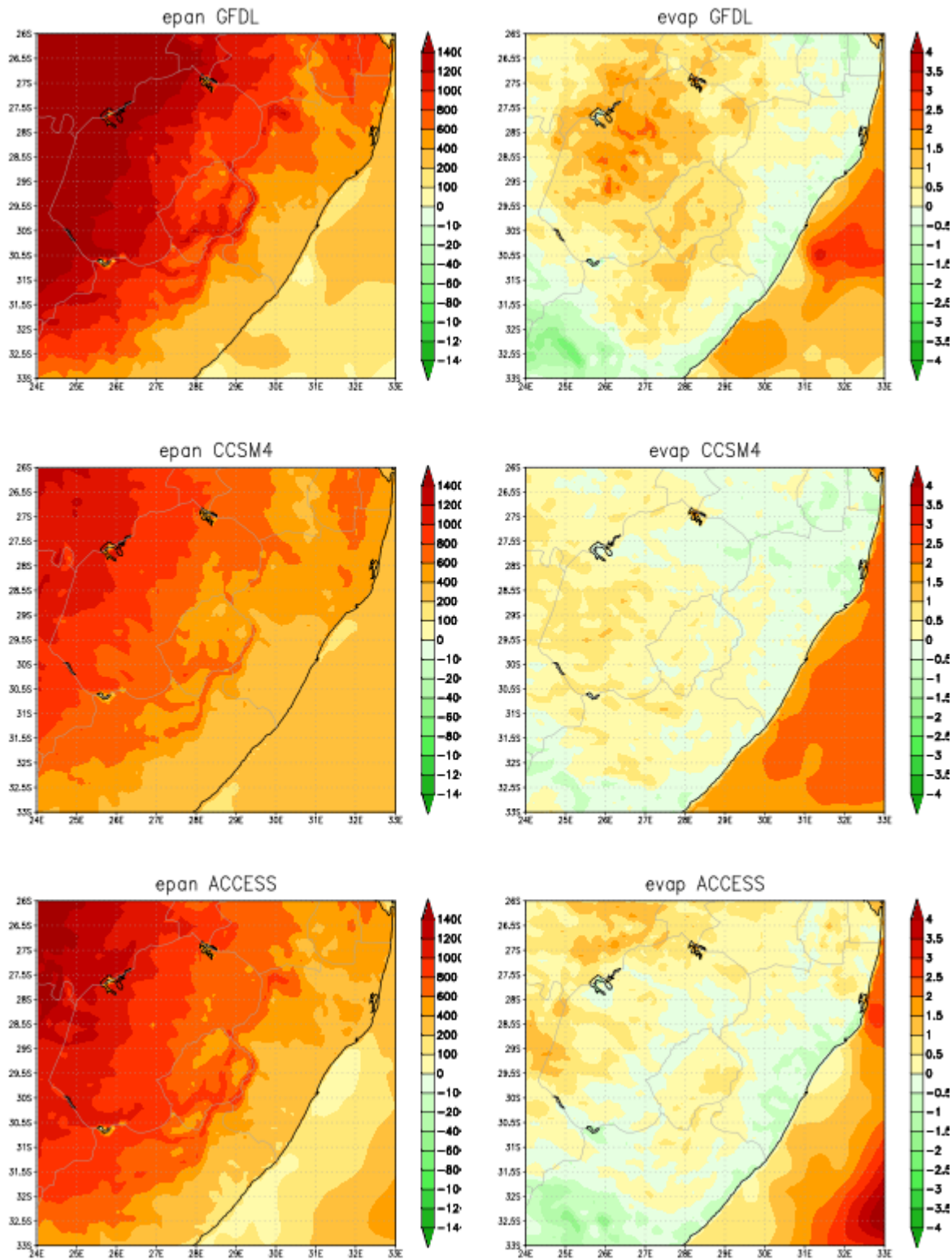


**Figure 5.12:** Projected changes in annual average climatologies over the mega-dam area, for the variables of potential pan evaporation ( $W/m^2$ ; left) and evaporation (mm; right). Changes are shown for the future period 2070-2099 relative to the present-day baseline period of 1961-1990, and across three different downscaled GCMs.

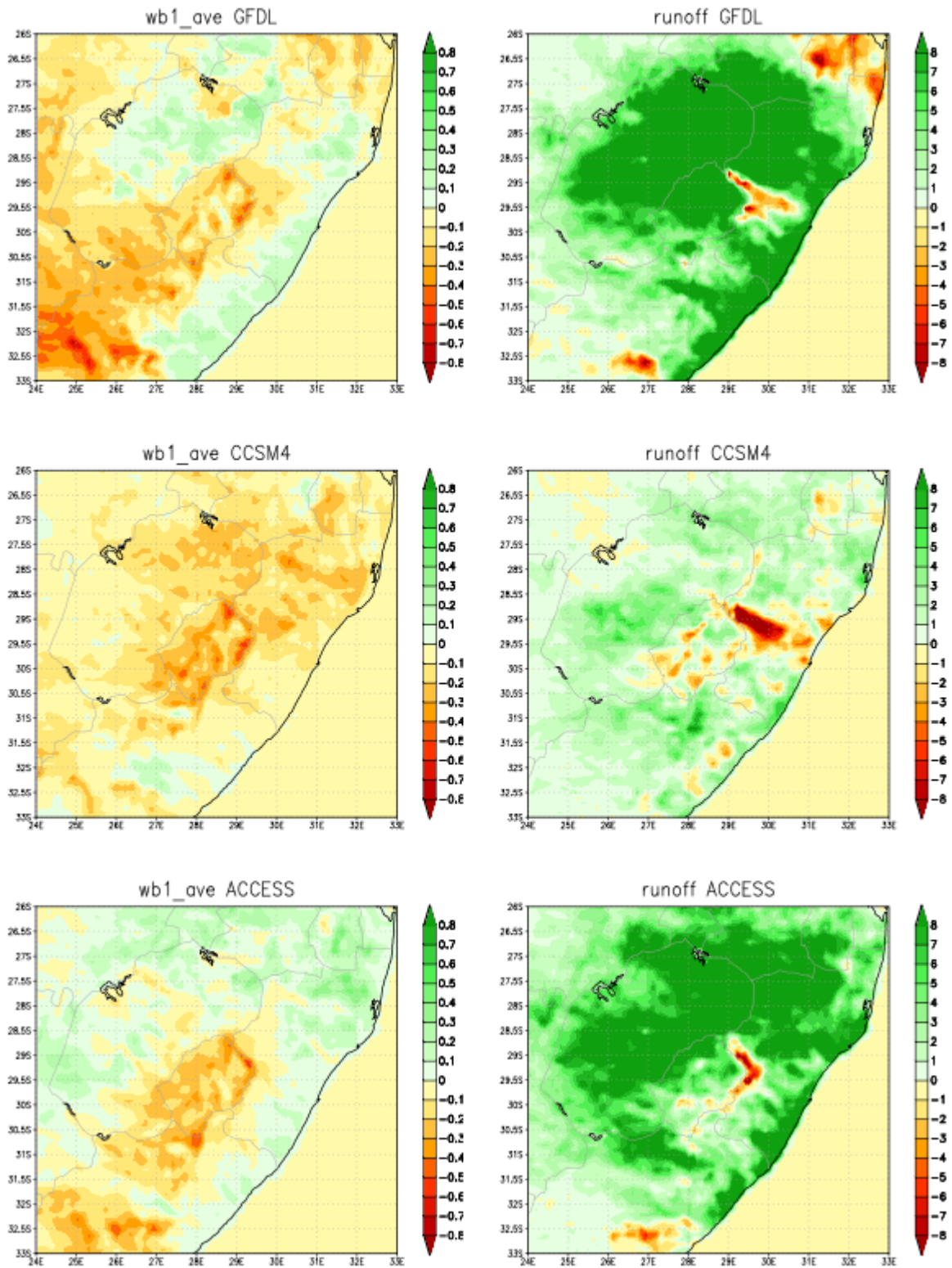


**Figure 5.13:** Projected changes in annual average climatologies over the mega-dam area, for the variables of runoff (mm/day; right and near-surface soil moisture ( $\text{m}^3/\text{m}^3$ ; left). Changes are shown for the future period 2070-2099 relative to the present-day baseline period of 1961-1990, and across three different downscaled GCMs.

The projected changes in potential pan evaporation and evaporation are shown in Figure 3.12 for future period 2070-2099 relative to the present-day period 1961-1990, and for three different GCMs downscaled using the coupled CCAM-CABLE system with hydrology under RCP8.5. Corresponding changes for run-off and soil-moisture are displayed in Figure 3.13. Large increases in potential pan evaporation are projected to occur (Figure 3.12), in response to the drastic increase in temperature that are projected to occur over the mega-dam area (not shown). As a consequence, general reductions in soil-moisture are likely (Figure 3.13). However, run-off is projected to increase significantly in response to the increases in convective rainfall projected for the mega-dam area.

This signal of drying in terms of soil moisture is of particular importance for southern Africa where yields of rainfed maize production are known to be highly sensitive to extreme temperature events that occur in the absence of adequate soil moisture. Even in eastern South Africa where rainfall totals are projected to increase, decreasing soil moisture in response to drastic warming may lead to reduced crop yield despite increases in rainfall. The projected increases in temperature may have additional implications for the water balance in the mega dams, skewing the uncertain projections of precipitation changes towards reductions in dam levels (through enhanced evaporation).

#### *5.3.4 Projections of streamflow over eastern South Africa under climate change*

As a first step towards understanding the observed variability in streamflow, 12 SOM nodes that depict variability in ONDJFM rainfall (mm) over the period 1920/1921 to 2008/9 are shown in Figure 5.14. Much of the well-known rainfall variability over southern Africa can be discerned from the SOM. Nodes 1 and 2 are representative of seasons of wet conditions (above average rainfall) over the western and central interior. Seasons exhibiting this type of rainfall pattern are associated with the frequent formation of tropical-temperate troughs over the central to western interior. The systems that typically occur in association Nodes 9, 10 and 5, on the other hand, are associated with anomalously wet conditions over the eastern and northeastern interior. Such seasons are typically associated with tropical-temperate cloud bands forming over the eastern to northeastern parts in combination with strong mid-level anticyclones being present over the Indian Ocean, thereby contributing to moisture transport from the east into southern Africa. Nodes 9 and 10 also exhibiting rainfall patterns that are indicative of tropical lows and cyclones making landfall over southern Mozambique or northeastern South Africa. Nodes 11 and 12, 7 and 8 and 15 and 3 and 4 are indicative of drought over southern Africa, and typically occur during seasons when tropical-temperate troughs rarely occur over the region.

Nodes 1, 2, 5, 9 and 10 represent the wettest conditions over Lesotho and the mega-dam region. That is, Lesotho and the larger mega-dam region of eastern South Africa experience anomalously wet conditions either during seasons of enhanced tropical-temperature trough formation over the central to eastern interior (nodes 1, 2, 5) or during seasons with pronounced easterly flow with rainfall peaks in the northeast extending to Lesotho (nodes 9 and 10). The drier summer seasons over Lesotho and the mega-dam region (nodes 3, 4, 7, 8, 11 and 12) carry the distinct signature of tropical-temperature cloud bands being largely absent or displaced to the west.

Each of the summer rainfall seasons between 1920/21 and 2008/9 can be associated with one of the nodes of the SOM, and by using this relationship the associated DJF accumulated streamflow anomalies can be mapped onto the SOM. This mapping is displayed in Figure 5.15. Generally, the positive rainfall anomalies on the left-hand side of the SOM (Figure 5.14) translate to positive streamflow anomalies (Figure 5.15), whilst the negative rainfall anomalies on the right-hand side of the SOM (Figure 5.14) translate to negative streamflow anomalies (Figure 5.15). However, the relationship is not linear and important exceptions can be noted. For example, node 12 is associated with below normal rainfall across South Africa (Figure 1) but with above normal streamflow over the Limpopo river basin in northeastern South Africa. Over Lesotho and the mega-dam region a similar quasi-linear relationship exists between rainfall and streamflow, with wet seasons typically associated with positive streamflow anomalies. Once again, exceptions exist –

node 10 for example is associated with above normal rainfall over Lesotho, but streamflow is below normal.

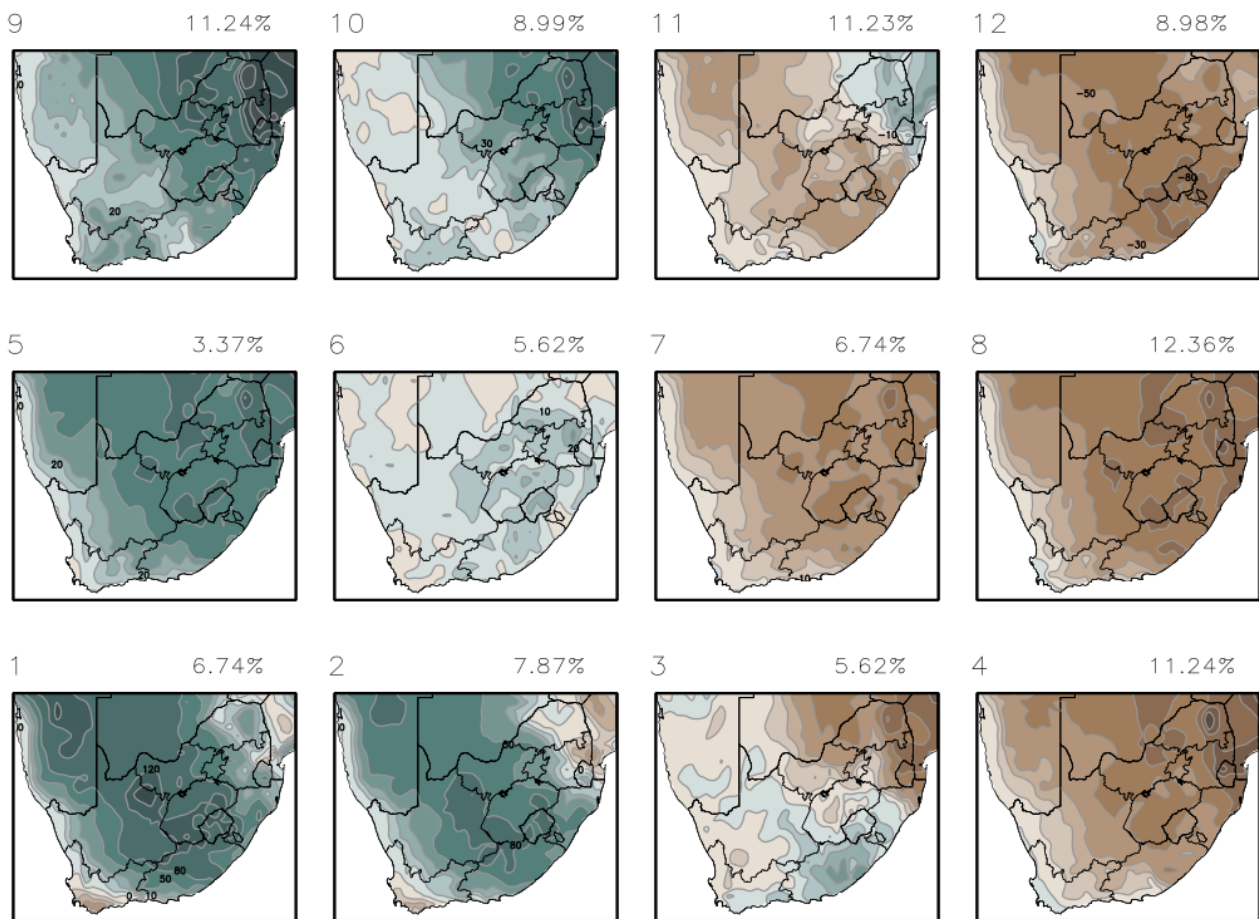


**Figure 5.14:** SOM characterisation of 12 dominant summer (DJF) rainfall anomalies over southern Africa as calculated from CRU TS\_3.2 data.

In order to determine the plausible impacts of climate change on streamflow over Lesotho and the mega-dam region, a first step is to consider the projected changes in rainfall. Figure 5.16 shows the projected changes in annual rainfall over southern Africa under a low mitigation (e.g. RCP8.5) scenario, for the future period 2070-2099 relative to the present-day period of 1961-1990, for an ensemble of six GCMs downscaled to high-resolution using the regional climate model CCAM (see Chapter 2). Four of the six ensemble members are indicative of rainfall decreases over the eastern escarpment areas, and generally over southern Africa, consistent with the findings of Assessment Report Four (AR4) and AR5 of the IPCC (Christensen et al., 2007; Niang et al., 2014; also see Chapter 2). However, when only ONDJFM rainfall is considered, many of the ensemble members are indicative of slight rainfall increases over the central interior and northeastern parts (Figure 5.17), including the mega-dam area. Qualitatively, the downscalings are indicative of increases in convective rainfall during the significantly warmer ONDJFM period under future climate change (also see Chapter 3). More frequent intense convective rainfall events may well impact positively on run-off and stream-flow, but may also result into increased sedimentation of the mega-dams.

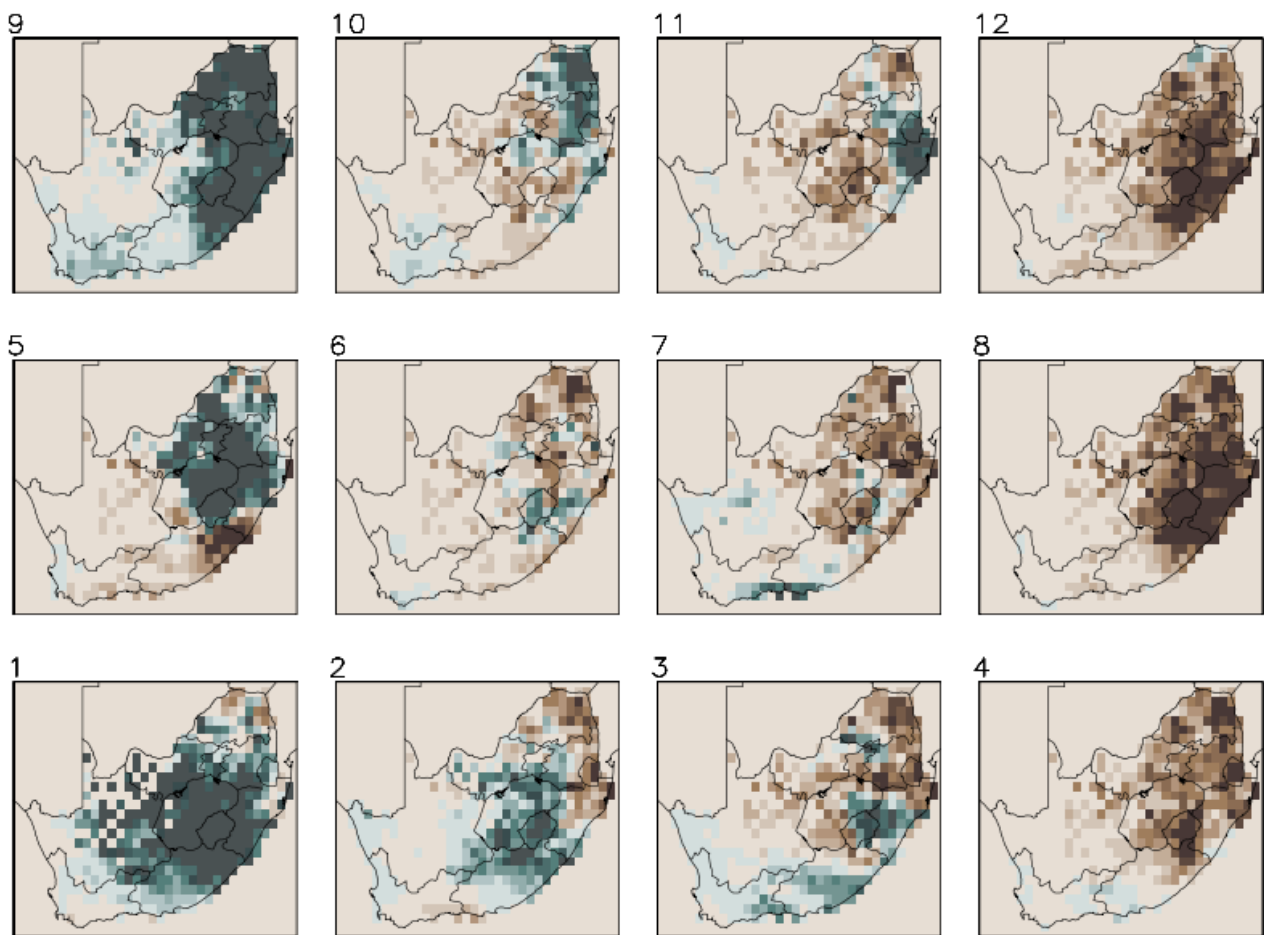


**Figure 5.15:** Accumulated summer (DJF) streamflow anomalies mapped onto the SOM characterisation of 12 dominant summer (DJF) rainfall anomalies over southern Africa.

The statistical relationship derived between streamflow and rainfall (Figures 5.14 and 5.15) was subsequently used to project future streamflow. This was achieved by mapping each simulated ONDJFM season over a future period of 30 years onto the SOM (Figure 5.14), for each ensemble member, thereby enabling the deduction of projected streamflow patterns. The results (Figure 5.18) are indicative that under low mitigation climate change, summer rainfall seasons would increasingly induce seasons with streamflow that are above the present-day average over much of the mega-dam region – according to the majority of downscalings performed. This signal is particularly robust over Lesotho and the important Lesotho highland scheme. It should be noted that increased streamflow over the mega-dam region may not offer only benefits – it may well also be associated with increased sedimentation.

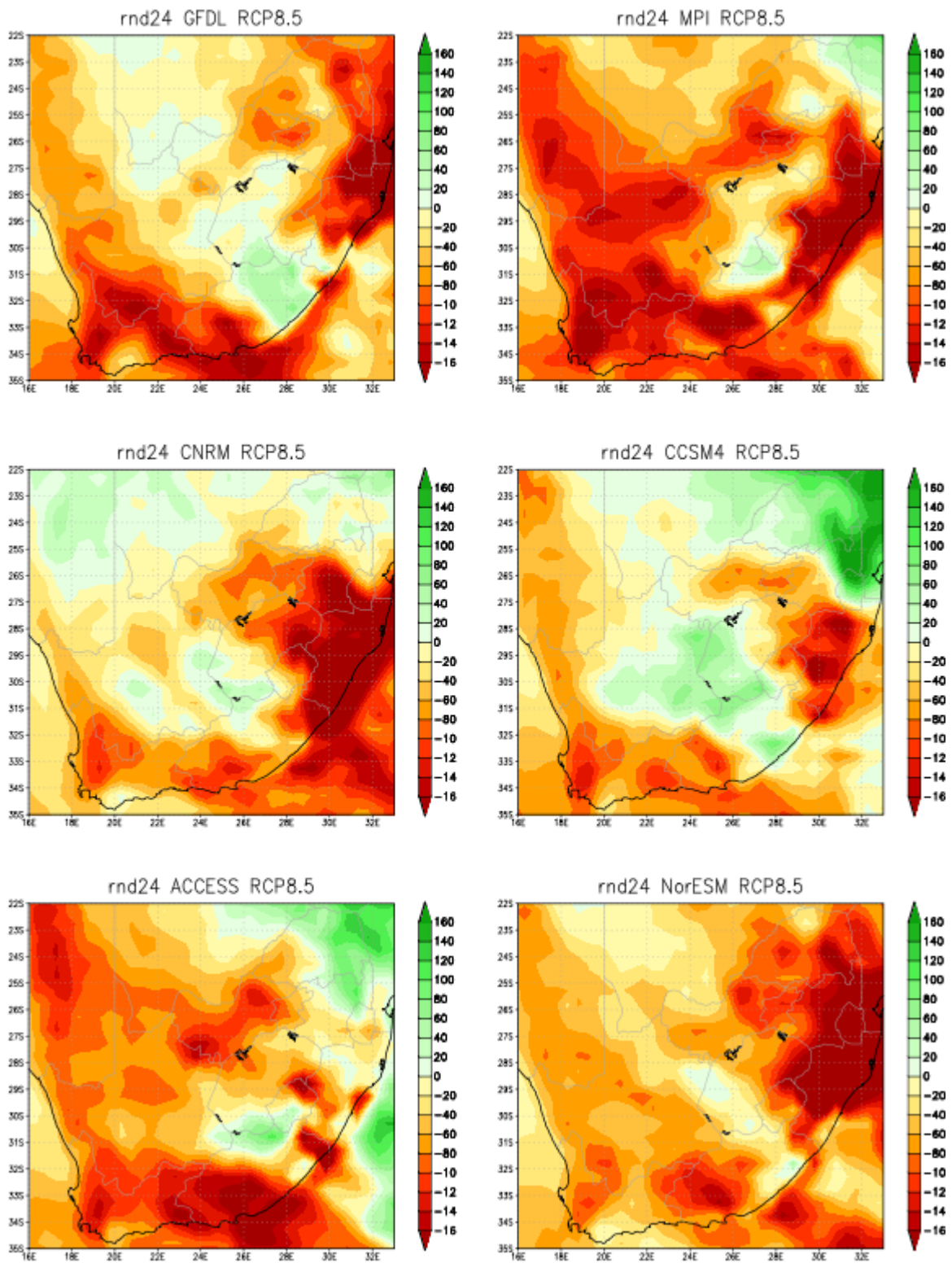


**Figure 5.16:** CCAM projected change in the annual average rainfall totals (units mm/day) over southern Africa for the time-slab 2070-2099 relative to 1961-1990. The downscalings were obtained from six different CMIP5 GCM projections under low mitigation (RCP8.5).

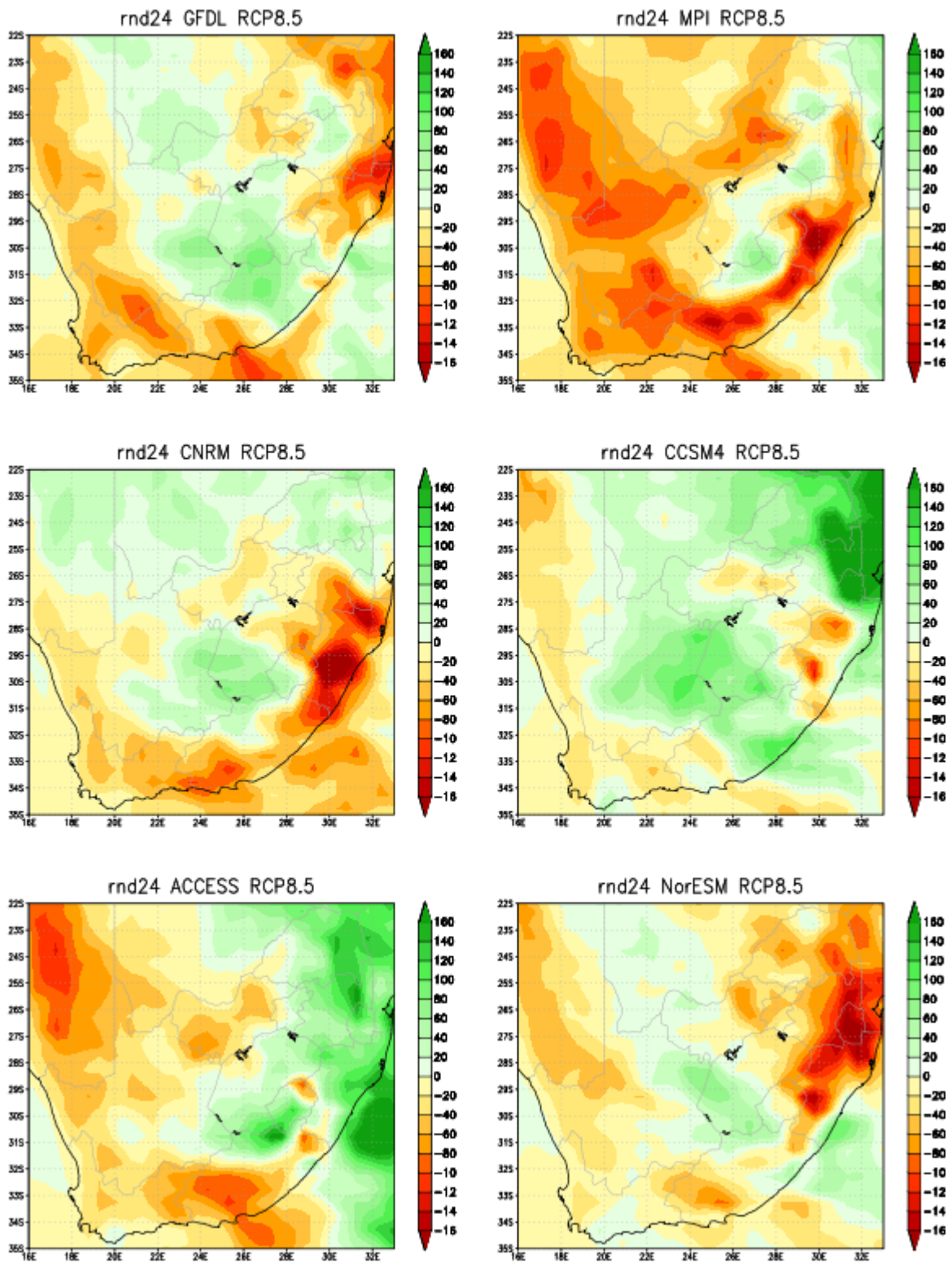


**Figure 5.17:** CCAM projected change in the summer average rainfall totals (units mm/day) over southern Africa for the time-slab 2070-2090 relative to 1961-1990. The downscalings were obtained from six different CMIP5 GCM projections under low mitigation (RCP8.5).

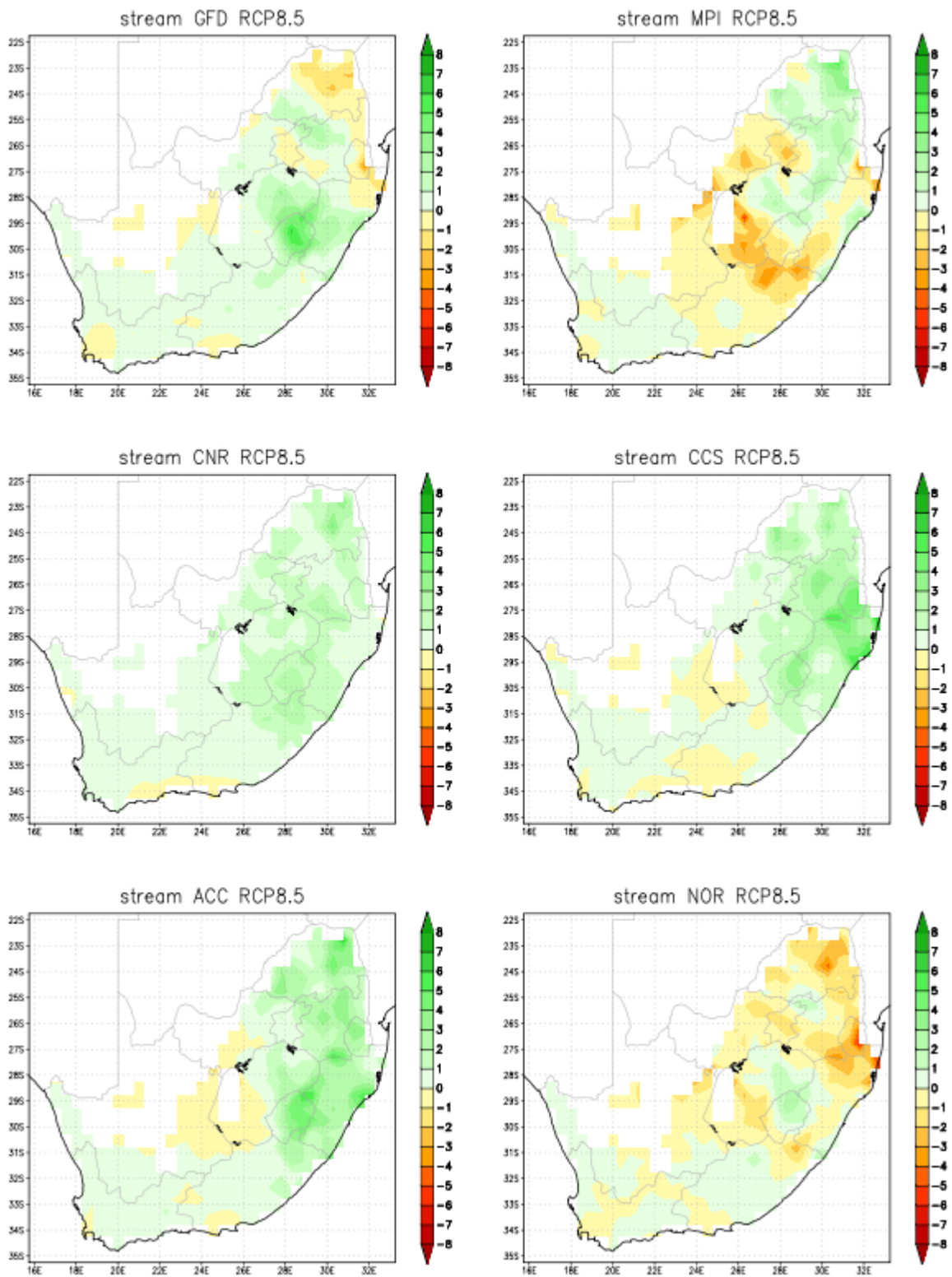


**Figure 5.18:** CCAM projected change in the summer half-year (ONDJFM) streamflow over South Africa for the time-slab 2070-2090 relative to 1961-1990. The downscalings were obtained from six different CMIP5 GCM projections under low mitigation (RCP8.5).

## 5.4 Summary

This chapter provides an overview of the statistical behaviour of rainfall (at an annual temporal resolution) and associated changes in the levels of dams, together with an indication of the association between the two time series. While the (significantly positive) association between rainfall per catchment and the levels of dams is expected (despite management interventions), the importance of cumulative, multi-year anomalies of the climate system on the storage of the mega dams also appears consistently for all dams considered. Consideration of longer periods of cumulative rainfall may yield better correlation results especially when considering lower values (drought impacts), but flood events have an abrupt influence and will therefore weaken the correlation at longer time scales. The similarity between the periods of lower levels in all dams once more emphasize the importance of extensive, multi-year droughts in the South African hydro-meteorological landscape.

The 8 km resolution projections are indicative of a plausible increase in extreme convective rainfall events over the central interior regions under climate change, which implies associated increases in run-off. Associated increases in streamflow may benefit water yield in the mega-dam region. Large increases in potential pan evaporation are projected to occur in response to the drastic increased in temperature that are projected to occur over the mega-dam area. As a consequence, general reductions in soil-moisture are likely and dam levels are to be impacted upon negatively.

Changes in the variability of the hydrological cycle were explored for the southern African region, with a focus on Lesotho and the mega-dam region of eastern South Africa. The variability in present-day summer rainfall anomalies was explored, and 12 characteristic patterns of rainfall, with associated patterns of streamflow, were identified using SOMs. Projections of future climate change that were subsequently analysed are indicative of more frequent summer half-years associated with above normal rainfall over eastern southern Arica, including Lesotho and the mega-dam region. This is projected to result in increased streamflow, consistent with the dynamic hydrological modelling what is indicative of increased run-off over eastern South Africa.

## Chapter 6 Conclusions

The overarching aim of the project was to explore the hydro-climatic futures of eastern South Africa, including systematic changes in mean variables, changes in extreme events and changes in variability. Areas of particular focus were the eastern escarpment of South Africa, Lesotho and the larger mega-dam area. It should firstly be noted that both AR4 and AR5 of the IPCC have concluded that the southern African region is likely to become generally drier under low mitigation climate change futures. Against this background, regional projections of future climate change over Africa were generated by the project as a contribution to CORDEX of the WCRP. These simulations spanned the period 1961-2100, and downscaled six CMIP5 GCMs for both low and high mitigation scenarios to a horizontal resolution of 50 km across the globe. The simulations are the first projections of future climate change contributed by an African institute to CORDEX, and thus represent an important outcome of the project. The downscalings performed are largely consistent with those of the GCMs described in AR4 and AR5 in terms of their climate change signals, indicating that the southern African region is likely to become generally drier under climate change. Moreover, the projections are indicative that rainfall decreases over the eastern escarpment of South Africa, including Lesotho, may well be substantial under low mitigation by the end of the century. In fact, under low mitigation unprecedented dry years may occur as early as the period 2016-2035, and by the mid-future period of 2046-2065 multi-year droughts may be frequently occurring over eastern South Africa. Such changes may seriously compromise South Africa's water security, including that of Gauteng, and may significantly hamper future industrial development in the country. Further to the north, rainfall increases are projected over much of Mozambique, a signal of change that is likely the result of more landfalling tropical cyclones. Some of the downscalings are indicative of this pattern of change extending southwards into northeastern South Africa. Under modest-high mitigation, a generally drier climate remains likely over eastern South Africa by the mid-future, although the amplitudes of rainfall reductions are reduced. However, by the end of the century under modest-high mitigation, the pattern of stronger easterlies over Mozambique is projected to be displaced southwards, extending into eastern South Africa, with generally wetter conditions projected for much of the region. It should also be noted that drastic increases in temperature are projected for South Africa under low mitigation, and that even under modest-high mitigation the country is committed to significant increases in temperature. Rising temperatures are projected to have a range of negative impacts on southern Africa, including reductions in crop yield and live-stock production, but may also directly impact on water security through inducing enhanced evaporation and land-use change.

Detailed simulations of present-day climate (8 km resolution in the horizontal) have been performed over the eastern escarpment of South Africa, and verified against observations from CRU, TRMM and SAWS. Rainfall features around Lesotho such as the wetter eastern parts of KwaZulu-Natal and the drier western parts in the Free State and Eastern Cape are captured well in the CCAM simulations. However, the model simulations exhibit very large wet biases north east of Lesotho that are at some stations up to 3 times the rainfall observed at SAWS stations. CCAM is able to simulate the well-defined west-east gradient in rainfall over the eastern escarpment of southern Africa and provides a reasonable presentation of the diurnal cycle in convection. On the eastern side of the escarpment there is a systematic bias in the model simulations of the timing of convection, with the rainfall peaking too late in the day compared to observations. The CORDEX projections of future climate change were subsequently downscaled to 8 km resolution over South Africa to obtain the most detailed set of projections ever obtained for eastern South Africa. The 8 km resolution projections are indicative of drastic temperature increases in near-surface temperatures and related extreme events over the mega-dam region. Already for the mid-future period of 2021-2050, high fire-danger days, heat-wave days and very hot days are likely to occur at unprecedented frequencies. The projected changes are similar for low (RCP8.5) and modest-high (RCP4.5) mitigation futures for the mid-future period. The changes may reach devastating proportions by the far-future period (2071-2099) under low mitigation futures, at least in terms of impacts on agriculture. However, the modelling indicates that under modest-high mitigation, changes in temperature and related extremes are significantly mitigated for the far-future period. The projections also provide evidence of a plausible increase in extreme convective rainfall events

over the central interior regions under climate change. Associated increases in streamflow may benefit water yield in the mega-dam region, although increases sedimentation may also result from the enhanced run-off.

In response to a generally warmer global climate under low mitigation, the austral summer inter-annual variability of both temperature and rainfall are projected to increase over the eastern parts of southern Africa. This is the case in particular for the Limpopo river basin, which exhibits the strongest ENSO signal in southern Africa under present-day climate. Most projections are also indicative of increased variability over the mega-dam area of eastern South Africa, but variability is projected to decrease over the Cape south coast region and also over the central and western interior regions. However, increasing variability does not necessarily imply decreasing predictability. In fact, the research is indicative that the inter-annual variability of austral summer circulation may become more predictable over the eastern parts of southern Africa under enhanced greenhouse gas warming – and specifically over the Limpopo river basin. This may be due to a stronger ENSO cycle and teleconnection to southern Africa under climate change, a signal already well captured and simulated by climate models, thereby yielding increased predictability. The present-day predictability of streamflow over the mega-dam region was also investigated through a typical statistical downscaling approach. Predictability of circulation (predictor) is high for summer, due to the strong influence of ENSO on atmospheric circulation over southern Africa during this season. With summer also the most important season in terms of streamflow and the replenishment of dams, this is an important result. It follows that the skill in predicting circulation as streamflow predictor for DJF, the predictions for the predictant (streamflow) is also skilful. This is an important finding, implying that water managers responsible for decision making around flows and dam-levels in the mega-dam area can with confidence make use of seasonal forecasts of streamflow as an aid in decision making.

The potential advantages of downscaling typical low-resolution CCAM seasonal forecasts, such as those used to generate the seasonal predictions of streamflow, to very high resolution (8 km in the horizontal) to South Africa was also explored. The primary motivation for pursuing this computationally expensive model configuration, lies on the fact that this level of detail (if rigorously skilful) is vital for various climate change impact studies. There is also the possibility that higher resolution may result in increased skill in predicting rainfall over regions of steep topography such as the eastern escarpment. The high-resolution probabilistic forecasts for the austral summer season for daily accumulated rainfall were found to be fairly skilful. The model was able to discriminate significantly wet and dry summers over southern Africa. Climatologically, the dynamical downscaling was also found to further improve the rainfall pattern simulated by its driving GCM. Short-range predictability over southern Africa was explored for the present-day climate, followed by an analysis of how this predictability may be altered by climate change. A SOM-based analysis revealed that rainfall is predicted best for synoptic-types associated with well-defined westerly wave characteristics, including well defined tropical-temperate troughs occurring over southern Africa. Such weather patterns are projected to occur more frequently under climate change, implying that rainfall over southern Africa may become more predictable. Conversely, synoptic types associated with moisture fluxes from the east, including easterly wave systems, are projected to occur less frequently under climate change. Such systems, although the least predictable, are also the most important in terms of the occurrence of rainfall over southern Africa. Qualitatively, therefore, the results are indicative of a generally drier climate over southern Africa under climate change, but in which individual rainfall events may be more predictable.

The statistical behaviour of rainfall (at an annual temporal resolution) and associated changes in the levels of dams was explored, in combination with the association between the two time series. While the (significantly positive) association between rainfall per catchment and the levels of dams is expected (despite management interventions), the importance of cumulative, multi-year anomalies of the climate system on the storage of the mega dams also appears consistently for all dams considered. Consideration of longer periods of cumulative rainfall may yield better correlation results especially when considering lower values (drought impacts), but flood events have an abrupt influence and will therefore weaken the correlation at longer time scales. The similarity between the periods of lower levels in all dams once more emphasize the importance of extensive,

multi-year droughts in the South African hydro-meteorological landscape.

The 8 km resolution projections are indicative of a plausible increase in extreme convective rainfall events over the central interior regions under climate change, which implies associated increases in run-off. Associated increases in streamflow may benefit water yield in the mega-dam region. Large increases in potential pan evaporation are projected to occur in response to the drastic increased in temperature that are projected to occur over the mega-dam area. As a consequence, general reductions in soil-moisture are likely and dam levels are to be impacted upon negatively. Changes in the variability of the hydrological cycle were explored for the southern African region, with a focus on Lesotho and the mega-dam region of eastern South Africa. The variability in present-day summer rainfall anomalies was explored, and 12 characteristic patterns of rainfall, with associated patterns of streamflow, were identified using SOMs. Projections of future climate change that were subsequently analysed are indicative of more frequent summer half-years associated with above normal rainfall over eastern southern Arica, including Lesotho and the mega-dam region. This is projected to result in increased streamflow, consistent with the dynamic hydrological modelling that is indicative of increased run-off over eastern South Africa.

It may finally be noted that understanding the climate change futures of the mega-dam region also presents a rich set of research questions to post-graduate students in climatology and hydrology. As such, this project was associated with a strong capacity building programme, with three post-graduate students contributing to the research. Their contributions and involvement, as well as a list of external publications generated in relation to the project research, are presented in Appendix A of this report.

## References

- Andrews, W.R.H. and Hutchings, L. (1980). Upwelling of the Southern Benguela Current. *Progress in Oceanography* **9** 1-8.
- Barnston, A.G., Leetmaa, A., Kousky, V., Livezey, R., O'Lenic, E, Van den Dool, H., Wagner, A.J. and Unger, D. (1999). NCEP forecasts of the El Niño of 1997-98 and its U.S. impacts. *Bull. Am. Meteorol. Soc.* **80** 1829-1852.
- Beraki, A.F., DeWitt, D.G., Landman, W.A. and Olivier, C. (2014). Dynamical seasonal climate prediction using an ocean-atmosphere coupled climate model developed in partnership between South Africa and the IRI. *J. Climate* **27** 1719-1741. doi:10.1175/JCLI-D-13-00275.1.
- Beraki, A.F., Landman, W., DeWitt, D. and Olivier, C. (2016). Global Dynamical Forecasting System Conditioned to Robust Initial and boundary forcings: Seasonal Context. *Int. J. Climatol.* DOI: 10.1002/joc.4643.
- Blamey, R.C. and Reason, C.J.C. (2009). Numerical simulation of a mesoscale convective system over the east coast of South Africa. *Tellus* **61A** 17-34.
- Christensen, J.H., Hewitson, B., Busuioc, A., Chen, A., Gao, X., Held, I., Jones, R., Kolli, R.K., Kwon, W-T., Laprise, R., Magana Rueda, V., Mearns, L., Menendez, C.G., Raisanen, J., Rinke, A., Sarr, A., Whetton, P. (2007). *Regional climate projections*. In: Solomon S, Qin D, Manning M, Chen Z, Marquis M, Averyt, AB, Tignor M, Miller HL (eds). Climate change 2007: the physical science basis. Contribution of Working Group I to the Fourth Assessment Report of the Inter-governmental Panel on Climate Change. Cambridge University Press, Cambridge.
- Dedekind, Z., Engelbrecht, F.A. and Van der Merwe, J. (2016). Model simulations of rainfall over southern Africa and its eastern escarpment. *Water SA* **42** 129-143.
- Doi, T., Behera, S.K., and Yamagata, T. (2016). Improved seasonal prediction using the SINTEX-F2 coupled model. *J. Adv. Model. Earth Syst.* **8** 1847-1867. doi:10.1002/2016MS000744.
- Dyer, T.G.J. and Tyson, P.D. (1977). Estimating above and below normal rainfall periods over South Africa, 1972-2000. *J. Appl. Meteorol.* **16** 145-147.
- Engelbrecht, F., Adegoke, J., Bopape, M.M., Naidoo, M., Garland, R., Thatcher, M., McGregor, J., Katzfey, J., Werner, M., Ichoku, C. and Gatebe, C. (2015). Projections of rapidly rising surface temperatures over Africa under low mitigation. *Environ Res Lett.* doi:10.1088/1748-9326/10/8/085004.
- Engelbrecht, F.A. and Bopape, M.J. (2011). High-resolution projected climate futures for southern Africa. *27<sup>th</sup> Annual Conference of the South African Society for Atmospheric Sciences*, September 2011, Hartebeeshoek. ISBN 978-0-620-47333-0.
- Engelbrecht, C.J., Engelbrecht, F.A. and Dyson, L.L. (2013). High-resolution model projected changes in mid-tropospheric closed-lows and extreme rainfall events over southern Africa. *Int J Climatol* **33** 173-187. doi:10.1002/joc.3420.
- Engelbrecht, F.A., Landman, W.A., Engelbrecht, C.J., Landman, S., Bopape, M.M., Roux, B., McGregor, J.L. and Thatcher, M. (2011). Multi-scale climate modelling over Southern Africa using a variable-resolution global model. *Water SA* **37** 647-658.

- Engelbrecht, F.A., McGregor, J.L. and Engelbrecht, C.J. (2009). Dynamics of the conformal-cubic atmospheric model projected climate-change signal over southern Africa. *Int J Climatol* **29** 1013-1033.
- Engelbrecht, F.A., McGregor, J.L. and Rautenbach, C.J. deW. (2007). On the development of a new nonhydrostatic atmospheric model in South Africa. *SA J. of Sci.* **103** 127-134.
- Engelbrecht, F.A., Rautenbach, C.J. deW. and Katzfey, J.J. (2002). January and July climate simulations over the SADC region using the limited area model DARLAM. *Water SA* **28** 361-374.
- Fauchereau, N., Trzaska, S., Rouault, M. and Richard, Y. (2003). Rainfall Variability and Changes in Southern Africa during the 20th Century in the Global Warming Context. *Nat. Hazards* **29** 139-154.
- Funk, C., Peterson, P., Landsfeld, M., Pedreros, D., Verdin, J., Shukla, S., Husak, G., Rowland, R., Harrison, L., Hoell, A. and Michaelsen, J. (2015). The climate hazards infrared precipitation with stations-a new environmental record for monitoring extremes. *Scientific Data* **2** 150066. doi:10.1038/sdata.2015.66 2015.
- Garland, R.M., Matoane, M., Engelbrecht, F.A., Bopape, M-J. M., Landman, W.A., Naidoo, M., Van der Merwe, J. and Wright, C.Y. (2015). Regional projections of extreme apparent temperature days in Africa and the related potential risk to human health. *International Journal of Environmental Research and Public Health* 10/2015 **12** 12577-12604. DOI:10.3390/ijerph121012577.
- Goddard, L., Mason, S.J., Zebiak, S.E., Ropelewski, C.F., Basher, R. and Cane, M.A. (2001). Current approaches to seasonal-to-interannual climate predictions. *Int. J. Climatol.* **21** 1111-1152.
- Harris, I., Jones, P.D., Osborn, T.J. and Lister, D.H. (2013). Updated high-resolution grids of monthly climatic observations – the CRU TS3.10 Dataset. *International Journal of Climatology* **34** 623-642.
- Hernandez-Diaz, L., Laprise, R., Sushama, L., Martynov, Winger, K. and Dugas, B. (2013). Climate simulation over CORDEX Africa domain using the fifth-generation Canadian Regional Climate Model (CRCM5). *Clim. Dyn.* **40** 1215-1433.
- Holtstag, A.A.M. and Boville, B.A. (1993) Local versus non-local boundary layer diffusion in a global climate model. *J. Climate* **6** 1825-1842.
- Houze, R.A., Rudledge, S.A., Biggerstaff, M.I. and Smull, B.F. (1989). Interpretation of Doppler Weather Radar Display of Midlatitude Mesoscale Convective Systems. *American Met. Soc.* **70** 608-619.
- James, R. and Washington, R. (2013). Changes in African temperature and precipitation associated with degrees of global warming. *Climatic Change* **117** 859-872. DOI 10.1007/s10584-012-0581-7.
- Jones, P.D., Lister, D.H., Osborn, T.J., Harpham, C., Salmon, M. and Morice, C.P. (2012). Hemispheric and large-scale land-surface air temperature variations: An extensive revision and an update to 2010 *J. Geophys. Res.* **117** D05127. doi:10.1029/2011JD017139.
- Joubert, A.M., Katzfey, J.J., McGregor, J.L. and Nguyen, K.C. (1999). Simulating mid-summer climate over southern Africa using a nested regional climate model. *J. Geophys. Res* **104** 19015-19025.
- Jury, M.R. (2012). An intercomparison of model-simulated east-west climate gradient over South Africa. *Water SA* **38** 467-478. <http://dx.doi.org/10.4314/wsa.v38i4.1>.

- Kanamitsu, M., Ebisuzaki, W., Woollen, J., Yang, S.K., Hnilo, J.J., Fiorino, M. and Potter, G.L. (2002). NCEP-DOE AMIP-II reanalysis(R-2). *Bull. Am. Meteorol. Soc.* **83** 1631-1643.
- Katzfey, K.K., McGregor, J.M., Nguyen, K. and Thatcher, M. (2009). Dynamical downscaling techniques: Impacts on regional climate change signals. 18<sup>th</sup> World IMACS/MODSIM Congress, Cairns, Australia, July 2009.
- Kgatuke, M.M., Landman, W.A., Beraki, A. and Mbedzi, M.P. (2008). The internal variability of the RegCM3 over South Africa. *Int. J. Climatol.* **28** 505-520. doi:10.1002/joc.1550.
- Klopper, E., Landman, W.A. and Van Heerden, J. (1998). The predictability of seasonal maximum temperature in South Africa. *Int. J. Climatol.* **18** 741-758.
- Kowalczyk, E.A., Wang, Law, R.M., Davies, H.L., McGregor, J.L. and Abramowitz, G. (2006). The CSIRO Atmosphere Biosphere Land Exchange (CABLE) model for use in climate models and as an offline model. *CSIRO Marine and Atmospheric Research Paper* 13, 37 pp.
- Landman, W.A. and Beraki, A. (2012). Multi-model forecast skill for midsummer rainfall over southern Africa. *Int J Climatol* **32** 303-314. doi:10.1002/joc.2273
- Landman, W.A., Beraki, A., De Witt, D. and Lötter, D. (2014). SST prediction methodologies and verification considerations for dynamical mid-summer rainfall forecasts for South Africa. *Water SA* **40** 615-622.
- Landman, W.A. and Goddard, L. (2002). Statistical recalibration of GCM forecasts over southern Africa using model output statistics. *J. Clim.* **15** 2038-2055.
- Lazenby, M., Landman, W.A., Garland, R. and DeWitt, D. (2014). Seasonal temperature prediction skill over southern Africa and human health. *Meteorol Appl* **21** 963-974. doi:10.1002/met.1449
- Madec, G. (2006). NEMO ocean engine. Note du Pôle de Modélisation IPSL Rep., 110 pp.
- Malherbe, J., Dieppois, B., Maluleke, P. et al. (2016). South African Droughts and Decadal Variability, *Nat Hazards* **80** 657. doi:10.1007/s11069-015-1989-y.
- Malherbe, J., Engelbrecht, F.A. and Landman, W.A. (2013). Projected changes in tropical cyclone climatology and landfall in the Southwest Indian Ocean region under enhanced anthropogenic forcing. *Clim Dyn* **40** 2867-2886.
- McGregor, G. and Nieuwolt, S. (1998). An introduction to the climates of the low latitudes. Tropical Climatology. 339. John Wiley & Sons. England.
- McGregor, J.L. (1996). Semi-Lagrangian advection on conformal-cubic grids. *Mon. Wea. Rev.* **124** 1311-1322.
- McGregor, J.L. (1997). Regional Climate Modelling. *Met. Atmos. Phys.* **63** 105-117.
- McGregor, J.L. (2003). A new convection scheme using a simple closure. In "Current issues in the parameterization of convection", *BMRC Research Report* **93**, 33-36.
- McGregor, J.L. (2005a). Geostrophic adjustment for reversibly staggered grids. *Mon. Wea. Rev.* **133** 1119-1128.
- McGregor, J.L. (2005b). C-CAM: Geometric aspects and dynamical formulation. CSIRO Atmospheric research Tech. Paper No. 70, 43 pp.

- McGregor, J.L. and Dix, M.R. (2001). The CSIRO conformal-cubic atmospheric GCM. In IUTAM Symposium on Advances in Mathematical Modelling of Atmosphere and Ocean Dynamics, P. F. Hodnett (Ed.), Kluwer, Dordrecht, 197-202.
- McGregor, J.L. and Dix, M.R. (2008). An updated description of the Conformal-Cubic Atmospheric Model. In High Resolution Simulation of the Atmosphere and Ocean, eds. K. Hamilton and W. Ohfuchi, Springer, 51-76.
- McGregor, J.L., Gordon, H.B., Watterson, I.G., Dix, M.R. and Rotstayn, L.D. (1993). The CSIRO 9-level atmospheric general circulation model. CSIRO Div. Atmospheric Research Tech. Paper No. 26, 89.
- McKee, T.B., Doesken, N.J. and Kleist, J. (1993). The relationship of drought frequency and duration of time scales. *Eighth Conference on Applied Climatology, American Meteorological Society* Jan 17-23, 1993, Anaheim CA, pp. 179-186.
- McKee, T.B., Doesken, N.J. and Kleist, J. (1995). Drought monitoring with multiple time scales. *Ninth Conference on Applied Climatology, American Meteorological Society* Jan 15-20, 1995, Dallas TX, pp. 233-236.
- Mitchell, T.D. and Jones, P.D. (2005). An improved method of constructing a database of monthly climate observations and associated high-resolution grids. *International Journal of Climatology* **25** 693-712 DOI: 10.1002/joc.1181.
- Muthige, M.S., Malherbe, J., Engelbrecht, F.A., Grab, S., Beraki, A., Van der Merwe, J. and Lennard, C. (2018). Projected changes in tropical cyclones over the southwest Indian Ocean under different degrees of global warming. *Environmental Research Letters*. *In review*.
- Niang, I., Ruppel, O.C., Abdrabo, M., Essel, A., Lennard, C., Padgham, J., Urquhart, P., Adelekan, I., Archibald, S., Barkhordarian, A., Battersby, J., Balinga, M., Bilir, E., Burke, M., Chahed, M., Chatterjee, M., Chidzie, C.T., Descheemaeker, K., Djoudi, H., Ebi, K.L., Fall, P.D., Fuentes, R., Garland, R., Gaye, F., Hilmi, K., Gbobaniyi, E., Gonzalez, P., Harvey, B., Hayden, M., Hemp, A., Jobbins, G., Johnson, J., Lobell, D., Locatelli, B., Ludi, E., Otto Naess, L., Ndebele-Murisa, M.R., Ndiaye, A., Newsham, A., Njai, S., Nkem, Olwoch, J.M., Pauw, P., Pramova, E., Rakotondrafara, M-L., Raleigh, C., Roberts, D., Roncoli, C., Sarr, A.T., Schleyer, M.H., Schulte-Uebbing, L., Schulze, R., Seid, H., Shackleton, S., Shongwe, M., Stone, D., Thomas, D., Ugochukwu, O., Victor, D., Vincent, K., Warner, K., Yaffa, S. (2014). *IPCC WGII AR5 Chapter 22* pp 1-115.
- Nel, W. and Sumner, P. (2006). Trends in rainfall total and variability (1970-2000) along the KwaZulu-Natal Drakensberg foothills. *S.A Geog. J.* **88** 130-137.
- Nickless, A., Ziehn, T., Rayner, P.J., Scholes, R.J. and Engelbrecht, F. (2015). Greenhouse gas network design using backward Lagrangian particle dispersion modelling – Part 2: Sensitivity analyses and South African test case. *Atmospheric Chemistry and Physics* **15** 2051-2069. doi:10.5194/acp-15-2051-2015.
- Palmer, T.N. and Anderson, D.L.T. (1994). The prospects for seasonal forecasting – a review paper. *Q. J. R. Meteorol. Soc.* **120** 755-793.
- Potgieter, C.J. (2006). Accuracy and skill of the conformal-cubic atmospheric model in short-range weather forecasting over southern Africa. *M.Sc. Thesis*, University of Pretoria. 172 pp.
- Ratnam, J.V., Behera, S.K., Doi, T., Ratna, S.B. and Landman, W.A. (2016). Improvements to the WRF seasonal hindcasts over South Africa by bias correcting the driving SINTEX-F2v CGCM fields. *J. Clim.* **29** 2815-2829. doi:10.1175/JCLI-D-15-0435.1.

- Reason, C.J.C. and Rouault, M. (2002). ENSO-like decadal variability and South African rainfall. *Geophys. Res. Lett.* **29** 1638. DOI: 10.1029/2002GL014663.
- Reason, C.J.C. and Rouault, M. (2005). Links between the Antarctic Oscillation and winter rainfall over western South Africa. *Geophys. Res. Lett.* **32** L07705. doi: 10.1029/2005GL022419.
- Roeckner, E. and co-authors (2003). The atmospheric general circulation model ECHAM5. Part I: Model description. Max-Planck-Institut für Meteorologie Rep. 349, 127 pp. Available online at [https://www.mpimet.mpg.de/fileadmin/publikationen/Reports/max\\_scirep\\_349.pdf](https://www.mpimet.mpg.de/fileadmin/publikationen/Reports/max_scirep_349.pdf).
- Rotstayn, L.D. (1997). A physically based scheme for the treatment of stratiform clouds and precipitation in large-scale models. I: Description and evaluation of the microphysical processes. *Quart. J. Roy. Meteor. Soc.* **123** 1227-1282.
- Rouault, M. and Richard, Y. (2003). Intensity and spatial extension of drought in South Africa at different time scales. *Water SA* 29 489-500.
- Rouault, M., Roy, S.S. and Balling, R.C. Jr. (2013). The diurnal cycle rainfall in South Africa in the austral summer. *Int. J. of Clim.* 33 770-777.
- Rouault, M., White, S.A., Reason, C.J.C., Lutjharms, J.R.E. and Jobard, I. (2002). Ocean-Atmosphere Interaction in the Agulhas Current Region and a South African Extreme Weather Event. *Wea. Forecasting* **17** 655-669.
- Sasaki, W., Richards, K.J. and Luo, J.J. (2013). Impact of vertical mixing induced by small vertical scale structures above and within the equatorial thermocline on the tropical Pacific in a CGCM. *Climate Dyn.* **41** 443-453, doi:10.1007/s00382-012-1593-8.
- Sasaki, W., Doi, T., Richards, K.J. and Masumoto, Y. (2014). Impact of the equatorial Atlantic sea surface temperature on the tropical Pacific in a CGCM. *Climate Dyn.* **43** 2539-2552. doi:10.1007/s00382-014-2072-1.
- Sasaki, W., Doi, T., Richards, K.J. and Masumoto, Y. (2015). The influence of ENSO on the equatorial Atlantic precipitation through the Walker circulation in a CGCM. *Climate Dyn.* **44** 191-202. doi:10.1007/s00382-014-2133-5.
- Schulze, B.R. (1965). Hail and thunderstorm frequency in South Africa. *Notos* **14** 67-71.
- Tennant, W.J. and Hewitson, B.C. (2002). Intra-seasonal rainfall characteristics and their importance to the seasonal prediction problem. *Int. J. Climatol.* **22** 1033-1048.
- Thatcher, M. and McGregor, J.L. (2009). Using a scale-selective filter for dynamical downscaling with the conformal cubic atmospheric model. *Mon. Weather Rev.* **137** 1742-1752.
- Thatcher, M. and McGregor, J.L. (2010). A technique for dynamically downscaling daily-averaged GCM datasets over Australia using the Conformal Cubic Atmospheric Model. *Mon. Weather Rev.* **139** 79-95.
- Thornton, P.K., Jones, P.G., Ericksen, P.J. and Challinor, A.J. (2011). Agriculture and food systems in sub-Saharan Africa in a 4°C+ world. *Philosophical Transactions of the Royal Society A* **369** 117-36.
- Tozuka, T., Babatunde, J.A. and Engelbrecht, F.A. (2014). Impacts of convection schemes on simulating tropical-temperate troughs over southern Africa. *Climate Dynamics* **42** 433-451. DOI 10.1007/s00382-013-1738-4.

- Tyson, P.D., Preston-Whyte R.A. and Schulze, R.E. (1976). The climate of the Drakensberg. Natal Town and regional planning commission: Pietermaritzburg.
- Van der Beek, P., Summerfield, M.A., Braun, J., Brown, R.W. and Fleming A. (2002). Modeling postbreakup landscape development and denudational history across the southeast African (Drakensberg Escarpment) margin. *J. of Geoph. Research: Solid Earth* (1978-2012), 107(B12), ETG-11.
- Wang, G., Cai, W., Gan, B., Wu, L., Santoso, A., Lin, X., Chen, Z., McPhaden, M.J. (2017). Continued increase of extreme El Niño frequency long after 1.5°C warming stabilization. *Nature Climate Change* **7** 568-572. doi:10.1038/nclimate3351
- Winsemius, H.C., Dutra, E., Engelbrecht, F.A., Archer Van Garderen, E., Wetterhall, F., Pappenberger, F. and Werner, M.G.F. (2014). The potential value of seasonal forecasts in a changing climate in southern Africa. *Hydrol. Earth Syst. Sci.* 18 1525-1538.
- Yang, G.Y. and Slingo, J. (2001). The diurnal cycle in the Tropics. *Mon. Weather Rev.* **129** 784-801.

## APPENDIX A

### List of publications and post-graduate students related to/contributing to WRC project K5/2457

#### A1. List of publications

##### *Published*

Dedekind Z., Engelbrecht F.A. and Van der Merwe J. (2016). Model simulations of rainfall over southern Africa and its eastern escarpment. *Water SA* **42** 129-143.

Dedekind Z (2016). Modelling cumulus convection over the eastern escarpment of South Africa. *MSc Manuscript, North West University*.

Dedekind Z., Engelbrecht F.A. and Van der Merwe J. (2015). High resolution rainfall modelling over the eastern escarpment of South Africa. 31st Annual Conference of South African Society for Atmospheric Sciences, Hennops River Valley, South Africa, 21-22 September 2015.

Mavhungu M., Malherbe J., Engelbrecht, F., Grab S., Beraki A., Maisha R., Van Der Merwe J. (2018). Projected changes in tropical cyclones over the South West Indian Ocean under different extents of global warming. *Env. Res. Letters* 104541.R1. *In Press*.

##### *In preparation*

Dedekind Z. and Engelbrecht F.A. (2018). High Resolution Rainfall Modelling over the Eastern Escarpment of South Africa. *Water SA*. *In preparation*.

Engelbrecht F.A., Engelbrecht C.J. and Lumsden T. (2018). When can we expect day zero in Gauteng? *Water Wheel*. *In preparation*.

Engelbrecht F.A., Engelbrecht C.J. and Lumsden T. (2018). Projecting the hydrodynamic futures of eastern South Africa. *Water SA*. *In preparation*.

Ngwana I, Engelbrecht FA and Grab S (2018). Predictability of different synoptic types over southern Africa. *Weather and Forecasting*. *In preparation*.

#### A2. Capacity building report

Three students are/were involved in this project through post-graduate research.

Mr. Zane Dedekind obtained an MSc (Environmental Sciences) degree in 2016 with manuscript entitled: "Modelling cumulus convection over the eastern escarpment of South Africa". At the time, he was a candidate researcher within the CSIR Natural Resources and the Environment.

Mr. Mavhungu Muthige is a candidate researcher at the CSIR Natural Resources and the Environment and has registered for his PhD research at the University of the Witwatersrand (Wits) in April 2015. His work focuses on landfalling tropical lows and cyclones over southern Africa under climate change, and as such he is analysing the CCAM CORDEX projections generated through the project. His first PhD paper has recently been accepted for publication.

Mr. Isaac Ngwana (previously from SAWS) is a PhD student at Wits and is receiving support through the project in the forms of data sets generated, and his research has in fact directly

contributed to the project. He has to date prepared a full PhD paper draft of which the findings are described in the project final report.

<b>Student</b>	<b>University</b>	<b>Topic</b>	<b>Status</b>
Mavhungu Muthige	Wits	Projected changes in tropical rainfall-producing systems impacting on the eastern parts of southern Africa under climate change.	Registered April 2015
Zane Dedekind	North West University	Modelling cumulus convection over the eastern escarpment of South Africa.	Graduated (MSc) in 2016
Isaac Ngwana	Wits	Short-range predictability over southern Africa under present-day and future forcings.	Initially registered 2013.